ENP

ANL-7685

PROCEEDINGS OF THE CONFERENCE ON FLOW-INDUCED VIBRATIONS IN REACTOR SYSTEM COMPONENTS

May 14 and 15, 1970

RETURN TO REFERENCE FILE
TECHNICAL PUBLICATIONS
DEPARTMENT

PROPERTY OF
ANL-W Technical Library

ARGONNE NATIONAL LABORATORY
ARGONNE, ILLINOIS

The facilities of Argonne National Laboratory are owned by the United States Government. Under the terms of a contract (W-31-109-Eng-38) between the U. S. Atomic Energy Commission, Argonne Universities Association and The University of Chicago, the University employs the staff and operates the Laboratory in accordance with policies and programs formulated, approved and reviewed by the Association.

MEMBERS OF ARGONNE UNIVERSITIES ASSOCIATION

The University of Arizona
Carnegie-Mellon University
Case Western Reserve University
The University of Chicago
University of Cincinnati
Illinois Institute of Technology
University of Illinois
Indiana University
Iowa State University
The University of Iowa
Kansas State University
The University of Kansas
Loyola University
Marquette University
Michigan State University
The University of Michigan
University of Minnesota
University of Missouri
Northwestern University
University of Notre Dame
The Ohio State University
Ohio University
The Pennsylvania State University
Purdue University
Saint Louis University
Southern Illinois University
University of Texas
Washington University
Wayne State University
The University of Wisconsin

LEGAL NOTICE

This report was prepared as an account of Government sponsored work. Neither the United States, nor the Commission, nor any person acting on behalf of the Commission:

A. Makes any warranty or representation, expressed or implied, with respect to the accuracy, completeness, or usefulness of the information contained in this report, or that the use of any information, apparatus, method, or process disclosed in this report may not infringe privately owned rights; or

B. Assumes any liabilities with respect to the use of, or for damages resulting from the use of any information, apparatus, method, or process disclosed in this report.

As used in the above, "person acting on behalf of the Commission" includes any employee or contractor of the Commission, or employee of such contractor, to the extent that such employee or contractor of the Commission, or employee of such contractor prepares, disseminates, or provides access to, any information pursuant to his employment or contract with the Commission, or his employment with such contractor.

Printed in the United States of America
Available from
Clearinghouse for Federal Scientific and Technical Information
National Bureau of Standards, U. S. Department of Commerce
Springfield, Virginia 22151
Price: Printed Copy $3.00; Microfiche $0.65

ANL-7685
Reactor Technology

ARGONNE NATIONAL LABORATORY
9700 South Cass Avenue
Argonne, Illinois 60439

Proceedings of the Conference on

FLOW-INDUCED VIBRATIONS IN REACTOR SYSTEM COMPONENTS

May 14 and 15, 1970

G. S. Rosenberg
Program Director

M. W. Wambsganss
Meeting Program Chairman

R. P. Carter
Program Coordinator

TABLE OF CONTENTS

Preface v

* * * * *

Welcome 1
M. V. Nevitt, *Argonne National Laboratory*

Opening Remarks 3
N. Grossman, *U. S. Atomic Energy Commission*

SESSION 1
Chairman: G. S. Rosenberg
Argonne National Laboratory

Response of a Flexible Rod to Near-field Flow Noise 5
S. S. Chen and M. W. Wambsganss, *Argonne National Laboratory*

Experimental Determination and Analysis of Vibrations Induced by the Near-field Flow Noise in Tubes 32
A. K. Addae, *Massachusetts Institute of Technology*, and H. Fenech, *University of California, Santa Barbara*

Calculation of the Response of Rods to Boundary Layer Pressure Fluctuations 47
R. M. Kanazawa, *General Electric Co., San Jose*, and A. P. Boresi, *University of Illinois, Urbana*

Dynamic Response of Slender Tubes in Parallel Flow when Subjected to Time Varying Boundary Conditions 64
S. A. Knudson, *Esso Research and Engineering Co.*, and G. M. Smith, *University of Nebraska*

Unsteady Momentum Fluxes in Two-phase Flow and the Vibration of Nuclear System Components* 91
T. S. Yih, *Stone and Webster Engineering Corp.*, and P. Griffith, *Massachusetts Institute of Technology*

SESSION 2
Chairman: K. A. Gardner
Liquid Metal Engineering Center

Measurement, Interpretation and Characterization of Nearfield Flow Noise 112
M. W. Wambsganss and P. L. Zaleski, *Argonne National Laboratory*

Conductivity Cells for Flow Induced Vibration Measurements 141
G. R. Sawtelle, *Battelle Northwest Laboratory*

* Not presented orally at Conference

Application of Noise Analysis Techniques to Study of Flow Induced Vibration in Reactor System Components 177
R. L. Randall, *Atomics International*

An Engineering Approach to Tube Flow-induced Vibrations 205
C. R. Gerlach and F. T. Dodge, *Southwest Research Institute*

Lift and Strouhal Frequency for Bluff Shapes in Constricted Passages. 225
G. H. Toebes, *Purdue University*, and A. S. Ramamurthy, *Sir George Williams University*

Proposed Analytical Model for the Cross-flow-induced Vibrations of a Circular Cylinder 248
H. Halle, *Argonne National Laboratory*

SESSION 3
Chairman: M. Bender
Oak Ridge National Laboratory

Introduction 270
M. Bender, *Oak Ridge National Laboratory*

Big Rock Point Vibration Analysis 272
J. E. Corr, *General Electric Co., San Jose*

Investigation of Methods for Coupled Structural-Hydrodynamic Analysis of Reactor Internals 290
S. Fabic, *Westinghouse Electric Corp., Pittsburgh*

Generation of Positive and Negative Damping with a Flow Restrictor in Axial Flow 304
Excitation of a Pure Tone by Flow through an Orifice 308
Flow-induced Instability of a Thin-walled Cylindrical Shell 312
D. R. Miller, *Knolls Atomic Power Laboratory*

Stability Analysis of a Rigid Blade in Parallel Fluid Flow 321
E. A. Zanoni and P. A. Lowe, *Bettis Atomic Power Laboratory*

Analysis of the Fundamental Vibration Frequency of a Radial Vane Internal Steam Separator Structure 335
E. Kiss, *General Electric Co., San Jose*

Summary Remarks 344
M. W. Wambsganss, *Argonne National Laboratory*

* * * *

Attendees 347

PREFACE

Vibration of reactor core components, such as fuel pins, fuel assemblies, and control rods, has the potential for causing failure by fretting, wear and fatigue, as well as causing anomalous reactor behavior as exhibited in neutron-flux oscillations; vibration-induced failures of reactor heat exchanger tubes are documented in the literature. The primary source of energy exciting these vibrations is the flowing coolant, which additionally alters various vibrational characteristics of the component.

To provide a basis for assessing the state-of-the-art of flow-induced vibration, to encourage the systematic application of diversely developed techniques, and to provide a forum for currently developing insights into the subject area, a conference on Flow-Induced Vibration in Reactor System Components was planned to be held May 14, 1970, at Argonne National Laboratory. On December 19, 1969, an announcement and call for papers was issued. The response was excellent and a one-and-a-half-day technical program featuring 15 papers was prepared. (An additional paper was submitted for publication without presentation.) The meeting was attended by 62 registered participants; 41 from outside Argonne representing 19 different organizations including AEC Laboratories, AEC Industrial Contractors, Private Industry, and Universities. The papers which were presented discussed basic studies relating to parallel-flow- and crossflow-induced vibrations, and the analysis of specific problems and generalized approaches.

We would like to express our appreciation to Mr. Nicholas Grossman, not only for his opening remarks, but also for his interest and support for the meeting.

Mr. Ralph Carter served efficiently as program coordinator. We are indebted to him especially for his liaison work with the services, editing, and publishing groups, and also for collection of the papers, maintenance of the registration list, and design of the program.

Our sincere thanks also to Mrs. Dorothy Carlson, for handling the transportation, lodging, and banquet arrangements; to Mrs. Joyce Kopta for invaluable assistance as proceedings coordinator, and in preparing this volume for publication; and to Miss Joyce Stephens for secretarial work involved in preparation of the initial mailing and transcribing the discussions from tape.

Finally, we thank the authors for taking the time to prepare their papers and for discussing their particular research activities.

To expedite publication and distribution of the proceedings the discussion was edited without subsequent review by the discussers. Comments of minor importance were neglected and some editorial work was required in cases where the discussion was not clearly "picked-up" by the microphone. We extend our apologies to those discussers who find their comments missing or unintentionally changed in meaning through editorial changes.

It is our hope that this publication will be useful as a reference document and will also form the basis upon which work in the subject area can be continued and expanded.

G. S. Rosenberg, Program Director
M. W. Wambsganss, Meeting Program Chairman
Argonne National Laboratory

June 30, 1970

WELCOME

M. V. Nevitt
Deputy Laboratory Director
Argonne National Laboratory

I have the distinct pleasure and privilege to call to order this conference on Flow-induced Vibrations in Reactor Systems Components and to extend a word of welcome on behalf of the Laboratory. We have quite a few conferences here at Argonne, and I'm sure it's no surprise to you that frequently my boss Dr. Robert Duffield, the Laboratory Director, or I may be called on to extend a welcome at the beginning of a meeting. We have remarked to each other many times that although we do it frequently, we always feel a genuine sense of exhilaration in opening a conference. We have this feeling particularly when the meeting involves a relatively small group, such as this one, so that exchanges of ideas can take place in a very informal way. We hope this meeting follows the pattern of being stimulating and useful to all of you in attendance.

In a sense the topic suggests the extent to which there is specialization nowadays: You will be discussing cyclic translational motion in a select group of bodies and assemblies, namely reactor internals and reactor components. You will be treating a rather specific excitation source, the coolant. On the other hand, vibration effects occur widely in reactor systems, so the subject does permit you to generalize to some degree.

If you don't mind a materials man - I'm a metallurgist - introducing one caveat, I'll remind you that it is of equal importance to have an understanding, in the same depth, of the influence of these vibrational effects on the materials of which the reactor components are composed. I judge from the preamble to this conference, where comments were made about fretting corrosion, about fatigue, and about wear, that at least a part of your time will be given to materials considerations.

I'm not going to tell you very much about Argonne National Laboratory. Our next speaker, Mr. Grossman, is going to review some of Argonne's past and current interests and achievements in reactors and reactor components. I shall simply say again we're glad you are here. Mr. Rosenberg and his staff have tried to think of all of the things that can be useful to you and that are necessary to make this a good conference. If they have forgotten anything, call it to their attention so that the Laboratory can be the responsible host it wishes to be.

Thank you for coming, and I hope your conference is successful.

OPENING REMARKS

Nicholas Grossman
Chief, Special Technology Branch
Division of Reactor Development and Technology
U. S. Atomic Energy Commission
Washington, D. C.

It is appropriate to briefly review the historical role Argonne National Laboratory played in the development of commercial nuclear power. The historical events that took place in December of 1942 under the Stagg Field stadium, where the first nuclear chain reaction occurred, is well known to all. The purpose of this first "pile" was both to establish the proof of principle of the chain reaction and to serve as a working model for the graphite moderated plutonium production reactors. Perhaps it is lesser known that the Manhattan Project staff explored other types of reactor concepts with the specific thought of utilizing the heat of the nuclear fission for practical power generation purposes. A patent application--naturally classified as secret--was prepared--OSRD-97--and submitted to the Manhattan District Patent Officer on "Cooling a Reactor by Latent Heat of Evaporation of a Liquid" in anticipation of the practicality for such reactors. The patent officer reviewed and withdrew the application and attached a statement to it stating in part: "In view of the indication that no way has been worked out for controlling a reactor of the type under consideration, the case will be given inactive status until such time as an operative device can be disclosed."

Shortly after the establishment of the Atomic Energy Commission in 1947, long range plans were formulated to explore the potential uses and assess the attendant risks involved in pursuing one of the mandates of the Commission; namely, the development of the peaceful applications of nuclear energy. One of the first steps taken was to design and build a Materials Test Reactor--to be located at some remote test site. The basic experiments were conducted here at Argonne to study the expulsion of the water coolant under a variety of assumed operating conditions. These experiments confirmed the soundness of the design approach and vindicated the foresight of the pioneer Manhattan District staff. The next milestone came in connection with the design of the CP-5, the Argonne Heavy Water Research Reactor, when it was necessary to demonstrate experimentally that steam would be expelled fast enough to shut down the reactor before the fuel plates would melt, should the control rods fail to shut down the reactor. Again, the experiments verified the premise that the steam formation was sufficiently fast to control the reactor.

Early in 1950 a proposal was submitted by Argonne for a series of experiments to establish more quantitatively the operating limits of reactors under transient conditions. This proposal later became known as the Boiling Water Reactor Experiment (BORAX). The success of these early experiments led to a whole series of BORAX reactor experiments that provided the engineering foundation for a whole family of liquid cooled reactor designs. It was a natural follow-up that in 1954 Argonne proposed to build a 20 megawatt Experimental Boiling Water Reactor power plant (EBWR); the significant part of the proposal was that the reactor was to be built not at some remote test site, but right here at Argonne in the metropolitan Chicago area.

One of the most unique aspects of the self-sustained nuclear chain reaction is the production of new fissionable material in addition to the heat generation. The desirability to design and build practical systems where this gain in fissionable material, compared with the material consumed is substantial, has also been recognized at the very outset of the reactor program, and here again Argonne took an early lead. You all know about the event of the lighting of an electric light bulb from energy derived from a controlled nuclear power source that took place for the first time in the Argonne designed Experimental Breeder Reactor (EBR) at Idaho--a scant nine years after the first successful nuclear chain reaction was established under the Stagg Field stadium.

There is a common element in all these events: a systematic and orderly approach going from the relatively simple tests to the more and more complex systems; a program that has been pursued on a systematic basis with carefully thought out experiments designed to establish, or refute, the validity of concepts, propositions, or assumptions. As we are all aware, from the standpoint of nuclear physics, a variety of mechanical assemblies can be constructed in order to convert nuclear heat to electricity. The fundamental cornerstone of the Atomic Energy Commission's reactor development program rests on an orderly approach to assure a practical design that is economical, safe, and provides the greatest potential for conserving our national resources within a balanced environment. Needless to say, there is no easy solution to these complex problems--and our jobs, as engineers, are safe for a few more years.

One of the salient aspects of this working meeting is that it cuts across traditional engineering disciplines and provides a strong interplay among the various groups. It should also highlight the state of art pertaining to the flow-induced vibration aspects in reactor design and assist all of us to continue on a sound program. It is very appropriate for Argonne National Laboratory to sponsor such a working meeting and I know it will substantially contribute to our reactor development efforts.

RESPONSE OF A FLEXIBLE ROD TO NEAR-FIELD FLOW NOISE

by

S. S. Chen and M. W. Wambsganss

Theoretical and Applied Mechanics Section
Engineering and Technology Division
Argonne National Laboratory
Argonne, Illinois

ABSTRACT

An analytical solution is obtained for the displacement statistics of a simply-supported rod in parallel flow. The system is described by Paidoussis' equation of motion and the mathematical model for the turbulent-boundary-layer pressure statistics is based on a phenomenological model developed by Corcos. The derived model is successful in predicting the basic trends and essential features of parallel-flow-induced vibration. Numerical examples are given for comparison with the experimental measurements and the reasons for the differences between the theoretical prediction and experiment result are discussed. A parameter study is also made for the ranges associated with typical reactor components. The study shows theoretical prediction and experimental correlations to be in good agreement.

INTRODUCTION

The vibration of reactor internals, such as fuel pins, fuel assemblies, and control rods, has the potential for causing component failure by fretting, wear and fatigue, as well as causing anomalous behavior as exhibited in neutron-flux oscillations. A number of studies [1-7] have been conducted in order to predict the amplitude of vibration, to understand the mechanism of parallel-flow-induced vibration, and to obtain design fixes to eliminate it.

Earlier studies of parallel-flow-induced vibration of flexible rods can be divided into two groups, those involving a deterministic approach [1,2,3,6] and those involving a probabilistic approach [4,5,7]. In the

first group, no complete solution to the equation of motion was presented and analyses were hampered by the lack of a complete description of the forcing functions. Several empirical expressions were correlated based on the postulated causes of self-excitation, cross-flow, secondary circulation etc., yet the real forces exciting the vibration were unknown. The second group offered an alternative approach to the problem, postulating the vibration was excited by random pressure fluctuations in the turbulent flow. Reavis [4] treated the rod vibration using the turbulent-boundary-layer pressure obtained for turbulent pipe flows and for turbulent boundary layers on flat plates. An integrated experimental-theoretical study of the problem was initiated at Argonne National Laboratory [5]. Gorman [7] conducted an experimental study of the pressure statistics around a rod. Although it is shown that fairly good agreement between experiment and theory is achieved, a basic result is in question; the lateral cross-correlation of pressure does not agree with that given in the other reports.

The best features of the existing information are utilized and an analytical approach to the study of rod displacement statistics due to turbulent-boundary-layer pressure fluctuations is presented in this paper. The approach is essentially the same as that of Reavis, but the equation of motion is that of Paidoussis [8] which accommodates the effects of added mass, damping, axial force and the flow velocity on natural frequencies. The data characterizing the pressure field is that obtained by Bakewell [9]; measurements on a body of revolution. The analysis is presented in dimensionless form in an effort to achieve maximum applicability.

MATHEMATICAL MODEL AND ANALYSIS

Consider a simply supported rod immersed in an incompressible fluid flowing with an average velocity V parallel to the x-axis (Fig. 1). The rod has mass per unit length m and flexural rigidity EI. The vibration of the rod is excited by the random pressure fluctuations in the turbulent flow along the rod. The equation of small lateral motion was formulated by Paidoussis [8] in his study of stability. If the damping and random pressure are included, the equation of motion becomes

$$EI \frac{\partial^4 y}{\partial x^4} + \lambda I \frac{\partial^5 y}{\partial x^4 \partial t} + \left\{ MV^2 - \left[T_o + \frac{1}{2} \frac{MV^2}{d} c_T \left(\frac{1}{2} \ell - x \right) \right] \right\} \frac{\partial^2 y}{\partial x^2}$$

$$+ 2MV \frac{\partial^2 y}{\partial x \partial t} + \frac{1}{2} c_N \left(\frac{M}{d} \right) V \left(\frac{\partial y}{\partial t} + V \frac{\partial y}{\partial x} \right) + \frac{1}{2} \frac{M}{d} c_T V^2 \frac{\partial y}{\partial x}$$

$$+ c \frac{\partial y}{\partial t} + (M + m) \frac{\partial^2 y}{\partial t^2} = q(x,t) \tag{1}$$

where

$$q(x,t) = -\int_o^{2\pi} \frac{d}{2} p(x,\theta,t) \cos\theta d\theta \tag{2}$$

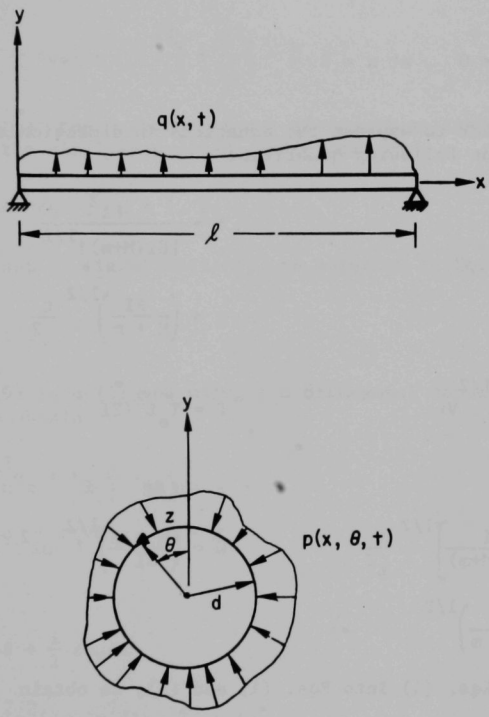

Fig. 1. Simply-Supported Rod in Parallel Flow and Pressure Distribution on the Surface of the Rod

and λ is internal viscous damping coefficient; c is effective viscous damping coefficient which includes possible flow-dependent damping mechanisms not already accounted for in the model, therefore, $c = c(V)$; T_o is initial axial tension; ℓ is length of the rod; M is added mass of fluid; d is diameter of the rod; c_N and c_T are drag coefficients in normal and tangential directions respectively [8].

The appropriate boundary conditions are

$$y = \frac{\partial^2 y}{\partial x^2} = 0 \quad , \quad \text{at } x = 0$$

$$y = \frac{\partial^2 y}{\partial x^2} = 0 \quad , \quad \text{at } x = \ell \tag{3}$$

It is convenient to express the equations in dimensionless terms by introducing the following quantities

$$\xi = x/\ell \qquad \delta = \frac{c\ell^2}{[EI(M+m)]^{1/2}}$$

$$w = y/\ell \qquad \tau = \left(\frac{EI}{M+m}\right)^{1/2} \frac{t}{\ell^2}$$

$$u = \left(\frac{M}{EI}\right)^{1/2} V\ell \qquad \Gamma = T_o \ell^2/EI$$

$$Q = \frac{q\ell^3}{EI} \qquad \varepsilon = \ell/d \tag{4}$$

$$\alpha = \left[\frac{I}{EI(M+m)}\right]^{1/2} \frac{\lambda}{\ell^2} \qquad \Omega = \left(\frac{M+m}{EI}\right)^{1/2} \omega\ell^2$$

$$\beta = \left(\frac{M}{M+m}\right)^{1/2}$$

Substituting Eqs. (4) into Eqs. (1) and (3), we obtain

$$\frac{\partial^4 w}{\partial \xi^4} + \alpha \frac{\partial^5 w}{\partial \xi^4 \partial \tau} + \{u^2[1 - \frac{1}{2}\varepsilon c_T(1-\xi)] - \Gamma\} \frac{\partial^2 w}{\partial \xi^2}$$

$$+ \frac{1}{2}\varepsilon(c_N + c_T)u^2 \frac{\partial w}{\partial \xi} + 2\beta u \frac{\partial^2 w}{\partial \xi \partial \tau} + (\delta + \frac{1}{2}\varepsilon c_N \beta u) \frac{\partial w}{\partial \tau} + \frac{\partial^2 w}{\partial \tau^2} = Q \tag{5}$$

The boundary conditions are

$$w = \frac{\partial^2 w}{\partial \xi^2} = 0 \quad , \quad \text{at } \xi = 0$$

$$w = \frac{\partial^2 w}{\partial \xi^2} = 0 \quad , \quad \text{at } \xi = 1 \tag{6}$$

Due to the presence of the Coriolis force term, $2\beta u \frac{\partial^2 w}{\partial \xi \partial \tau}$, the system does not possess classical normal modes [10]. We will look for the normal modes by neglecting the Coriolis force term, damping effects and variable coefficient term, and considering

$$\frac{\partial^4 w}{\partial \xi^4} + [u^2(1 - \frac{1}{2}\varepsilon c_T) - \Gamma] \frac{\partial^2 w}{\partial \xi^2} + \frac{\partial^2 w}{\partial \tau^2} = 0 \tag{7}$$

It is easy to see that the orthonormal set of functions associated with this equation and the simply-supported conditions are

$$\phi_n(\xi) = \sqrt{2} \sin n\pi\xi \quad , \quad n = 1, 2, \ldots \tag{8}$$

Having a complete set of eigenfunctions, the solution to Eq. (5) is taken as

$$w = \sum_n q_n(\tau)\phi_n(\xi) \tag{9}$$

Substituting Eq. (9) into (5) and using the orthogonal condition of the eigenfunctions, we obtain

$$\ddot{q}_n + \eta_n \dot{q}_n + \lambda_n^2 q_n + \varepsilon_1 \sum_j a_{nj}\dot{q}_j$$

$$+ \varepsilon_2 \sum_j b_{nj} q_j + \varepsilon_3 \sum_j a_{nj} q_j = Q_n \tag{10}$$

where

$$\eta_n = n^4\pi^4\alpha + \delta + \frac{1}{2}\varepsilon c_N \beta u$$

$$\lambda_n^2 = n^4\pi^4 + n^2\pi^2[\Gamma - u^2(1 - \frac{1}{2}\varepsilon c_T)]$$

$$\varepsilon_1 = 2\beta u \tag{11}$$

$$\varepsilon_2 = \frac{1}{2}\varepsilon c_T u^2$$

$$\varepsilon_3 = \frac{1}{2}\varepsilon(c_N + c_T)u^2$$

$$a_{nj} = \int_0^1 \phi_n \frac{\partial \phi_j}{\partial \xi} d\xi = \begin{cases} 0 \quad , & n = j \\ j\left[\frac{1-(-1)^{n-j}}{n-j} + \frac{1-(-1)^{n+j}}{n+j}\right], & n \neq j \end{cases}$$

$$b_{nj} = \int_0^1 \xi\phi_n \frac{\partial^2 \phi_j}{\partial \xi^2} d\xi = \begin{cases} -\frac{1}{2} n^2\pi^2 \quad , & n = j \\ j^2\left[\frac{1-(-1)^{n-j}}{(n-j)^2} - \frac{1-(-1)^{n+j}}{(n+j)^2}\right], & n \neq j \end{cases} \tag{11}$$

contd.

$$Q_n = \int_0^1 Q\phi_n d\xi$$

The system of equations are coupled. However, making the following simplifications:

(1) The terms induced by Coriolis force, $\varepsilon_1 \Sigma\, a_{nj}\, \dot{q}_j$ are neglected. The effects due to these terms are quite small when the flow velocity is small compared with its critical value [10];

(2) The terms of $\varepsilon_3 \Sigma\, a_{nj}\, q_j$ are the coupling between odd modes and even modes, similar to that associated with $\varepsilon_1 \Sigma\, a_{nj}\, \dot{q}_j$. Since ε_3 is a small parameter, they are neglected;

(3) The matrix b_{nj} has strong diagonal elements as can be seen from Eqs. (11), and ε_2 is a small parameter, therefore, the off-diagonal terms are neglected;

the equations of motion decouple and we obtain

$$\ddot{q}_n + 2\zeta_n \Omega_n \dot{q}_n + \Omega_n^2 q_n = Q_n \tag{12}$$

where

$$\Omega_n^2 = n^4\pi^4 + n^2\pi^2\left[\Gamma - u^2\left(1 - \frac{1}{4}\varepsilon c_T\right)\right]$$

$$\zeta_n = \eta_n/(2\Omega_n) \tag{13}$$

Recall that the dimensionless generalized force $Q_n(\tau)$ is random with time. Assuming that the pressure field is homogeneous, the power spectral density of the resulting line load, $\Phi_{QQ}(\Omega)$, is independent of position along the rod, and the power spectral density of displacement, Φ_{ww}, at point ξ may be shown to be

$$\Phi_{ww}(\xi,\Omega) = \Phi_{QQ}(\Omega) \sum_n |H_n(\Omega)|^2 \phi_n^2(\xi) J_n^2(\Omega) \tag{14}$$

where

$$H_n(\Omega) = \left[\frac{1}{(\Omega_n^2-\Omega^2)^2 + 4\zeta_n^2\Omega_n^2\Omega^2}\right]^{1/2}$$

$$\phi_n(\xi) = \sqrt{2}\ \sin n\pi\xi \tag{15}$$

$$J_n^2(\Omega) = \int_o^1 \int_o^1 R_{QQ}(\xi,\xi',\Omega)\phi_n(\xi)\phi_n(\xi')d\xi d\xi'$$

$R_{QQ}(\xi,\xi',\Omega)$ is the longitudinal spatial cross-correlation function of the forcing field at the particular frequency Ω and $J_n^2(\Omega)$ is called the joint acceptance of the pressure and mode concerned. The mean-square displacement $\bar{w}^2$ is given by

$$\bar{w}^2(\xi) = \int_o^\infty \Phi_{ww}(\xi,\Omega)d\Omega \tag{16}$$

These results are similar to those obtained by Powell [11]. The problem left is to find the joint acceptance and power spectral density of the pressure field.

TURBULENT-WALL-PRESSURE CROSS-POWER SPECTRAL DENSITY

The statistical properties of the wall-pressure fluctuations beneath a turbulent boundary layer have been measured by many experimenters. The data for the pressure statistics used in this analysis is that obtained by Bakewell [9]. The reason for this selection is that Bakewell measured the data on the surface of a body of revolution and in water tunnel, thus closely approximating our case. Most of the other information has been obtained for turbulent pipe flows [12,13] or for turbulent boundary layer on flat plates [14,15,16].

Corcos [17] proposed the following expression for the cross-spectral density of the fluctuating wall pressure

$$\Psi_{pp}(\omega,\bar{x},\bar{z}) = \Phi_{pp}(\omega)A\left(\frac{\omega\bar{x}}{V_c}\right) B\left(\frac{\omega\bar{z}}{V_c}\right) \cos\left(\frac{\omega\bar{x}}{V_c}\right) \tag{17}$$

where V_c is the mean convection velocity of the turbulent boundary layer; $\bar{x} = x - x'$ and represents the longitudinal spatial separation between x and x'; and $\bar{z} = z - z'$ and represents the lateral spatial separation between z and z'. The experimental results for V_c, $A(\omega\bar{x}/V_c)$, $B(\omega\bar{z}/V_c)$ and $\Phi_{pp}(\omega)$ obtained by Bakewell [9] are replotted in Figs. 2, 3, 4 and 5, where δ^* is the boundary-layer displacement thickness and $\Phi_{pp}(\omega)$ has been plotted on logarithmic paper.

The convection velocity V_c is a weak function of frequency. It is higher for low frequencies and lower for high frequencies. In the calculations, it will be taken as

$$r = V_c/V = 0.6 + 0.4 \exp[-2.2(\omega\delta^*/V)] \tag{18}$$

This expression correlates Bakewell's and Schloemer's [16] data quite well as shown in Fig. 2. The expressions selected to represent the A and B functions are

$$\begin{aligned} A(\omega\bar{x}/V_c) &= \exp(-0.10\ |\omega\bar{x}/V_c|) \\ B(\omega\bar{z}/V_c) &= \exp(-0.55\ |\omega\bar{z}/V_c|) \end{aligned} \tag{19}$$

which are shown plotted in Figs. 3 and 4. In these two figures, Willmarth and Wooldridge's [15] data are also included for comparison. Fig. 5 presents a comparison of the experimental data of Bakewell [9] for a body of revolution in water flow, Clinch [13] for water pipe flow, Willmarth and Wooldridge [15] for air flow on plate, and Skudrzyk and Haddle phenomenological model [14]. For computational convenience, the normalized power spectra of the pressure field (Fig. 5) are represented by

$$\begin{aligned} \Phi_{PP}(f) &= 5.25 \times 10^{-5} \quad , \quad S < 0.2 \\ &= (1.05 \times 10^{-5})S^{-1} \quad , \quad 0.2 \le S \le 3.5 \\ &= (12.9 \times 10^{-5})\ S^{-3} \quad , \quad S > 3.5 \end{aligned} \tag{20}$$

where

$$\begin{aligned} \Phi_{PP}(f) &= \Phi_{pp}(f)/\rho^2 V^3 \delta^* \\ S &= \omega\delta^*/V, \ f = \omega/2\pi \end{aligned} \tag{21}$$

and ρ is the density of fluid. The expressions (20) correlate the data of Bakewell and Clinch very well. It should be mentioned that dependable data have not been obtained for values of S less than 0.07; Clinch [13] reported the existence of extraneous noise at low frequencies, and Willmarth and Wooldridge [15] found that the power spectra contain a large energy density at low frequencies. The spectra measured at the same day with different amounts of sunlight differred by an order of magnitude. Consequently, there is a lower cut-off frequency below which the signals were rejected in the measured spectra. This is important in discussion of the rod vibration and will be explored again later.

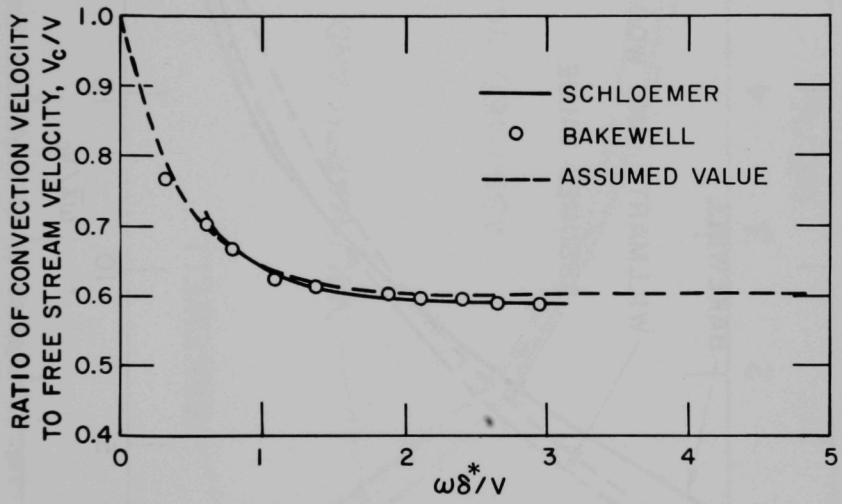

Fig. 2. Dependence of Convection Velocity on Dimensionless Frequency

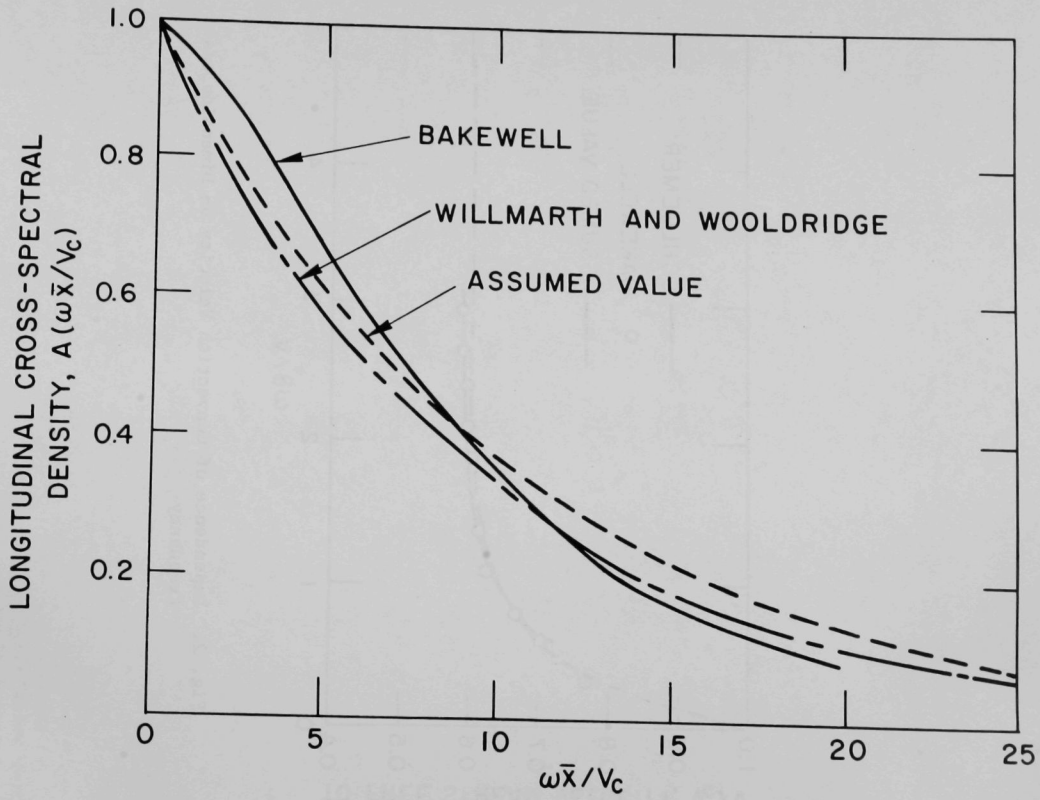

Fig. 3. Magnitude of the Longitudinal Cross-Spectral Density of the Turbulent-Wall-Pressure

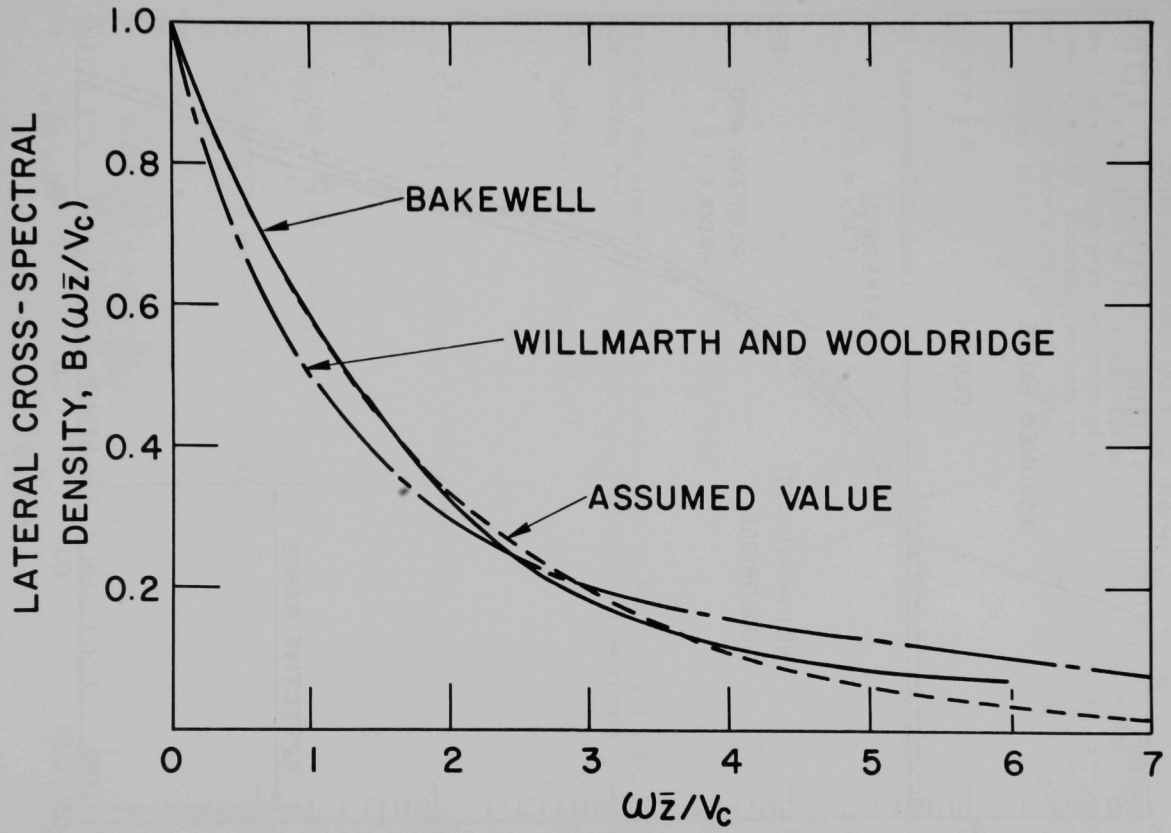

Fig. 4. Magnitude of the Lateral Cross-Spectral Density

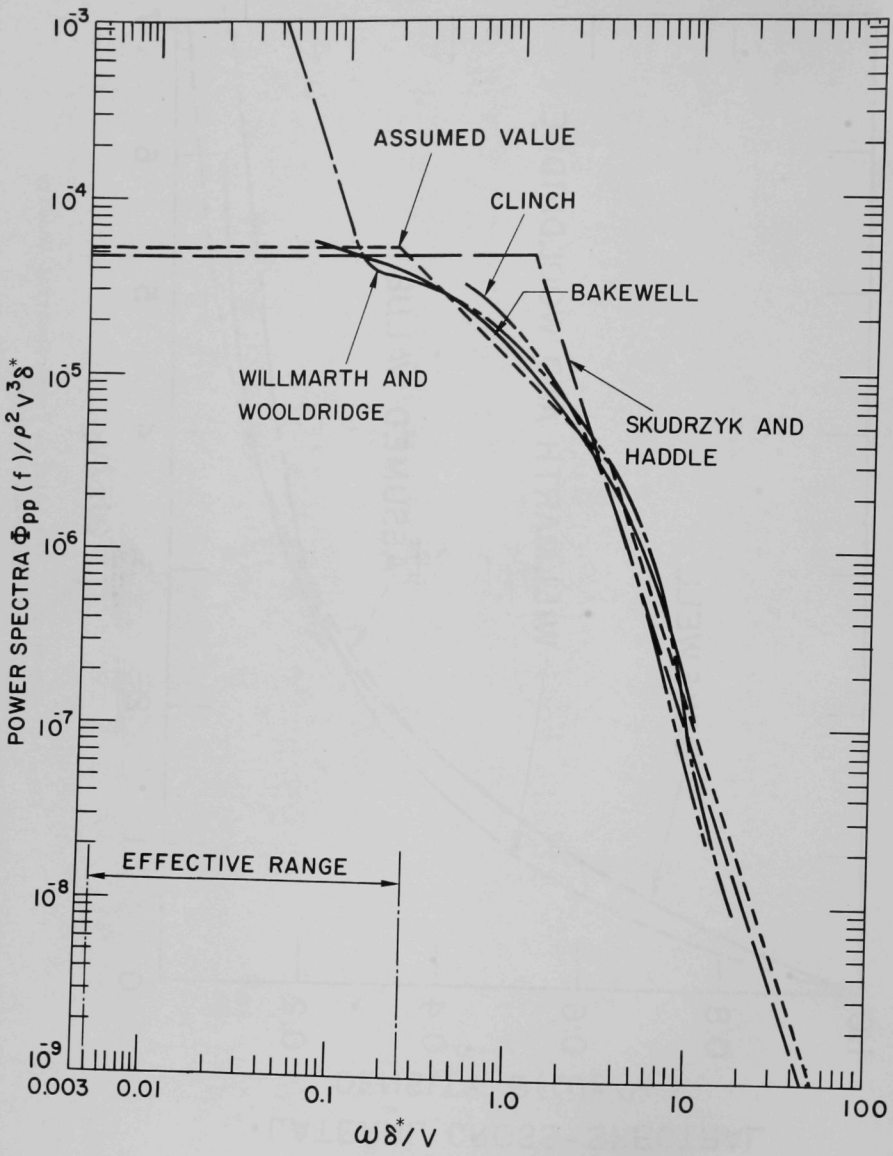

Fig. 5. Turbulent-Wall-Pressure Power Spectra

JOINT ACCEPTANCE AND POWER SPECTRA OF LINE LOAD

The statistics of the random force required is a one dimensional line load while the power spectrum given by Eq. (17) is a two dimensional pressure field. Therefore we have to convert the peripherally distributed pressure into a line load. This is accomplished by using Eq. (2) and noting (Fig. 1)

$$z = \frac{d}{2}\,\theta \tag{22}$$

The cross-spectral density of the line load q(x,t) is easily shown to be

$$\Psi_{qq}(\omega,\bar{x}) = \chi^2 d^2 \Phi_{pp}(\omega)\; A\left(\frac{\omega\bar{x}}{V_c}\right) \cos\left(\frac{\omega\bar{x}}{V_c}\right) \tag{23}$$

where

$$\chi^2 = \frac{1}{4}\int_0^{2\pi}\int_0^{2\pi} B\left(\frac{\omega\bar{z}}{V_c}\right) \cos\theta\cos\theta' d\theta d\theta' \tag{24}$$

Employing the dimensionless parameters, given by Eqs. (4) and (21), and substituting Eqs. (18) - (21) into Eqs. (23) and (24) we obtain

$$\Psi_{QQ}(\Omega,\xi,\xi') = \Phi_{QQ}(\Omega) R_{QQ}(\Omega,\xi,\xi') \tag{25}$$

and

$$\chi^2(\Omega) = \frac{1}{4}\int_0^{2\pi}\int_0^{2\pi} \exp(-\nu|\theta - \theta'|)\cos\theta\cos\theta' d\theta d\theta' \tag{26}$$

where

$$\Phi_{QQ}(\Omega) = \frac{16}{\pi^2}\,\beta\bar{\delta}\varepsilon^2\chi^2 u^3 \Phi_{PP}(\Omega) \tag{27}$$

$$R_{QQ}(\Omega,\xi,\xi') = \exp(-0.1\gamma|\xi - \xi'|)\cos(\gamma|\xi - \xi'|) \tag{28}$$

and

$$\nu = 0.275\left(\frac{\omega d}{V_c}\right) = 0.275\left(\frac{\beta\Omega}{\varepsilon r u}\right)$$

$$\gamma = \frac{\ell\omega}{V_c} = \frac{\beta\Omega}{ru} \tag{29}$$

$$\bar{\delta} = \frac{\delta^*}{\ell}$$

Carrying out the integral of Eq. (26), we have

$$\chi^2 = \frac{\nu}{2(\nu^2+1)}\left[\pi - \frac{\nu(1-e^{-2\pi\nu})}{\nu^2+1}\right] \tag{30}$$

which is shown in Fig. 6. By substitution of Eq. (28) into (15), the integration yields

$$J_n^2 = F(n\pi+\gamma) + F(n\pi-\gamma) \tag{31}$$

where

$$F(n\pi\pm\gamma) = \frac{\exp(-0.10\gamma)[-0.10\gamma\sin(n\pi\pm\gamma)-(n\pi\pm\gamma)\cos(n\pi\pm\gamma)]+n\pi(1+0.10\gamma)\pm\gamma}{n\pi[(n\pi\pm\gamma)^2+(0.10\gamma)^2]}$$

$$+\frac{\exp(-0.10\gamma)\{[(0.10\gamma)^2-(n\pi\pm\gamma)^2]\cos(n\pi\pm\gamma)-0.20\gamma(n\pi\pm\gamma)\sin(n\pi\pm\gamma)\}-(0.10\gamma)^2+(n\pi\pm\gamma)^2}{[(n\pi\pm\gamma)^2+(0.10\gamma)^2]^2} \tag{32}$$

Using these expressions, the values of the joint acceptance were easily calculated; plots are given for the first five modes in Fig. 7. The physical significance of the joint acceptance is that it represents the "effectiveness" of the pressure in exciting a mode of the rod. It will be relatively large when the pressure correlation has a significant contribution at the wavelength predominating in the mode concerned [11].

RESULTS

A. Qualitative Results

The parametric dependence of the solution may be expressed as

$$\bar{w}(\xi) = \bar{w}(\alpha,\beta,\delta,\bar{\delta},\varepsilon,\Gamma,\varepsilon c_T,\varepsilon c_N,u,\xi) \tag{33}$$

Of course, other quantities of interest, such as bending stress, can also be calculated.

Instead of presenting extensive numerical results, only a few representative results are given. From the mathematical model, the following qualitative conclusions may be reached:

(1) The response of the first mode dominates; the contribution from higher modes is less than five percent. From a practical consideration, a one-mode-approximation will give sufficient accuracy. This is consistent with the experimental observation [2,5,6].

(2) With the magnitude of the power spectral density of the pressure field proportional to the axial flow velocity cubed, as indicated by available experimental results (Fig. 5), the rms rod displacement

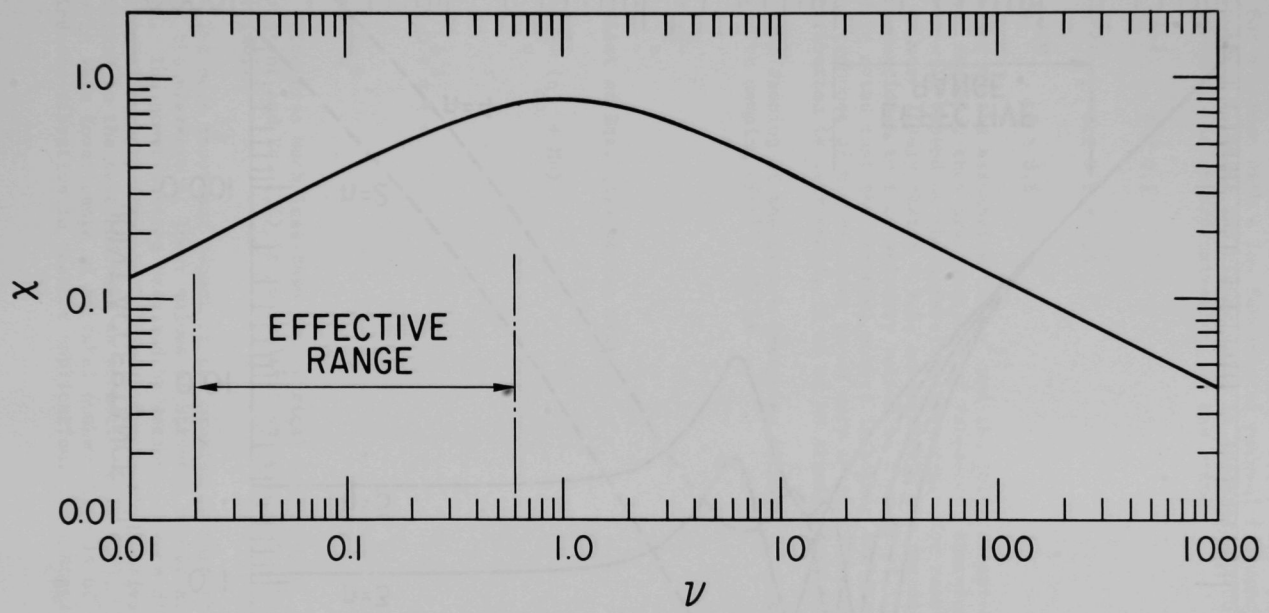

Fig. 6. Dependence of the Parameter χ on ν

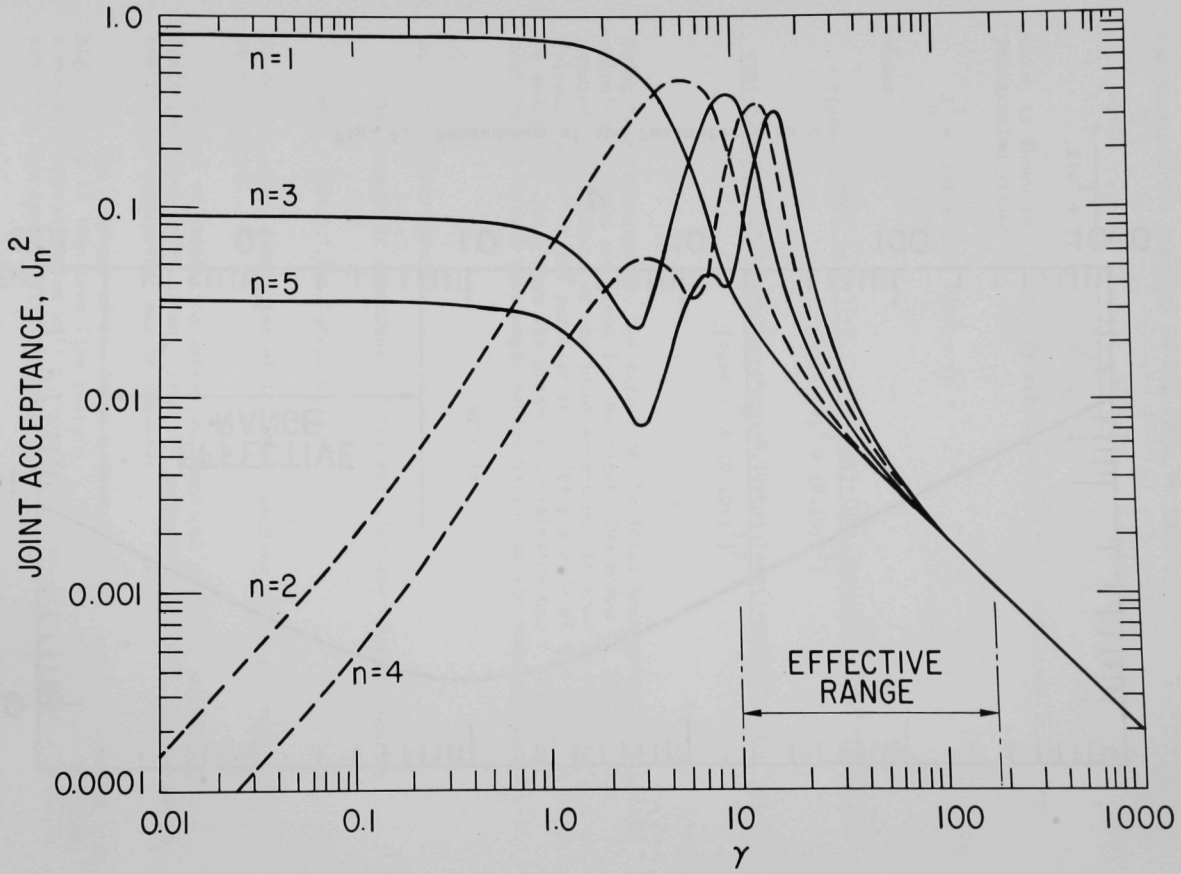

Fig. 7. Joint Acceptance for a Simply-Supported Rod Subjected to Turbulent-Boundary-Layer Pressure

is proportional to flow velocity to the 1.5 to 3.0 power. The lower value is for a system with a low fundamental natural frequency, hence low Strouhal number, S, while the higher value is associated with higher Strouhal numbers. As an approximation, we can write

$$\bar{w} \propto u^{1.5} \quad , \quad S < 0.2$$

$$\bar{w} \propto u^{2.0} \quad , \quad 0.2 < S < 3.5 \tag{34}$$

$$\bar{w} \propto u^{3.0} \quad , \quad S > 3.5$$

This is based on the assumption that χ^2 and the joint acceptance are constants. However, they are functions of frequency, therefore, the exact power will depend on the parameters involved. For reactor components it is most likely that $S < 3.5$, consequently the rms displacement will be proportional to flow velocity raised to a power of 1.5 to 2.0. It should be noted that the Strouhal number is higher for the higher modes, the response of higher modes could vary to the 3.0 power. Since their contribution is very small, it is of no significance in practice.

(3) The damping of the system increases linearly with the flow velocity. The damping of nth mode is

$$\zeta_n = \frac{\eta_n}{2\Omega_n} \tag{35}$$

From the first of Eqs. (11) we can write

$$\zeta_n = \frac{1}{2\Omega_n} (\eta_{no} + Nu) \tag{36}$$

where

$$\eta_{no} = n^4 \pi^4 \alpha + \delta$$

$$N = \frac{1}{2} \varepsilon c_N \beta \tag{37}$$

For flow velocities much less than the critical velocity, Ω_n is approximately constant and Eq. (36) is in qualitative agreement with experimental results [5,18].

(4) The most important aspect of the problem is that the power spectra of the pressure at lower values of Strouhal number are not known accurately. The power spectra measured by various workers differ widely at low Strouhal numbers (Fig. 5). This is due to the spurious disturbances arising in the test channels as acoustic waves [19]. It is precisely in this lower range of Strouhal number which is of importance to flow-induced-vibration in reactor application. This suggests the

pressing necessity of making power-spectra measurements in this range of Strouhal number.

B. Quantitative Results

Turning now to a specific numerical example, consider the following dimensional values: $d = 0.5$ in; $m = 0.1675$ lb/ft; $M = 0.085$ lb/ft; $E = 15 \times 10^6$ lb/in^2; $I = 1.28 \times 10^{-3}$ in^4; $\ell = 36$ in; $V = 10$ to 20 ft/sec; this is the system of Test D in Ref. 5. These quantities lead to the following nondimensional parameters; $\beta = 0.58$; $\varepsilon = 72$; $u = 0.133 - 0.266$. The other parameters are unknown. Here we will assume that $\Gamma = 0$; $\varepsilon c_T = \varepsilon c_N = 1.0$; $\alpha = 0$; $\delta = 0.2$; and $\bar{\delta} = 0.002$. The power spectra of dimensionless rod displacements at midspan and quarter-point are shown in Fig. 8. Due to the symmetry, the even modes do not contribute to the midspan response. Also, these modes which are multiples of four contribute little to the quarter-point response, since the quarter-point is close to the nodal point of those modes. The rms displacement along with the experiment data [5] are shown in Fig. 9. The experimental results are measured at two perpendicular directions.

The theory predicts that the rms displacement is proportional to the flow velocity with a power of 2.0 for $V < 10$ ft/sec and 1.5 for $V > 10$ ft/sec. The general trends are in agreement with the experimental measurements. The theoretical prediction at midspan ($x = \ell/2$) is lower than those of experimental data. However, at quarter point ($x = \ell/4$), the experimental data for the two directions differ considerably and the theoretical values lie in between. In general, the theoretical results and experimental data agree within order of magnitude. The discrepancy might result from the following factors:

(1) The uncertainty of the parameters involved contributes to the difference. The exact values of the parameters δ, $\bar{\delta}$, α and Γ are not available for this particular system. Also no experimental data are available for estimation of εc_T and εc_N which makes direct quantitative comparison difficult.

(2) When V is larger than 10 ft/sec, the Strouhal number, S, is less than 0.2 in which dependable data for power spectra are not available. This is important when the flow velocity is large. As Willmarth and Wooldridge [15] pointed out they obtained differences amounting to a factor of ten from an air tunnel. In a water tunnel, the differences might not be that large, however, there is still uncertainty associated with the spectral density in the low range of Strouhal numbers.

(3) Acoustic and other effects can contribute to the experimental results; the theoretical prediction is based on the turbulent-boundary-layer pressure fluctuations only.

PARAMETER STUDY

Three different Strouhal number relationships have been utilized in the normalization of the mean-square-value spectra, and in representation of the effective diameter and joint acceptance associated with the random pressure field; they are respectively

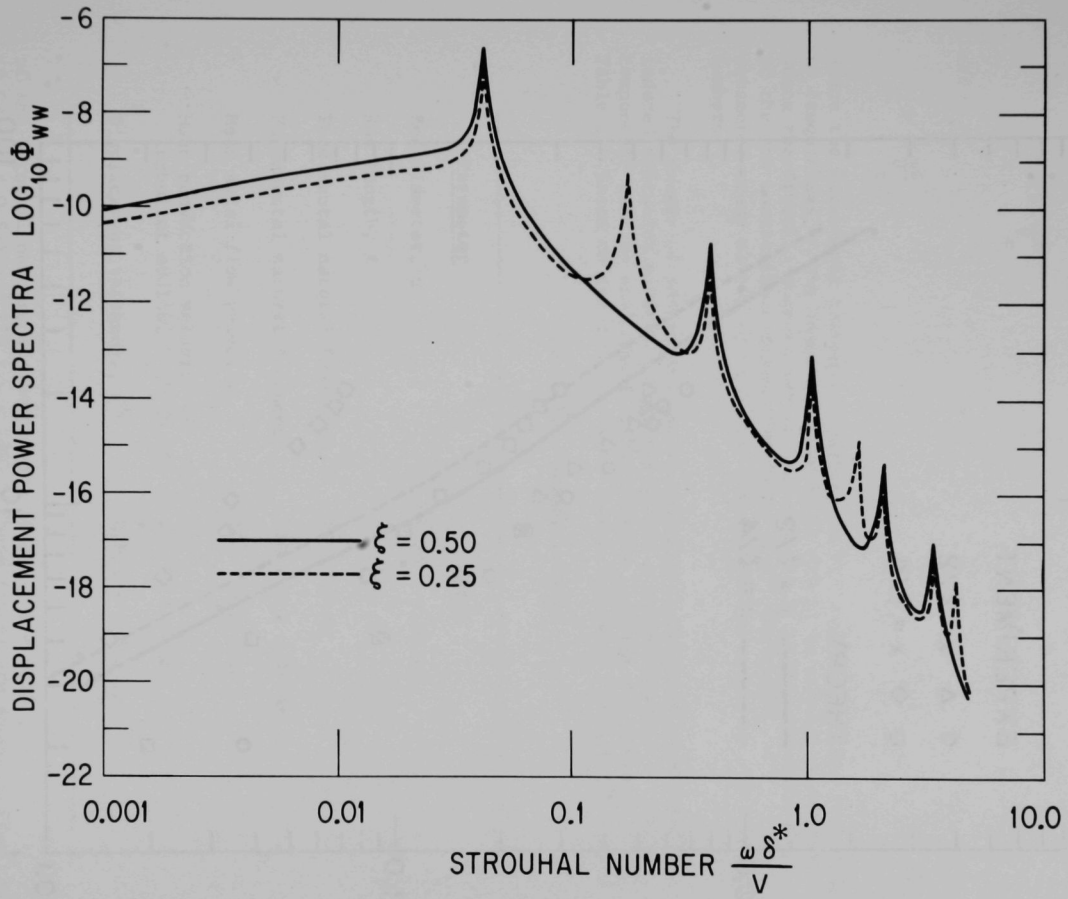

Fig. 8. Power Spectral Density Curves of Dimensionless

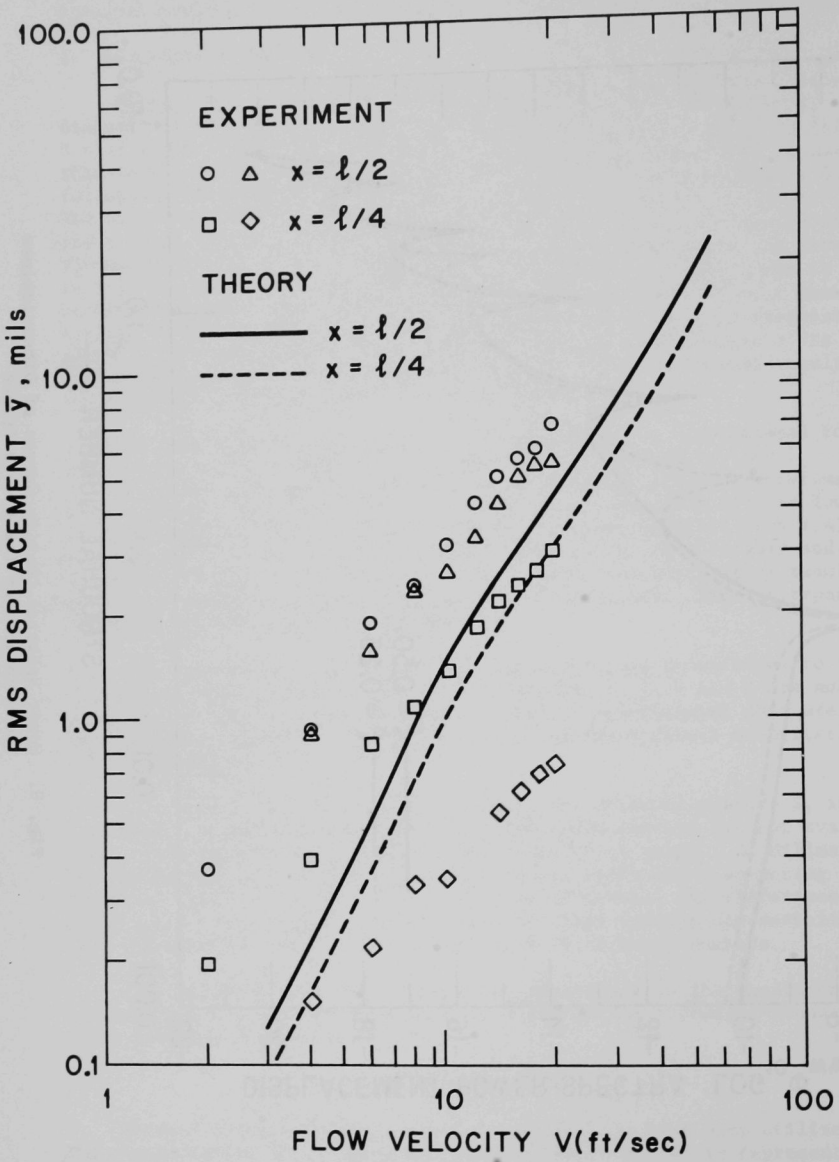

Fig. 9. RMS Displacement versus Mean Axial Flow Velocity

$$S = \frac{\omega\delta^*}{V}$$

$$\nu = 0.275\,\frac{\omega d}{V_c} \tag{38}$$

and

$$\gamma = \frac{\omega\ell}{V_c} \tag{39}$$

Since the first-mode response is dominant, the rod will respond primarily to frequencies in the range centered about its first natural frequency, hence the Strouhal numbers associated with the first natural frequency of the rod locate their respective range of effectiveness. A parameter study allows us to define the realizable ranges on the Strouhal numbers.

The ranges of parameters associated with our planned parallel-flow-induced vibration experiments (these ranges are also typical of reactor components and the environment in which they operate) are given in Table 1. Based on the data in Table 1, the following "effective" ranges

Table 1. Parameter Range

Parameter	Range
Rod diameter, d	0.25 - 0.50 in.
Rod length, ℓ	36 - 48 in.
Fundamental natural frequency, f	20 - 50 Hz
Fundamental natural frequency, ω	125 - 315 rad/sec
Mean axial flow velocity, V	10 - 50 ft/sec
Mean convection velocity of turbulent eddies, $V_c (V_c \approx 0.7V)$	7 - 35 ft/sec
Displacement thickness, δ^*	0.023 - 0.094 in.

of the Strouhal numbers are computed: $(0.004 < S < 0.25)$, $(0.02 < \nu < 0.52)$ and $(10 < \gamma < 180)$. These ranges are shown on Figs. 5-7 respectively.

From Fig. 5 it is readily observed that data in the effective range of S are lacking. As discussed earlier, various investigators [13,15,19] encountered measurement difficulties in making these low Strouhal number

measurements. From Figs. 6 and 7, it is seen that curves of the effective diameter, χ, and the square of the joint acceptance of the first mode, J_1^2, can be approximated by straight lines of slopes 0.5 and -1, respectively. The straight-line approximations on log-log paper imply power function relationships and we obtain

$$\chi(\omega) = 1.3\nu^{1/2} = 0.68\ (\omega d/V_c)^{1/2} \quad , \quad 0.02 < \nu < 0.52 \tag{40}$$

and

$$J_1(\omega) = 0.45\gamma^{-1/2} = 0.45\ (\omega\ell/V_c)^{-1/2} \quad , \quad 10 < \gamma < 180 \tag{41}$$

Substituting Eq. (27) into Eq. (14), the mean-square-value spectral density of displacement can be written as

$$\Phi_{ww}(\xi,\Omega) = \frac{16}{\pi^2}\ \bar{\delta}\beta\varepsilon^2 u^3 \chi^2(\Omega) J_1^2(\Omega)\,|H_1(\Omega)|^2 \phi_1^2(\xi)\Phi_{PP}(\Omega) \tag{42}$$

which assumes the first-mode is dominant. Let us further assume a relatively lightly-damped system such that the rod is selective in responding to frequencies near its first natural frequency. We can now use the approximations given by Eqs. (40) and (41); substituting in Eq. (42), the frequency dependence of the effective diameter and joint acceptance cancels and we obtain

$$\Phi_{ww}(\xi,\Omega) = \frac{1.5}{\pi^2}\ \bar{\delta}\beta\varepsilon u^3 |H_1(\Omega)|^2 \phi_1^2(\xi)\Phi_{PP}(\Omega) \tag{43}$$

Within the effective range of Strouhal number, S, and considering the effect of disturbances as discussed by Wills [19], approximate the power spectral density of the turbulent wall pressure as

$$\Phi_{PP}(\omega) = k_1 \left(\frac{\omega\delta^*}{V}\right)^{-k_2} \tag{44}$$

where k_1 and k_2 are constants depending on the particular system flow conditions. Substituting Eq. (44) into (43) and integrating we obtain for rms displacement of the rod

$$\bar{y}(x) = 1.73 \times 10^{-3} \left(\frac{\sqrt{k_1}}{\Omega_1^{1.50+0.5k_2}}\right) G(k_2,\zeta_1)\sin\left(\frac{\pi x}{\ell}\right)$$

$$d^{-0.5}\ell^{2.5+k_2}(M+m)^{-\left(\frac{1-k_2}{4}\right)} M\ (EI)^{-\left(\frac{3+k_2}{4}\right)} V^{\left(\frac{3+k_2}{2}\right)} \delta^{*\left(\frac{1-k_2}{2}\right)} \tag{45}$$

where

$$\Omega_1^2 = \pi^2 \left\{1 - \frac{\ell^2}{\pi^2 EI}\left[T - MV^2\left(1 - \frac{\varepsilon C_T}{4}\right)\right]\right\} \tag{46}$$

and $G(k_2,\zeta_1)$ is a function depending on k_2 and modal damping factor ζ_1 (Fig. 10). For known system properties, the rms displacement is easily calculated.

In typical reactor systems, the coolant velocity is relatively small in comparison with the critical flow velocity, therefore the frequency, Ω_1, is a weak function of V. In general, experiment has shown the constant k_2 to vary from 0 to 1.0. With these observations Eq. (45) can be expressed as

$$y \alpha d^{\alpha_1} \ell^{\alpha_2} V^{\alpha_3} (EI)^{\alpha_4} \tag{47}$$

$$\left.\begin{aligned} \alpha_1 &= 1 \sim 1.5 \\ \alpha_2 &= 2.5 \sim 3.5 \\ \alpha_3 &= 1.5 \sim 2.0 \\ \alpha_4 &= -0.75 \sim -1.0 \end{aligned}\right\} \tag{48}$$

This result compares favorably with the empirical correlations of Paidoussis [6] and Burgreen et al [1] as shown in Table 2. It should be noted that the development of their correlations are based on experimental results while Eq. (47) represents an analytical reduction of a mathematical model. The general agreement between the theoretical prediction and experimental results lends support to the validity of the mathematical model.

Table 2. Comparison of Exponents with Experimental Correlations

parameters	d	ℓ	V	EI
theory	$1 \sim 1.5$	$2.5 \sim 3.5$	$1.5 \sim 2.0$	$-0.75 \sim -1.0$
Paidoussis [6]	$0.35 \sim 1.0$	3.2	1.85	-0.8
Burgreen [1]	0.77	3.1	2.3	-0.77

DISCUSSION

The mathematical model has been successful in predicting most of the essential features of parallel-flow-induced vibration: (1) the increase of damping is proportional to the flow velocity; (2) the first mode dominants; and (3) the rms displacement is proportional to the flow velocity with a power of 1.5 to 2.0 for practical system.

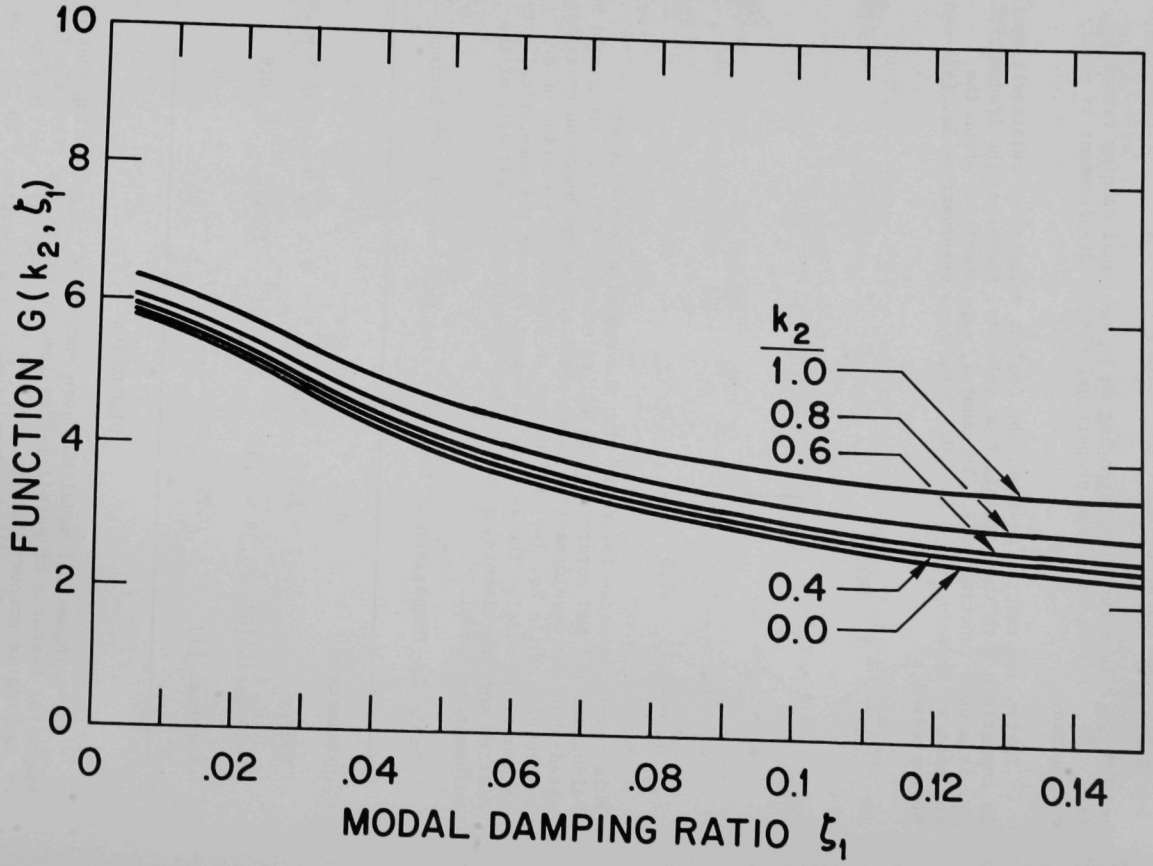

Fig. 10. Function $G(k_2, \zeta_1)$

In design, Eq. (45) can be used to estimate the rms displacement of a component satisfying the basic assumptions of the analysis. In general, k_1 is taken as 5.25×10^{-5} according to the experimental data (Fig. 5). The value of k_2 is unknown, and may be dependent on the system conditions; it is taken to range from 0 to 1.

It should be noted that the model was formulated without considering system-dependence-factors, such as pump pulsations [20], support excitation, far-field effects, etc. The response obtained from the proposed model will represent the basic level of vibration. If the other system-dependence excitations do exist, the vibration level is undoubtedly increased.

In order to predict rms displacement more accurately, the experimental data for the power spectrum of turbulent-wall-pressure in the lower range of Strouhal number is urgently needed. Although the response is relatively insensitive to the pressure correlation [21], there is no experimental data for the pressure statistics on the surface of the rod, except those measured by Gorman [7] who measured the pressure difference at two points diametrically opposite. Therefore the measurements of the pressure-field correlation on the rod surface are helpful in assessing the selected values used in this model. Of course, the measurements of the other parameters, such as the drag coefficients, are also required in order to make an analytical prediction more accurately.

ACKNOWLEDGMENT

This work was performed under the sponsorship of the Special Technology Branch, Division of Reactor Development and Technology, U. S. Atomic Energy Commission.

REFERENCES

1. D. Burgreen, J. J. Byrnes, and D. M. Benforado, "Vibration of Rods Induced by Water in Parallel Flow," Trans. Am. Soc. Mech. Engrs., 1958, pp. 991- 1003.

2. E. P. Quinn, "Vibration of Fuel Rods in Parallel Flow," USAEC Report GEAP-4059, General Electric Company, July 1962.

3. M. P. Paidoussis, "Vibration of Flexible Cylinders with Supported Ends, Induced by Axial Flow," Proc. Instn. Mech. Engrs., Vol. 180, 1966, p. 268-278.

4. J. R. Reavis, "WVI-Westinghouse Vibration Correlation for Maximum Fuel Element Displacement in Parallel Turbulent Flow," Trans. Am. Nucl. Soc., Vol. 10, No. 1, 1967, pp. 369-370.

5. M. W. Wambsganss and B. L. Boers, "Parallel-Flow-Induced Vibration of a Cylindrical Rod," Presented at ASME Winter Annual Meeting and Energy Systems Exposition, N.Y., N.Y., Dec. 1968, ASME Paper No. 68-WA/NE-15.

6. M. P. Paidoussis, "An Experimental Study of Vibration of Flexible Cylinders Induced by Nominally Axial Flow," Nucl. Sc. and Engr., Vol. 35, 1969, pp. 127-138.

7. D. J. Gorman, "The Role of Turbulence in the Vibration of Reactor Fuel Elements in Liquid Flow," Atomic Energy of Canada Limited, Chalk River, Ontario, AECL-3371, May 1969.

8. M. P. Paidoussis, "Dynamics of Flexible Slender Cylinders in Axial Flow, Part I: Theory," J. Fluid Mech., Vol. 26 (Part 4) Dec. 1966, pp. 717-736.

9. H. P. Bakewell, Jr., "Turbulent Wall-Pressure Fluctuations on a Body of Revolution," J. Acoust. Soc. Am., Vol. 43, 1968, pp. 1358-1363.

10. S. S. Chen, G. S. Rosenberg, and M. W. Wambsganss, Jr., "Vibrations and Stability of a Tube Conveying Fluid," to be published.

11. A. Powell, "On the Response of Structures to Random Pressures and to Jet Noise in Particular," in Random Vibration, S. H. Crandall, Ed., The MIT Press, Cambridge, Mass., 1958, Vol. 1, Chapt. 8.

12. G. M. Corcos, "The Structure of the Turbulent Pressure Field in Boundary-Layer Flows," J. Fluid Mech., Vol. 18, Part 3, 1964, pp. 353-378.

13. J. M. Clinch, "Measurements of the Wall Pressure Field at the Surface of a Smooth-Walled Pipe Containing Turbulent Water Flow," J. Sound Vib., Vol. 9, 1969, pp. 398-419.

14. E. J. Skudrzyk and G. P. Haddle, "Noise Production in a Turbulent Boundary Layer by Smooth and Rough Surfaces," J. Acoust. Soc. Amer., Vol. 32, 1960, pp. 19-34.

15. W. W. Willmarth and C. E. Wooldridge, "Measurements of the Fluctuating Pressure at the Wall Beneath a Thick Turbulent Boundary Layer," J. Fluid Mech., Vol. 14, Part 2, 1962, pp. 187-210.

16. H. H. Schloemer, "Effects of Pressure Gradients on Turbulent-Boundary-Layers Wall-Pressure Fluctuations," J. Acoust. Soc. Am., Vol. 42, 1967, pp. 93-113.

17. G. M. Corcos, "Resolution of Pressure in Turbulence," J. Acoust. Soc. Am., Vol. 35, 1963, pp. 192-199.

18. M. W. Wambsganss and P. L. Zaleski, "Flow-Velocity-Dependence of Damping in Parallel-Flow-Induced Vibration," Paper presented at the 1969 Winter Meeting of the American Nuclear Society, San Francisco, Calif., Nov. 30-Dec. 4, 1969, Trans. Am. Nucl. Soc., Vol. 12, 1969.

19. J. A. B. Wills, "Spurious Pressure Fluctuations in Wind Tunnels," J. Acoust. Soc. Am., Vol. 43, 1968, pp. 1049-1054.

20. S. S. Chen and G. S. Rosenberg, "Vibration and Stability of Tube Exposed to Pulsating Flow," Paper to be presented at the 1970 Annual Meeting of the American Nuclear Society, Los Angeles, Calif., June 28-July 2, 1970.

21. M. J. Crocker, "The Response of a Supersonic Transport Fuselage to Boundary Layer and to Reverberant Noise," J. Sound Vib., Vol. 9, 1969, pp. 6-20.

DISCUSSION

G. M. Smith (U. of Nebraska): What is the significance of the minus sign on the exponent of the flexural rigidity?

Chen: If the flexural rigidity is increased, then the vibration level decreases, and vice versa.

Smith: I see.

G. S. Rosenberg (ANL): I think that one characteristic coming out of this study may be somewhat different from the kind of thing that Grossman described. There was presumably one program under the stands. I don't think there is going to be one acoustic excitation vibration or boundary-layer excitation vibration study going on at a time.

I further hope we don't make the seemingly embarassing but erroneous comparison between the time scales necessary for the detailed and reliable understanding of the range of phenomena considered here and the nine-year period between controlled fission and production of power from fission. (See Grossman's Opening Remarks.) It is not at all uncommon for the efforts to produce refinements to exceed, by far, the efforts to demonstrate concepts. Enough philosophy, for now.

I think, however, you'll see some of the relationships between the separate studies pretty soon. I gather that at least one consideration will be given to the way in which dumping energy into the supports influences the response.

EXPERIMENTAL DETERMINATION AND ANALYSIS OF VIBRATIONS INDUCED BY THE NEAR-FIELD FLOW NOISE IN TUBES

Andrews K. Addae
Massachusetts Institute
of Technology
Cambridge, Massachusetts

Henri Fenech
University of California
Santa Barbara, California

ABSTRACT

Boundary layer turbulence as a source of excitation in single phase parallel coolant flow as well as the near field and acoustic field components of this flow noise are considered in this work.

The mid-span response of a tube excited by the near-field component of boundary layer turbulence is determined experimentally.

Results show that only the fundamental mode of the tube is excited. The RMS response predicted by the boundary layer turbulence wall pressure correlation is found to be of the same order of magnitude as the measured RMS response.

However, the maximum amplitude predicted by Paidoussis' empirical correlation is a factor of 4 to 15 times greater than the measured RMS response. The near field component of boundary layer turbulence thus appears not to be very important under conditions in which its empirical correlation has been found to apply.

INTRODUCTION

In a nuclear reactor, fuel rod and fuel assembly vibrations due to parallel coolant flow can cause fatigue failure of components, wear, and reactivity fluctuations, and set an upper limit on coolant flow velocity.

Single rod and fuel-assembly vibrations data[1-5] have been empirically correlated by many investigators[1-4]. The latest correlation due to Paidoussis[1] has been found to apply satisfactorily to a wide variety of experimental data[5,13]. Paidoussis empirical correlation was derived by dimensional analysis from an equation of motion of the vibrating rod. The forcing function used in his analysis was not clearly defined and effects associated with damping were not explicitly accounted for in the correlation.

Assuming boundary layer turbulence as the forcing function and using the correlation function for the fluctuating pressure at the wall in a turbulent boundary layer as described by Corcos[14] and Bakewell[15], Reavis[6] derived the fundamental mode RMS response of a pinned beam. A comparison of the reported data [1-5] with his predicted RMS response revealed that the reported maximum displacement ranged from 3.5 times the predicted RMS response for small hydraulic diameters to 420 times the predicted response for large hydraulic diameters. Taking the uncertainties in the reported data [1-5] into account, the discrepancies between the reported data and his predicted response thus appeared too large to be satisfactorily accounted for by the forcing function used in Reavis[6] analysis.

The present work was carried out to determine experimentally the contribution of only the near field boundary layer noise to parallel flow induced vibrations. The apparatus was carefully designed to eliminate all other far-field external noises and thus bring-out the relative importance of the two types of noise in vibrations of structures.

FORCED VIBRATIONS INDUCED BY SINGLE PHASE PARALLEL FLOW NOISE

Equation of Motion

The equation of motion of a cylindrical rod, excited by single phase parallel flow noise is given by the equation

$$EI \frac{\partial^4 y}{\partial x^4} + m\left(\frac{\partial}{\partial t} + V \frac{\partial}{\partial x}\right)^2 y + C \frac{\partial y}{\partial t} + M \frac{\partial^2 y}{\partial t^2} = F(x,t) \qquad (1)$$

in which M = mass of rod per unit length
EI = rod flexural rigidity
m = virtual mass per unit length

V = mean velocity of flow
C = structural viscous damping constant
y = displacement at the axial distance x from one end of the rod
$F(x,t)$ = lateral forcing function per unit length of rod.

In this equation, the effects due to tension and axial frictional force as well as transverse drag force on the rod have been neglected. The term $m(\frac{\partial}{\partial t} + V\frac{\partial}{\partial x})^2 y$ arises from the motion of the virtual mass of fluid associated with the vibrating rod.

The same equation (1) represents the equation of motion of a tube with water flowing inside it. The term $m(\frac{\partial}{\partial t} + V\frac{\partial}{\partial x})^2 y$ in this case arises from the transverse motion of the mass of fluid per unit length inside the tube.

At sufficiently high mean velocity of flow and $F(x,t)=0$, the free vibrations described by equation (1) exhibits static and dynamic instabilities. These instabilities, in the case of a cylindrical rod surrounded by axial flow are considered by Paidoussis[19] while those exhibited by a tube with internal flow are discussed by Housner[20] and Harold[21]. The experiment described by this paper was limited to low velocities to exclude such instabilities.

The forcing function, $F(x,t)$, in equation (1) is the lateral force per unit length exerted on the rod due to the pressure fluctuations at the surface of the rod. This forcing function depends on the flow conditions as well as the vibrations of structures in contact with the fluid. In general, there are three sources that contribute to the pressure fluctuations.

First, the turbulence generated by the dynamics of the fluid set up fluctuating stresses in the fluid and these result in a fluctuating pressure field[7,8,22]. Secondly, the vibrations of structures in contact with the fluid result in the radiation of a pressure field[12,22]. Thirdly, the pressure field radiated by the dynamics of either the fluid or structures in contact with the fluid has a near field component as well as a far (acoustic) field component[9,22]. Thus, the acoustic pressure field component associated with processes occuring far from the vibrating rod may be transmitted at the velocity of sound through the fluid medium to the surface of the rod.

When the vibrating rod forms part of a closed loop flow circuit, such as the primary coolant loop of a nuclear reactor, sources of acoustic noise in the entire coolant circuit must be taken into account. In flow circuits, with high velocity water,

some of the important processes which contribute to the acoustic pressure field are :

1. Turbulence generated by sharp bends and sudden section transitions.
2. Vortex shedding over submerged objects
3. Boundary layer turbulence.
4. Flow pulsations caused by pumps.
5. Other vibrating structures in contact with the fluid.
6. Coupling of the pressure fluctuations in a turbulent source of flow to the flow circuit.

EXPERIMENTAL WORK

Introduction

In all of the reported parallel flow experimental studies in the literature, boundary layer noise was always present and in addition all the other sources of single phase flow noise were also present in varying relative strengths. This experimental work was not aimed at developing vibration response prediction correlation for this complex situation. Rather, interest was focused on the response of a system excited by boundary layer noise only. Furthermore, the study was limited to the effects of the near field component only of boundary layer noise so as to determine the relative importance of this noise. The net effect of the acoustic field component of the boundary layer noise depends on a larger number of factors and so should be studied at a later stage. For instance, the larger the hydraulic diameter of the flow field for a given Reynolds Number, the larger is the effective acoustic noise radiation volume; the nature of the boundary of the flow field influences both the spatial and frequency pattern of the pressure waves that are set up; and the relative spatial location of the vibrating structure in the pressure field influences the net force exerted on the structure.

Object of the Experimental Work

For forcing functions that are random, the root-mean-square response is a more appropriate response to determine rather than the maximum displacement as reported in other experimental data; the mode of response is also of interest to know since most investigators agree that only the fundamental mode of vibration is dominant. These two pieces of information may be extracted from the power spectral density curve of the response.

The object of the experimental work was to obtain the power spectral density curve of the mid-span displacement of a long thin tube with turbulent flow of water inside it, and to compare the mid-span RMS response with that response predicted by presently available boundary layer wall pressure correlation.

Equipment and Procedure

A schematic diagram of the experimental apparatus is shown in Figure 1. It was designed to reduce sources and effects of the acoustic field component of single phase flow noise to the minimum. Pumps, sudden section transitions, and sharp bends were eliminated from the test loop. The source of excitation in this experiment was primarily the near field component of boundary layer noise.

Water for the tests was provided by a galvanized tank, 2 feet in diameter, 5 feet long, a capacity of 120 gallons, and pressurized by a bottle of compressed air. Velocity of the water through the test section was varied by regulating the constant pressure maintained in the tank.

The test section was the middle portion of a stainless steel tube of an outside diameter of 0.250 inches, a wall thickness of 0.010 inches, and a length of 6 feet. The tube was supported vertically by two precision single row radial ball bearings of an inside diameter of 0.250 inches and attached permanently to the tube so that the separation between them was exactly 5 feet and 9 inches.

The test section was connected to the tank through a vibration isolating joint and a conical reducer as shown in Figure 2. The conical reducer had a smooth conical bore of cone half angle of 19 degrees, a diameter at the large cone end of 3 inches and a diameter at the small end of 0.230 inches. This construction reduced the likelihood of generating turbulence upstream of the test section to the minimum.

The lower end of the test section was fitted with a 15 inch long polyethylene tube whose lower end was about 2 inches above the bottom of a collecting tank. The collecting tank rested on two coils of flexible rubber hose, which acted as a shock absorber to damp out any fluctuating momentum flux on the collecting tank. The mid-span vibrations were measured using an optical transducer and an amplification system. Schematic diagrams of the transducer and the amplification system are shown in Figures 3 and 4 respectively.

Referring to Figure 3, the phototube was placed inside a shield which had 1/8 inch diameter slit. The light source emitted a nearly isotropic beam of light through an 1/8 inch square slit. The light source and the shield were positioned relative to each other such that when the tube was deflected from the path of the light beam, a certain amount of light was transmitted through the slit in the shield; the phototube was placed well inside the shield so that all this amount of light was incident on the phototube active face. When the tube was allowed to return to the freely hanging position, the phototube output current was reduced to about one half. Small displace-

ments of the tube from this equilibrium position were found to be linear with changes in the output current.

Referring to the schematic diagram of the amplification system of Figure 4, the biasing current was used to remove the large d.c. component of the phototube output current. The feedback gain of the operational amplifier was adjusted so that 0.001 inch displacement of the tube produced approximately 7 volts change in the amplifier output voltage.

The recorded signal was analyzed using the power spectral analysis system shown schematically in Figure 5. A typical power spectral density curve obtained is as shown in Figure 6. The fundamental mode frequency of the tube was calculated and found to be 9.64 cycles/sec. The results showed there was no response beyond 15 cycles/sec. at either the mid-span or quarter-point of the tube, and hence only the fundamental mode of the tube was excited.

The shape of the power spectral density curve about the fundamental mode frequency was due largely to the finite frequency band-width of the analyzer's filter. The narrowest band width available was $\Delta f = 5$ cps. By playing back the recorded signal at four times the recording speed, it was possible to reduce the effective band width to $\Delta f = 1.25$ cps. Further effects of the finite band width of the filter were eliminated by normalizing the area under the power spectral density curve with respect to the area obtained for a sine wave of known RMS value. The measured RMS deflection was deduced from the normalized area under the power spectral density curve.

Discussion of Results

The results of the experiment are summarized in Table 1. The measured experimental RMS response and the corresponding response predicted by Reavis' expression[6] are given in Table 2 for comparison; the maximum amplitudes predicted by Paidoussis' revised expression[1] with K = 1 are also given in Table 2.

The correlations due to Reavis and Paidoussis apply to the vibrations of a rod surrounded by external flow. In this work, a tube with internal flow was found to be experimentally convenient. Although equation (1) has been shown to apply to either a rod or a tube with internal flow under the approximations stated, there are two important aspects in which differences may be expected between external and internal flows.

First, the near field boundary layer noise experienced by an infinitely rigid tube due to internal flow will be similar to the corresponding flow noise exerted on an infinitely rigid cylindrical rod of diameter equal to the bore of the tube[17,18]. If the rod and tube are not infinitely rigid, then differences

in the fluctuating pressure field may be expected due to circulation generated by the transverse motion of the vibrating structure [23]. However under conditions of high mean flow velocities but small amplitude and low frequency transverse vibrations as in this experiment, circulation effects will be negligible.

Secondly, the forces exerted on the vibrating structure by the transverse motion of the mean flow are, in general, different. In external flow only, the transverse motion results in dissipative drag force exerted on the vibrating rod[19], though such transverse drag force is not expected to have significant effects for small amplitude and low frequency vibrations with moderate damping. The second term of equation (1), namely

$$m\left(\frac{\partial}{\partial t} + V\frac{\partial}{\partial x}\right)^2 y = m\frac{\partial^2 y}{\partial t^2} + 2mV\frac{\partial^2 y}{\partial x \partial t} + mV^2\frac{\partial^2 y}{\partial x^2} \qquad (2)$$

represents the inertia forces generated by the transverse motion of the mean flow, m being equal to either the virtual mass associated with the vibrating rod for external flow[19], or the mass per unit length inside the tube[20]. The term $2mV\frac{\partial^2 y}{\partial x \partial t}$ is the inertia force associated with the Coriolis acceleration of the mean flow and its effect is different for external and internal flows. Its influence can be understood by rewriting equation (1) in a form where $2mV\frac{\partial^2 y}{\partial x \partial t}$ is considered as an external force as done by Housner[20].

For external flow, the inertia forces exerted by the virtual mass are conservative[19]; but for internal flow the net effect of the Coriolis acceleration force may be nonconservative depending on the shape assumed by the vibrating tube.

In the study of a similar problem of articulated pipes conveying fluid, Benjamin[23] noted that if the free end of the pipe was permitted to move transversely to the direction of the mean flow, the hydrodynamic forces on the pipe were nonconversative. Housner[20] shows that if the shape of a mode of a tube with both ends supported is symmetrical about the midpoint of the tube and the Coriolis acceleration force antisymmetrical, the latter force does no work on that mode. In particular, if only the fundamental mode of the tube is excited and the mode shape $y(x,t)$ and its first spatial derivative satisfy the relationship

$$\frac{\partial y(x\ t)}{\partial x} = C_1 y(x\ t) \qquad (3)$$

in which C_1 is either a positive constant or a weakly varying positive function of x such that both $y(x,t)$ and $\frac{\partial y(x\ t)}{\partial x}$ are symmetrical about the mid-point of the tube, then the Coriolis acceleration force is of the nature of a damping force.

The damping effect of the mean flow on the fundamental mode vibrations of a simply supported pipe with internal flow was observed experimentally by Harold[22]; a similar damping effect was observed in this experiment. Thus, treating the mixed-derivative Coriolis acceleration term as an external damping force on the tube, the fundamental mode variation of a tube with internal flow will be expected to be similar to the corresponding mode vibration of a rod surrounded by axial flow.

Referring to Table 2, the results show that the measured RMS response is within 50% of the response predicted by Reavis' expression[6] derived from boundary layer theory. This agreement was expected: the boundary layer forcing function used by Reavis to derive his expression has been found to apply satisfactorily to experimental data with water as well as air[17,18], and his assumption that only the fundamental mode of the tube is excited as been borne out by the experimental results.

The calculated maximum amplitudes using Paidoussis' empirical correlation are within a factor of 24 of the experimental RMS response. Good agreement was not expected for several reasons. First, the difference in the experimental set up and the lack of far field noise in the present work make the forcing conditions different. The noise level in the present work is comparatively low. Secondly, the damping ratio which is an important physical quantity is absent from his empirical correlation. The effective damping in this experiment was considerably greater than the structural damping expected in the structures of the reported data[1-5]. Assuming the dependence of vibration amplitude on the damping ratio as it appears in Reavis' expression[6], it is estimated that the increased damping may contribute by a factor of 4 to the discrepancy. Thirdly, for forcing functions that are random, there is no simple exact relationship between the RMS response and the maximum amplitude. If reasonable corrections are made for the second and third observations, his corresponding RMS response would be a factor of 4 to 15 times the measured response. The near field boundary layer noise thus appears not to be very important under the conditions his empirical correlation has been found to apply satisfactorily.

CONCLUSIONS

The results show that only the fundamental mode response of the tube was excited. This finding confirms other investiga-

tors' conclusion that for parallel flow induced vibrations in fuel rods, the fundamental mode response is dominant[4-6].

The results also show good agreement with the RMS response predicted by Reavis[6] expression derived from boundary layer theory. The calculated maximum amplitudes using Paidoussis empirical correlation are within a factor of 4 to 15 of the experimental result. This large factor discrepancy suggests that the near field boundary layer flow noise does not make a very significant contribution to the parallel flow induced vibrations under the conditions Paidoussis empirical correlation has been found to apply satisfactorily.

As a general observation, the acoustic noise, which is present in most experimental work reported previously, makes an important contribution to the amplitude of the vibrations in the structures. This is because the relatively long wave length (inch to feet) of this noise results in large net resultant forces applied to the vibrating structure. This acoustic noise is not only produced in the test section, but mostly at the inlet and outlet of the section and also in the outside loop. Experimental data reported should therefore attempt to clearly separate the inherent and characteristic far-field noise caused by the loop and the one generated in the test section. Because of its importance, a greater emphasis in future work should be given to the far-field noise and an attempt should be made to characterize the noise for a well specified flow system.

Table 1. Experimental Results

Run	1	2	3	4	5
Mean Pressure in Tank(psi)	233	162.5	121.5	102.5	87.5
Flow Velocity(ft/sec)	53.1	48.8	44.3	39.4	37.0
Voltage/0.001 in. defl.	6.25	7.00	7.75	7.00	7.75
Measured δ_{RMS}(10^{-3} in)	$\pm^{0.503}_{0.100}$	$\pm^{0.486}_{0.100}$	$\pm^{0.433}_{0.090}$	$\pm^{0.421}_{0.080}$	$\pm^{0.343}_{0.070}$

Table 2. A Comparison of the Experimental Results With RMS Deflection Predicted by Reavis[6] and Maximum Amplitude Predicted by Paidoussis[1].

Run	1	2	3	4	5
Flow Velocity(ft/sec)	53.1	48.8	44.3	39.4	37.0
Experimental δ_{RMS}(10^{-3} in)	$\pm^{0.503}_{0.100}$	$\pm^{0.486}_{0.100}$	$\pm^{0.433}_{0.090}$	$\pm^{0.421}_{0.080}$	$\pm^{0.343}_{0.070}$
δ_{RMS} (Reavis[6]) (10^{-3} in)	0.416	0.403	0.312	0.270	0.252
δ_{max} (Paidoussis[1]) (10^{-3}in)	12.8	12.6	12.3	11.8	11.6

REFERENCES

1. M.P. Paidoussis, "An Experimental Study of the Vibration of Flexible Cylinders Induced by Axial Flow," Trans. Am. Nucl. Soc., 11, 352 (1968).

2. D. Burgreen, et al., "Vibration of Rods Induced by Water in Parallel Flow," Trans. ASME, 80, 991-1003 (1958).

3. E.P. Quinn, "Vibration of Fuel Rods in Parallel Flow," GEAP-4059, (July 1962).

4. SoGRÉAH, "Study of Vibrations and Load Losses in Tubular Clusters," Special Report No. 3, EUREAC-288 (1962).

5. R.T. Pavlica and R.C. Marshall, "An Experimental Study of Fuel Assembly Vibrations Induced by Coolant Flow," Nuclear Engineering and Design, 4 (1966)

6. J.R. Reavis, "WVI - Westinghouse Vibration Correlation for Maximum Fuel-Element Displacement in Parallel Turbulent Flow," Trans. ANS, 10, No. 1 (June 1967) pp. 369.

7. M.J. Lighthill, "On Sound Generated Aerodynamically. I General Theory," Proc. Roy. Soc. A211, pp. 564 (1952).

8. M.J. Lighthill, "On Sound Generated Aerodynamically. II Turbulence as Source of Sound," Proc. Roy. Soc. A255, pp. 1 (1954).

9. J.B. Ollerhead, "On the Prediction of the Near Field Noise of Supersonic Jets," NASA CR-857 (August 1967).

10. D.H. Tack and R. F. Lambert, "Response of Bars and Plates to Boundary Layer Turbulence," J. Aero. Sci., 311-322 (1962).

11. H. Fenech, et al., "Acoustic Fatigue Life Study in Components of Nuclear Reactors," Trans. ANS, 10, No. 1, pp. 323 (1967).

12. W.A. Strawderman, "The Acoustic Field in a Closed Space Behind a Rectangular Simply Supported Plate Excited by Boundary Layer Turbulence," U.S. Navy Underwater Sound Laboratory Report No. 827. (May 1967).

13. M.P. Paidoussis, "The Amplitude of Fluid-Induced Vibration of Cylinders in Axial Flow," AECL-2225 (March 1965).

14. G.M. Corcos, "Pressure Fluctuations in Shear Flows," pp. 65-66, University of California, Berkeley, Inst. of Engineering Research, Series No. 183, issue No. 2 (July 1962).

15. H.P. Bakewell, Jr., "Narrow-Band Investigations of the Longitudinal Space-Time Correlation Function in the Turbulent Airflow," J.A.S.A. 36, No. 1, pp. 146 (1964).

16. A.K. Addae, "An Experimental Power Spectral Analysis of the Effect of Turbulent Flow Noise on Pipes," S.M. Thesis, Massachusetts Institute of Technology, Department of Nuclear Engineering, Cambridge, Massachusetts (February 1968).

17. G.F. Carey, J.E. Chlupsa, and H.H. Schloemev, "Acoustic Turbulent Water-Flow Tunnel," J.A.S.A. 41, 373-379, (1967).

18. H.P. Bakewell, Jr., "Turbulent Wall-Pressure Fluctuations on a Body of Revolution," J.A.S.A. 43, No. 6, 1358-1363, (1968)

19. M.P. Paidoussis, "Dynamics of Flexible Slender Cylinders in Axial Flow. Part 1, Theory," J. Fluid Mech., Vol. 26, Part 4, pp. 717-736 (December 1966).

20. G.W. Housner, "Bending Vibrations of a Pipe Line Containing Flowing Fluid," J. Appl. Mech., Vol. 19, No. 2, pp. 205-208 (June 1952).

21. L. Harold, et al.,"Effect of High-Velocity Fluid Flow on the Bending Vibrations and Static Divergence of a Simply Supported Pipe," NASA TN D-2870 (June 1965).

22. N. Curle, "The Influence of Solid Boundaries upon Aerodynamic Sound," Proc. Royal Soc. Series A, Vol. 231, pp. 505-514 (1955).

23. T.B. Benjamin, "Dynamics of a System of Articulated Pipes Conveying Fluid," Proc. Royal Soc. Series A, Vol. 261, pp. 457-499 (1961).

24. Max M. Munk, "Notes on Vortices and on their Relation to the Lift of Airfoils," NACA Technical Note No. 184 (1924).

DISCUSSION

P. A. Lowe (Westinghouse-Bettis): I have a couple of questions. I didn't understand whether in the Reavis correlation you were using the high-noise or the low-noise correlation to compare your results.

Fenech: We used a high-noise correlation.

Lowe: Okay. Then I was wondering about the applicability of the correlation, if you had flow inside of a tube and, I believe, Reavis' and the Paidoussis' experimental results are for flow around the outside of tubes.

Fenech: We have sorted this out very clearly in our paper and didn't want to go into the sort of complicated mathematics this would require. We realize that in most cases flow inside tubes would be different from flow outside tubes as far as vibrations are concerned. In the case at hand, the differences are mostly due to the viscous friction in the transverse direction to the flow; that is, when the tube is vibrating perpendicularly to the flow of the liquid. The frequency measured is very low, about nine cycles per second in the shell. These differences due to transverse frictions are negligible. The other effect which is due to the convection effect has been accounted for; that is, we corrected the Reavis correlation to account for the different situations between inside and outside flow.

M. W. Wambsganss (ANL): I'm in general agreement with your conclusions; however, I would like to clear up one point. I think in your opening remarks you suggested that Dr. Chen's theory was in agreement with Paidoussis' correlation. This is not what Dr. Chen was implying. In fact, if you compare the two, I think Paidoussis would probably be an order of magnitude or two greater. The comparison at the end of Dr. Chen's paper was the result of a parameter study which showed that he was in agreement with the way the parameters varied, but not in the overall magnitude.

Fenech: I didn't understand that part of Chen's paper and I'm glad that point has been resolved.

G. S. Rosenberg (ANL): I think the agreement that Chen found had to do with the functional form rather than with the ultimate numerical value, but in the context of the last slide you displayed what seems interesting is that there didn't appear to be any great disparity in the functional relations. For the way in which the displacements change with flow velocity including your experiments, Reavis' correlation or Paidoussis' correlation, it seemed that there is simply a systematic gross translation of the curve. If true, this means that a possibility for scaling is near.

Fenech: I agree with your statement. I am personally worried about the acoustic noise produced outside, in the experimental loop, and propagated into the experimental test tube. This noise is usually of very long wavelength and, although its amplitude may not be high, because of the high wavelength, its effectiveness on the amplitude of the vibration of the tube would be greater than the nearfield noise.

Lowe: I might add one more comment about Paidoussis' work. I have just been looking at it, and he recently reissued his correlation and the amplitudes have increased by maybe 25 times. You indicated they were already too large.

Fenech: I wish either he or Reavis would be here to justify such action.

J. C. Simonis (Babcock & Wilcox): In comparing your studies, say, your study and Paidoussis' study, I wondered if you had looked at peak-to-peak amplitudes, or maximum displacements as apparently Paidoussis had. Do they agree when you look at them in this light any better than when you look at them in terms of the rms value?

Fenech: We feel that when we talk about vibration induced by statistical phenomena, like nearfield noise, the maximum amplitude is meaningless because you always find there is a probability that you are going to have an infinite displacement. Therefore, the meaning of maximum amplitude is somewhat ill-defined. We did do some correction to try to breach a gap between our measurement of the displacement and the maximum displacement calculated by Paidoussis. And I think we did this using the correction that you have between the maximum and the rms for a sine wave, or this sort of thing. I think that brought in a factor of about 4, but we are still off with Paidoussis by a good factor of about 25, after making this adjustment between rms and maximum.

Simonis: So then you are saying that even if you'd go ahead and look at your peak-to-peak values, you are still off.

Fenech: Well, when we adjust the maximum Paidoussis value to an rms value, and compare our rms values with those of Paidoussis, we are still off by a factor of 25 or so.

E. Kiss (GE-San Jose): I'm troubled by a question that was asked before--the difference between flow internal to a tube and flow external to it. I haven't seen your paper, so I can't know what's in it, but it seems to me there is a fundamental difference between internal and external flow. That is, in internal flow you don't have a chance for crossflow. I wonder if you'd comment on this--crossflow as an exciting mechanism?

Fenech: Essentially that was contained in my answer to Dr. Lowe. That is, at low frequencies, which is the case in our experiment (9.67 cycles per second), the effect of the viscous force on the tube due to crossflow is insignificant compared with the force due to flow of liquid longitudinally to the tube, whether it's inside or outside. If the frequency were of the order of 500 or 1000 cps, then I would think that the correction for crossflow would be significant, but not in the low frequency range we had.

B. L. Boers (ANL): I was wondering if you had compared your data to that taken at IIT by Clinch, where he used a loop which had flow interior to the tube. He was also very careful to eliminate extraneous vibrations.

Fenech: No, we haven't done this for the simple reason that we didn't know about this result when we did our work. There is a possibility that we will do this in the future.

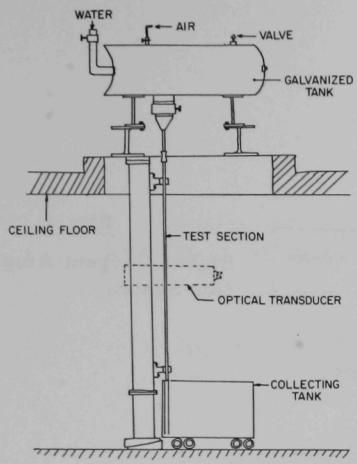

Fig. 1

Diagram of Test Loop

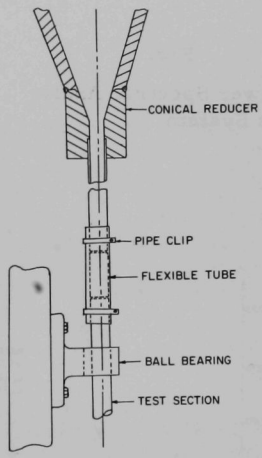

Fig. 2

Upstream Isolation Joint

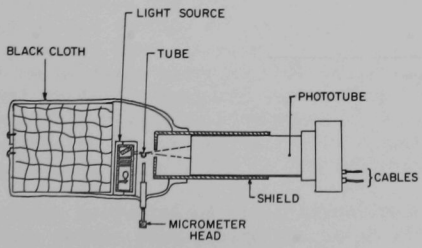

Fig. 3

Arrangement of Optical Transducer

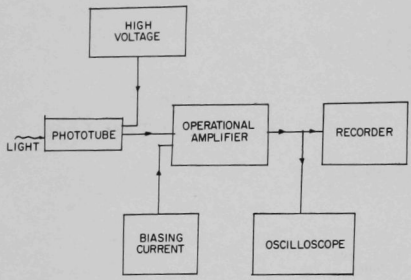

Fig. 4

Signal Current Amplification System

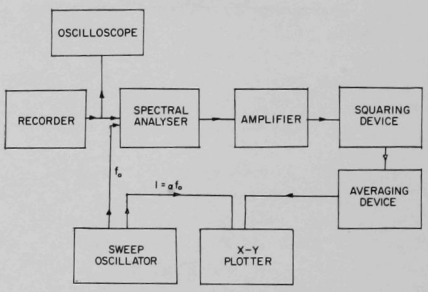

Fig. 5

Power Spectral Analysis System

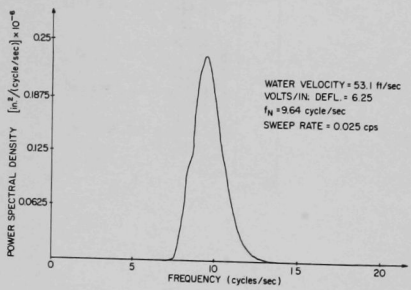

Fig. 6

Power Spectral Density Curve for Run 1

CALCULATION OF THE RESPONSE OF RODS TO BOUNDARY LAYER PRESSURE FLUCTUATIONS

R. M. Kanazawa
General Electric Company
Nuclear Energy Division
San Jose, California

A. P. Boresi
University of Illinois
Urbana, Illinois

ABSTRACT

A method for calculating the probable response of a rod to pressure fluctuations on its surface is shown in detail. The random pressure field which acts on the surface of the rod is assumed to be similar to the pressure fields which have been measured on flat plates in wind tunnels. The mathematical model for a rod in parallel flow which is used in the calculations is based on Bernoulli-Euler beam theory and includes viscous damping. The results are presented in a series of figures which expose the influence of various parameters on the rod response.

INTRODUCTION

The general problem of flow-induced vibration is obviously quite complicated. The crux of the problem seems to exist in describing the interaction between the motion of the structure and the fluid forces which act on the surface of the structure. For some problems, such as rods in parallel flow, it seems logical to assess the effects of the interaction by first assuming that no interaction exists. If the structural response, measured experimentally, cannot be satisfactorily described analytically as a response to fluid forces which are assumed to be unaffected by the motion of the structure, then the effects of interaction must be included in the analysis.

However, exclusion of the interaction between motion of the structure and surface forces does not result in an effortless calculation. Numerous papers have been published on the response of plates to turbulent pressure fields. The most recent paper (1) refers to but a few of them.

Clinch (2) has calculated the response of the wall of a pipe to turbulent flow and obtains very good agreement with experimental data for the averaged higher modes of shell vibration. Reavis (3) has presented a method for calculating the response of a rod to turbulent boundary layer pressure fluctuations which eliminates the requirement of a large digital computer but which is restricted to the fundamental bending mode of response. In this paper, the identical problem is solved except that no assumptions are made which restrict the results to the fundamental mode of vibration. A digital computer is used to explore the effects of various parameters on the response of the rod to turbulent water flow.

ANALYSIS

The response of a simply-supported rod to boundary layer pressure fluctuations can be expressed in the form of the cross-spectral density function, $\Phi_{YY}(x,x',\omega)$ and its integral over-all frequencies, the mean-square value, $\overline{y^2}(x,x')$. It can be shown (4) that Φ_{YY} and $\overline{y^2}$ take on the following form.

$$\Phi_{YY}(x,x',\omega) = \frac{4}{L^2}\sum_{m=1}^{\infty}\sum_{n=1}^{\infty} \sin\frac{m\pi x}{L}\sin\frac{n\pi x'}{L} H_m(\omega) H_n^*(\omega) \int_0^D\int_0^D\int_0^L\int_0^L \Phi_{PP}(\xi-\xi',\eta-\eta',\omega)\sin\frac{m\pi\xi}{L}\sin\frac{n\pi\xi}{L}\, d\xi\, d\xi'\, d\eta\, d\eta' \tag{1}$$

$$\overline{y^2}(x,x') = \int_0^{\infty}\Phi_{YY}(x,x',\omega)\,d\omega \tag{2}$$

where $H_n(\omega)$ is the frequency response function for the simply-supported rod, and $\Phi_{PP}(\xi,\eta,\omega)$ is the cross-spectral density function of the random pressure field.

In the calculations, the following expression for $H_n(\omega)$ was used (5).

$$H_n(\omega) = \left(\lambda_n^4 EI\right)^{-1}\left[1-\frac{\pi}{4}\frac{\rho D^2 U^2}{EI\lambda_n^2} - \left(\frac{\omega}{\omega_n}\right)^2 + i2\zeta\left(\frac{\omega}{\omega_n}\right)\right]^{-1} \tag{3}$$

where

$$2\zeta = \frac{c}{\mu\omega_n}$$

$$\lambda_n = \frac{n\pi}{L}$$

$$\omega_n^2 = \lambda_n^4\frac{EI}{\mu}$$

It is postulated that the random pressure field acts on only one side of the rod and can be described by Corcos' (6) analytical expression for $\Phi_{pp}(\xi, \eta, \omega)$. The cross-spectral density function, as proposed by Corcos, is separable into its rectangular Cartesian spatial coordinates. Corcos proposes that

$$\Phi_{pp}(\xi, \eta, \omega) = \phi(\omega)\, A\left(\frac{\omega|\xi|}{U_c}\right) B\left(\frac{\omega|\eta|}{U_c}\right) \exp\left(-i\,\frac{\omega\xi}{U_c}\right) \tag{4}$$

where $\phi(\omega)$ is the spectral density function for the pressure fluctuations,

$A\left(\frac{\omega|\xi|}{U_c}\right)$ is the amplitude function for Φ_{pp} in the longitudinal (downstream) direction, and

$B\left(\frac{\omega|\eta|}{U_c}\right)$ is the amplitude function for Φ_{pp} in the lateral (cross-stream) direction.

It is interesting to note that the cross-spectral density function in the lateral direction is real, namely

$$\Phi_{pp}(0, \eta, \omega) = \phi(\omega)\, B\left(\frac{\omega|\eta|}{U_c}\right) \tag{5}$$

while in the longitudinal direction, the cross-spectrum is

$$\Phi_{pp}(\xi, 0, \omega) = \phi(\omega)\left(A\,\frac{\omega|\xi|}{U_c}\right) \exp\left(-i\,\frac{\omega\xi}{U_c}\right) \tag{6}$$

In general, cross-spectral densities are complex functions.

The spectral density of the wall pressure was obtained by drawing a straight line, fitted by eye, through data points plotted in Figure 2 of reference (6). The expression used is

$$\phi(\omega) = \begin{cases} \dfrac{\tau_0^2\,\omega s}{U}\left(\dfrac{\omega s}{2\pi U}\right)^{-\frac{1}{2}}, & \left(\dfrac{\omega s}{2\pi U}\right) \le 10 \\[2ex] 0, & \left(\dfrac{\omega s}{2\pi U}\right) > 10 \end{cases} \tag{7}$$

The cut-off frequency, $\left(\frac{\omega s}{2\pi U}\right) = 10$, is somewhat arbitrary, although the data indicate a sharp drop in spectral density beyond $\left(\frac{\omega s}{2\pi U}\right) = 10$. However, it was found that the frequency limit was never reached in the calculations.

The shearing stress at the wall, τ_0, is calculated from well-known facts of the turbulent boundary layer (7).

$$\tau_0 = \frac{1}{8} \lambda \rho U^2 \tag{8}$$

$$\frac{1}{\sqrt{\lambda}} = 2.0 \log\left(Re\sqrt{\lambda}\right) - 0.8 \tag{9}$$

Equation (9) is the famous von Karman-Prandtl universal law of friction and has been verified for Reynolds number up to 3.4×10^6. The largest value of Re used in the calculations is 3.1×10^5. In order to evaluate λ by means of equation (9), the Blasius formula was used to begin the iteration process in the calculations.

$$\lambda = 0.3164 \; Re^{-\frac{1}{4}} \tag{10}$$

By itself, equation (10) is accurate up to Re = 1×10^5 and so the iteration procedure was quite short (to 1% accuracy) for values of Reynolds number below 1×10^5.

Willmarth and Roos (8) have fitted curves through data reported by Corcos (9) to determine the amplitude functions A and B of equation (4). The results are

$$A(\gamma) = \exp\left(-0.1145|\gamma|\right) + 0.1145|\gamma| \exp\left(-2.5|\gamma|\right) \tag{11}$$

$$\begin{aligned} B(\beta) = {} & 0.155 \exp\left(-0.092|\beta|\right) + 0.70 \exp\left(-0.789|\beta|\right) \\ & + 0.145 \exp\left(-2.910|\beta|\right) + 0.99|\beta| \exp\left(-4.0|\beta|\right) \end{aligned} \tag{12}$$

where $\gamma = \dfrac{\omega \xi}{U_c}$ and $\beta = \dfrac{\omega \eta}{U_c}$

Finally, the convection speed of the random pressure field was determined by using published data and fitting lines through the data points. [Figure 9, reference (6)].

$$\frac{U_c}{U} = \begin{cases} 0.9 - 0.06\,\dfrac{\omega s}{2\pi U}, & \dfrac{\omega s}{2\pi U} \le 3 \\[2ex] 0.7, & \dfrac{\omega s}{2\pi U} > 3 \end{cases} \tag{13}$$

Since the largest non-dimensional frequency used in the calculations was $\frac{\omega s}{2\pi U} = 2.81$, the point of discontinuity was never exceeded.

The spectral density and mean-square value of the rod displacement, equation (1) and (2) respectively, were evaluated using a digital computer. The first attempts at digital analysis of the problem used an excessive amount of machine time. Consequently, the double integrals over the length and diameter of the rod were evaluated in closed form. Since the results of the integrations are quite lengthy, only the general procedure followed is presented.

By substituting equation (4) into equation (1), the following expression is obtained:

$$\Phi_{YY}(x,x',\omega) = \frac{4}{L^2}\sum_{m=1}^{\infty}\sum_{n=1}^{\infty} \sin\frac{m\pi x}{L}\sin\frac{n\pi x'}{L}\, H_m(\omega)\, H_n^*(\omega)\, \phi(\omega) \int_0^L\!\!\int_0^L A\left(\frac{\omega|\xi-\xi'|}{U_c}\right)$$
$$\exp\left(-i\,\frac{\omega(\xi-\xi')}{U_c}\right)\sin\frac{m\pi\xi}{L}\sin\frac{n\pi\xi'}{L}\,d\xi\,d\xi' \int_0^D\!\!\int_0^D B\left(\frac{\omega|\eta-\eta'|}{U_c}\right)d\eta\,d\eta' \tag{14}$$

The portion of Φ_{YY} which is the double integral over the length of the rod, DIL, is written as follows:

$$\begin{aligned} DIL = &\int_0^L\!\!\int_0^L e^{-.1145\left|\frac{\omega(\xi-\xi')}{U_c}\right|}\cos\left(-\left|\frac{\omega(\xi-\xi')}{U_c}\right|\right)\sin\frac{m\pi\xi}{L}\sin\frac{n\pi\xi}{L}\,d\xi\,d\xi' + \\ &.1145\int_0^L\!\!\int_0^L \left|\frac{\omega(\xi-\xi')}{U_c}\right| e^{-2.5\left|\frac{\omega(\xi-\xi')}{U_c}\right|}\cos\left(-\left|\frac{\omega(\xi-\xi')}{U_c}\right|\right)\sin\frac{m\pi\xi}{L}\sin\frac{n\pi\xi'}{L}\,d\xi\,d\xi' + \\ &i\int_0^L\!\!\int_0^L e^{-.1145\left|\frac{\omega(\xi-\xi')}{U_c}\right|}\sin\left(-\frac{\omega(\xi-\xi')}{U_c}\right)\sin\frac{m\pi\xi}{L}\sin\frac{n\pi\xi'}{L}\,d\xi\,d\xi' + \\ &i\int_0^L\!\!\int_0^L \left|\frac{\omega(\xi-\xi')}{U_c}\right| e^{-2.5\left|\frac{\omega(\xi-\xi')}{U_c}\right|}\sin\left(-\frac{\omega(\xi-\xi')}{U_c}\right)\sin\frac{m\pi\xi}{L}\sin\frac{n\pi\xi'}{L}\,d\xi\,d\xi' \end{aligned} \tag{15}$$

The introduction of absolute value signs to the arguments of the cosine terms in the above expression is noted. Since the cosine is an even function, the net effect is a mathematical convenience for setting up the integration of the real part of DIL.

The integrands in the double integrals of DIL can be written without the absolute values and integrated. For example, the first term of DIL becomes

$$\int_0^L e^{-\alpha_1 \xi} \sin\beta_1 \xi \cos\gamma\xi \int_0^{\xi} e^{\alpha_1 \xi'} \sin\beta_2 \xi' \cos\gamma\xi' \, d\xi' \, d\xi \; +$$

$$\int_0^L e^{-\alpha_1 \xi} \sin\beta_1 \xi \sin\gamma\xi \int_0^{\xi} e^{\alpha_1 \xi'} \sin\beta_2 \xi' \sin\gamma\xi' \, d\xi' \, d\xi \; +$$

$$\int_0^L e^{-\alpha_1 \xi'} \sin\beta_2 \xi' \cos\gamma\xi' \int_0^{\xi'} e^{\alpha_1 \xi} \sin\beta_1 \xi \cos\gamma\xi \, d\xi \, d\xi' \; +$$

$$\int_0^L e^{-\alpha_1 \xi'} \sin\beta_2 \xi' \sin\gamma\xi' \int_0^{\xi'} e^{\alpha_1 \xi} \sin\beta_1 \xi \sin\gamma\xi \, d\xi \, d\xi' \qquad (16)$$

where $\alpha_1 = .1145 \dfrac{\omega}{U_c}$, $\beta_1 = \dfrac{m\pi}{L}$, $\beta_2 = \dfrac{n\pi}{L}$, $\gamma = \dfrac{\omega}{U_c}$

The second term in DIL, expanded in the same way as the first term, results in eight integrable terms.

The integration of the expanded terms is carried out by direct methods and with the help of a table of integrals. Although the integration process is not difficult, it is a tedious one.

The imaginary part of DIL was not evaluated. This restricts the solution of equation (14) to cases in which m = n. That is, the cross-spectral densities between different modes of vibration were not calculated. Note that for m = n, the imaginary part of DIL is zero due to the fact that the sine function is odd with respect to its argument.

The value of DIL down to a few simple, single integrals is as follows for m = n:

$$DIL = A\left(\frac{L}{2}\right) + B\int_0^L e^{-\alpha_1 \xi} \sin\beta\xi \cos\gamma\xi \, d\xi \; +$$

$$C\int_0^L e^{-\alpha_1 \xi} \sin\beta\xi \sin\gamma\xi \, d\xi + D\int_0^L \xi e^{-\alpha_2 \xi} \sin\beta\xi \cos\gamma\xi \, d\xi \; +$$

$$E\int_0^L \xi e^{-\alpha_2 \xi} \sin\beta\xi \sin\gamma\xi \, d\xi + F\int_0^L e^{-\alpha_2 \xi} \sin\beta\xi \cos\gamma\xi \, d\xi \; +$$

$$G\int_0^L e^{-\alpha_2 \xi} \sin\beta\xi \sin\gamma\xi \, d\xi + H\left(\frac{L}{2}\right) \tag{17}$$

where $\alpha_1 = .1145 \frac{\omega}{U_c}$, $\alpha_2 = 2.5 \frac{\omega}{U_c}$, $\beta = \frac{m\pi}{L}$, $\gamma = \frac{\omega}{U_c}$

and A through H are constants containing the above four constants.

Returning to equation (14), the portion of Φ_{YY} which contains the double integral over the diameter of the rod, DID, is written as follows:

$$DID = \int_0^D\int_0^D \left[.155\, e^{-.092 \frac{\omega|\eta-\eta'|}{U_c}} + .7 e^{-.789 \frac{\omega|\eta-\eta'|}{U_c}} + .145\, e^{-2.916 \frac{\omega|\eta-\eta'|}{U_c}} + \right.$$

$$\left. .99 \frac{\omega|\eta-\eta'|}{U_c} e^{-4.0 \frac{\omega|\eta-\eta'|}{U_c}} \right] d\eta \, d\eta' \tag{18}$$

The procedure and results of the integration of DIL and DID were checked carefully. Skepticism in regards to the accuracy of the results persisted until the value of $\Phi_{YY}(x, x', \omega)$ calculated by using the "exact" method checked with those obtained by the slower digital method. It was found that the FORTRAN IV program for the "exact" solution was

12-1/2 times as fast as the digital integration program. Consequently, more extensive calculations were possible.

RESULTS

The results of the computer calculations are plotted in Figures 1 and 2.

Figure 1 is a series of plots showing the variation of root-mean-square displacement with a) water velocity, b) bending modulus, c) critical damping ratio, and d) rod natural frequency. Table 1 shows the rod response at the mid-point and quarter-point of the rod for the first three modes of vibration. All of the rms values have been divided by 32.4 mils which is the calculated response for the following case: $U = 30$ ft/sec., $\zeta = 0.05$, $f_o = 15$ Hz., $EI = 200\ lb_f\text{-}ft^2$.

TABLE 1 NORMALIZED DISPLACEMENT AT MID- AND QUARTER-POINTS FOR FIRST THREE MODES OF VIBRATION

Mode No.	Normalized Displacement	
	Mid-Point	Quarter-Point
1	1.000	0.707
2	0	0.0475
3	0.0078	0.0056
Total	1.0078	0.760

Figure (2) is a series of plots which shows the variation of the normalized spectrum of rod response with a) water velocity, b) bending modulus, c) critical damping ratio, and d) rod natural frequency. Only the first mode response at $x/L = 1/2$ was calculated for the preceding plots. The higher mode response as well as displacement at $x/L = 1/4$, $3/4$ is shown in a separate plot d). All of the spectra have been normalized to unit mean square value.

The following parameters were assigned the values shown:

$$s = 0.125 \text{ ft.}$$

$$\rho = 1.936 \text{ slugs/ft}^3 \ (H_2O \text{ at } 70° \text{ F.})$$

$$\nu = 1.06 \times 10^{-5} \text{ ft}^2\text{/sec. } (H_2O \text{ at } 70°\text{F.})$$

$$L = 4 \text{ ft.}$$

$$D = 0.0416 \text{ ft.}$$

$$E = 4.32 \times 10^9 \text{ lb/ft}^2$$

The results show a strong dependence of rod displacement on water velocity. The slope of the line in Figure 1 (a) is approximately = 2. Also, the calculated displacement is inversely proportional to the bending modulus. Damping and natural frequency appear to play secondary roles in determining the rod response, at least over the ranges explained for these parameters. According to the calculations, higher mode response to turbulent boundary layer excitation is quite small. It can be mentioned that the variation in rod response with damping is in agreement with the results for a single degree of freedom system excited by white noise (4).

The spectra show the relative frequency distribution of the mean square rod displacement. It is interesting to note the shifts in the spectrum due to changes in water velocity and rod damping. The spectra for increasing water velocity show a relative decrease in the lowest frequencies with increasing fluid velocity, and the results for increased damping show a flattening and broadening of the peak at the rod natural frequency, as one would expect. Also, the spectra for increasing rod natural frequency show a relative increase in the portion of the spectra just below the resonance peak. This result indicates that the excitation spectrum begins to drop in power density within the frequency range through which the rod natural frequencies were varied.

CONCLUSION

It has been shown that the response of rods to a random pressure field can be calculated provided that certain statistical descriptions of the pressure field are known. Also, no approximations are necessary in the calculational process (other than standard methods of numerical analysis) provided that the analytical expressions which describe the pressure field lend themselves to closed form integration over the space variables. It should be mentioned that Bakewell (10) has measured the pressure field on a body of revolution in water and has reported results which indicate the pressure field is similar to air

flows over flat plates and in pipes. However, the reader must refrain from deducing that the description of the pressure field used in the present analysis, accurately describes the pressure field acting on a rod in parallel water flow. Among other things, it remains to be shown that the instantaneous pressures acting on opposite sides of a cross-section of a rod, are statistically independent or uncorrelated. In general, it can be said that the precise measurements required to assess the response of structures to the highly disturbed flows which exist in nuclear reactors do not exist. Consequently, the investigator who desires to carry out an exercise similar to the one presented must take great liberties with the information presently available. An additional paper which may prove useful toward this end is that of Schloemer (11) who has assessed the effects of pressure gradients on wall pressure fluctuations in air flows.

ACKNOWLEDGMENT

This work was part of an investigation carried out in the University of Illinois. The senior author would like to thank the Nuclear Engineering Program and the Department of Theoretical and Applied Mechanics for their support during the investigation.

REFERENCES

1. W. A. Strawderman, "Turbulence-Induced Plate Vibrations: an Evaluation of Finite-and Infinite-Plate Models", J. Acous. Soc. Am., Vol. 46, No. 5 (Part 2) pp. 1294-1307 (1969).

2. J. M. Clinch, "Study of Vibrations Induced in Thin-Walled Pipes under Varying Flow Conditions", NASA Tech. Brief 67-10518, June 1967.

3. J. R. Reavis, "Vibration Correlation for Maximum Fuel-Element Displacement in Parallel Turbulent Flow", Nuc. Sci. Eng., Vol. 38, pp. 63-69 (1969).

4. Y. K. Lin, Probablistic Theory of Structural Dynamics, McGraw-Hill, 1967.

5. R. M. Kanazawa, "Hydroelastic Vibration of Rods in Parallel Flow", Ph. D. Thesis, University of Illinois, Urbana (1969).

6. G. M. Corcos, "The Structure of the Turbulent Pressure Field in Boundary-Layer Flows", J. Fluid Mech., Vol. 18, pp. 353-378 (1964).

7. H. Schlichting and J. Kestin, Boundary Layer Theory, Fourth Edition, McGraw-Hill, New York, 1960.

8. W. W. Willmarth and F. W. Roos, "Resolution and Structure of the Wall Pressure Field Beneath a Turbulent Boundary Layer", J. Fluid Mech., Vol. 22, pp. 81-94 (1965).

9. G. M. Corcos, "Resolution of Pressure in Turbulence", J. Acous. Soc. Am., Vol. 35, pp. 192-199 (1963).

10. H. P. Bakewell, Jr., "Turbulent Wall-Pressure Fluctuations on a Body of Revolution", J. Acoust. Soc. Am., Vol. 43, No. 6, pp. 1358-1363 (1968).

11. H. H. Schloemer, "Effects of Pressure Gradients on Turbulent-Boundary-Layer Wall-Pressure Fluctuations", J. Acoust. Soc. Am., Vol. 42, No. 1, pp. 93-113 (1967).

DISCUSSION

G. H. Toebes (Purdue U.): In order to get the picture clear, what you did essentially is to compute the response of a strip, a flat strip, loaded on one side, which is rather different from the rod case.

Kanazawa: Right. That is somewhat misleading in that I said a rod, although it's a matter of conjecture as to how you should warp the measured pressure fields. The data for flat-plate measurements, probably should be changed to conform to the boundary layer that exists on a rod. There is data from Bakewell for some type of projectile on which he claims they measured surface pressure fluctuations. However, I am very skeptical about his results.

Toebes: Would you care to make a preliminary comment? If you have the same strip loaded on both sides at the same time, the displacements could, of course, get larger.

Kanazawa: That is a very good point. It brings up the problem of correlating the pressure fluctuations on diametrically opposite positions on a rod. Those are measurements that also have to be made. I didn't mention it, but I meant to include it when I discussed the measurements that had to be made. They should include the net transverse pressure that acts on the rod. That is a very important point. If they are uncorrelated, of course, you just double the intensity. Until somebody comes up with those measurements, I think we are grasping at straws.

Toebes: One other comment. Students, as a classroom exercise, looked at the loading of such a strip with transverse correlation, and we put on not white noise but spectra that had a predominant frequency, like you would expect due to wakes, and it made a large difference.

Kanazawa: Do you mean screens and grids?

Toebes: Yes.

G. S. Rosenberg (ANL): The only thing I'd like to throw up for consideration is that, after listening to this, I am getting more and more curious about what the chances are of getting "some kind of characteristic distribution function" to permit one to "do something" about crossing-rate statistics, amplitude distributions, etc.

Kanazawa: You mean, using a forced random-vibration type of model? I myself think that if it's ever going to succeed, it's on this large simply-supported model in an annulus. This is a very good case to try this out on, and I think the results of Chen and Reavis show that parametrically you can do a pretty good job of describing what goes on. It's just a matter of getting the proper data for the forcing field acting on the rod. I don't think the structure of the forcing field changes too much, and we can rely on some data for spatial behavior of the pressure field from people dealing with wind tunnels. But until we have more reliable data taken in the same test section in which the displacement measurements are made, to get the two consistent, we're all sort of spinning our wheels conjecturing.

Rosenberg: Well, let me take one more spin. In the context of what we have been doing here, I think it's a big step to even bring up the subject of rod bundles. But some of us are most interested in getting to it. What I was wondering is, don't we have to account a little more for the test-chamber configuration, at least more than has been accounted for in some of the work that I've seen presented here so far? There may also be some practical conditions, where the acoustic properties of the media and test geometry, for example, might be significant in adjusting the displacement of the description functions.

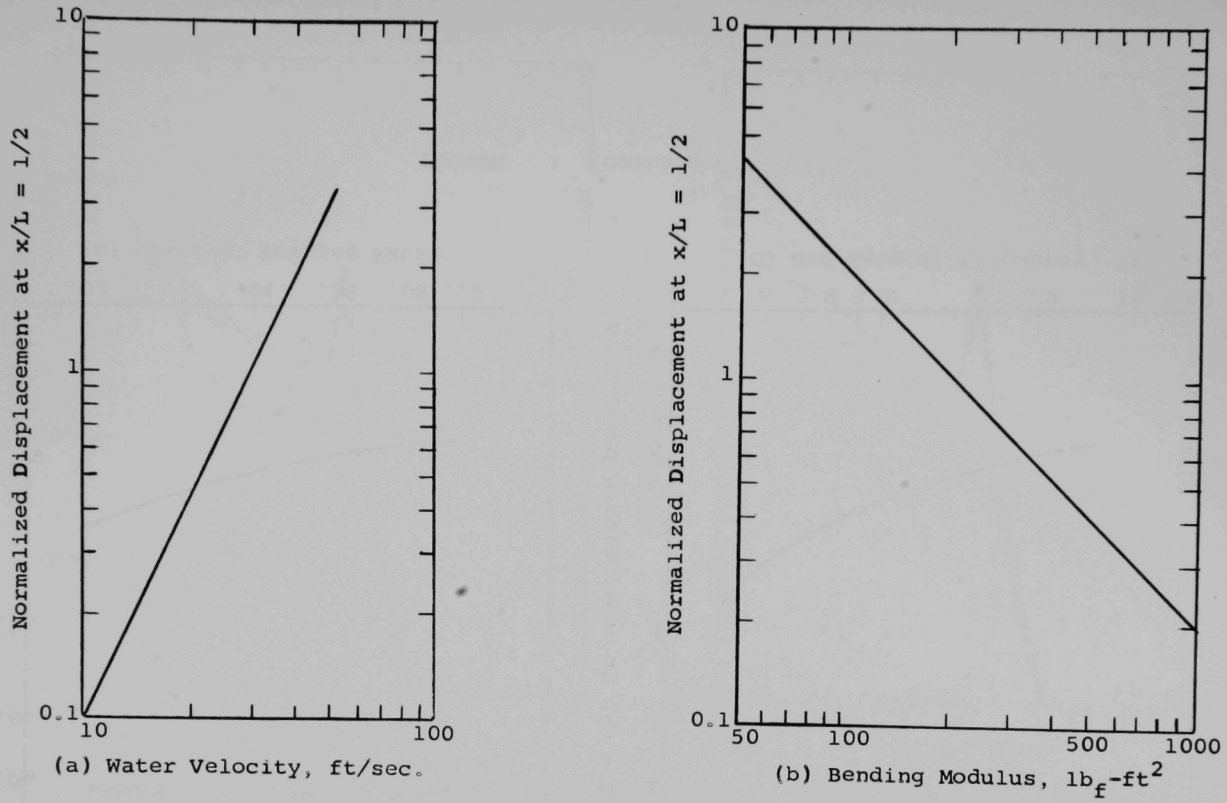

FIGURE 1 VARIATION OF RMS DISPLACEMENT WITH (a) WATER VELOCITY (b) BENDING MODULUS (c) DAMPING (d) ROD NATURAL FREQUENCY

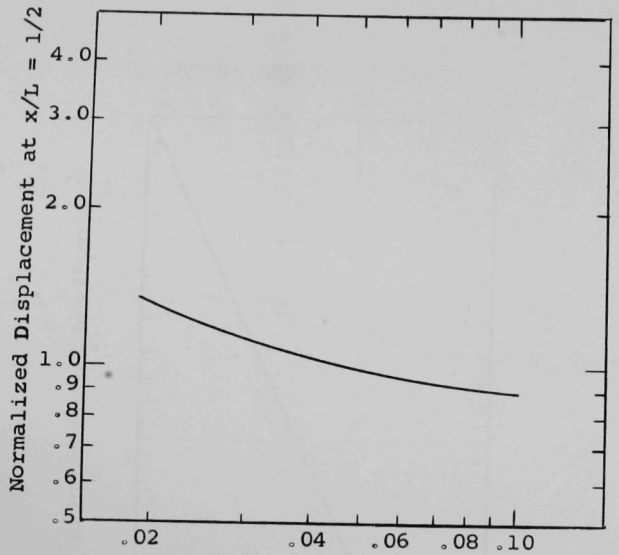

(c) Critical Damping Ratio

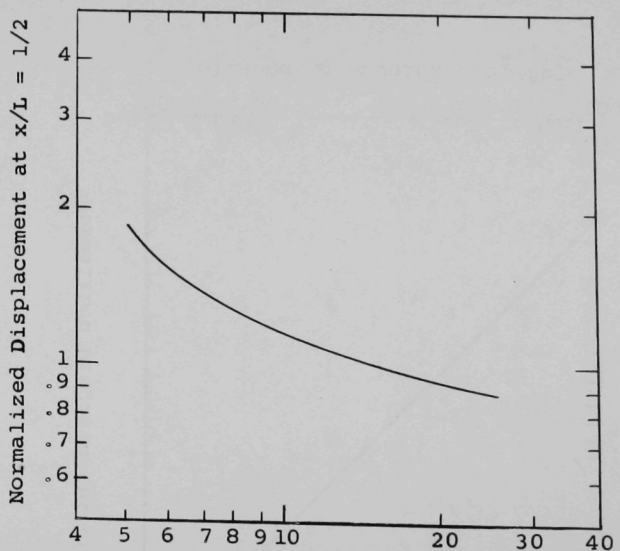

(d) Rod Natural Frequency, Hz

FIGURE 1 (Continued)

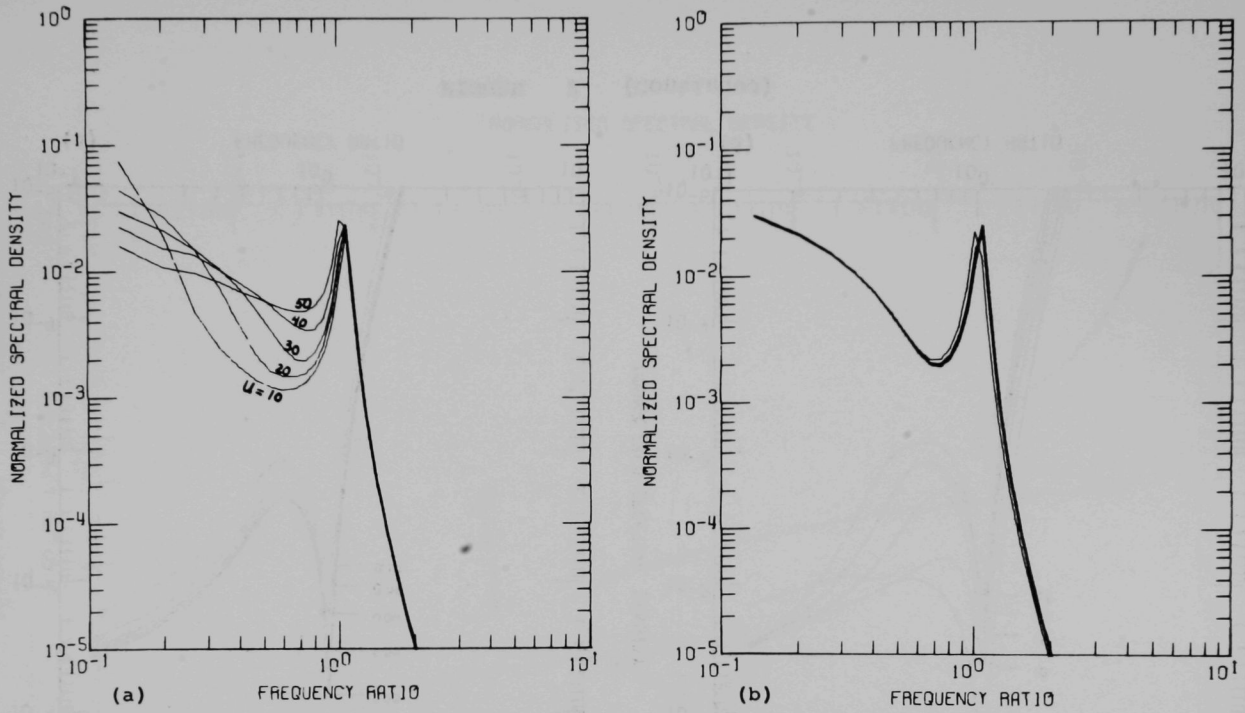

FIGURE 2 NORMALIZED SPECTRA OF ROD RESPONSE TO TURBULENT BOUNDARY LAYER PRESSURE FLUCTUATION. EFFECTS OF (a) WATER VELOCITY, (b) BENDING MODULUS, (c) DAMPING, (d) ROD NATURAL FREQUENCY, AND (e) POSITION ALONG ROD AND HIGHER MODES OF VIBRATION

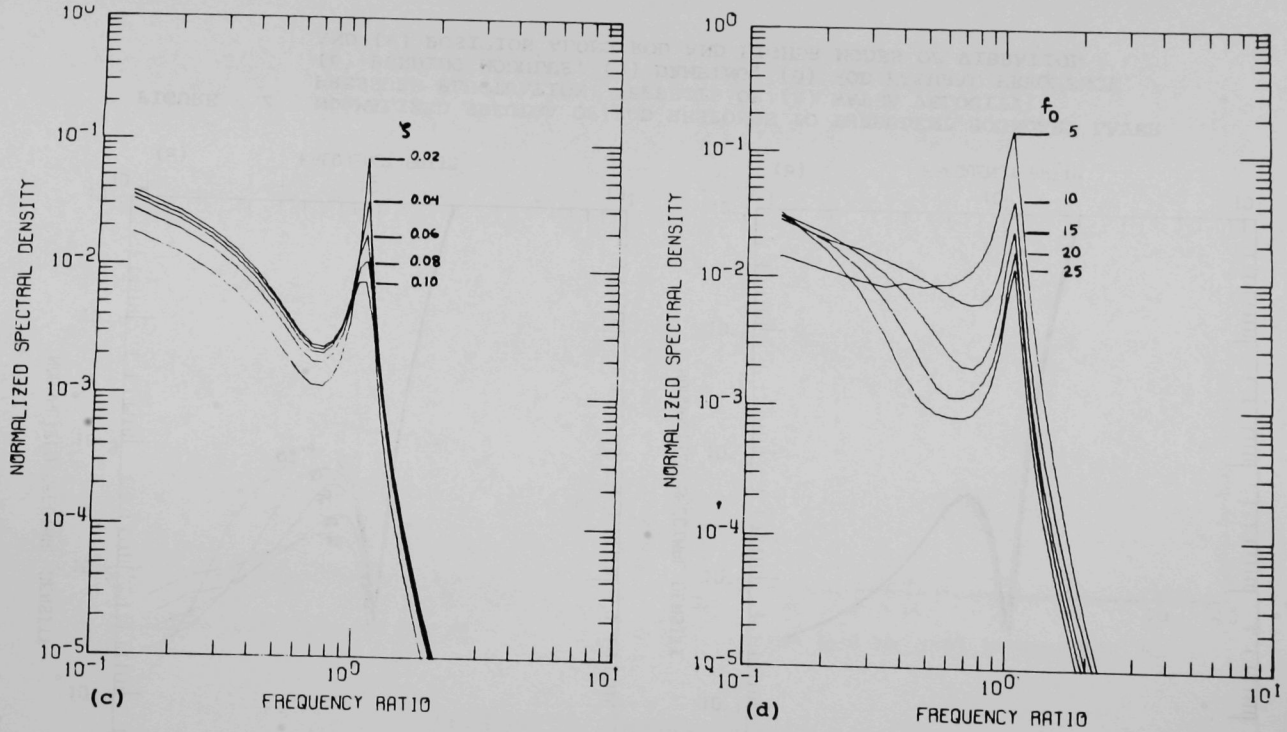

FIGURE 2 (Continued)

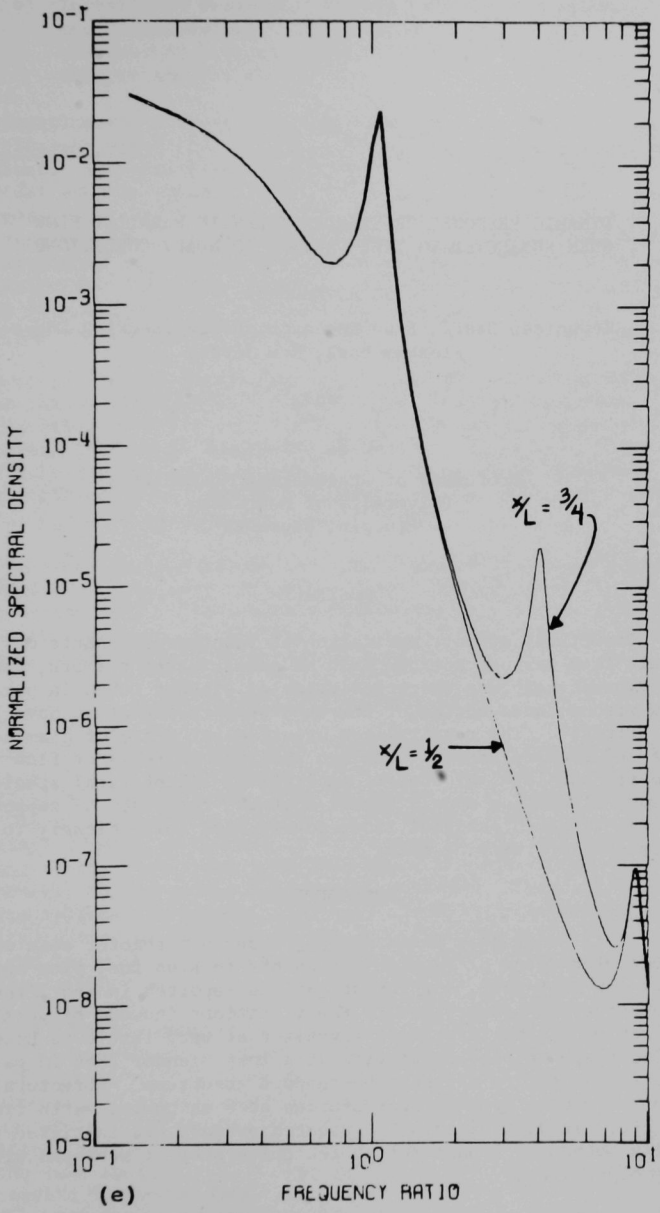

(e)

FIGURE 2 (Continued)

DYNAMIC RESPONSE OF SLENDER TUBES IN PARALLEL FLOW WHEN SUBJECTED TO TIME VARYING BOUNDARY CONDITIONS

S. A. Knudson

Technical Staff, Esso Research and Engineering Co.
Florham Park, New Jersey

and

G. M. Smith

Professor of Engineering Mechanics
University of Nebraska
Lincoln, Nebraska

ABSTRACT

Structural support excitation of reactor components may result from various sources such as pumps, earth tremors, etc. The dynamic response characteristics of slender tubes in parallel flow with induced motion of the tube support structure have been investigated. The results from experimental tests of clamped-free and clamped-pinned tubes are analyzed in terms of flow velocity and level of support excitation. Theoretical studies of several damping models reveal that the response, of support excited tubes in parallel flow, corresponds quite closely to a viscous type damping model.

INTRODUCTION

It is well known that fluid flowing through a reactor core can cause undesirable vibrations of reactor components such as fuel pins and control rods. For the most part, the investigations reported in the literature have been concerned primarily with the vibrations induced by parallel fluid flow. A review of the literature reveals that very little is known about the dynamic response characteristics of a long slender tube in parallel flow with forced motion of the tube support structure. Structural support excitations can come from various sources such as pumps, earth tremors, valving, etc. In view of this, a research project was initiated in the Engineering Mechanics Department at the University of Nebraska with the following objectives:

a) Determine functional relationships of fluid flow velocities and base excitation in relation to the dynamic response.

b) Investigate analytical models with various damping mechanisms suitable for predicting the dynamic response of slender tubes in coaxial flow with support excitation.

The experimental results obtained from tests conducted on clamped-free and clamped-pinned slender tubes (clamped end upstream) are presented in this paper. The data show the effects of the flow velocity and level of sinusoidal support excitation on the steady-state response. In the case of a clamped-free tube, the parallel flow velocity appears to have a significant damping effect on the tube vibrations. However, in the case of the clamped-pinned tube the damping mechanism is essentially independent of the flow velocity. Theoretical studies of the various types of damping mechanisms (complex modulus, viscous, and viscoelastic) reveal that this phenomenon can be explained to some extent from a theoretical point of view.

A study of the characteristics of the damping models investigated shows that the peak response of clamped-free tubes for the first two modes is best described by the linear viscous damping model. (Size of shaker system limited studies to the first two modes.) It is also found that the effect of tube length on the response can be taken into account by simply considering the relation between a viscous damping parameter α and the fundamental circular frequency ω_o of the tube.

Of considerable interest is the comparison of the damping parameter α of a clamped-free tube with that of a clamped-pinned tube. In the case of the clamped-free tube, α increases considerably as a linear function of the flow velocity. However, in the case of a clamped-pinned tube, α is found to be essentially independent of the flow velocity.

TEST FACILITIES AND PROCEDURES

In general, the test facilities (see Fig. 1) for the experimental studies consist of a water-recirculating system with a test section mounted horizontally on a shaker table which is driven by an electrodynamic shaker system. The test section consists of a 4-ft plexiglass tube 1-1/2 inches inside diameter which is mounted on the shaker table with flexible hose connections at the ends. The test cylinder (1/4-inch copper tube) is mounted concentrically within the plexiglass tube. The clamped end condition of the cylinder is accomplished by a combination of slender struts and an airfoil section as shown in Fig. 2. To eliminate swirling motion of the flow and to ensure uniform turbulence, a 6-inch-long straightener section (small tubes and screens) is inserted in front of the clamped-end support structure for the tube. The plexiglass tube, test tube support section, and flow straightener section, are securely attached to a 2" x 6" x 5' plank which is bolted to the shaker table. The shaker table consists of a 2-inch-thick aluminum plate supported by two thin vertical plates which act as elastic springs for motion in the horizontal plane. The shaker table is driven by an electrodynamic shaker so that the motion of the entire test section is horizontal and transverse to the longitudinal axis of the test section. Thus, the motion of the end supports of the tube tends to excite flexural vibrations of the test tube in the horizontal plane. The mean flow velocity is measured downstream from the test tube. Vibration tests in air showed the support or anchoring system for the

upstream end of the test tube to be essentially that of a fixed, or clamped, end condition.

The dynamic response of the test tubes (clamped-free and clamped-pinned) were measured by the output from two strain gages mounted internally in the test tube near the clamped end. One strain gage is located on a horizontal diameter and the other on a vertical diameter in order to measure strains due to bending in both the horizontal and vertical planes. The end of the tube downstream is sealed shut and the strain gage leads are brought out through the airfoil support section.

The steady-state strains (ϵ_h and ϵ_v) due to bending in the horizontal and vertical planes were monitored by a true root-mean-square meter. The resultant strain ϵ_r was used as a measure of the total dynamic response. It can be shown that the mean-square value of the resultant strain, $\langle \epsilon_r^2 \rangle$, is

$$\langle \epsilon_r^2 \rangle = \langle \epsilon_h^2 \rangle + \langle \epsilon_v^2 \rangle \tag{1}$$

where $\langle \epsilon_h^2 \rangle$ and $\langle \epsilon_v^2 \rangle$ are the mean-square values of the corresponding rms values of ϵ_h and ϵ_v. Since the rms value of a variable is simply the square root of the mean-square value, then the rms value of the resultant strain, $\bar{\epsilon}_r$, is simply

$$\bar{\epsilon}_r = \sqrt{\langle \epsilon_h^2 \rangle + \langle \epsilon_v^2 \rangle} \ . \tag{2}$$

Thus, the rms resultant strain $\bar{\epsilon}_r$ was easily obtained without giving consideration to any phase relationship between ϵ_h and ϵ_v.

Experimental data was first obtained for the vibration response of a clamped-free tube 28 inches long in which the double amplitude λ of the support excitation ranged from 0.02 inch to 0.14 inch. The flow velocity u was varied from 0 to approximately 20 ft/sec. To determine the effect of tube length on the viscous damping parameter α, data were obtained for 25- and 22-inch clamped-free tubes that were provided by cutting off the free end of the 28-inch tube.

The 22-inch tube was pinned at the end downstream for the clamped-pinned end condition. The pinned connection for the 22-inch tube was obtained by soldering a 1/4" copper tube 1 inch long at right angles to the test tube. This served as a bearing for a brass pin inserted through the walls of the plexiglass tube. The brass pin was aligned vertically for pinned action to bending in the horizontal plane but with considerable resistance to bending in the vertical plane. For comparable strain levels, the required displacement amplitudes of the support excitation for the clamped-pinned tube were considerably less than for the clamped-free tubes. Due to low displacement amplitudes and higher frequencies of excitation, it was necessary to control on acceleration with the electrodynamic shaker system used. The support excitation level for the clamped-pinned tube ranged from 1g to 2.5g's (g = 386 in/sec^2). The acceleration levels of 1g to 2.5g's resulted in double amplitude displacements ranging from approximately 0.006 to 0.0165 inch. The displacement amplitudes were calculated from the sinusoidal acceleration levels and corresponding frequencies.

To facilitate the comparison of the experimental data with the viscous damping model discussed later, the vibration response was expressed in terms of the dimensionless quantity $2\bar{\epsilon}_r \ell^2/\rho\bar{\lambda}$, where $\bar{\epsilon}_r$ is the rms value of the resultant strain, ℓ is the length of the tube, ρ is the distance from the neutral axis to the measured strain, and $\bar{\lambda}/2$ is the rms value of the support excitation amplitude. For a given flow velocity and support excitation amplitude, the response was determined as a function of the frequency ratio F/F_o, where F_o is the first mode natural frequency of the tube.

VIBRATION RESPONSE OF CLAMPED-FREE TUBES

Typical strain-time responses of vertical and horizontal motions at resonance ($F/F_o = 1$) are shown in Fig. 3. The predominant horizontal motion is due to the tube support excitation in the horizontal plane. The vertical motion is due to the vertical excitation resulting from vortex formations which are caused by the horizontal flexural vibrations of the tube.

The general effects of the flow velocity on the ratio $\bar{\epsilon}_v/\bar{\epsilon}_h$ of the rms values of strain due to the vertical and horizontal motions are shown in Fig. 4. Although the maximum value of $\bar{\epsilon}_v/\bar{\epsilon}_h$, for zero flow, depended to some extent on the level of support excitation, the ratio was above unity for all levels of support excitation used. It is noted that the inverted peaks become more pronounced as the flow velocity increases. In addition, it was observed during the tests that the vertical motion tended to remain essentially constant throughout a frequency sweep for the higher flow velocities. For a given value of F/F_o, the increase in the ratio $\bar{\epsilon}_v/\bar{\epsilon}_h$ is due primarily to the self-induced excitation caused by the parallel flow. These observations indicate that the "wiping" action of the coaxial flow in effect disturbs or inhibits vortex formations.

As reported by other investigators (1, 2, 3), the vibrations induced by fluid flow only ($\lambda = 0$) were found to depend upon the flow velocity u to some power as shown in Fig. 5. It is of interest to note that the resultant rms strains for the 22- and 25-inch tubes are essentially identical with $\bar{\epsilon}_r \propto u^{1.73}$. This is considerably different than $\bar{\epsilon}_r \propto u^{1.16}$ for the 28-inch tube. At this time the authors have no logical explanation as to why the exponent for the 28-inch length is considerably different from that of the other two lengths.

The resultant rms strains for the 22-inch tube at resonance ($F/F_o = 1$) with parallel flow and tube support excitation are shown in Fig. 6. If the flow-induced vibrations (zero support excitation) are excluded, it is apparent that the resultant rms strains at resonance are a linear function of the support excitation amplitudes for each of the different flow velocities shown. It is also apparent that the coaxial flow acts as a strong damping mechanism and that the magnitude of damping increases with an increase in flow velocity. With sufficient support excitation, it is noted that the response data for the lower flow velocity (u = 5.88 ft/sec) begins to deviate from the linear relationship and tends to merge with the zero data. Thus, it appears that the zero flow condition describes an upper bound for the support excited system.

The response data for the 25- and 28-inch-long tubes exhibited the same general response characteristics as that of the 22-inch tube shown in Fig. 6. For a given flow velocity, the resultant rms strain $\bar{\epsilon}_r$ in the linear region may be expressed in terms of a slope β as

$$\bar{\epsilon}_r \propto \beta\lambda = f(u)\lambda$$

in which the slope β is a function, f(u), of the flow velocity u. Log-log plots of the slopes β as a function of u are shown in Fig. 7 for the three different lengths. From Fig. 7 it is found that

$$\beta = Su^{-0.81} \tag{3}$$

where S is simply a constant of proportionality which depends upon the tube length. Thus, the resultant rms strain at resonance from the clamped-free tubes in the linear regions may be expressed in the form

$$\bar{\epsilon}_r = S\lambda u^{-0.81} \quad . \tag{4}$$

Equation 4 shows that the peak response of clamped-free tubes can be described by the product of a linear function of support excitation and a nonlinear function of flow velocity.

For the clamped-free tubes, it appears (see Fig. 6) that the dynamic response is characterized by three separate regions as shown in Fig. 8. It is realized that in reality the three regions are not as clearly defined as those shown in Fig. 8, but that there is a gradual transition from one region to another. The response to the left of dashed line 1 is due primarily to a flow-induced forcing function. Between dashed lines 1 and 2, the response can be described by a linear function (see Eq. 4) in which the slope depends upon the flow velocity. Beyond 2, the response tends to approach a limit described by the condition of zero flow.

VIBRATION RESPONSE OF CLAMPED-PINNED TUBE

The resultant rms strains at resonance for the 22-inch tube are shown in Fig. 9. It is noted that the flow velocities for the clamped-pinned tube are of the same order of magnitude as those used in the clamped-free tube tests. However, it should be noted that the support excitation amplitudes, $\lambda/2$, are in the order of only one tenth of those for the clamped-pinned tubes. A comparison of Fig. 9 with Fig. 6 shows that the strains for the small support excitations of the clamped-pinned tube are, in general, above the strain levels of the clamped-free tube.

It is imperative to note that the response characteristics, Fig. 9, of the clamped-pinned tube are significantly different in several respects from those of the clamped-free tube, Fig. 6. First, it is noted that the resultant rms strains of the clamped-pinned tube, for the different flow velocities, are linear functions of the support excitation which do not pass through zero. Since the strains due to the flow-induced vibrations ($\lambda = 0$) were very small (around 5 micro-inches per in.), it can be concluded that the response must increase quite rapidly for small support excitations somewhere below 0.005 inch DA. It is further noted that the slopes of the response data are essentially independent of the flow velocity.

The results shown in Fig. 9 suggest that the strain $\bar{\epsilon}_r$ in the straight line region is of the form

$$\bar{\epsilon}_r = b + m\lambda = g(u) + m\lambda \tag{5}$$

where b is the hypothetical intercept which is a function, g(u), of the flow velocity u, and m is the slope. Relevant information on g(u) in relation to system parameters is lacking at this time due to the limited studies conducted to date on clamped-pinned tubes.

Another significant difference between the results shown in Figs. 6 and 9 is that the parallel flow acts as a strong damping mechanism in the case of clamped-free tubes but is a rather weak damping mechanism in the case of clamped-pinned tubes.

Some of the differences found between the response characteristics of the two types of end conditions can be rationalized to some extent from a study of damping models which now follows.

SYNTHESIS OF DAMPING MODELS FOR BEAMS GOVERNED BY EULER'S BEAM EQUATION

In order to get a quantitative insight into the effect of system parameters on the dynamic response of support-excited tubes in coaxial flow, various types of damping models were investigated for comparison with the experimental studies of the clamped-free tubes. The linear damping models included complex modulus damping, viscoelastic damping, and viscous damping. In the case of support excitation of beams, the motion of the supports correspond to time-varying boundary conditions.

The partial differential equations governing the damping models investigated are as follows:

a) <u>Complex Modulus Damping</u>

$$\frac{E^* r^2}{\gamma} \frac{\partial^4 y}{\partial x^4} + \frac{\partial^2 y}{\partial t^2} = 0 \tag{6}$$

where $E^* = E(1 + j\delta)$ = complex modulus
E = modulus of elasticity
$j = \sqrt{-1}$
δ = loss factor
γ = mass density
r = radius of gyration

b) <u>Viscoelastic Damping</u>

$$\frac{Er^2}{\gamma} \frac{\partial^4 y}{\partial x^4} + \frac{Fr^2}{\gamma} \frac{\partial^5 y}{\partial x^4 \partial t} + \frac{\partial^2 y}{\partial t^2} = 0 \tag{7}$$

where E, r, and γ are as previously defined. The viscoelastic constant F is a parameter for the Kelvin model which is described by

$$\sigma = E\epsilon + F\dot{\epsilon}$$

where σ = stress due to bending
ϵ = strain
$\dot{\epsilon}$ = strain rate

c) Viscous Damping (proportional to velocity)

$$\frac{Er^2}{\gamma}\frac{\partial^4 y}{\partial x^4} + \frac{C}{A\gamma}\frac{\partial y}{\partial t} + \frac{\partial^2 y}{\partial t^2} = 0 \tag{8}$$

where C = damping coefficient
A = cross-sectional area of beam

If the ends (one or both) of the beam are subjected to sinusoidal motion, steady-state solutions to Eq. 6, 7, or 8 may be taken in the form

$$y = Xe^{j\omega t} \qquad j = \sqrt{-1} \tag{9}$$

where ω is the circular frequency of the support excitation and X is a function of x which depends on the conditions at the ends of the beam. The substitution of Eq. 9 into either Eq. 6, 7, or 8, results in the equation

$$X^{IV} - (k^*)^4 X = 0 \tag{10}$$

where k* is a complex quantity in which the imaginary part describes the system damping. The general solution to Eq. 10 is the familiar equation

$$X = C_1 \cosh k^*x + C_2 \sinh k^*x + C_3 \cos k^*x + C_4 \sin k^*x \tag{11}$$

where the complex constants (C_1, C_2, C_3, and C_4) depend upon the boundary conditions which include the support excitation at the ends. For comparison purposes, the complex quantity k* for the different damping models are shown in table I.

For a given set of conditions, such as exciting frequency, temperature, etc., the steady-state response of a given beam may be described by any one of the models if an appropriate value for the imaginary part of k* is selected. However, a damping parameter value for a particular type of damping may give poor results under different conditions than those for which it was determined. A suitable linear model with an appropriate damping parameter for the first mode should also describe higher order mode response. In the experimental studies of the clamped-free tubes, it was found that the second mode resonant response was in the order of 10 times that of the first mode for a given support excitation and flow velocity. The ratio of the second mode response to the first mode response was considerably less than the factor of 10 for the complex and viscoelastic type damping. However, when the viscous model was fitted to the first mode response of the experimental data, the theoretical results of the viscous model were, in all cases, within 10 percent or less (usually within 5 percent) of the second mode response for the range of support excitations and flow velocities used. Therefore, the experimental studies to date have been analyzed in terms of the viscous damping model.

TABLE I - Complex terms for different damping models

Damping Model	k*	Remarks
Complex Modulus	$\left(\frac{\gamma\omega^2}{Er^2}\right)^{\frac{1}{4}} (1+j\delta)^{-\frac{1}{4}}$	For a constant loss factor δ, the damping is independent of frequency
Viscoelastic	$\left(\frac{\gamma\omega^2}{Er^2}\right)^{\frac{1}{4}} \left(1+\frac{j\omega F}{E}\right)^{-\frac{1}{4}}$	For constant values of E and F, the damping parameter, $\omega F/E$, increases with frequency
Viscous	$\left(\frac{\gamma\omega^2}{Er^2}\right)^{\frac{1}{4}} \left(1-\frac{jC}{A\gamma\omega}\right)^{\frac{1}{4}}$	For constant values of C, A, and γ, the damping parameter, $C/A\gamma\omega$, decreases with ω.

SUPPORT EXCITATION OF CLAMPED-FREE AND CLAMPED-PINNED TUBES WITH VISCOUS DAMPING

For further discussion of the experimental results, it is essential that we consider the effect of end conditions on viscously damped beams with support excitation. The coordinate system and end conditions for the clamped-free and clamped-pinned end conditions are shown in Fig. 10.

From Eq. 11, the strain at x = 0 is found to be

$$\epsilon(0,t) = \rho\frac{\partial^2 y}{\partial t^2} = \rho(k^*)^2 \left[C_1 - C_3\right] e^{j\omega t} \tag{12}$$

where ρ is the distance from the neutral axis to the measured strain. For viscous damping (see table I), we may write

$$(k^* \ell) = \left(\frac{\gamma\omega^2 \ell^4}{Er^2}\right)^{\frac{1}{4}} \left(1 - j\,\frac{C}{A\gamma\omega}\right)^{\frac{1}{4}} . \tag{13}$$

We now define a damping parameter α in terms of the fundamental circular frequency ω_o as

$$\alpha = C/A\gamma\omega_o \tag{14}$$

where C is a viscous damping coefficient and $A\gamma$ is the mass per unit length which includes the virtual mass of the fluid. From Euler's beam theory we also have

$$\left(\frac{\gamma\omega^2 \ell^4}{Er^2}\right)^{\frac{1}{4}} = \left(\frac{\omega}{\omega_o}\right)^{\frac{1}{2}} (k_o \ell) \tag{15}$$

where $k_o\ell$ is the eigenvalue corresponding to the first mode. Thus, we may write from Eq. 13

$$k^*\ell = \left(\frac{f}{f_o}\right)^{\frac{1}{2}} (k_o\ell)\left(1 - \alpha\frac{f_o}{f}\right)^{\frac{1}{4}} \tag{16}$$

where $k_o\ell$ = 1.875 (clamped-free)
$k_o\ell$ = 3.928 (clamped-pinned)
f = Exciting frequency, cps
f_o = Natural frequency of first mode, cps

From Eq. 11 and the end conditions shown in Fig. 10, we find for the clamped-free beam

$$\left.\begin{aligned} C_1 &= \frac{\lambda}{2}\,\frac{(\cosh k^*\ell \cos k^*\ell + \sinh k^*\ell \sin k^*\ell + 1)}{2(\cosh k^*\ell \cos k^*\ell + 1)} \\ C_3 &= \frac{\lambda}{2} - C_1 \\ C_1 - C_3 &= 2C_1 - \frac{\lambda}{2} \end{aligned}\right\} \tag{17}$$

Similarly for the clamped-pinned beam, we find

$$\left.\begin{aligned} C_1 &= \frac{\lambda}{2}\,\frac{(\sinh k^*\ell + \sin k^*\ell - 2\cos k^*\ell \sinh k^*\ell)}{2(\cosh k^*\ell \sin k^*\ell - \cos k^*\ell \sinh k^*\ell)} \\ C_3 &= \frac{\lambda}{2} - C_1 \\ C_1 - C_3 &= 2C_1 - \frac{\lambda}{2} \end{aligned}\right\} \tag{18}$$

Denoting $C_1 = \lambda C_1'/2$ and $C_3 = \lambda C_3'/2$, the <u>magnitude</u> of the steady-state response can be formulated from Eq. 12 in the dimensionless form

$$\frac{2\epsilon\ell^2}{\lambda\rho} = \left|(k^*\ell)^2(C_1' - C_3')\right| \tag{19}$$

where $k^*\ell$, C_1', and C_3' depend upon the frequency ratio f/f_o and the damping parameter α as noted in Eqs. 16, 17, and 18. An IBM 360/65 computer was used to evaluate the right-hand side of Eq. 19 with a variation in the variables f/f_o and α. A typical frequency-response curve comparing the results of Eq. 19 (α = 0.225) with some experimental data is shown in Fig. 11.

The computed results from Eq. 19 for the resonant response as a function of α for the two different end conditions are shown in Fig. 12.

DISCUSSION

Values of the damping parameter α were determined from Eq. 19 so as to match the resonant response of the experimental data for the first mode. For comparison purposes, α values were also determined for tests in air.

Ratios of $\alpha_{fluid}/\alpha_{air}$ for the 22-inch tubes are shown in Fig. 13 as a function of the flow velocity. It is noted that the ratio for the clamped-free case is, in general, considerably greater than the ratio for the clamped-pinned case. Also the ratio for the clamped-free tube shows an appreciable increase with flow velocity while the ratio for the clamped-pinned tube changes very little with the flow velocity. These observations are consistent with the results previously shown in Figs. 6 and 9.

In order to explain the results shown in Fig. 13, we refer again to Fig. 12 and note the values of α shown for the two types of end conditions with u slightly less than 6 ft/sec. The value of $\alpha = 0.1125$ (clamped-pinned curve) falls in the region where small changes in α tend to result in an appreciable change of the dimensionless quantity $2\epsilon_r \ell^2/\rho\lambda$. Therefore, this is one possible explanation as to why there is no appreciable change in α with the flow velocity in the case of the clamped-pinned tube. However, the value of $\alpha = 0.225$ (clamped-free) is in a region where the response is rather insensitive to changes in α. Thus, a small change in the quantity $2\epsilon_r \ell^2/\rho\lambda$ requires an appreciable change in α for clamped-free tubes. This means that if the quantity $2\epsilon_r \ell^2/\rho\lambda$ decreases slightly with an increase in flow velocity an appreciable increase in α is to be expected. Therefore, it seems logical to expect a significant increase in α with flow velocity as shown in Fig. 13.

From a basic point of view, we must consider the damping parameter in relation to the variables C, A, γ, and ω_o. Undoubtedly the damping coefficient C depends to some extent upon the fluid viscosity, tube diameter, and parallel flow velocity. If C, A, and γ are assumed to be the same for identical tubes having two different end conditions, then the α values for the different end conditions should be related to each other by the system frequencies since $\alpha = C/A\gamma\omega_o$. Considering the eigenvalues for clamped-free and clamped-pinned tubes, this hypothesis gives

$$\frac{\alpha(\text{clamped-free})}{\alpha(\text{clamped-pinned})} = \left(\frac{3.928}{1.875}\right)^2 = 4.4 \ .$$

We note that the ratio of 4.4 is more than twice the ratio of the α values (0.225/0.1125 = 2) shown in Fig. 12. This indicates that C is quite different for the two end conditions. The authors are of the opinion that the fluid shear at the free end of a clamped-free tube has a significant effect on the apparent value of C which was assumed constant all along the tube in deriving Eq. 8.

The analysis of the data for the tests of the clamped-free tubes of different lengths showed that α, for a given flow velocity, varied inversely with the resonant frequencies of the different lengths. Since the frequency ω_o is inversely proportional to the square of the length, we may write

$$\frac{\alpha_1}{\alpha_2} = \frac{(\omega_o)_2}{(\omega_o)_1} = \left(\frac{\ell_1}{\ell_2}\right)^2$$

where the subscripts 1 and 2 refer to tubes of lengths ℓ_1 and ℓ_2. Table II shows that the ratio of the α's for the 28- and 22-inch tubes, for different

TABLE II. Comparison of α values for 28- and 22-inch clamped-free tubes

Flow Velocity, ft/sec	$\left(\frac{\ell_1}{\ell_2}\right)^2 = \left(\frac{28}{22}\right)^2 = 1.61$	$\frac{\alpha_1 \text{ (28-in. tube)}}{\alpha_2 \text{ (22-in. tube)}}$
5.88	1.61	1.60
10.25	1.61	1.57
14.65	1.61	1.66
18.5	1.61	1.66

flow velocities, are all within 3 percent of the theoretical ratio $(\ell_1/\ell_2)^2 = 1.61$. The good correlation between the damping parameter α and tube length ℓ is further evidence that a clamped-free tube in parallel flow with support excitation behaves according to a viscous damping model.

In the case of clamped-pinned tubes, the effect of length on the damping parameter α is currently not known since the tests to date have involved only the 22-inch-long tube.

SUMMARY AND CONCLUSIONS

The following conclusions are based on the experimental and theoretical studies of slender tubes (clamped-free and clamped-pinned) in parallel flow with sinusoidal support excitation:

1) The vibration response characteristics of a clamped-free tube are quite different from those of a clamped-pinned tube.

2) The resonant response of clamped-free tubes is directly proportional to the support excitation level in which the slope of the linear function depends upon the flow velocity (see Eq. 4).

3) The resonant response of clamped-pinned tubes also varies linearly with the level of support excitation in which the straight-line intercept at $\lambda = 0$ appears to be a function of the flow velocity (see Eq. 5). However, the straight-line slopes are independent of the flow velocity.

4) The general response characteristics can be described in terms of a viscous damping parameter α. For clamped-free tubes and a given flow velocity, the second-mode response at resonance can be predicted quite accurately from a value of α selected to match the resonant response of the first mode. As further evidence in support of the viscous damping model, it was found that α varies as the square of the tube length for a given flow velocity. This follows from the fact that $\alpha = C/A\gamma\omega_0$ in which ω_0 is inversely proportional to the square of the length.

5) In the case of clamped-free tubes, the parallel flow acts as a strong damping mechanism which is characterized by a significant increase in the damping parameter α as the flow velocity increases. However, in the case of the clamped-pinned tube, the parallel flow had very little effect on the vibration response and as a result the damping parameter α appears to be essentially independent of the flow velocity.

It is hoped that the research reported in this paper will serve as a foundation for further studies of support-excited tubes in parallel flow. Certainly more basic studies are needed to determine the effects and relations of tube diameter, flow velocity, and fluid viscosity on the damping coefficient C. The validity of the viscous damping model for predicting higher mode response of clamped-pinned and clamped-clamped tubes also needs to be investigated. In addition, there is a need for studies of other types of support excitation such as narrow- and wide-band random excitation.

ACKNOWLEDGMENTS

The authors are appreciative of NSF funds granted for the purchase of vibration equipment used on the research project. We also want to thank Mr. Rao Kommineni for his efforts in obtaining some of the computer results.

REFERENCES

1. Paidoussis, M. P., "The Amplitude of Fluid-Induced Vibration of Cylinders in Axial Flow," AECL-2225, 1965 (Atomic Energy of Canada Limited), Chalk River Nuclear Laboratories, Canada.

2. Quinn, E. P., "Vibration of Fuel Rods in Parallel Flow," USAEC Report GEAP-4059, July 1962, General Electric Co., San Jose, California.

3. Wambsganss, Jr., M. W., and Boers, B. L., "Parallel-Flow-Induced Vibration of a Cylindrical Rod," ASME Publication, 68-WA/NE-15, Nuclear Engineering Division, Presented at Winter Meeting, Dec. 1-5, 1968.

DISCUSSION

D. R. Miller (KAPL): I would like to offer a possible explanation of a factor that would contribute to the damping behavior you observed. When the tube vibrates laterally, water oscillates circumferentially in the angular space between the rod and the tube. The water then has kinetic energy. If I have longitudinal flow, some of the kinetic energy is lost. There is the kinetic energy that would have been converted back to potential energy in bending the tube when it's brought to rest. Some of that energy is swept downstream. That effect is more pronounced with a cantilever than it is with a clamped-pinned tube. So, I presume that this effect might have been contributory. One way to get some insight into whether this might be true is to note whether the natural frequency changed perceptibly with flow velocity.

Smith: No, it did not.

Miller: I recall a paper published in the Civil Engineering Journal, a paper on crossflow excited vibration of a cylinder. There they found the frequency of vibration to diminish with increasing flow velocity and with increasing response, and also the response curve was chopped off. Apparently what was happening, after they passed the peak of response, was that damping was being introduced by virtue of kinetic energy being carried away rather than being converted back into elastic deformation.

Smith: We recognize that there now have to be some basic studies. We're convinced that the viscous model is the best one; at least what we've done so far indicates it's by far the best model. You can change conditions for a given flow velocity, you can change length of tube and end conditions, or you can select parameters from one test and go to other conditions, but we need more basic information on this constant C that includes a lot of things.

Miller: I'd like to make another comment. I would not be surprised if, having reversed the velocity in the tube, the direction of the flow in the tube, with a cantilever, would very likely be unstable. I have seen situations where that is true. With the flow impinging on the free end of the cantilever, it is very likely to be set into the self-excited vibration.

G. H. Toebes (Purdue U.): Possibly I did miss something in the presentation, but when a rod is moved, there will be a transient lift. This transient lift propagates downstream with the outer flow velocity. Therefore, data of this kind always should be presented in terms of the so-called reduced frequency, as is common in all flutter calculations. You presented a graph that showed damping as a function of velocity. If you plot this as a function of reduced frequency, that is, displacement times excitation frequency divided by flow velocity, you should probably find that the slope of these curves is inversely proportional to the flow velocity. Now, this had nothing to do with viscous damping of any kind. It is a very normal reduced frequency that was being used in flutter calculations.

P. M. Moretti (Westinghouse): I was puzzled by something you said about the vertical vibration related to the horizontal vibration. What was the frequency relationship between the vertical and horizontal vibrations? Was it the same?

Smith: Yes, the same.

Moretti: That's the way it looked in the picture. Do you know anything about the phase relationship?

Smith: No, we didn't make a study of it.

Moretti: It just struck me that if it had the same frequency, then the explanation that it was coupled in by some kind of hydrodynamic phenomenon like vortex shedding or eddy formation or something like that is not applicable. It would probably be some peculiarity of the foundation of either the whole tube or of the cantilever, or whatever is in the tube, and the fact that this does appear with flow velocity was only due to the effects that have been discussed now, which are these apparent damping effects due to the translation of the induced velocities in the

fluid. In any case, I don't think you could deduce from the horizontal vibration that there is some kind of a boundary-layer vortex-shedding phenomenon involved. This would appear then at a double or even higher frequency, if it did appear.

Smith: Well, the strength of the vortex shedding should depend somewhat upon the amplitude and relative velocity between the fluid and the tube. We get the largest amplitudes around resonance, of course, in the horizontal plane.

S. S. Chen (ANL): For the clamped-pinned rod, I think you can see that is a conservative system. In my judgment it is perfectly all right to consider the rod, supported at both ends as a conservative system. But I wonder about a cantilevered rod, because that is essentially the same as a cantilevered rod subject to the follower force; that is not a conservative system but you treat it as a conservative system. I wonder if that may explain some discrepancy over there. Since a clamped-free rod is the nonconservative system, my question is how good is it to treat a nonconservative system as a conservative system?

Smith: I didn't follow that.

Chen: Well, if you have a rod immersed in parallel flow and supported at one end only, then that is the same as a rod subject to a follower force; that is, a force which is always tangent to the free end.

Smith: The whole system moved parallel. We didn't just move one end.

Chen: Yes. But the fluid force always acted directly tangent to the end of the deformed rod.

G. S. Rosenberg (ANL): I think what he was trying to do was account for the possibility of a longitudinal drag force which is tangential to the rod and acts as a follower force. That is where you have a nonconservative system.

Smith: Once again, this hasn't been a basic study. We lumped a lot of things into this constant C and were looking for a mathematical model we could use.

Fig. 1 - Closed loop test facilities.

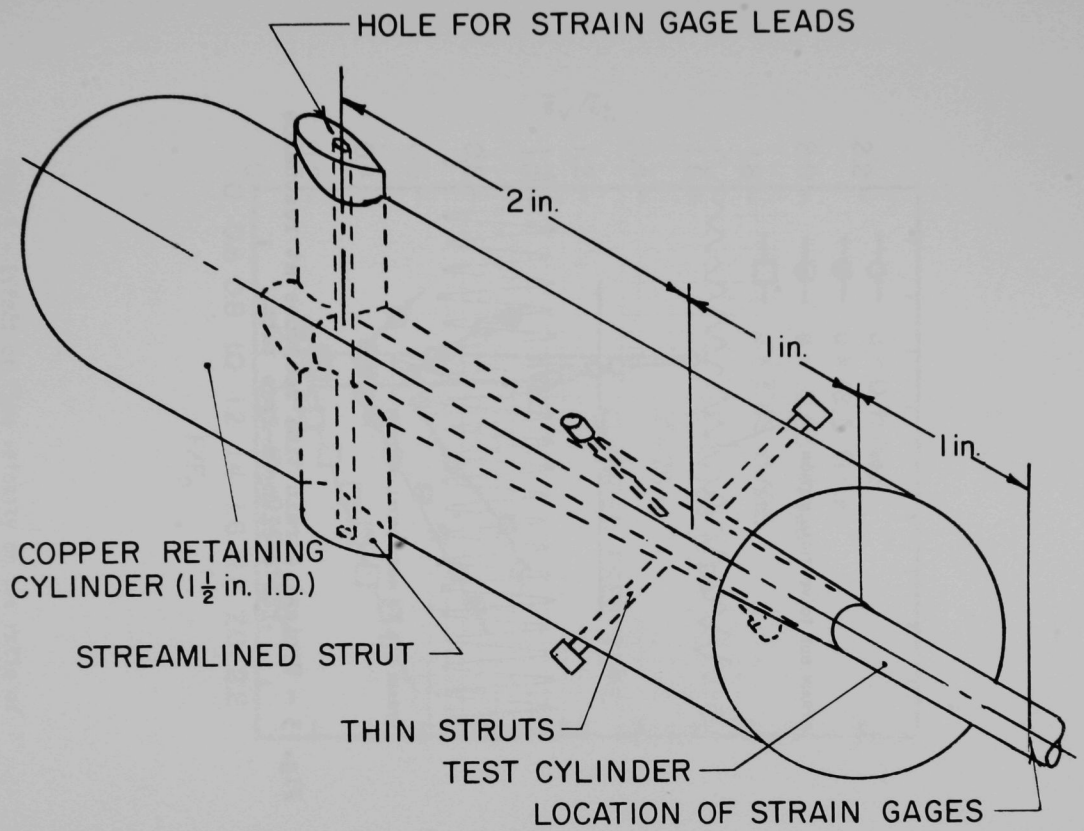

Fig. 2 Clamped-end support structure assembly.

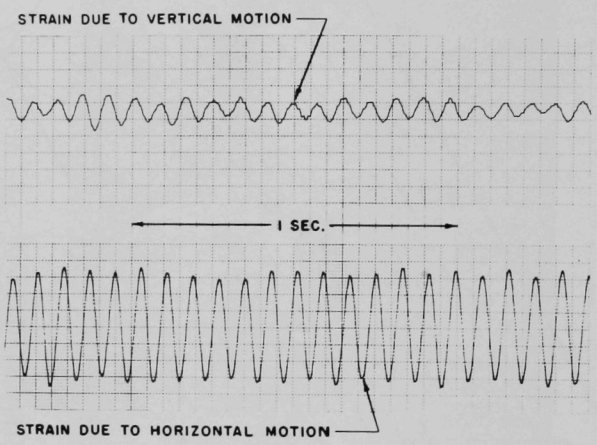

Fig. 3 - Typical strain time response at resonance for a clamped-free tube.

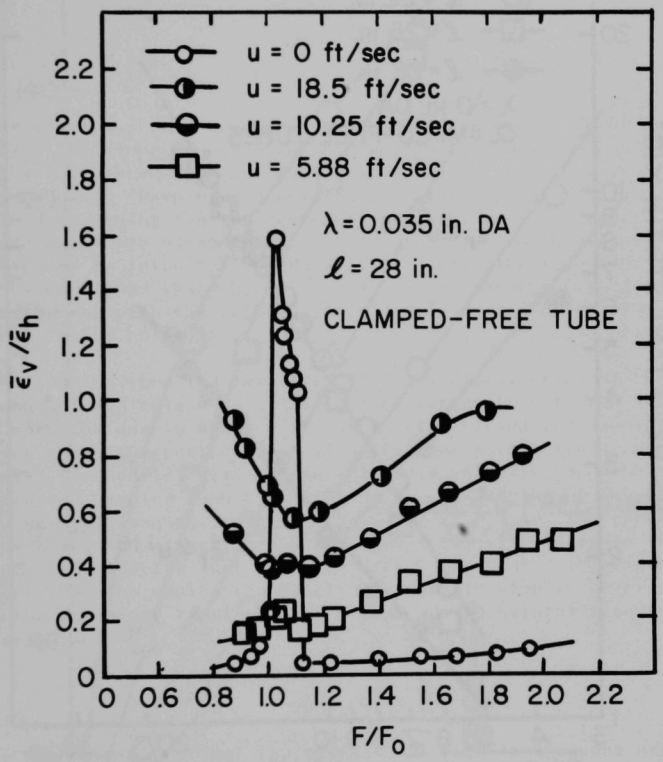

Fig. 4 - Effect of flow velocity on the ratio of strains resulting from bending in the vertical and horizontal planes.

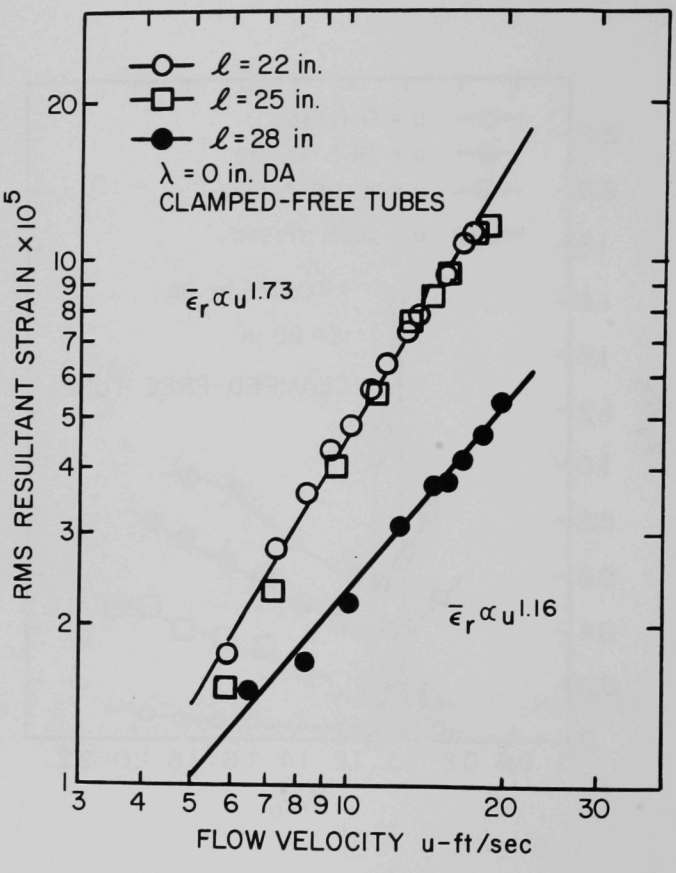

Fig. 5 - Resultant rms strain due to only flow-induced vibrations.

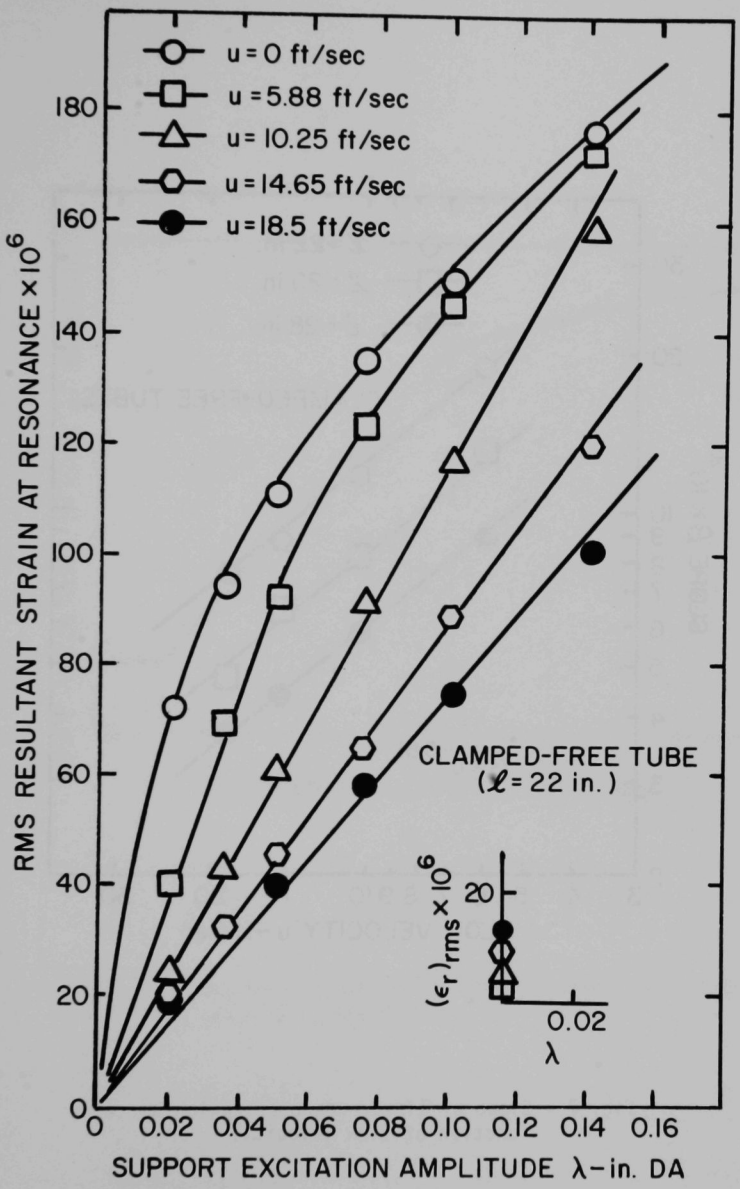

Fig. 6 - Effect of flow velocity and support excitation on the resonant response of the 22 inch clamped-free tube.

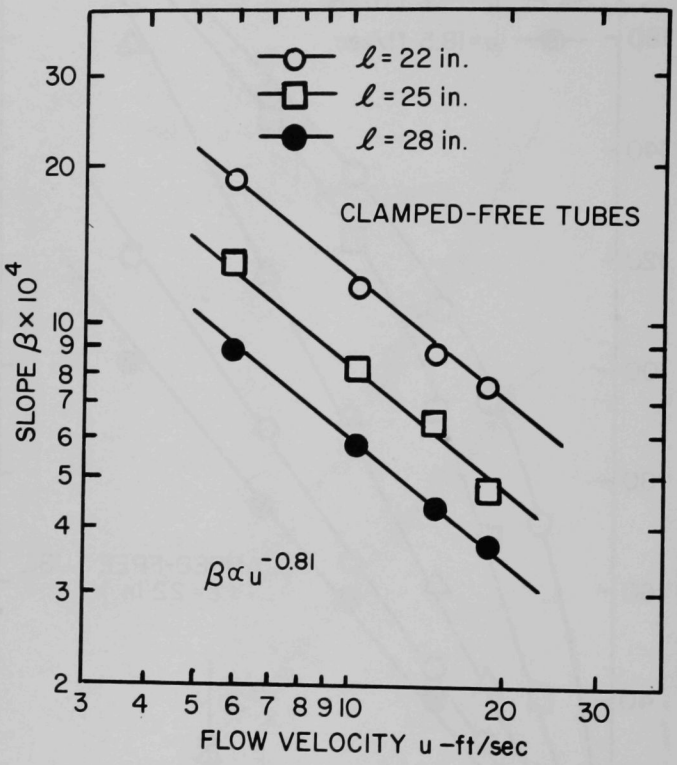

Fig. 7 - Slope of linear response region as a function of flow velocity.

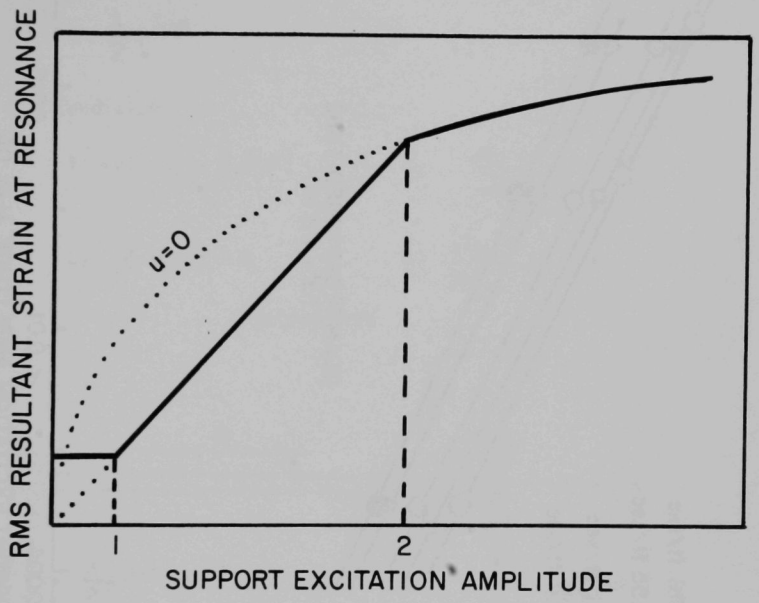

Fig. 8 - Response of clamped-free tubes characterized by three separate regions.

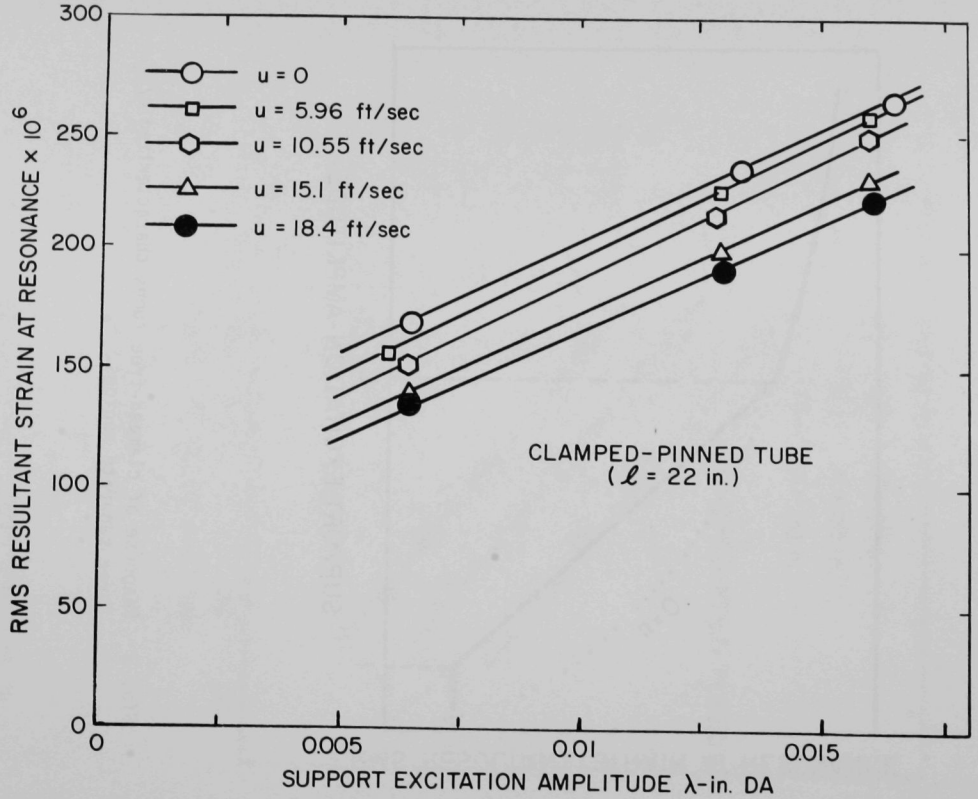

Fig. 9 - Effect of flow velocity and support excitation on the resonant response of the 22 inch clamped-pinned tube.

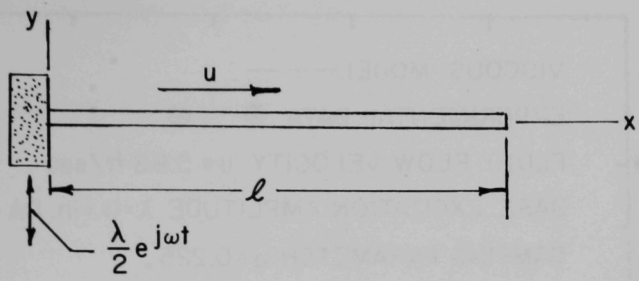

End Conditions:

1) $v(0,t) = \frac{\lambda}{2} e^{j\omega t}$

2) $\frac{\partial y}{\partial x}(0,t) = 0$

3) $\frac{\partial^2 y}{\partial x^2}(\ell,t) = 0$

4) $\frac{\partial^3 y}{\partial x^3}(\ell,t) = 0$

Clamped-Free

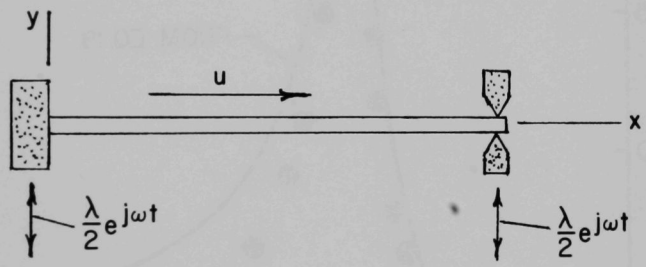

End Conditions:

1) $y(0,t) = \frac{\lambda}{2} e^{j\omega t}$

2) $\frac{\partial y}{\partial x}(0,t) = \frac{\lambda}{2} e^{j\omega t}$

3) $y(\ell,t) = \frac{\lambda}{2} e^{j\omega t}$

4) $\frac{\partial^2 y}{\partial x^2}(\ell,t) = 0$

Clamped-Pinned

Fig. 10 - End conditions for Clamped-free and Clamped-pinned beams.

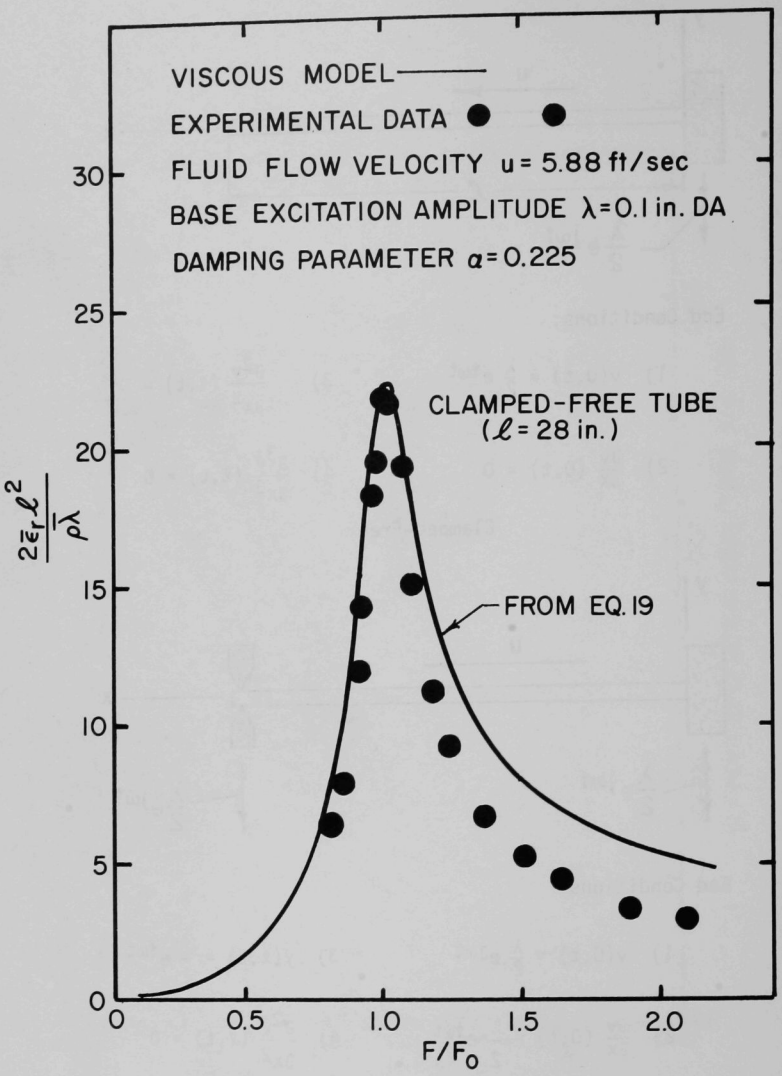

Fig. 11 - Comparison of frequency response of viscous damping model with experimental data.

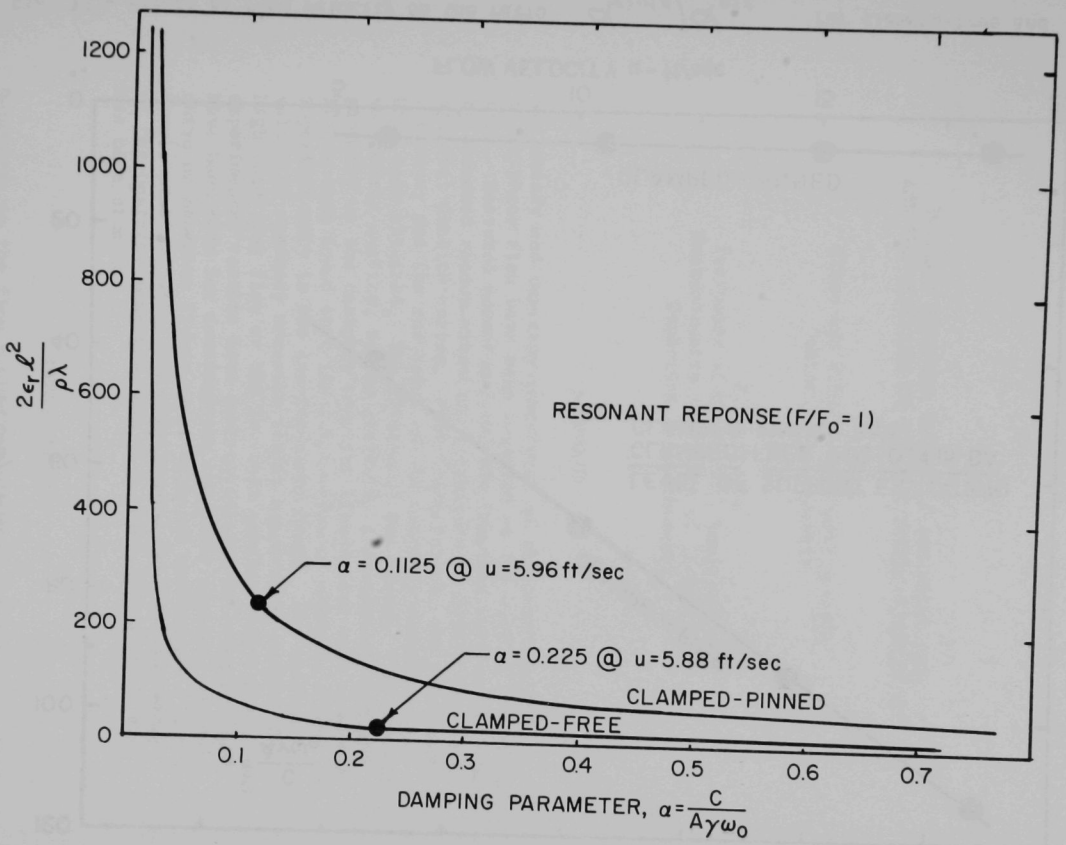

Fig. 12 - Steady-state response of viscous damping model as a function of α.

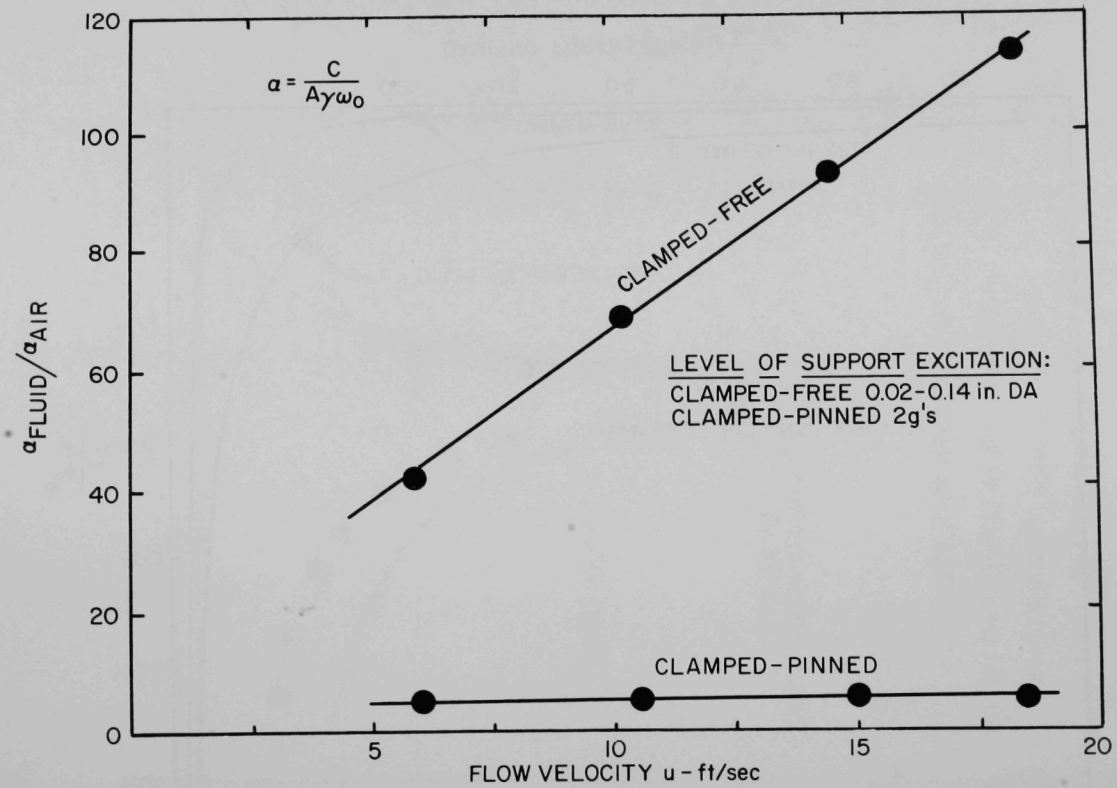

Fig. 13 - Effect of flow velocity on the ratio $\alpha_{fluid}/\alpha_{air}$ for clamped-free and clamped-pinned tubes.

UNSTEADY MOMENTUM FLUXES IN TWO-PHASE FLOW AND THE VIBRATION OF NUCLEAR SYSTEM COMPONENTS*

T. S. Yih
Stone and Webster Engineering Corp.
Boston, Massachusetts

and

P. Griffith
Professor of Mechanical Engineering
Massachusetts Institute of Technology
Cambridge, Massachusetts

ABSTRACT

The steady and unsteady components of the momentum flux in a two-phase flow have been measured at the exit of a vertical pipe. Measured momentum-flux data have been machine processed by standard random-vibration techniques to obtain the power spectral density curves. From these curves, the predominant frequency and the rms value of the unsteady momentum flux have been obtained. The effects of the average flow velocity, volumetric quality, system pressure, flow-channel size, and geometry on the unsteady momentum fluxes have been observed. It has been found that the fluctuation of momentum fluxes is important only in the low-frequency range. The maximum values of unsteady momentum fluxes appeared in either the high void slug flow or the low void annular flow regime. The experimental results have been correlated and suggestions have been made for constructing the power spectral density curve of momentum fluxes under untested conditions. In the sample problem, using the experimental results, the effect of the unsteady momentum flux on a steam generator U-tube has been studied.

INTRODUCTION

Depending on the flow regime one might find either gas bubbles, liquid drops, slugs, or waves in a two-phase flow. These are all accompanied with severe pulsations in pressure, void fraction, and momentum fluxes. The knowledge of these fluctuations is of considerable importance to the development of the two-phase flow technology and its application

* Not presented orally at Conference.

to engineering problems. In spite of this, little work relating to the unsteady nature of two-phase flow has been done. Semenov[1] is the first investigator known to have made a systematic investigation of the unsteadiness in the wall pressure of an air-water mixture flowing in horizontal pipes. His method of data reduction was not specified. Therefore, the use of his results is limited. Hubbard and Duckler[2] also made pressure-time measurements of an air-water flow in a horizontal pipe. Random vibration techniques were applied in their data processing. Because they primarily aimed at the characterization of flow regimes, complete data of fluctuating wall pressure were not presented. Recently, Nishikawa, Sekoguchi, and Fukano reported the measurements of pulsating pressure in upward air-water flow through a vertical tube.[3] Their data were presented in terms of auto- and cross-correlation, standard deviation, and frequency function of pulsating pressure. The results of unsteady pressure investigations are closely related to those found in this work but are not the same because the quantity measured here, momentum flux, is not the same as pressure drop.

Since the three time-varying quantities, void fraction, pressure, and momentum flux, are all interrelated, measurements of the fluctuation in either one of them would lead to the understanding of the others. However, the momentum flux variations are the best to work with because they are defined experimentally at a surface while the void fraction and the pressure drop are defined over a volume and a length, respectively. Furthermore, our knowledge of unsteady momentum fluxes may be very useful in solving some important engineering problems. For example, the fluctuation of momentum flux in a two-phase flow is a possible source of the structural vibrations of heat exchanger U-tubes and reactor fuel elements.

Recently, much attention has been devoted to the study of flow-induced vibrations, especially that of reactor fuel elements.[4-9] In most publications on this subject, investigations were restricted to single-phase flow. Quinn[5] is the first investigator known to have conducted tests on single rods and multirod assemblies in both single- and two-phase flow. Paidoussis[6] made the attempt to deal with two-phase flow by introducing a time-independent void fraction into the density term of his empirical expression. A fluctuating two-phase flow, however, can excite vibrations which no steady flow can, and such a model will not show these vibrations.

The objectives of this investigation were twofold: (1) to obtain information of the unsteady nature of two-phase flow which could be useful in the fundamental understanding of the two-phase phenomena; and (2) to provide basic information that can be applied to various two-phase flow-induced vibration problems.

Since no previous work has been done on this subject, every aspect of the unsteady momentum fluxes needs to be studied. In this work, effort has been made to explore the effects of geometry, pressure, and flow rate on the unsteady momentum flux. As this is an exploratory investigation, none of these variables has been investigated in great depth.

PHYSICAL BASIS OF MOMENTUM FLUCTUATIONS

From the geometries of the various flow regimes shown in Fig. 1, it is obvious that when a two-phase mixture flows through a pipe section there

is the random variation of flow density with respect to time and position in the plane of that section. In either the bubbly or the mist flow, the variation of the total mass flux across a section is very small. In high-void annular flow, one would expect a moderate variation of flow density. In low void annular flow and slug flow, violent fluctuations of flow density take place.

The velocity distribution in a two-phase flow of one flow regime is quite different from that of other flow regimes. For the bubbly upflow, the discrete gas bubbles move at higher speeds than the liquid phase. In a mist upflow the liquid drops move at much lower velocities than the gas phase. For the slug flow, the core of liquid in the center of a pipe moves at a velocity about 20% faster than the mean velocity in the pipe.[10] The gas bubbles move even faster than the liquid slugs. The average velocity of the waves at the interface of an annular flow is on the order of one-tenth of the gas core velocity.[11] The waves may account for a large part of all of the liquid flow; under some conditions the thin film between waves is stationary or even downward-moving.

In the bubbly and mist flow regimes, although the density and velocity are not uniform at a flow section, the total momentum efflux from a section is almost a constant with respect to time. For slug and annular flow regimes, the velocity of the increased liquid portion, i.e., waves in annular flow or core of liquid in slug flow, is always higher than the average velocity of the liquid phase. Thus, one can expect the momentum flux fluctuation to be in phase with the flow density fluctuation but with somewhat larger amplitude than the latter. The pictures in Fig. 2 are samples of the momentum flux fluctuation in different flow regimes. In Fig. 2a, the voltage reading representing the average momentum flux is 0.105 volt. This can be considered in the annular flow regime as sketched in Fig. 1e. When liquid waves passed through a flow section, the momentum flux sharply increased and appeared in the picture as separate upward peaks. In Fig. 2b, the voltage reading of average momentum flux is 0.57 volt. This is probably in the slug flow regime corresponding to Fig. 1b. As a large gas bubble moved across a section the momentum fluxes suddenly dropped to almost zero. The picture in Fig. 2c shows the fluctuation of momentum fluxes of a two-phase flow which may be in the flow regime shown in Fig. 1c or 1d.

EXPERIMENTAL MEASUREMENTS

The experimental apparatus is shown schematically in Fig. 3. By means of a turning tee the momentum fluxes of the air-water flow at the exit plane of the vertical test pipe are converted into a force which acts upon the beam built inside the tank. Appendix A describes how the turning tee actually works. The displacement of the beam is then picked up by a transducer. In the measurement of the steady momentum fluxes, the voltage reading on the vacuum tube volt meter (VTVM) is proportional to the time average of the momentum fluxes. In the unsteady momentum flux measurement, the turning tee and beam combination is a dynamic system and can be treated as a linear time-invariant vibratory system of single degree of freedom. In the frequency domain, the response of a dynamic system is equal to the excitation times the transfer function of this system. The momentum fluxes

of the two-phase flow from the test pipe are the excitation to the beam-tee system while the beam deflection is the response. A special filter set simulating the inverse of the transfer function of the beam-tee system has been designed to convert the response signals to the excitation signals. After being rectified, amplified, and filtered, the electric signals from the transducer are recorded on the magnetic tape.

The fluctuation of momentum fluxes in a two-phase flow is closely related to the flow regimes which can be determined by the average flow velocity, $V = (Q_g + Q_f)/A_p$, and the volumetric quality, $\beta = Q_g/(Q_g + Q_f)$.[12,13] Hence, the average flow velocity and the volumetric quality have been chosen as two major variables in this investigation. Most of the experiments were conducted in the velocity range of 55 ft/sec to 250 ft/sec and volumetric quality range of 50 to 100%. Test pipes with different sizes and cross-section geometries have been used. The diameters of three round pipes are 1, 5/8, and 1/4 in. The different geometries are round, rectangular, triangular, and annular. The cross-sectional areas of these pipes are shown in Fig. 4. The flow areas in the four pipes in Fig. 4a-d are approximately equal. The length of the 1/4-in.-diameter pipe is 7½ ft and the lengths of the other five pipes are all about 8½ ft. In the annular pipe three sets of spacers were soldered on the inner tube. The distances from the pipe inlet to these three sets of spacers are about 2, 4, and 6 ft, respectively. The pressure at the exit of the test pipe was maintained at one atmospheric pressure for most of the experiments. To investigate the effect of pressure upon the unsteady momentum fluxes, a few tests were run with the exit pressure kept at two atmospheric pressure.

The random nature of the two-phase flow fluctuations suggests the application of statistical analysis to the recorded signals of unsteady momentum fluxes in two-phase flow. Figure 5 shows the arrangements of instruments for obtaining the power spectral density curves of the unsteady momentum fluxes $W_p(f)$. The area under the power spectral density curve is the mean square of the momentum flux.[14]

$$E\,[P^2] = \int_0^\infty W_p(f)\,df. \qquad (1)$$

From the spectral density curves obtained in most of the experiments it has been seen that beyond 50 cps the magnitude of unsteady momentum flux in two-phase flow is very small. As an approximation, the upper integration limit in Eq. 1 can be replaced by 50 cps.

EXPERIMENTAL RESULTS

The steady component of momentum fluxes P_{st} was measured directly in the experiments; the root-mean-square value of the unsteady momentum fluxes P_{rms} was obtained from the power spectral density curve by using Eq. 1. As a measure of the relative magnitude of the fluctuation, the ratio P_{rms}/P_{st} is defined to be the unsteadiness of the momentum fluxes. The energy in the spectral density curves was distributed in a very broad frequency band. However, in most of the curves there was a region which contained more energy than the rest. The frequency at the center of this region is designated as f_c, the predominant frequency. This is one of the quantities

which is needed to complete the statistical description of the unsteady two-phase flow.

General Observations

In the experiments using rectangular pipe, appreciable transverse vibrations of the test pipe occurred. No such appreciable structural vibrations were observed in the tests using other pipes. This is probably due to the fact that the rectangular pipe has a low natural frequency of vibration in the direction of its small dimensions. This natural frequency falls in the range which contains the major part of the fluctuation energy of momentum fluxes.

When experiments were run with the annular test pipe, the flow resistance to the two-phase mixture was much higher than in other test pipes. The power spectral density curves of these runs are quite different from those using test pipes of other geometries. Shown in Fig. 6 is a typical set of spectral density curves of the unsteady momentum flux under the same flow conditions but with different channel geometries. For annular test pipe, the energy in the spectral density curve is so evenly distributed that no specific location along the frequency axis can be assigned as the predominant frequency f_c. The spacers between the inner and outer tubes and the relatively small hydraulic diameter were both suspected of being responsible for the high flow resistance. Regarding the even distribution of the energy in the spectral density curve, the spacers were thought to have broken some of the large disturbances in the two-phase flow and increased the number of small disturbances. It resulted in a reduction of the total fluctuation energy.

When the volumetric quality β was less than 70%, another pattern of spectral density curves appeared. A sample curve of this pattern is shown in Fig. 7a. In contrast to the curve pattern shown in Fig. 7b, it seems impossible to assign a single value of f_c to curve a. Since at high volumetric quality the waves or the slugs of the liquid phase are the disturbances in the two-phase flow, whereas in the relatively low β region, presumably the slug flow regime, the lengths of liquid slugs and gas bubbles are comparable and both may be viewed as the disturbances. Therefore, there is no single value of frequency that can be assigned as f_c.

General Trends

The maximum value of P_{rms} has been found to occur in either the low void annular or the high void slug flow regime.

The effects of the average flow velocity and pipe diameter on the unsteadiness of momentum fluxes are shown by the correlation presented in Fig. 8. The value of P_{rms}/P_{st} is seen to increase with decreasing V. This implies that when V increases, the unsteady component of momentum fluxes increases at a slower rate than the steady component. The fact that the unsteadiness of momentum fluxes increases with decreasing pipe diameter indicates the better mixing of the gas and liquid phases in a large pipe than in a small pipe. Probably surface tension (through the Weber number) determines the size of dispersion. It has been observed that, for the same flow conditions, the unsteadiness is the greatest for the flow in the rectangular pipe and is the smallest in the annular pipe. Spacers in the

annulus appear to break up the flow. The result presented in Fig. 9 shows that a higher system pressure tends to depress the unsteadiness of the momentum fluxes. Since in a low- or moderate-pressure system the density of the gas phase is increased almost in proportion with pressure, the difference between the densities of the liquid and the gas phase is reduced. As a result, the density fluctuation as well as the momentum fluctuation is reduced too. It is felt that in going to higher pressure in a steam-water system the changes in gas density are the most important changes in property which take place.

For the predominant frequency of unsteady momentum fluxes, all the experimental results were correlated together in the form of f_c/V versus β and presented in Fig. 10. In the range of β above 70%, f_c is proportional to V and increases with decreasing β. In the relatively high β range, the increase of V is equivalent to the increase of gas flow rate; the decrease of β is equivalent to the increases of liquid flow rate. Both of them will increase the number of liquid slugs or waves in a two-phase flow which is the frequency of disturbance in the flow. It has been reported in references 11 and 15 that the disturbance wave frequency in a two-phase flow does increase with liquid or gas flow rate. The frequency of pressure fluctuation in a two-phase flow has a similar trend except it has been reported to be inversely proportional to the pipe diameter,[1] whereas f_c has been found almost independent of pipe diameter. It can be seen from Fig. 10 that the predominant frequency is slightly increased under higher system pressure.

Since the unsteady momentum fluxes of a two-phase flow may be affected by surface tension and gravity force, it is suggested to correlate the P_{rms}/P_{st} data and the f_c data by the dimensionless groups, $W_e^{0.4}P_{rms}/P_{st}$ and $(f_cD/V)(F_r/W_e^{0.5})$ respectively. Scales in terms of these dimensionless groups are also shown in Figs. 8 and 10.

CONSTRUCTING A SPECTRAL DENSITY CURVE FOR UNTESTED CONDITIONS

From the observation made on the spectral density curves plotted in the experiments, it has been found that most of the curves can be represented approximately by a triangle as shown in Fig. 11a. If the area under the spectral density curve is denoted by A_{psd} then Eq. 1 can be written as

$$A_{psd} = \int_0^\infty W_p(f)df = (P_{rms})^2. \tag{2}$$

The area of the triangle is

$$\tfrac{1}{2}hL_f = (P_{rms})^2. \tag{2}$$

Two empirical equations relating the value of f_c to the length and position of the triangle base line were obtained statistically from available spectral density curves. The two equations have the form

$$L_f = f_c + 22 \tag{4}$$

$$L_L = 0.6\ f_c + 3, \tag{5}$$

where L_f and L_L are all in units of cycles per second. With the aid of Eqs. 3-5 one can construct an approximate spectral density curve from given values of P_{rms} and f_c. For the purpose of comparison, a pair of the true and the approximate spectral density curves are shown in Fig. 11b.

For a two-phase flow with $\beta < 70\%$ or a two-phase mixture passing through an annular pipe with spacers inside, the spectral density curves are close to the band-limited white noise spectrum. In these cases a rectangle can be used to simulate the spectral density curves for untested conditions.

In general it is possible to estimate the values of P_{rms} and f_c of the unsteady momentum fluxes in any two-phase flow from the limited results of this investigation and then to construct the spectral density curve. The only limitations on this statement are there is no high-pressure data and no very low volume quality data available. For a two-phase flow with low values of β, the unsteady component of momentum fluxes is not important, as shown in Fig. 8. For a two-phase flow at very high pressure, the density difference between the liquid and the gas phases is small and the unsteady momentum fluxes are also probably unimportant. The suggested procedure for constructing a power spectral density curve for untested conditions is as follows.

1. To estimate the steady component of momentum fluxes either from Ref. 16 or by the simplified relation

$$P_{st} = \rho_f(1 - \beta)\, V^2 \tag{6}$$

for low system pressure, and by

$$P_{st} = [\rho_f(1 - \beta) + \rho_g\beta]\, V^2 \tag{7}$$

for high system pressure.

2. For given values of V, D, and β, pick P_{rms}/P_{st} from Fig. 8 and designate this value as $(P_{rms}/P_{st})_0$.

3. The unsteadiness of the momentum flux being considered is

$$\frac{P_{rms}}{P_{st}} = \left(\frac{P_{rms}}{P_{st}}\right)_0 (0.85)^{\log_2\left(\frac{\rho_g}{\rho_a}\right)}, \tag{8}$$

where ρ_g is the density of the gas phase in the two-phase flow to be studied and ρ_a is the density of air under standard conditions. This adjustment of the value of unsteadiness is made on the grounds that the increase of gas density will reduce the difference between the densities of liquid and the gas phases and depress the fluctuations of momentum fluxes. In Fig. 9 the average reduction rate of P_{rms}/P_{st} by doubling the system pressure is about 15%. Since no other information is available, it is suggested to use the result in Fig. 9 as a rule of thumb, i.e., when the density of the gas phase is doubled the unsteadiness is reduced by 15%. This rule takes care of the primary property variable in two-phase flow systems, the gas density.

4. Combining Eq. 6 or 7 with Eq. 8, the value of P_{rms} can be determined.

5. For given values of V and β obtain f_c from Fig. 10.

6. Construct the desired power spectral density curve by applying Eqs. 3, 4, and 5.

Equations 6 and 7 are based on the homogeneous model for evaluating the momentum flux. This model is used in spite of the fact that the bulk of the data taken are in the annular or dispersed flow regime. The justification for this is contained in Ref. 16, where it was found that the momentum flux in two-phase flow was generally described better by a homogeneous model than by a separated flow model even though the slip velocity ratio was appreciably different from 1. As far as the errors associated with this procedure are concerned, the homogeneous model was used to reduce the low-pressure data which are reported here. It should then be used to predict untested conditions by using these data. As the pressure increases, the homogeneous and slip models for evaluating momentum flux approach each other, so extrapolating to higher pressure is not dangerous. As indicated in Ref. 16, better estimates of the momentum flux can be made if another parameter was used to describe the momentum flux data. This would add appreciably to the complication of using the suggested procedure without, it is felt, a compensating increase in the accuracy of the resulting predictions.

EXAMPLE PROBLEM APPLYING THESE RESULTS

The sample problem to be presented is the two-phase flow-induced vibration of a U-tube in a steam generator. The major assumptions in the following analysis are:

1. The U-tube is treated as an equivalent mass spring system with a single degree of freedom, since an excessive amount of energy is required to cause a mechanical system to vibrate with significant amplitude at a mode higher than the fundamental one.

2. The two-phase momentum fluctuations travel at the average velocity of the mixture.

The U-tube model is shown in Fig. 12. Being treated as a vibrating system of single degree of freedon, its equation of motion is

$$M_e\ddot{x} + C\dot{x} + kx = F, \tag{9}$$

where k is the stiffness of a cantilever beam,

$$k = \frac{3EI_Y}{L^3}, \tag{10}$$

and M_e is the equivalent mass of the U-tube. The transfer function of this system takes the form

$$H(\omega) = \frac{1}{k - M_e\omega^2 + iC\omega}. \tag{11}$$

It can be shown that the relation between the spectral density of the excitation F(t) and the spectral density of the response x(t) has the following form:[14]

$$S_x(\omega) = |H(\omega)|^2 \, S_F(\omega). \tag{12}$$

Consequently, the power density spectrum of the response is

$$S_x(\omega) = \frac{S_F(\omega)}{(k - M_e\omega^2)^2 + C^2\omega^2}. \tag{13}$$

In terms of experimental spectral density,

$$W_x(f) = \frac{W_F(f)}{[k - M_e(2\pi f)^2]^2 + C^2(2\pi f)^2}. \tag{14}$$

Now, the remaining problem is to find the spectral density of the transverse force F. Referring to the model in Fig. 12, at time t, if the momentum flux in the two-phase flow at the upper bend is P(t), then that at the lower bend is $P(t + \tau_o)$, where τ_o is the time interval for the flow to travel through the distance L_b and can be expressed as

$$\tau_o = \frac{L_b}{V}. \tag{15}$$

Therefore, the total vertical force acting on the U-tube is

$$F(t) = A_t[P(t) - P(t + \tau_o)], \tag{16}$$

where A_t is the flow area inside the U-tube. The auto-correlation function of F is

$$R_F(\tau) = E[F(t)\, F(t + \tau)]. \tag{17}$$

Substitute Eq. 16 into 17 and consider the limiting case of $\tau = 0$.

$$R_F(0) = A_t^2[2R_P(0) - 2R_P(\tau_o)], \tag{18}$$

where

$$R_P(0) = \int_{-\infty}^{\infty} S_P(\omega)\, d\omega, \tag{19}$$

$$R_P(\tau_o) = \int_{-\infty}^{\infty} S_P(\omega)\, e^{i\omega\tau_o}\, d\omega. \tag{20}$$

Therefore, Eq. 18 becomes

$$\int_{-\infty}^{\infty} S_F(\omega)\, d\omega = 2\sqrt{2}\, A_t^2 \int_{-\infty}^{\infty} (1 - \cos \omega\tau_o)^{\frac{1}{2}}\, S_P(\omega)\, d\omega. \tag{21}$$

The relation between the power spectral density curves of F(t) and P(t) is thus found to be

$$S_F(\omega) = 2\sqrt{2}\, A_t^2 (1 - \cos \omega\tau_o)^{\frac{1}{2}}\, S_P(\omega), \tag{22}$$

or

$$W_P(f) = 2\sqrt{2}\, A_t^2 (1 - \cos 2\pi f\tau_o)^{\frac{1}{2}}\, W_P(f). \tag{23}$$

The term $(1 - \cos 2\pi f\tau_o)^{\frac{1}{2}}$ is a periodic function.

From the spectral density curve of the momentum flux in the two-phase mixture flowing within a U-tube, one can construct the spectral density curve of the vibration amplitude by using the relation

$$W_x(f) = \frac{2\sqrt{2}\, A_t^2 (1 - \cos 2\pi f\tau_o)^{\frac{1}{2}}}{[k - M_e(2\pi f)^2]^2 + C^2(2\pi f)^2}\, W_P(f). \tag{24}$$

The mean square of the vibration amplitude of the U-tube is

$$E[x^2] = \int_0^{\infty} W_x(f)\, df. \tag{25}$$

Suppose the physical quantities of a steam generator U-tube are given as the following:

<u>Tube data</u>:

Stainless steel tubing

O.D. = 0.5 in., Wall thickness = 0.05 in.

L = 20 ft, L_b = 1 ft (Fig. 12)

C/C_c = 0.01 (assumed)

<u>Flow data</u>:

Steam and water mixture

p = 2400 psi, V = 70 ft/sec, β = 90%

By following the suggested procedure, the power spectral density curve of the momentum fluxes in this steam-water flow was constructed. With the help of Eq. 24, the power spectral density curve of the U-tube vibration amplitude was also constructed. Then the mean square and the rms value of the vibration amplitude were found to be $E[x^2] = 0.13$ in.^{2} and $x_{rms} = 0.36$ in.

On the general subject of flow-induced vibration, many investigations have proceeded directly from the flow conditions to the vibration solutions without studying the nature of the interactions between the flow and the mechanical structure. Obviously, the results of these investigations can only be applied to systems similar to those which have been investigated. Furthermore, following the approach used in the other investigations, it is difficult to understand the actual mechanism of the flow-induced vibration. For instance, the vibration frequencies of rods subjected to parallel flow are found close to the natural frequencies of rods in many experimental studies. Based on this fact, some investigators believe the mechanism of parallel flow-induced rod vibration to be a self-excited vibration. In the example presented here, the U-tube problem is essentially a forced-vibration case because the tube bend will still receive the impulses of the two-phase flow even if it is rigidly fixed by some means. Nevertheless, the major vibration frequencies of the U-tube were found to be close to its natural frequency. This shows that the frequencies of forced vibrations may also be close to the natural frequencies of the mechanical systems if the excitation is of a random nature. In the present study, the flow-induced vibration problem was solved by applying the exciting force of known magnitude and frequency to a model appropriate to the system being studied. This is a more fundamental way of approaching such problems although the model and the analysis in this study are by no means perfect.

CONCLUSIONS

The conclusions of this investigation may be summarized as follows:

1. The fluctuation of momentum fluxes is important only in a relatively low frequency range. Under all the tested flow conditions, the major part of the fluctuation energy is contained in the frequency range below 50 cycles/sec.

2. The unsteady component of the momentum fluxes in a two-phase flow increases with increasing average flow velocity at a smaller rate than the steady component does. The maximum values of unsteady momentum fluxes appear in either the high void slug flow or the low void annular flow regime.

3. The unsteadiness of momentum fluxes, the ratio of the rms value of the unsteady momentum flux to the steady momentum flux is inversely proportional to the average flow velocity to the 0.8 power and pipe diameter to the 0.4 power. Among the tested pipe geometries the unsteadiness is the greatest in the rectangular pipe. High system pressures tend to suppress the unsteadiness of momentum fluxes.

4. Above 70% volumetric quality, the predominant frequency of unsteady momentum fluxes increases in proportion with the average flow velocity and increases almost linearly with decreasing volumetric quality. The system pressure, the size, and the geometry of the flow channel do not have a significant effect on the predominant frequency. Below 70% volumetric quality, the fluctuation energy of unsteady momentum fluxes is distributed rather evenly in the low-frequency region.

5. Based on the experimental results, a method of constructing the power spectral density curves for untested conditions has been suggested.

6. The presence of obstacles in the flow channel, such as the spacers between the reactor fuel elements, depresses the pulsation of momentum fluxes and results in an even distribution of the fluctuation energy in the low frequency range.

7. In two-phase flow systems, appreciable structural vibrations can be excited by the unsteady momentum fluxes. With the experimental results in the present investigation, the rms value of the vibration amplitude can be predicted by applying random vibration techniques. The vibration energy of the mechanical system is concentrated around its natural frequency.

APPENDIX A

Accuracy of the Unsteady Momentum Flux Measurement Using the Turning Tee

The vertical force acting upon the beam through the turning tee is

$$F_y = \iint_{C.S.} \rho V^2 dA + \frac{\partial}{\partial t} \iiint_{C.V.} \rho V \, d\bar{v} - \iiint_{C.V.} \rho g \, d\bar{v}. \tag{26}$$

The control volume in which the change of the vertical component of momentum flux takes place is shown by the dotted lines in Fig. 13. Then Eq. 26 can be written as

$$F_y = \rho V^2 A_x + \frac{\partial}{\partial t} \rho V A_x L_t - \rho g A_x L_t, \tag{27}$$

where A_x is the inlet area of the tee and equal to $(\pi/4)D^2$. Suppose the density of the two-phase flow varies sinusoidally, namely,

$$\rho = \rho_m (1 + \sin \omega_k t), \tag{28}$$

where ρ_m is the mean flow density and ω_k is the fluctuation frequency. Thus, Eq. 27 becomes

$$\begin{aligned} F_y = {} & \rho_m V^2 A_x + \rho_m V^2 A_x \sin \omega_k t + \omega_k \rho_m V A_x L_t \cos \omega_k t \\ & - \rho_m g A_x L_t - \rho_m g A_x L_t \sin \omega_k t. \end{aligned} \tag{29}$$

For the larger turning tee used in the experiments, both D and L_t are equal to 1-3/8 in. The flow conditions are assumed to be β = 80% and V = 100 ft/sec. Having these numerical values, the term $\rho_m g A_x L_t$ in Eq. 29 is found to be negligibly small. The vertical dynamic force acting on the beam is then

$$F_d = F_m (\sin \omega_k t + \frac{\omega_k L_t}{V} \cos \omega_k t) \tag{30}$$

or

$$F_d = \sqrt{1 + \left(\frac{\omega_k L_t}{V}\right)^2} \, F_m \sin (\omega_k t + \varphi), \tag{31}$$

where F_m is the amplitude of the force due to the unsteady momentum fluxes in the flow

$$F_m = \rho_m V^2 A_x. \tag{32}$$

Since the upper limit of the frequency range of interest is 50 cps, the highest value of ω_k would be 100 π rad/sec. For the given values of ω_k, L_t, and V, Eq. 31 becomes

$$F_d = 1.06\ F_m \sin\ (100\pi t + \varphi). \tag{33}$$

This shows that, under the specified conditions, in the measurement of unsteady momentum fluxes, the maximum error which occurs at the highest frequency is 6%.

NOMENCLATURE

A_p	Cross section area of pipe
A_{psd}	Area under the spectral density curve of momentum fluxes
A_t	Flow area of U-tube
C	Damping coefficient
C_c	Critical damping coefficient
D	Diameter (in.)
E	Modulus of elasticity
F	Force
F_r	Froude number = Inertia force/Gravity force
f	Frequency
f_c	Predominant frequency of unsteady momentum fluxes (cps)
f_o	Central frequency of the narrow band filter
Δf	Band width of the narrow band filter
$H(\omega)$	Transfer function
h	Height of the triangle in Fig. 11a
I_Y	Moment of inertia of U-tube cross-section area about Y axis, Fig. 12
k	Spring constant
L	Length
L_b	Length of U-tube bend
L_f	Length, Fig. 11a
L_L	Length, Fig. 11a
M_e	Equivalent mass
P	Momentum flux
P_{rms}	rms value of unsteady momentum fluxes
P_{st}	Steady momentum fluxes
P_{rms}/P_{st}	Unsteadiness of momentum fluxes
Q_f	Volume flow rate of water
Q_g	Volume flow rate of air
$R_F(\tau)$	Auto-correlation function of force, Eq. 17
$R_p(\tau)$	Auto-correlation function of momentum fluxes
$S_F(\omega)$	Spectral density of force
$S_p(\omega)$	Spectral density of momentum fluxes
$S_x(\omega)$	Spectral density of vibration amplitude
t	Time
V	Average flow velocity (ft/sec)
W_e	Weber number = Inertia force/Surface tension force

$W_F(f)$	Experimental spectral density of force
$W_p(f)$	Experimental spectral density of momentum fluxes
$W_x(f)$	Experimental spectral density of vibration amplitude
x	Vibration amplitude
β	Volumetric quality, flowing void fraction
ρ_a	Density of air under standard conditions
ρ_f	Density of liquid phase
ρ_g	Density of gas phase
ρ_m	Average density of a two-phase flow
τ	Time lag, variable
τ_o	Time lag, constant
ω	Circular frequency
ω_k	Frequency of density fluctuation

ACKNOWLEDGMENT

This work was entirely supported by the U. S. Atomic Energy Commission.

REFERENCES

1. Semenov, N. I., "Pressure Pulsations during the Flow of Gas-Liquid Mixtures in Pipes," Heat Power Engineering Part I, USAEC, Div. of Technical Information, AEC-tr-4496, December 1961 (translation).

2. Hubbard, M. G., and Dukler, A. E., "The Characterization of Flow Regimes for Horizontal Two-Phase Flow," Proceedings of the 1966 Heat Transfer and Fluid Mechanics Institute.

3. Nishikawa, K., Sekoguchi, K., and Fukano, T., "Characteristics of Pressure Pulsation in Upward Two-Phase Flow," Presented at the International Symposium on Research in Cocurrent Gas-Liquid Flow, September 1968, Canada.

4. Burgreen, D., Byrnes, J. J., and Benforado, D. M., "Vibration of Rods Induced by Water in Parallel Flow," Trans. ASME, July 1958, 991-1003.

5. Quinn, E. P., "Vibration of Fuel Rods in Parallel Flow," GEAP-4059, USAEC, 1962.

6. Paidoussis, M. P., "The Amplitude of Flow-Induced Vibration of Cylinders in Axial Flow," Canadian Report AECL-2225, March 1965.

7. Pavlica, R. T., and Marshall, R. C., "An Experimental Study of Fuel Assembly Vibrations Induced by Coolant Flow," Nuclear Engineering and Design 4, 54-60 (1966).

8. Wambsganss, M. W., "Vibration of Reactor Core Components," Reactor and Fuel-Processing Technology 10(3), 208-219 (Summer 1967).

9. Reavis, J. R., "WVI-Westinghouse Vibration Correlation for Maximum Fuel-Element Displacement in Parallel Turbulent Flow," Trans. ANS 10(1), 369-371 (1967).

10. Griffith, P., "The Prediction of Low-Quality Boiling Voids," Trans. ASME, Journal of Heat Transfer, Paper No. 63-HT-20.

11. Hall-Taylor, N., and Hewitt, G. F., "The Motion and Frequency of Large Disturbance Waves in Annular Two-Phase Flow of Air-Water Mixtures, AERE-R3952, United Kingdom, 1962.

12. Griffith, P., "Two-Phase Flow in Pipes," M.I.T. Summer Session Notes, 1962.

13. Kozlov, B. K., "Regimes and Types of Flow for an Air-Water Mixture in Vertical Tubes," Hydrodynamics and Heat Transfer during Boiling in High Pressure Boiler, 7-18, AEC-tr-4490, 1954.

14. Crandall, S. H., and Mark, W. D., "Random Vibration in Mechanical Systems," Academic Press, New York, 1963, pp. 27-28 and 69-71.

15. Hinkle, W. D., "A Study of Liquid Mass Transport in Annular Air-Water Flow," Sc.D. Thesis, M.I.T., 1967.

16. Andeen, G.B., and Griffith, P., "Momentum Flux in Two-Phase Flow," Trans. ASME, Journal of Heat Transfer, Series C, 90(2), 211-222 (May 1968).

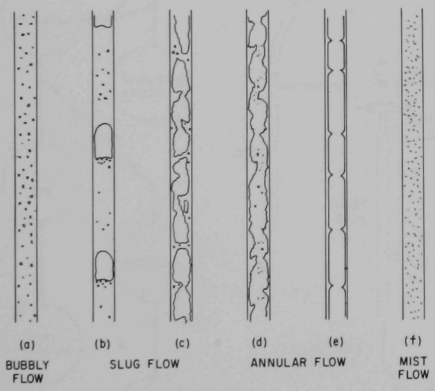

Fig. 1

Sketches of Flow Regime Geometries in Adiabatic Two-phase Vertical Upflow

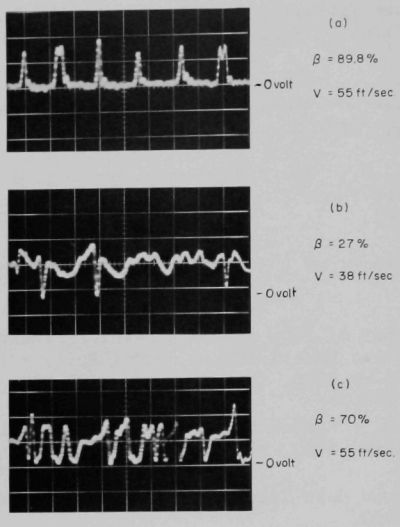

Fig. 2

Fluctuations of Momentum Fluxes.
Horizontal scale = 0.05 sec/unit.
Vertical scale = 0.5 volts/unit.

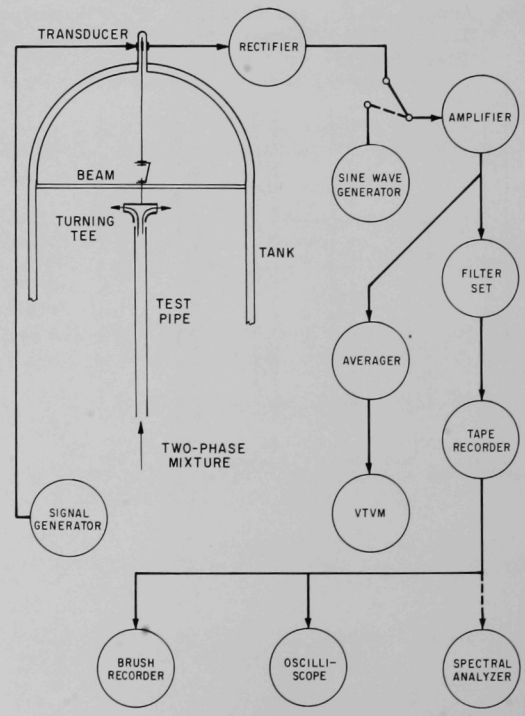

Fig. 3

Arrangement of Apparatus

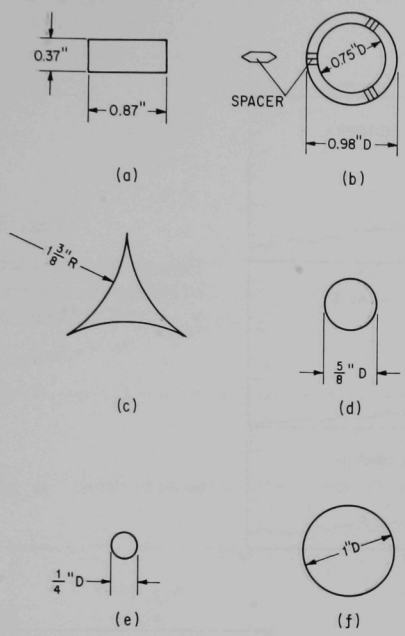

Fig. 4

Cross Sections of Test Pipes

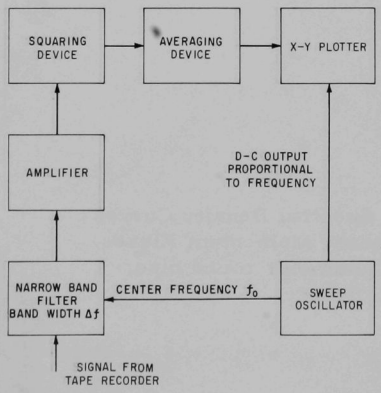

Fig. 5

Spectral Analysis System

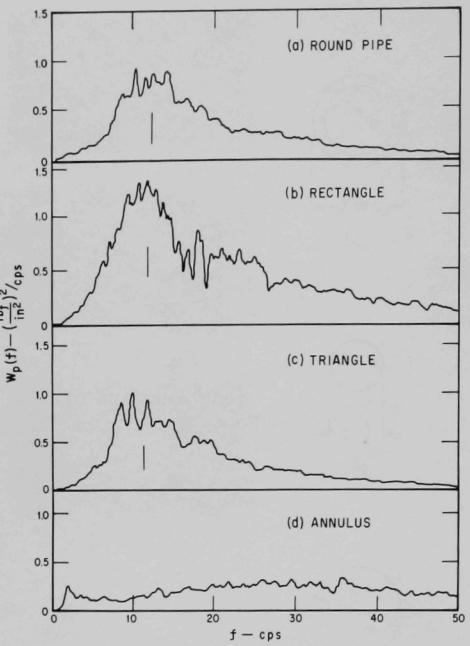

Fig. 6

Power Spectral Density Curves of Unsteady Momentum Fluxes. V = 100 ft/sec, β = 95.5%.

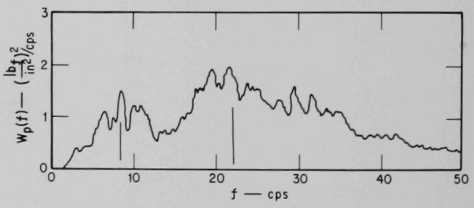

(a) β = 60 %

Fig. 7

Power Spectral Density Curves of Unsteady Momentum Fluxes. 1/4 in. diameter round pipe, V = 55 ft/sec.

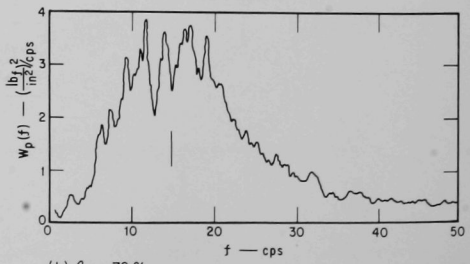

(b) β = 70 %

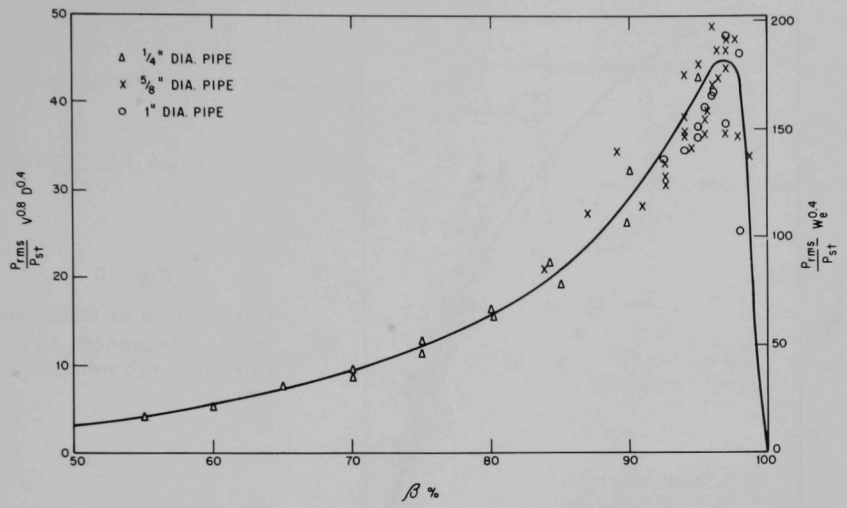

Fig. 8. Correlation of the Unsteadiness of Momentum Fluxes

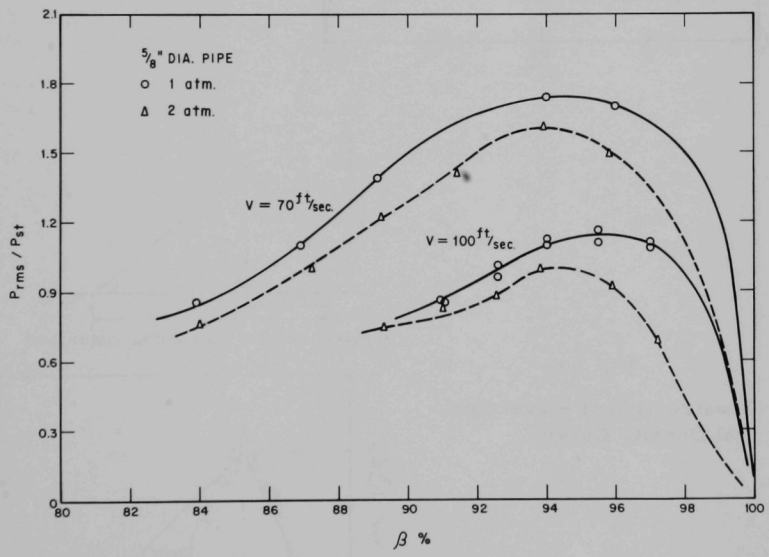

Fig. 9. Effect of Pressure on the Unsteadiness of Momentum Fluxes

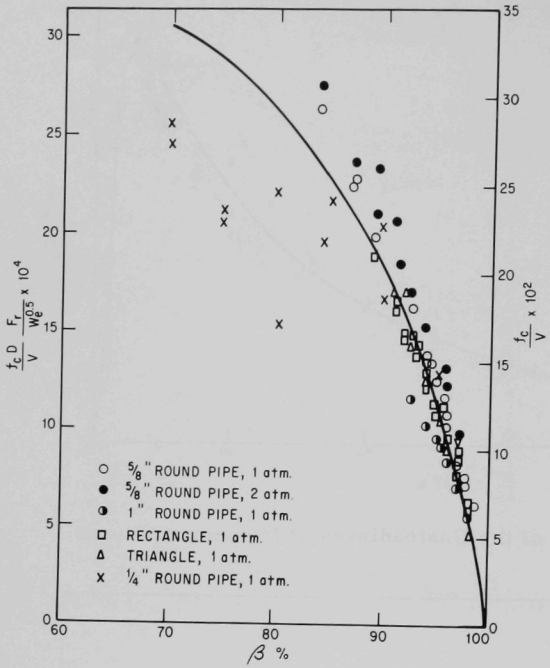

Fig. 10

Correlation of Predominant Frequency of Unsteady Momentum Fluxes

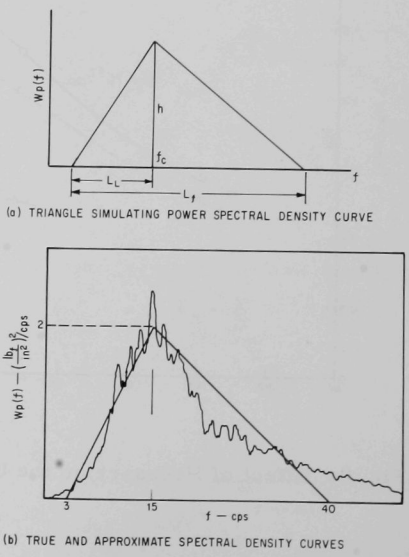

Fig. 11

Construction of Power Spectral Density Curve

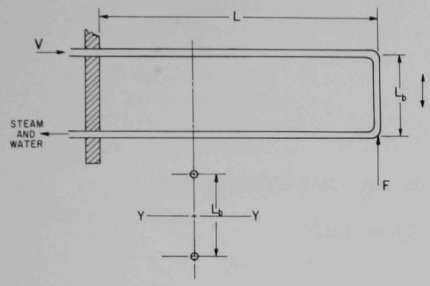

Fig. 12. U-tube Model

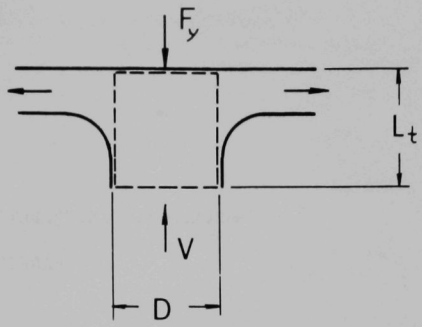

Fig. 13. Control Volume in Turning Tee

MEASUREMENT, INTERPRETATION AND CHARACTERIZATION OF NEARFIELD FLOW NOISE

M. W. Wambsganss and P. L. Zaleski

Theoretical and Applied Mechanics Section
Engineering and Technology Division
Argonne National Laboratory
Argonne, Illinois

ABSTRACT

The nearfield component of flow noise has been identified in earlier studies as a primary excitation source in the parallel-flow-induced vibration of flexible rods and its measurement and characterization as the cruxes of the problem. This paper reports on an experimental study of the flow noise on the surface of a test element in annular water flow. Three, longitudinally in-line, pairs of miniature pressure transducers were constructed on the surface of a tubular test element. The instrumented test element was concentrically mounted within a test section which is part of a water flow loop. This assembly was used to obtain pressure-time measurements of the flow noise. The nearfield mean-square-value spectral densities and rms pressure coefficients were computed from a pressure-difference signal using a subtraction process, with a diametrically opposite transducer pair, to null out the farfield noise. Normalization of the mean-square-value spectra is discussed. Convection velocity ratios, mean eddy lifetimes, and correlation lengths are computed from broad-band, longitudinal, space-time correlations. In general, the results are in agreement with those from independent studies of the statistics of wall-pressure fluctuations in pipe flows and flow over flat plates. The low-frequency behavior of the nearfield mean-square-value spectra is believed to represent new data.

INTRODUCTION

High-velocity, heat-removing coolant in reactors and associated plant equipment represents a source of energy which can excite the structural components which it contacts. With the trend toward increasing plant size and power density, resulting in higher coolant velocities, flow noise

as a source of excitation which can lead to structural damage is increasing in importance. It is difficult to reduce or eliminate flow noise since a significant portion of it is locally generated. Therefore, it is more practical to design the structural components to survive in the noise environment. This is an objective of the structure-fluid dynamics program at Argonne: to develop new methods of analysis and testing that can be used by designers in designing to avoid potentially detrimental flow-induced vibrations of in-core and out-of-core components.

Clearances between adjacent components within a reactor are inherently small, therefore, small displacements of these components can be critical. There have been a number of studies, both theoretical and experimental, of the parallel-flow-induced vibrational response of flexible rods, both singly and in clusters; for example, see references listed in Ref. 1. In these studies, flow noise has been identified as the primary excitation mechanism; and its measurement, interpretation, and characterization are the cruxes of the parallel-flow-induced vibration problem.

Flow-noise can be divided into nearfield and farfield components. In the nearfield the pressure fluctuations are due to the adjacent fluid only; the energy density remains close to the source and does not radiate outward. Pressure fluctuations generated by turbulent eddies do not propagate and are an example of the nearfield. The farfield consists of all true noise in the system. The associated pressure fluctuations propagate at the speed of sound and radiate to large distances. Sources of farfield noise include pump pulsations, valve scream, cavitation, and the like. Flow noise within a reactor can be expected to be made up of nearfield and farfield components, both of which can excite structural response.

In the study of parallel-flow-induced vibration of flexible rods, the test element is generally centrally located within the test section, that is, the test element and test section axes are coincident. It is reasonable to assume that the farfield (acoustic) noise travels through the test section as a one-dimensional wave at the speed of sound in the fluid. Therefore, at a given instant of time, and at a given section along the rod, the contribution from the farfield to the pressure on the surface of the rod is equal around the circumference of the rod. Since the wavelengths associated with the low-frequency acoustic noise are generally long in comparison with the wavelengths associated with vibration of the structure, it is assumed that the farfield does not significantly contribute to forcing structural motion. Based on these observations it is concluded that the nearfield represents the primary source of excitation.

Solution of the analytical model describing rod response requires mathematical characterization of the convecting, random pressure field associated with the nearfield [1]. Assuming a homogeneous pressure field, the cross-spectral density provides this characterization. Corcos [2] proposed a phenomenological model to describe the cross-spectral-density given by

$$\Psi_p(\xi,\eta,\omega) = \Phi_p(\omega)A(\omega\xi/U_c)B(\omega\eta/U_c)\exp(-j\omega\xi/U_c) \quad (1)$$

where ω is frequency, U_c is convection velocity, ξ and η are the separation distances in the longitudinal and lateral directions respectively, and $\Phi_p(\omega)$ is the wall-pressure, mean-square-value (power) spectral density, $A(\cdot)$ is the functional dependence of Ψ_p on the longitudinal (streamwise) coordinate, ξ, and $B(\cdot)$ is the functional dependence of Ψ_p on the lateral coordinate, η. Corcos' model provides good agreement with experiment as well as lends itself to mathematical computations because of the separability of the mean-square-value spectral density, and longitudinal and lateral effects. Therefore, Corcos' model is widely used and has been employed in the analysis of the response of a flexible rod to parallel-flow [1,3,4]. Upon inspection of Eq. 1 it is seen that characterization of the nearfield requires studies of the mean-square-value spectral density and of the narrow-band longitudinal and lateral space-time correlations.

There have been a considerable number of experimental studies performed over the past decade [for example 2,5-12], and many of the basic features of the nearfield are understood today. However, the majority of the experiments have been performed in air tunnels and involve measurement of the boundary-layer pressure fluctuations on the surface of a flat plate or the wall of a pipe. There have been only a few experiments performed in water tunnels; Bakewell [11] measured the statistical properties of the fluctuating pressure on a body of revolution and Clinch [12] studied the wall pressure field at the surface of a smooth-walled pipe.

While experimental results from independent studies agree well at the higher frequencies, the low-frequency spectra vary widely and, in general, it can be concluded that reliable results are not available in this frequency range. Yet this is precisely the range of interest in the study of flow induced vibration of flexible rods (simulating reactor components), since this low-frequency range encompasses the range of first-mode natural frequencies at which the rods predominantly respond [1]. Further, the majority of the studies have been concerned with fully-developed turbulent flow which exists after the flow has traversed a sufficient number of diameters down a uniform flow area channel. However, in a reactor system there are any number of flow disturbers present which can increase the flow noise intensity and contribute to increased displacement amplitudes. (Results of a preliminary experimental study which was conducted to determine the effect of external flow spoilers on vibration amplitude showed rms displacements to be three times greater when a 0.5 in diameter rod was mounted at the entrance to the test section, crosswise to the flow direction [13].) A question which arises is over what length will an increased turbulence level induced by an upstream obstruction be maintained. In general, a study of the flow noise field associated with flow conditions more closely approximating those in an actual reactor is indicated. Also, there has been little published on flow through an annulus [4].

Motivation for this study is provided by (1) the need for information in the low frequency range from annular flow tests under conditions more typical of those of reactor systems and (2) the lack of published state-of-the-art experiments to satisfy this need. The object of this paper is to describe the experimental facility, instrumentation and the initial results obtained from pressure-time measurements of the wall-pressure on a cylinder in annular water flow.

The experimental facility consists of a test section with an inside diameter of 2 in., capable of accepting test elements up to 48 in. long, and mounted in a 500-gpm water loop. The test element is a 1-in.-dia. tube on the surface of which are flush-mounted three, in-line pairs of diametrically opposite miniature pressure transducers. The low frequency behavior of the nearfield was obtained by using a subtraction process with a diametrically-opposite transducer pair to null out the acoustic noise. the rms pressure coefficient, mean-square-value spectral density and longitudinal decay properties of the convecting random pressure field are computed.

EXPERIMENTAL FACILITIES

The water flow loop (Fig. 1), used in the experimental study, is an open system in which a centrifugal pump delivers water to a 2-in. i.d. test section at flow rates up to 500 gallons per minute. Acoustic filter systems were designed and installed in the flow loop to attenuate extraneous low-frequency noise; the filters are similar to those used by Paidoussis [14]. As shown in Fig. 1, one filter system was installed upstream of the test section and one downstream in order to isolate the test section from possible sound sources in the rest of the loop. Each consists of three chambers (representing semi-infinite cavities) that are connected to the flow channel by a short pipe located near the bottom of each chamber. These cavities are mounted axially along the channel and are air-filled during operation. The response of the system is that of a high-pass filter; calculated cutoff frequencies are greater than 400 Hz. The effectiveness of the filter systems was evaluated and an attenuation of the low-frequency mean-square-value response of the pressure on the order of 20 db was achieved; this amount of attenuation while reducing the low-frequency farfield noise level is not in itself sufficient to eliminate the "masking" problem caused by the noise.

To obtain a flexurally-rigid test section, and thereby reduce acceleration effects, a relatively massive V-shaped stainless steel channel was designed (Fig. 2). This test section features a removable flat-plate cover and houses a 2-in. i.d., plexiglass tube which forms the flow channel. The tube is split to permit accessibility to the test element. The test section will accommodate test elements of 36 or 48 in lengths. The test-element supports approximate fixed end conditions. Provisions are made for applying a slight tensile force to the test element. Additional isolation of structural-borne vibration of the test section is provided by the use of flexible bellows and sections of rubber pipe (Fig. 1).

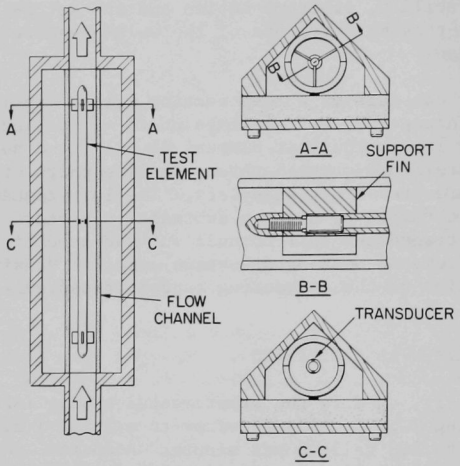

Fig. 1

Water Loop Schematic

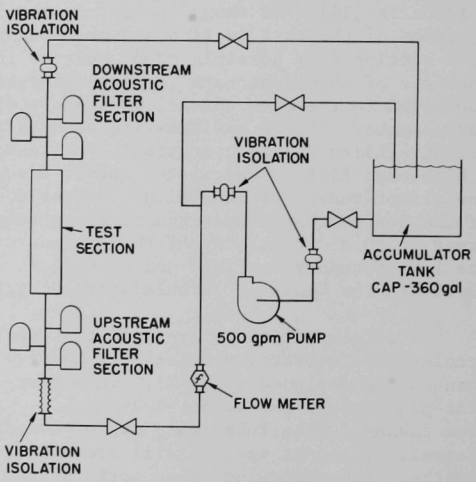

Fig. 2

Test Section and Test Element Support Details

INSTRUMENTATION AND DATA PROCESSING

As discussed in the Introduction, characterization of the nearfield requires knowledge of the mean-square-value spectral density and the narrow-band, longitudinal and circumferential space-time correlations. These characterizing properties are obtained from pressure-time histories measured at closely-spaced intervals along and around the test element. To make these measurements, miniature pressure transducers are needed. The small size is required to obtain direct pressure measurements over a sufficiently broad frequency range; larger sized transducers average the high frequency (small wavelength) eddies resulting in a loss of resolution. While there are relationships for correcting for finite transducer size [2], these corrections have certain inherent inaccuracies and, if possible, it is felt desirable to avoid their use. Small size is also required to obtain transducer spacings that will permit computation of the correlation (decay) lengths and other characterizing properties of the pressure field. This need for small size is made clear in the presentation of results to follow.

Sufficiently small transducers are not available commercially and since Clinch [15] showed the feasibility of constructing and using small units, it was decided to construct our own at Argonne from ceramic piezoelectric material. At the time the transducer work was initiated it was not believed to be as much of a development program as a construction effort. However, because our study required the sensors to be flush-mounted on the surface of a test element possessing inherent flexibility and because we were interested in the low frequency behavior of the nearfield it became apparent that some innovation beyond the work of Clinch was necessary, in particular, (1) the need to eliminate base strain sensitivity from the sensors, and (2) the necessity of obtaining devices which had good, demonstrable low frequency response, were identified.

A schematic of the miniature pressure transducer assembly is given in Fig. 3. The transducers are constructed in situ, that is, the units are built directly onto the tube, following a procedure, which evolved slowly with each set of transducers, as outlined in Appendix A. Originally the sensors were designed to be built on a 0.5-in. diam. tube using ceramic squares, 20 mils on a side. However, various problems associated with transducer construction, sensitivity and reliability of these small units were encountered. To circumvent several of these difficulties, a larger diameter test element (1-in. diam. tube) was used and the sensing area of the transducer was increased a factor of approximately 9 by using 1/16-in. ceramic squares for the sensors; this contributed to the ease of construction and improved the sensitivity and thus the signal-to-noise ratio. The 48 in. long, tubular test element was instrumented with three, longitudinally in-line pairs of diametrically-opposite pressure transducers located at a section 24 in. from the test section inlet. The transducer pairs were spaced 0.1 and 0.2 inches apart. The leads were run through the tube and out through a support fin so as not to disturb the flow field or oscillate the leads. (Transducer calibration and frequency response is discussed in Appendix

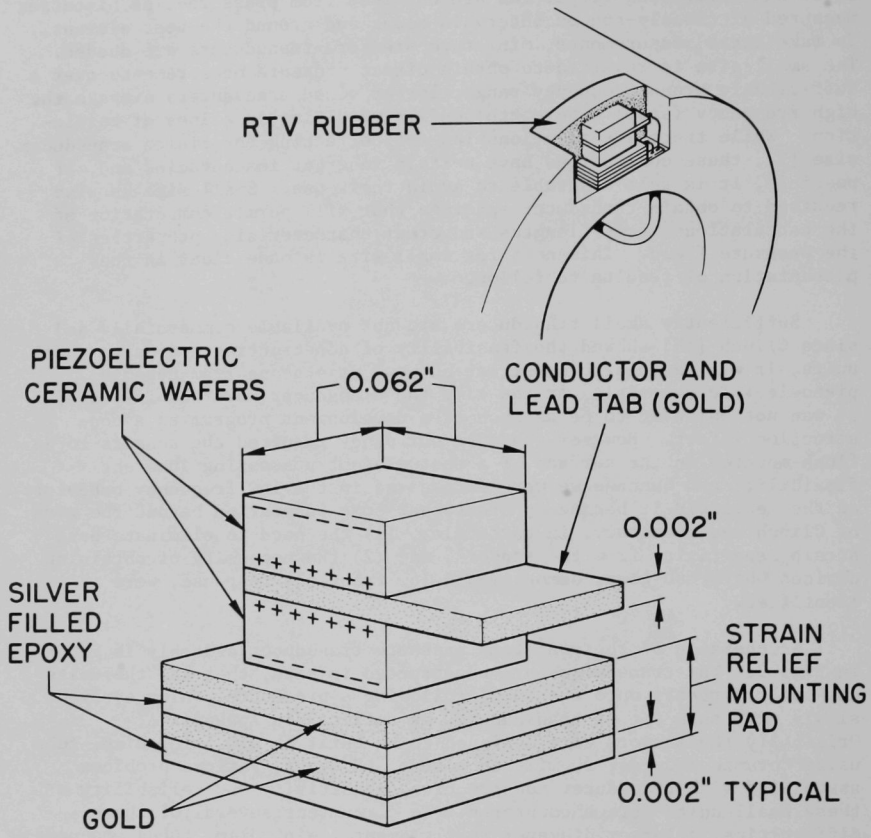

Fig. 3. Miniature Pressure Transducer Assembly

B.) For comparison purposes test section wall pressure was also measured at two locations using commercial transducers which were flush-mounted in the wall.

The test procedure called for measuring wall pressure-time histories for a range of mean axial flow velocities. (Mean flow velocity in the annulus is obtained indirectly by measuring the mean volumetric flowrate with a turbine-type flow meter.) A schematic showing the instrumentation and data processing sequence is given in Fig. 4. For each mean axial flow velocity tested, the pressure-time data were recorded on magnetic tape for subsequent processing. The mean-square-value spectral densities were obtained from an analog spectrum analyzer by slowly sweeping the frequency range with a constant-bandwidth filter while plotting the time-average of the square of the signal; the sweep-rates, filter-bandwidths, and averaging-times used are given in Table I. Broad-band space-time correlation plots were obtained using an electronic analog correlator which gives the time-averaged product of signals from two transducers, one signal delayed in time with respect to the other. The pressure difference from diametrically-opposite pairs was obtained using a sign-changer and adder built from operational amplifiers.

Table I. Spectrum Analysis Parameters

Frequency Range (Hz)	Filter Bandwidth (Hz)	Sweep Rate (sec/kHz)	Averaging Time (sec)
20 - 80	5	3600	1
80 - 500	10	1100	1
500 - 10K	50	210	1

MEAN-SQUARE-VALUE SPECTRAL DENSITY

In computing the response of a flexible rod to nearfield flow noise excitation, perhaps the most important quantity in characterizing the random pressure field is the mean-square-value (MSV) spectral density [1]. The MSV spectral density represents the frequency distribution of the mean-square of a signal. For a homogeneous pressure field, as assumed in the various studies referenced, the MSV spectrum is independent of position along the flow channel at which it is measured.

MSV-spectra were plotted from the six miniature pressure transducers flush-mounted on the instrumented test element. Transducers numbered 2 and 5 (Fig. 4) represent a typical diametrically-opposite transducer pair. Experimental curves* corresponding to a mean axial flow velocity

*The experimental data discussed in this paper were obtained prior to the installation of the acoustic filter systems in the loop.

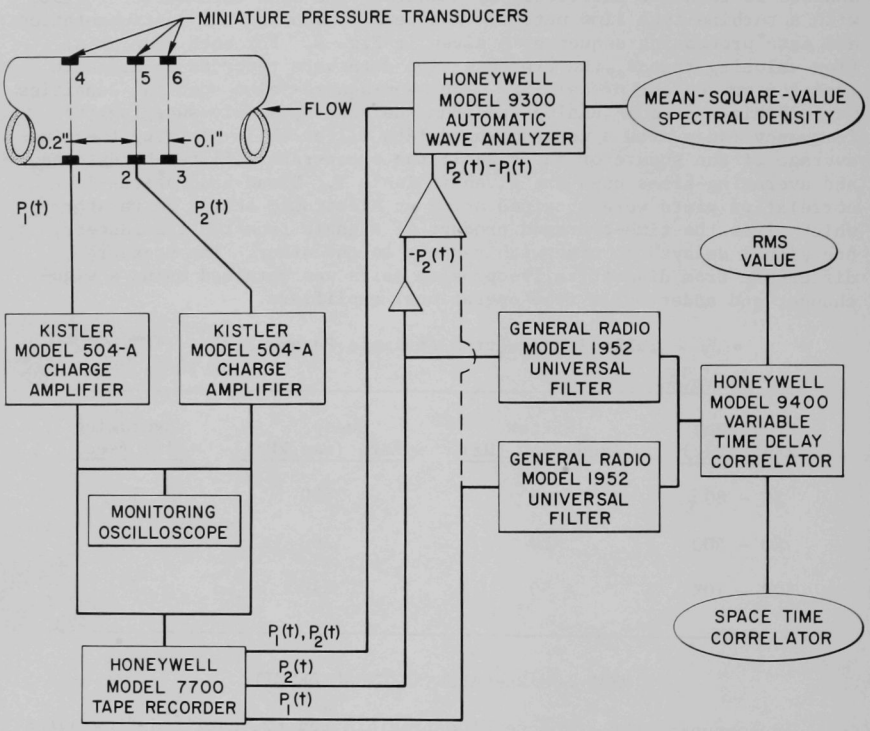

Fig. 4. Instrumentation and Data Processing Block Diagram

of 39 ft/sec are given in Figs. 5 and 6, as measured by transducers 2 and 5 respectively. In Figs. 5 and 6 distinct pressure peaks occurring at a frequency of 60 Hz and multiples up to 300 Hz can be observed. These pressure peaks have been identified as pump-induced pulses; 60 Hz corresponds to the running speed of the pump while 300 Hz represents the vane-passing frequency. In Figs. 7 and 8 MSV-spectra have been sketched from experimental curves for the range of flow velocities tested; the pressure peaks identified with the pumping operation have been neglected.

The corresponding spectra from each of the two transducers agree well, both qualitatively and quantitatively. This good agreement indicates a homogeneous pressure field at the particular section along the test element. In the high frequency range ($f > 600$ Hz) the spectra vary with flow velocity as expected; the energy content of the pressure field increasing with mean flow velocity. The results in this frequency range agree quantitatively with those of Clinch [12]. At the low frequencies ($f < 600$ Hz) there is a significant contribution due to extraneous noise; this was also observed by Clinch [12] and by Willmarth and Wooldridge [16]. This low frequency noise is nearly invariant with flow velocity as shown in Fig. 7 and 8.

The low frequency noise is suspected to be farfield noise which masks the contribution to the measured MSV-spectra from the nearfield. Its presence also makes it difficult, if not impossible, to obtain meaningful cross-correlation measurements in the lower frequency range.

As discussed briefly in the Introduction, it is reasonable to assume that the farfield noise travels as a one-dimensional wave at the speed of sound in the water. Therefore, at a given instant of time, and at a given section along the test element, the contribution to the surface pressure from the acoustic noise is equal around the circumference of the element. Since the wavelengths associated with the low-frequency acoustic noise are long in comparison with the length of the element, it is assumed that the acoustic noise does not significantly contribute to forcing motion of the element. In an attempt to circumvent the problems associated with the presence of low-frequency acoustic noise, the use of pressure differentials taken across the test element was considered. The reasoning here is that with the acoustic noise being equal in magnitude and phase on the circumference of the element it would subtract out.

Let us consider the process of computing the MSV-spectra from the pressure-difference signal

$$P(t) = p_B(t) - p_A(t) \quad . \tag{2}$$

where subscripts A and B refer to diametrically-opposite transducers. Mathematically the MSV-spectral density may be defined as

$$\Phi_P(\omega) = \frac{1}{\pi} \int_0^\infty R_P(\tau) e^{-j\omega\tau} \, d\tau \tag{3}$$

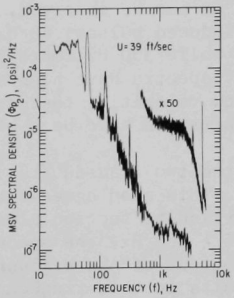

Fig. 5. Typical MSV Spectrum Measured by Transducer No. 2

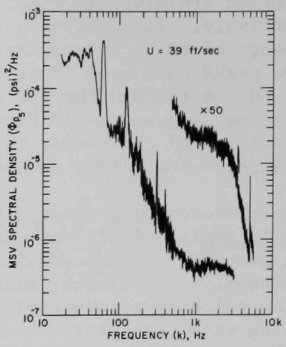

Fig. 6. Typical MSV Spectrum Measured by Transducer No. 5

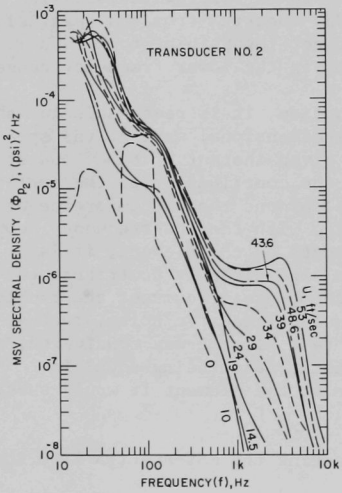

Fig. 7. Family of MSV Spectra Sketched from Experimental Data from Transducer No. 2

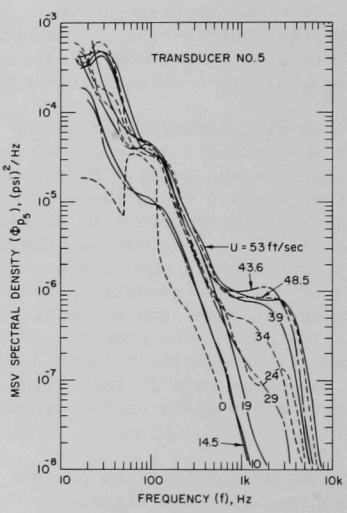

Fig. 8. Family of MSV Spectra Sketched from Experimental Data from Transducer No. 5

where $R_P(t)$ is the stationary auto correlation function for $P(t)$ given by

$$R_P(\tau) = \lim_{T\to\infty} \frac{1}{T} \int_o^T P(t)P(t + \tau)dt \tag{4}$$

An equivalent definition, which is more appropriate for those cases in which measurements are obtained on analog devices, can be written [17]

$$\Phi_P(f) = \lim_{T\to\infty} \lim_{\Delta f\to 0} \frac{1}{T(\Delta f)} \int_o^T P^2_{\Delta f}(f,t)dt \tag{5}$$

where $P^2_{\Delta f}(f,t)$ is the squared instantaneous amplitude of the signal in the narrow-frequency band from f to $(f + \Delta f)$. In actual practice the averaging times are finite and infinitesimally narrow frequency bands are unattainable. An approximation to the above equation which represents the machine computation of MSV-spectral density, can be written

$$\Phi_P(f) = \frac{1}{T(\Delta f)} \int_o^T P^2_{\Delta f}(f,t)dt = \frac{\langle P^2_{\Delta f}(f,t)\rangle}{(\Delta f)} \tag{6}$$

where < > denotes a time average.

Dropping the subscript Δf and substituting Eq. 2 into Eq. 6 obtains

$$\Phi_P(f) = \frac{1}{T(\Delta f)} \int_o^T [p_B(f,t) - p_A(f,t)]^2 dt \tag{7}$$

which expanded can be written

$$\Phi_P(f) = \frac{1}{T(\Delta f)} \int_o^T p^2_B(f,t)dt + \frac{1}{T(\Delta f)} \int_o^T p^2_A(f,t)dt$$

$$- \frac{2}{T(\Delta f)} \int_o^T p_B(f,t)p_A(f,t)dt \tag{8}$$

The first two integrals on the right-hand-side (RHS) represent the MSV-spectral density of the overall pressure measured by transducers B and A respectively, that is, $\Phi_{p_B}(f)$ and $\Phi_{p_A}(f)$. For a homogeneous field at the given section

$$\Phi_{p_B}(f) = \Phi_{p_A}(f) = \Phi_{total}(f) \tag{9}$$

The third integral on the RHS of Eq. 9 represents the cross-spectral density between pressure signals $p_A(t)$ and $p_B(t)$. The farfield contributions measured by each transducer will be in-phase, since the transducers are located at the same section, hence they will correlate. However,

the nearfield contributions are random and unrelated and thus will correlate to zero. Therefore, the third integral gives the MSV-spectral density of the farfield contribution only, $\Phi_{farfield}(f)$. In the computational process this is subtracted from the MSV-spectral density of the total pressure

$$\Phi_p(f) = 2[\Phi_{total}(f) - \Phi_{farfield}(f)] \tag{10}$$

and the term within the brackets in Eq. 10 then represents the desired quantity, the MSV-spectral density of the nearfield noise. The factor of two in front indicates that the spectrum computed from the pressure difference is twice the magnitude of the nearfield spectrum.

Pressure differences from diametrically-opposite transducer pairs were obtained using an analog subtractor made up from operational amplifiers. MSV-spectra for the pressure-differential signals were plotted for the range of mean flow velocities tested. A typical experimental plot is given in Fig. 9; nearfield MSV-spectra sketched from experimental results are shown in Fig. 10.

A comparison of curves from Figs. 5-8 with the corresponding curves in Figs. 9 and 10 shows that the subtraction process efficiently cancels the "extraneous" low-frequency noise and pump pulses and thus supports the hypothesis that is is acoustic in nature. In general, the nearfield spectra are relatively flat out to a cut-off frequency, implying band-limited white noise; the magnitude, or energy content, increases with mean axial flow velocity. However, it should be noted that the levels between the high-frequency (turbulent eddy) spectra obtained from a single transducer and those from a corresponding pressure-difference signal consistently differ by a factor greater than the two as given by Eq. 10. This discrepancy has not yet been resolved; equipment gains and calibrations are being checked as a possible source of error. The low-frequency behavior of the nearfield is believed to be new information and is of importance to the understanding and prediction of flow-induced vibration of reactor components, again since structural vibration frequencies can, in general, be expected to fall in the low frequency range.

The pressure peak exhibited by the curves of Fig. 10 occurs at a frequency which can be associated with the natural vibration frequency of the instrumented test element ($\sim$44 Hz). The pressure peak itself is assumed to be the result of a slight vibration of the test element. The bending strain induced by this motion (of the order of 0.1 mil) is sensed by the miniature pressure transducers which are somewhat strain sensitive despite design and development efforts (Appendix A) which, while greatly relieving the problem, were not completely successful in eliminating strain sensitivity. In the subtraction process the transducer "output" due to test element straining is doubled because the strains add. This doubling is further amplified through the squaring-process associated with the computation of MSV- spectra. It is interesting to note that the magnitude of the peak is greatest at the lowest flow velocity and shows a decreasing trend with increasing mean flow velocity. If we assume that the excitation causing the low-level

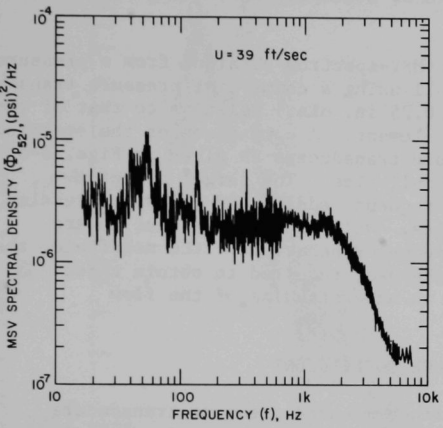

Fig. 9

Typical Pressure-difference MSV Spectrum from Transducers 2 and 5

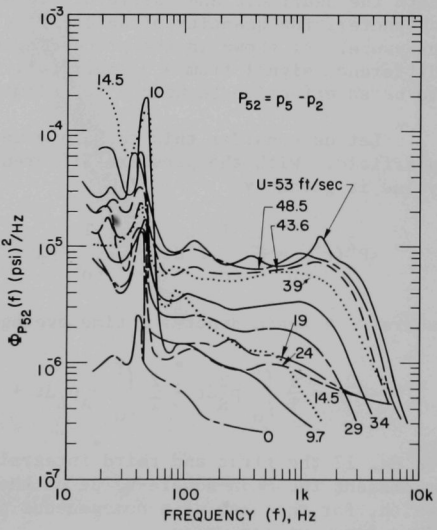

Fig. 10

Family of Pressure-difference MSV Spectra Sketched from Experimental Plots

test element vibration is independent of flow velocity (as it might be if it were structure-borne from an external source), the decrease in amplitude might be explained by the associated increase in effective system damping which has been shown to accompany increasing flow velocity [18].

In Fig. 11 we have plotted a MSV-spectrum obtained from a pressure measurement on the test section wall using a commercial pressure transducer with a large sensing area (∿0.25 in. dia.) relative to that of the miniature transducers on the test element. A comparison of the spectrum of Fig. 11 with those from miniature transducers as given in Figs. 5-8 clearly illustrates the need for small size. The larger diameter transducer averages out the high frequency eddies and a loss of resolution at the high frequencies results. While it is true that we are primarily interested in the low frequency behavior of the nearfield, the high frequency response is, nevertheless, required to obtain those insights and information basic to an understanding of the flow phenomenon.

RMS PRESSURE COEFFICIENT

As discussed earlier, the surface-mounted pressure transducers measure an overall pressure fluctuation containing contributions from both the nearfield and farfield. In our study of the nearfield, a characterizing quantity of interest is the root-mean-square (rms) pressure. As shown in the preceeding section, working with a pressure-difference signal from a diametrically-opposite transducer pair proved to be an effective technique for eliminating the farfield contribution.

Let us consider this technique in computing the rms pressure of the nearfield. With the pressure difference given by Eq. 2, the mean-square-value is given by

$$\langle P^2(t)\rangle = \frac{1}{T}\int_0^T P^2 dt = \frac{1}{T}\int_0^T (p_B - p_A)^2 dt \tag{11}$$

where < > again denotes a time average. Expanding Eq. 11 obtains

$$\langle P^2\rangle = \frac{1}{T}\int_0^T p_B^2 dt - \frac{2}{T}\int_0^T p_A p_B dt + \frac{1}{T}\int_0^T p_A^2 dt \tag{12}$$

In Eq. 12 the first and third integrals on the right-hand-side (RHS) represent the mean-square-value of the overall pressure fluctuations which, for the case of a homogeneous pressure field, will be equal. Therefore, we can write

$$\langle P^2\rangle = 2\left[\frac{1}{T}\int_0^T p_A^2 dt - \frac{1}{T}\int_0^T p_A p_B dt\right] \tag{13}$$

The second integral on the RHS of Eq. 13 represents a cross-correlation between pressure signals $p_A(t)$ and $p_B(t)$. The contributions from the

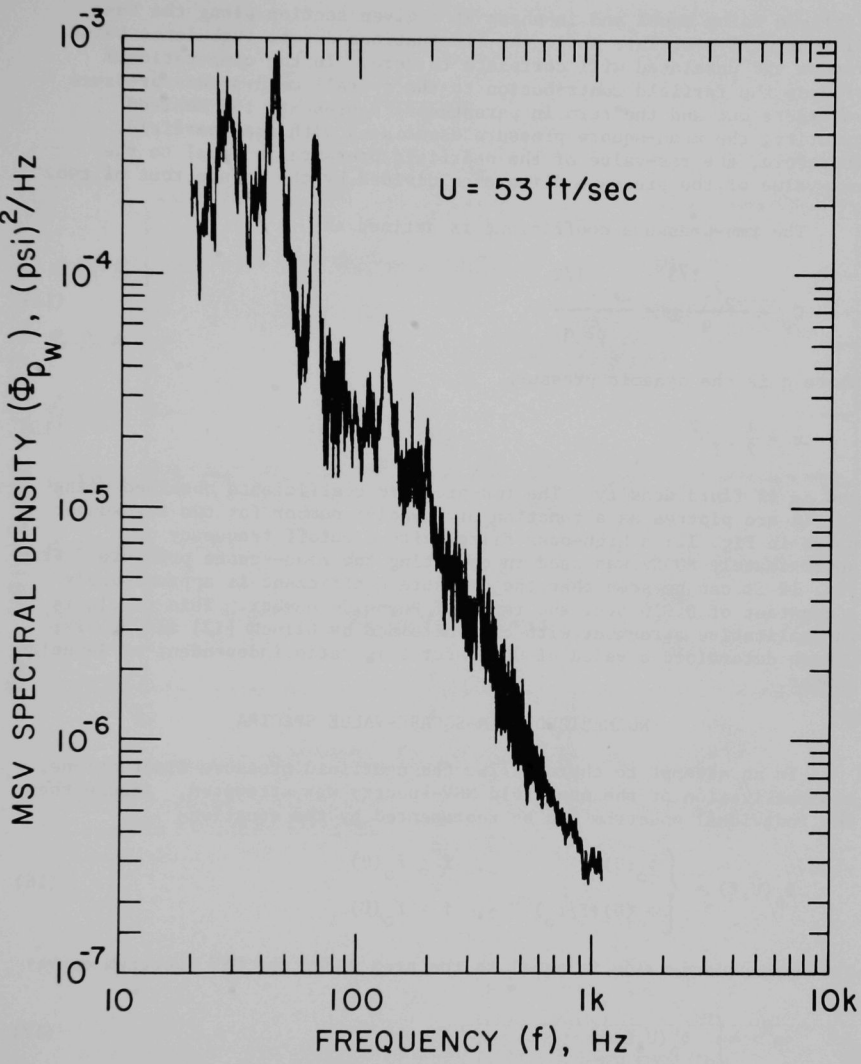

Fig. 11. Typical MSV Spectrum Measured at the Test Section Using a Relatively Large Transducer

farfield being equal and in-phase at a given section along the test element will correlate while the fluctuations due to turbulence being random and unrelated will correlate to zero. In the computational process the farfield contribution to the overall mean-square pressure subtracts out and the term in parenthesis represents the desired quantity, the mean-square pressure associated with the nearfield. Therefore, the rms-value of the nearfield pressure is equal to the rms-value of the pressure difference divided by the square root of two.

The rms-pressure coefficient is defined as

$$C_p = \frac{\langle p^2 \rangle^{1/2}}{q} = \frac{\langle p^2 \rangle^{1/2}}{\sqrt{2}\, q} \tag{14}$$

where q is the dynamic pressure

$$q = \frac{1}{2} \rho_f U^2 \tag{15}$$

and ρ_f is fluid density. The rms-pressure coefficients obtained using Eq. 14 are plotted as a function of Reynolds number for two transducer pairs in Fig. 12; a high-pass filter with a cutoff frequency of approximately 80 Hz was used in computing the mean-square pressure. From Fig. 12 it can be seen that the pressure coefficient is approximately a constant of 0.010 over the range of Reynolds number. This result is in qualitative agreement with that obtained by Clinch [12] and others; Clinch determined a value of 0.007 for this ratio independent of Reynolds number.

NORMALIZED MEAN-SQUARE-VALUE SPECTRA

In an attempt to characterize the nearfield pressure fluctuations, a normalization of the nearfield MSV-spectra was attempted. Assume that the individual spectrum can be represented by the equation

$$\Phi_p(U,f) = \begin{cases} \Phi_o(U) & , \quad f \le f_o(U) \\ \Phi_o(U)(f/f_o)^{-n} & , \quad f > f_o(U) \end{cases} \tag{16}$$

The mean-square-value is equal to the area under the MSV spectrum curve

$$\langle p^2 \rangle = \int_o^\infty \Phi_p(U,f)\,df \tag{17}$$

Substituting Eq. 16 into Eq. 17 and integrating gives

$$\langle p^2 \rangle = \frac{n}{n-1} \Phi_o f_o \tag{18}$$

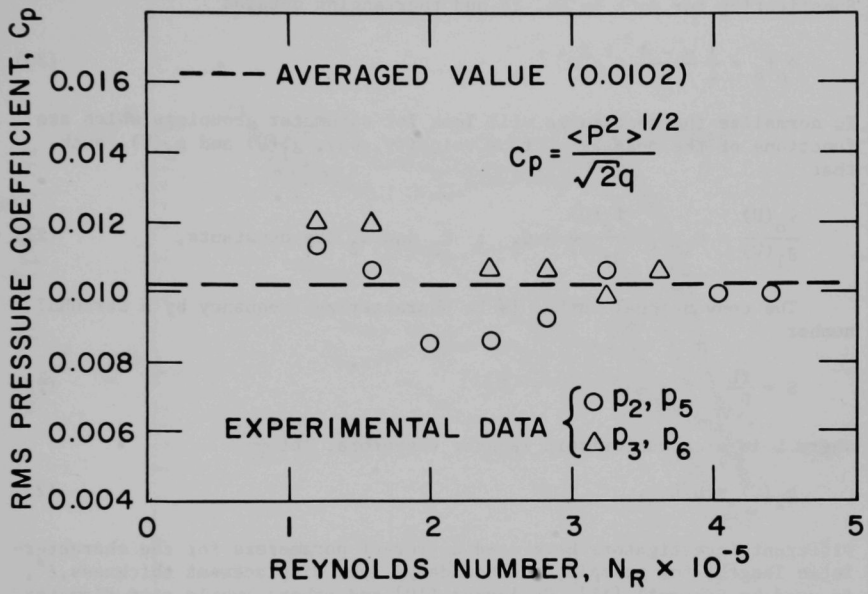

Fig. 12. RMS Pressure Coefficient for the Nearfield as a Function of Reynolds Number

From the results of other investigations and as shown in Fig. 12, the rms pressure coefficient is approximately a constant

$$C_p = \text{const} = \frac{\langle p^2 \rangle^{1/2}}{\frac{1}{2}\rho_f U^2} \tag{19}$$

Substituting for $\langle p^2 \rangle$ in Eq. 18 and rearranging obtains

$$\Phi_o f_o = \frac{1}{4}\frac{n-1}{n} C_p^2 \rho_f^2 U^4 \tag{20}$$

To normalize the spectra we will look for parameter groupings which are functions of the mean axial flow velocity, say, $g_1(U)$ and $g_2(U)$, such that

$$\frac{\Phi_o(U)}{g_1(U)} = C_1 \quad , \quad \frac{f_o(U)}{g_2(U)} = C_2 \quad ; \quad C_1 \text{ and } C_2 \text{ are constants,} \tag{21}$$

The conventional method is to characterize frequency by a Strouhal number

$$S = \frac{fL}{U} \tag{22}$$

where L is a characteristic length; therefore, let

$$g_2(U) = U/L \quad . \tag{23}$$

Different investigators have used different parameters for the characteristic length; for example, the boundary-layer displacement thickness, δ^*, is used by Bakewell [11], Schloemer [10] and others, while pipe diameter, d, has been used by Corcos [19] and Clinch [12]. Similarly both the free stream velocity and the mean convection velocity have been used for the characteristic flow velocity. Use of the boundary-layer displacement thickness and pipe diameter lend themselves to characterizing flow over a flat plate and pipe flow respectively. However, for annular flow we have chosen the hydraulic diameter,

$$d_h = D - d \tag{24}$$

where D is test section inside diameter and d is test element diameter. In Fig. 13 the nearfield MSV-spectra are plotted as a function of $S = fd_h/U$. As can be seen from Fig. 13, normalization of frequency using Eq. 23 does a reasonable job of correlating the spectra; the "break frequencies" of the spectra occur at an approximately constant Strouhal number value of 4.

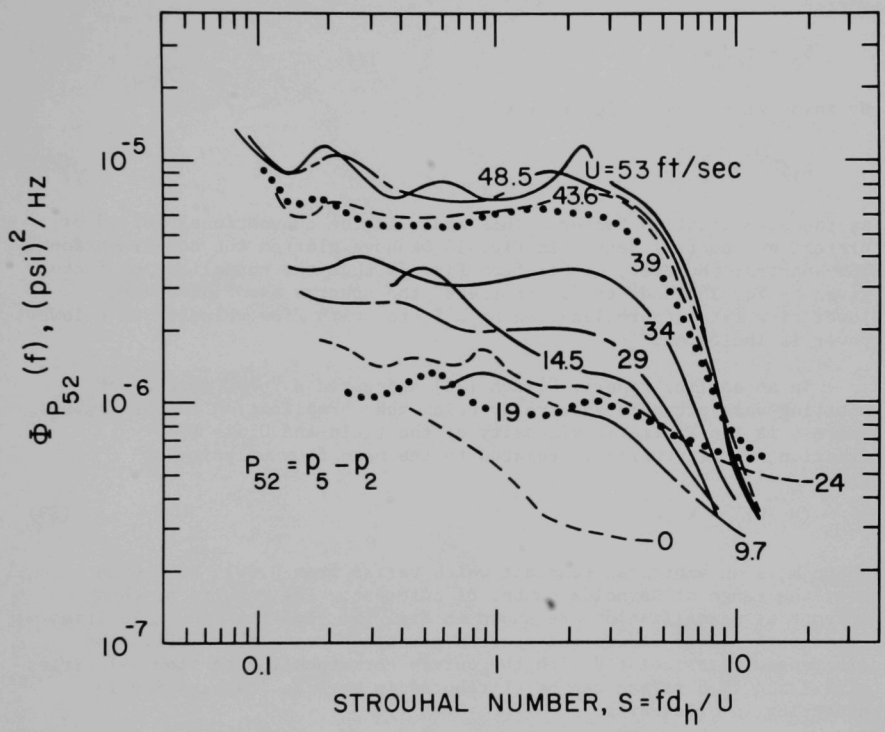

Fig. 13. Family of Nearfield Spectra as a Function of Strouhal Number

Using Eq. 25 with Eq. 20 gives

$$\frac{\phi_o S_o}{g_1(U)} = \frac{n-1}{4n} \frac{C_p^2 \rho_f^2 U^3 d_h}{g_1(U)} \tag{26}$$

where

$$S_o = f_o d_h / U \tag{27}$$

By inspection, one is led to try

$$g_1(U) = \rho_f U^3 d_h \tag{28}$$

as the normalization factor. This again is the conventional method of presenting spectral data. In Fig. 14 we have plotted the non-dimensional MSV-spectra. However, we see from Fig. 14 that the normalization factor given by Eq. 28 tends to "overcorrect" the spectra associated with lower flow rates; normalization by a factor with flow velocity to a lower power is indicated.

In an earlier report, Clinch [20] suggested a "new" method* of plotting wall pressure spectra by using the normalization factor $(\rho_f^2 \nu U_\tau^2)$, where ν is the kinematic viscosity of the fluid and U_τ is the friction velocity which is related to the mean flow velocity as

$$(U_\tau / U)^2 = k \tag{29}$$

where k is an empirical constant which varies from 0.0015 to 0.0016 over the range of Reynolds number of interest. The results of this attempt at normalization are shown in Fig. 15. For the flow velocities greater than 14.5 ft/sec the spectra normalize reasonably well. The discrepancies associated with the curves corresponding to flow velocities of 9.7 and 14.5 ft/sec can be attributed in part to inaccuracies in measuring low flowrates.

SPACE-TIME CORRELATIONS

Space-time correlations from longitudinally- and circumferentially-spaced transducers give information from which the convecting and decaying properties of the nearfield can be computed. For this initial study our instrumented test element gives us only three longitudinally-spaced measuring stations and none circumferentially-spaced. Broad-band space-time correlations using differential pressure signals were obtained from the variable time delay correlator (Fig. 4) for the frequency range from 300 Hz to 15 kHz. Typical correlation plots for two flow velocities are given in Figs. 16 and 17.

---

*It should be noted that in his later paper [12] Clinch reverts to the "conventional" method of normalizing with $(\rho_f^2 U^3 d)$.

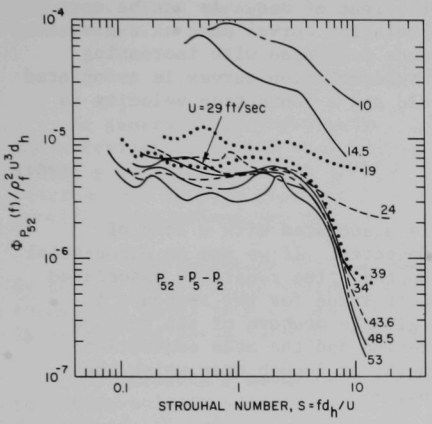

Fig. 14. Nondimensional, Near-field MSV Spectra

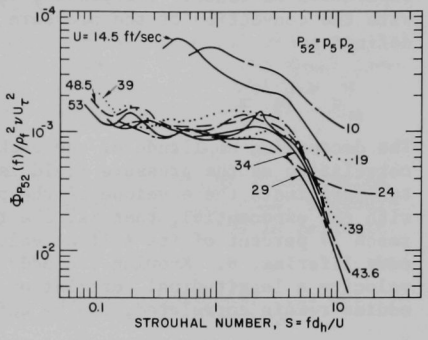

Fig. 15. Nondimensional, Near-field MSV Spectra

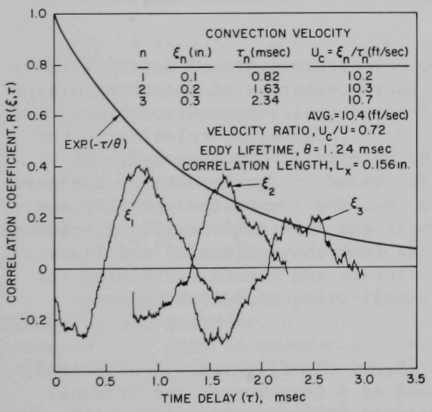

Fig. 16. Typical Broad-band, Longitudinal Space-Time Correlations; U = 14.5 ft/sec

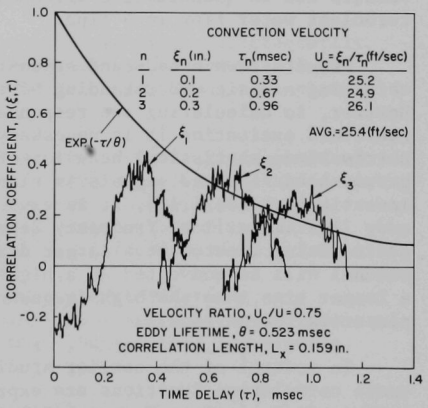

Fig. 17. Typical Broad-band, Longitudinal Space-Time Correlations; U = 34 ft/sec

The curves are plotted as a function of time delay with each curve representing a different pressure transducer separation. The curves have been normalized such that the zero time delay, or auto correlation, value corresponds to a correlation coefficient of one. As can be seen from Figs. 16 and 17 the individual correlation curves peak at a given value of time delay and the peak amplitude decreases with increasing separation distance. The peaking of the correlation curves is associated with the convection of the pressure field and a convection velocity is defined as

$$U_c = \xi_m/\tau_m \tag{30}$$

The decreasing amplitude of the peaks is associated with a loss of correlation as the pressure field is convected. If we use an exponential to approximate the envelope of the peaks, the "time constant" associated with the exponential, that is, the time it takes for the response to reach 37 percent of its initial value, gives a measure of the average eddy lifetime, θ. Knowing the eddy lifetime and the mean convection velocity a longitudinal correlation length, or length over which the eddies remain correlated, can be defined as

$$L_x = U_c\theta \tag{31}$$

The computed convection velocities, average eddy lifetime and longitudinal correlation length are given on Figs. 16 and 17. In general these results are in quantitative agreement with those of Clinch [12] for turbulent water flow in a pipe.

Results from broad-band space-time correlations are of interest in obtaining a basic understanding of the characteristics of the nearfield. However, in calculating the response of structural components to the nearfield excitation it is necessary to have information relating to the narrow-band, statistical behavior of the nearfield. Data analysis of narrow-band filtered signals is planned. Based on the results of earlier investigators [9,11,12], it is expected that the convection velocity and eddy lifetime will be frequency dependent; the low-frequency, large-size eddies being located at a larger distance from the surface of the flow channel will be convected at a higher velocity and remain correlated for a longer time than the high-frequency, small-size, eddies which are closer to the surface.

In several of the earlier studies [9,11] the filtered, longitudinal, space correlation functions are expressed as a function of the Strouhal number, $f\xi/U_c$, only. However, Clinch's data [12] do not conform with this manner of representation particularly at low frequencies. Clinch suggests expressing the longitudinal correlation amplitude A in the form

$$A = \exp(-\xi/L_x) \tag{32}$$

where the correlation length is frequency dependent. Because of this difference in interpretation and of the importance of low frequency behavior to our study further investigation is indicated and is, in fact, planned.

As can be seen from Figs. 16 and 17, close-spacing of pressure transducers is required to obtain a sufficient number of data points to characterize the longitudinal decay of correlation with sufficient accuracy. This requirement points out the need for small-size pressure transducers.

CONCLUDING REMARKS

In general, results obtained from an experimental study and characterization of the wall pressure on a cylinder in annular water flow showed good agreement with earlier investigations of wall pressure fluctuations in pipe flow and in flow over flat plates. The following specific conclusions may be drawn:

(1) Low-frequency "extraneous" noise can be effectively eliminated by taking the pressure difference from a diametrically-opposite, pressure transducer pair; this supports the hypothesis that the noise is acoustic in nature and not a part of the nearfield.

(2) Nearfield mean-square-value spectra are essentially flat out to a flow-velocity-dependent cutoff frequency. The data at low-frequencies is believed to constitute new information.

(3) RMS pressure coefficients are approximately constant over the range of Reynolds number tested. However, the average value of 0.010 is greater than the 0.007 value reported by several investigators of turbulent boundary-layer flow.

(4) A Strouhal number representation of frequency satisfactorily normalizes the spectra with respect to frequency. This result is in agreement with that arrived at from independent studies of flat plate and pipe flows with both air and water.

(5) The magnitude of the spectra was most effectively normalized by nondimensionalizing the spectra as $\Phi_p/\rho_f \nu U_\tau^2$, that is, by scaling with the square of the mean flow velocity. The conventional method of normalizing by scaling with the cube of the flow velocity tended to "overcorrect" the spectra associated with the lower flow velocities.

(6) Convection velocity ratios, average eddy lifetimes, and longitudinal correlation lengths obtained from broad-band space-time correlations were in general agreement with results from independent studies of turbulent flow in pipes.

In addition to the above conclusions which were drawn from the test results, the feasibility of constructing reliable miniature pressure transducers that are sufficiently strain insensitive to operate on the surface of a tubular test element possessing inherent flexibility was demonstrated in the course of carrying out the experimental program.

Plans for future work include:

(1) A study of the structure of the nearfield. In general, turbulent flow can be considered to be made up of turbulent eddies that are

continually being created and destroyed. These eddies have associated with them a length scale and a time scale. The upper limit on size is determined mainly by the size of the apparatus, or flow channel, while the lower limit is determined by viscosity effects [21]. If we take the wavelength given by

$$\lambda = U_c/f \tag{33}$$

to be representative of eddy size, it is easily seen that with an upper limit being the width of the annulus, low-frequency eddies (say $f < 300$ Hz) cannot exist for the range of flow velocities tested. It is hypothesized that the low frequency contribution to the mean-square-value spectra as shown on Figs. 9 and 10 is due to slow variations in fluid flow which, while not belonging to the turbulent flow per se, can be considered as part of the nearfield. Support for this notion is given in photographs of flow through a channel [21; Fig. 1-10, p. 13]. The statistical descriptions of these slow flow variations might be expected to be significantly different from those associated with the turbulent-eddy flow.

(2) The measurement of narrow-band space-time correlations and characterization of the results. This study will result in information relating to the frequency dependence of the statistical properties of the nearfield. Special consideration will be given to the interpretation of results from low-frequency-centered bandwidths as an aid to understanding the structure of the nearfield.

(3) Determination of the effect of various flow spoilers on altering or contributing to the energy content of the nearfield. Included will be a study of the feasibility of characterizing various spoilers via a pressure measurement. The homogeneity of the pressure field downstream from a spoiler and the decay length, as the length required for a disturbance to die out, will be investigated.

(4) Instrumentation of a 0.5-in. dia., tubular test element with from 5 to 7 longitudinally in-line, miniature pressure transducers. This instrumented test element will yield additional data points from space-time correlations and will be used to study the nearfield noise within a bundle of 7 elements with and without wire wrap.

ACKNOWLEDGMENTS

This work was performed under the sponsorship of the Special Technology Branch, Division of Reactor Development and Technology, U. S. Atomic Energy Commission.

The authors gratefully acknowledge the contributions of Messrs. J. A. Jendrzejczyk and W. Lawrence to the study. Mr. Lawrence carried out the construction of the instrumented test element, Mr. Jendrzejczyk was responsible for the data processing, and both were active in performance of the experiments and interpretation of results.

REFERENCES

1. S. S. Chen and M. W. Wambsganss, Response of a Flexible Rod to Near-Field Flow Noise, Proceedings of the Conference on Flow Induced Vibrations in Reactor System Components, Argonne National Laboratory, Argonne, Illinois, May 14-15, 1970.

2. G. M. Corcos, Resolution of Pressure in Turbulence, J. Acoust. Soc. Am. 35, 192-199 (1963).

3. J. R. Reavis, Vibration Correlation for Maximum Fuel-Element Displacement in Parallel Turbulent Flow, Nucl. Sci. and Eng. 38, 63-69 (1969).

4. D. J. Gorman, The Role of Turbulence in the Vibration of Reactor Fuel Elements in Liquid Flow, AECL-3371, Atomic Energy of Canada Limited, Chalk River, Ontario, May 1969.

5. E. J. Skudrzyk and G. P. Haddle, Noise Production in a Turbulent Boundary Layer by Smooth and Rough Surfaces, J. Acoust. Soc. Am. 32(1), 19-34 (January 1960).

6. D. H. Tack, M. W. Smith, and R. F. Lambert, Wall Pressure Correlations in Turbulent Airflow, J. Acoust. Soc. Am., 33(4): 410-418 (April 1961).

7. G. M. Corcos, Pressure Fluctuations in Shear Flows, Univ. Calif. Inst. Eng. Res. Rept., Ser. 183, Issue 2 (July 1962).

8. H. P. Bakewell, Jr., G. F. Carey, J. J. Lebuha, H. H. Schloemer and W. A. Von Winkle, Wall Pressure Correlations in Turbulent Pipe Flow, U. S. Navy Underwater Sound Laboratory Report USC-559 (August 1962).

9. H. P. Bakewell, Jr., Narrow-Band Investigations of the Longitudinal Space-Time Correlation Function in Turbulent Airflow, J. Acoust. Soc. Am., 36(1): 146-148 (January 1964).

10. H. H. Schloemer, Effects of Pressure Gradients on Turbulent-Boundary-Layer Wall-Pressure Fluctuations, J. Acoust. Soc. Am. 42(1): 93-113 (1967).

11. H. P. Bakewell, Jr., Turbulent Wall-Pressure Fluctuations on a Body of Revolution, J. Acoust. Soc. Am. 43(6): 1358-1363 (1968).

12. J. M. Clinch, Measurements of the Wall Pressure Field at the Surface of a Smooth-Walled Pipe Containing Turbulent Water Flow, J. Sound Vibr. 9(3): 398-419 (1969).

13. Reactor Development Program Progress Report, Argonne National Laboratory, ANL-7500, 109-110 (September 1968).

14. M. P. Paidoussis, An Experimental Study of the Vibration of Flexible Cylinders Induced by Nominally Axial Flow, Nucl. Sci. Eng. 35, 127-138 (Jan. 1969).

15. J. M. Clinch, Miniature Transducer Assembly for Measuring the Properties of the Wall-Pressure Field in Turbulent Flows, J. Acoust. Soc. Am. 40(1) (1966).

16. W. W. Willmarth and C. E. Wooldridge, Measurements of the Fluctuating Pressure at the Wall Beneath a Thick Turbulent Boundary Layer, J. Fluid Mech. 14 (Part 2): 187-210 (1962).

17. J. S. Bendat and A. G. Preisol, Design Considerations and Use of Analog Power Spectral Density Analyzers, printed and distributed by Minneapolis-Honeywell Regulator Company, Denver Division (1964).

18. M. W. Wambsganss and P. L. Zaleski, Flow-Velocity-Dependence of Damping in Parallel-Flow-Induced Vibration, Trans. Am. Nucl. Soc. 12(2): 839-840 (1969).

19. G. M. Corcos, Pressure Measurements in Unsteady Flows, Proceedings Symposium on Measurements in Unsteady Flow, ASME Hydraulics Conf., Worchester, Mass., May 21-23, 1962.

20. J. M. Clinch, Study of Vibrations Induced in Thin-Walled Pipes by Fluid Flow, IIT Research Institute Report for NASA Contract No. NAS8-11248 (1965).

21. J. O. Hinze, Turbulence, McGraw-Hill Book Co., New York, 1959.

APPENDIX A. TRANSDUCER CONSTRUCTION

The present construction details evolved slowly with each set of transducers which were built. The following techniques more or less represent the state of the art in transducer construction in our program.

Although these details are rather straightforward when described, it must be remembered that all construction was done using a 40 power microscope. The unit used was a Carl Zeiss operation microscope. Because of the self-illumination and large depth of field offered by this unit it is felt that this is an excellent choice for this type of work.

The 1 x 2 x 0.01 inch sheets of ceramic material* were sliced into 0.020 in. square wafers by the Argonne Optic Shop. Although the square shape effectly behaves as a larger diameter circular unit they were used because of the relative ease with which they were obtained. Also, in actual usage the effective sensing area is more dependent on the opening in which the transducer is placed rather than the ceramic size.

Upon receipt, the wafers were cleaned and inspected for chipping or size defects. The polarity of each piece chosen for assembly was determined and color coded with a colored lacquer. An additional purpose

*PZT 5H obtained from Clevite Corporation.

of this lacquer coating was to seal and insulate the sides or edges of the piezoelectric material. It was found that if this was not done it was possible to create a partial short circuit on the edges of the ceramic square with the silver filled epoxy solder used to cement the pieces together and thus greatly reduce the electrical output of the finished transducer. The paint was easily chipped and scraped free of the metal surfaces of the square in the appropriate spots for subsequent soldering.

Actual construction of the units was accomplished by stacking the elements in the order shown in Fig. 3. Because virtually any shift in orientation of the individual elements would result in gross misalignment on this miniature scale, the assembly is done in discrete steps allowing the epoxy solder to harden between steps.

The transducer construction was done in situ - that is, the units were built directly onto the test element rather than fabricated completely and installed when done. An oversize slot or flat was milled into the test elements where the construction was to take place and all penetrations were made on this flat for the coaxial lead wires which connect the completed unit to the charge amplifiers. The transducers were electrically connected to these coaxial lead wires with .002 in. gold wires. Silver filled epoxy solder was used to accomplish this also. The slot area immediately surrounding the pressure sensor was then built up to the original tube size, using an epoxy plastic. An annular gap of < .010 in. was maintained between this plastic and the transducer. This operation essentially formed a pressure port exposing the transducer only to the fluid immediately above it. The final operation consisted of plotting the sensor in an RTV silicone rubber. This provided electrical insulation for the transducer and filled all gaps so that no depressions or protrusions were present in the area surrounding the transducer. The area was inspected microscopically for smoothness so that the flow would not be disturbed.

APPENDIX B. CALIBRATION

Since one of the primary requirements of the transducers was to show good demonstrable frequency response in the range of 10 to 100 Hz, a small, low frequency dynamic pressure calibration chamber was built to operate in this region. This device consists of a small cylindrical (2-1/2 dia. x 4 in. long) pressure chamber fitted with an electromechanical valving system capable of oscillating the pressure in the region $5 < f < 150$ Hz. The ends are flanged for easy access and are sealed with O-rings.

The end flanges are fitted with a pressure tube penetration which allows the installation of a test rod through the chamber. In operation only the section of the test element on which the transducers are located is within the calibration chamber. The remainder of the test element protruded through the pressure tube penetrations. The chamber is thus kept to a small size yet permits the calibration of any length specimen.

Because of the variation in transducer sensitivity with ambient pressure, the calibration chamber is normally maintained at a fixed, preselected mean pressure level. During actual test loop operation, the test section pressure is also maintained at this same pressure level. This simple procedure eliminates the necessity of changing the equipment calibration settings during tests due to pressure variations and thus reduces the possibility of introducing calibration errors.

In operation the frequency of the pressure pulsations are varied over the region of interest using the Honeywell frequency sweep and tracking filter section of the data analysis system. The pressure level is servo-controlled at a pre-selected level using an Atlantic Research Model Lc-60 Transducer as a control. This commercial unit was initially calibrated using a step change in pressure. This procedure produced very good agreement with the calibration factor provided by the manufacturer. A block diagram of the control scheme is pictured on Fig. 18. With proper charge amplifier settings the constructed transducers have produced effective calibration factors of approximately 3.0 volts/psi.

DISCUSSION

None.

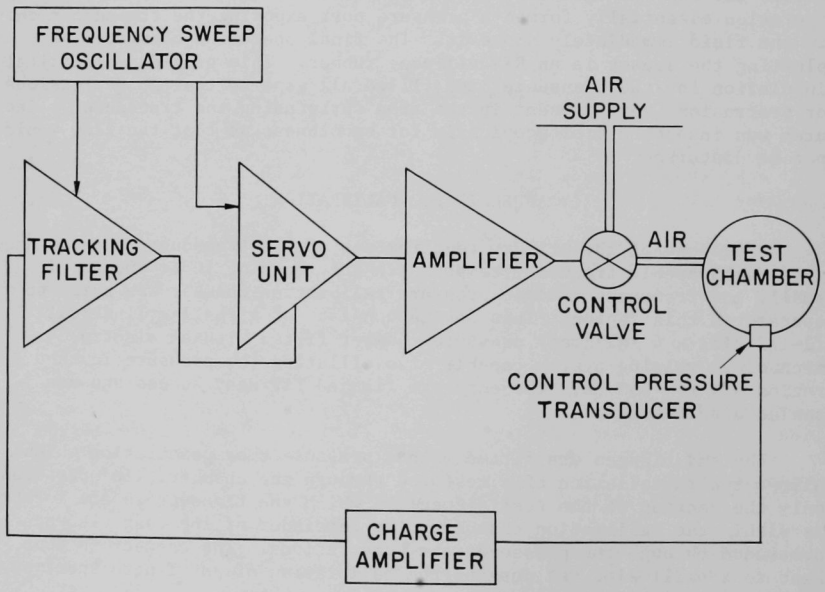

Fig. 18. Calibration Control Scheme

CONDUCTIVITY CELLS FOR FLOW INDUCED VIBRATION MEASUREMENTS*

G. R. Sawtelle

Engineering Mechanics Section
Physics and Engineering Division
Battelle Memorial Institute
Pacific Northwest Laboratories
Richland, Washington

ABSTRACT

This report describes the development of a conductivity cell instrumentation for measuring flow induced vibrations in long, slender fuel pins. The design, construction and evaluation of conductivity cells and associated signal conditioning equipment is discussed in detail, providing the background for the underlying theory, operating procedure and limitations of a particular instrument, the PNL Impedance Detector.

INTRODUCTION

The Vibration Problem

Flow induced vibrations have generated failures in various reactor components.(1) Generally these failures occurred in regions of highly turbulent flow and vortex shedding. In the Fast Test Reactor (FTR), heat generated in the fuel bundles will be removed by pumping large quantities of sodium past closely spaced, spiral wire wrapped fuel pins. The resulting turbulent flow conditions, ideal for removing heat efficiently, may generate flow induced vibrations. Failure of the fuel-element cladding can occur from vibration-induced fretting, and such an event could cause a costly reactor shutdown. The severity of vibrations must be evaluated for the contemplated design, so that if serious, appropriate measures can be taken to reduce or eliminate vibrations.

In general, theoretical methods to predict flow induced vibrations are not available; any theoretical treatment would be extremely difficult because of the complex geometric and

* This paper is based on work performed under United States Atomic Energy Commission Contract AT(45-1)-1830.

time varying boundary conditions present in the spiral wire wrap fuel design. Furthermore, the forcing function associated with flow induced vibrations is not well defined. Several investigators have derived empirical equations[2,3,4,5] for single pins with known support conditions; however, in comparing these equations with experimental results of other investigators, differences arise which have yet to be reconciled. Because of the uncertainties in predicting vibrations of single pins, experiments are required.

An experimental evaluation of flow induced vibrations requires appropriate measurements to establish the fatigue life and wear rate of fuel pins. Since the precise failure mechanism in a fuel pin is unknown, a knowledge of the mode shapes and frequencies may provide much of the information needed to relate pin motion to failure. Mode shapes and frequencies can be determined by measuring the displacement histories in two orthogonal directions at various axial locations along the pin. Since the spacing between fuel pins in a bundle can be quite small, vibration transducers (i.e., sensors) externally mounted on the pin may disturb the flowing coolant; hence internal or surface mounted transducers are required. In addition to being small enough to mount within the fuel pin, the transducer should be capable of resolving amplitudes of at least 1 mil and preferably 0.1 mil. Although vibration-induced damage might not be expected at amplitudes below a fraction of a mil, fretting corrosion has been encountered at relative motion amplitudes of much less than 1 mil.[6] From mode shapes and amplitude data relative motion amplitudes at the fuel pin wire wrap contact points can be estimated.

The preferred test would measure vibrations under prototypic reactor conditions which include exposing the fuel pin to sodium in excess of 1000 °F under a radiation environment. The ideal transducer would then be capable of operation in a 1000 °F, radioactive, sodium environment and be small enough to mount within the fuel pin diameter. Since state-of-the-art instrumentation does not meet these needs, a suitable low-temperature, out-of-reactor environment must be used to develop instrumentation and data analysis techniques. Water can be used as a Reynold-modeling coolant; it has the same kinematic viscosity at 200 °F as sodium at 900 °F. Therefore, transducers required for flow induced vibration measurements should be capable of 200 °F operation.

Apparently four transducers have been used for various fuel pin size and spacer configurations; each has different capabilities and limitations. Other types of available transducers may be potential candidates. For example a small rod or pin could be attached to a fuel cladding and extended through the wall of the flow duct to an external displacement sensor. This type of sensor may provide nonprototypic constraint and flow distortion and hence is not a desirable

instrument. The following discussion indicates the limitations of four types of transducers and why the conductivity cell method was chosen for flow induced vibration measurements at PNL.

Variable Reluctance Coils

Variable reluctance coils have been mounted inside a 1/2 inch OD thin wall tube about 3 feet in length and suspended on a taut wire to detect the tube vibrations.[7] In this case the pin must be supported from both ends such that the variable reluctance coil mounting wire can be placed in tension to provide rigid support. This device, requiring an internal support does not appear applicable to a long small diameter fuel pin.

Strain Gages

Strain gages have been mounted on the outer and inner wall[2,3,5,8] of fuel pins to measure flow induced vibrations. Although strain measurements provide a direct strain reading useful for fatigue failure prediction, the mode shape of the fuel element must be known to determine the amplitude of vibration. In grid spacer fuel design, the support locations are generally known; the fundamental mode shape and frequency (which has been found to be the dominant vibration frequency) can be determined readily from experiments and/or analysis. However in a wire wrap support design the location and constraint provided by the wire wrap is difficult to predict. The spiral wire wrap design provides a potential support at 6 locations, 60 degrees around the pin, and at 6 inch axial intervals as shown in Figure 1. However since a 217 pin bundle fits loosely in its flow duct; and because of construction tolerance and inherent pin bow, only a portion of the potential supports may be in contact at any instant in time. Hence the interaction between fuel pins is more complex in the wire wrap design because of the multiplicity of potential contact points whereas in the grid plate design the interaction of fuel pins takes place primarily at the grid spacer.

Assuming that the mode shape is known, the practical measurable threshold vibration amplitude using strain gages in an FTR fuel pin can be determined from the following analysis. Assume the fuel pin deforms into sine waves along its length.

$$y = A \sin \frac{\pi x}{L} \tag{1}$$

where A is the amplitude coefficient and L is the span length x is the axial location.

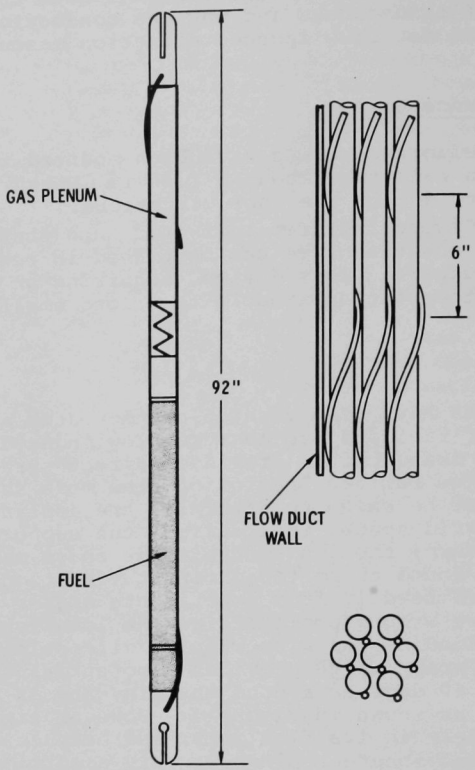

FIGURE 1. Fuel Pin and Spiral Wire Wrap Spacer Design

Recall that the strain (ε) for a uniform beam in flexure

$$\varepsilon = \frac{\sigma}{E} = \frac{Mc}{EI} = c\,\frac{\partial^2 y}{\partial x^2} \tag{2}$$

and thus

$$\varepsilon_{max} = \frac{c\pi^2}{L^2}\,A \tag{3}$$

where

σ is an outer fiber stress
E Youngs Modulus
M bending moment
I cross section moment of inertia
c distance from neutral axis to strain location, i.e., inside radius of the fuel pin (0.100 inch is the current design).

The maximum strain level occurs at ($x = {}^{L}/_{2}$) the midpoint of the span and is directly proportional to the amplitude of vibration(A), the fuel pin radius and inversely proportional to the square of the span length(L). Assuming a 10 microstrain threshold, the minimum detectable amplitude would be about 0.3 mil peak (0.6 mil p-p) for a 6 inch span length which corresponds to a frequency of about 300 Hz. Since each wire wrap contact may not act as a support, the effective span may range between 92 inches, the full length of the fuel pin, to 6 inches where every potential wire wrap contact acts as a rigid support.

Figure 2 indicates the predicted vibration threshold versus frequency (span length) for a strain gage sensor. For reliable measurements a signal to noise ratio of 10 to 1 is desired and the practical measuring level may be an order of magnitude above the indicated threshold. Hence the strain gage is not feasible for small vibration amplitudes.

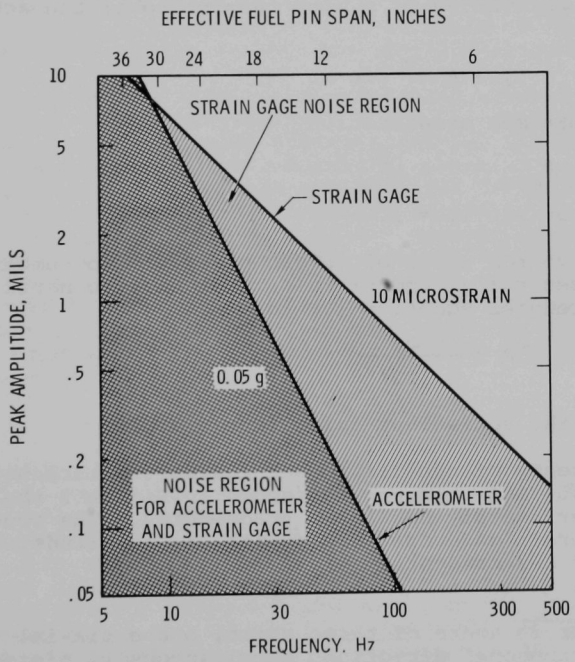

FIGURE 2. Strain Gage and Accelerometer Threshold Deflection Amplitude

Accelerometers

Accelerometers small enough to fit inside an FTR fuel pin (0.200 ID) have recently become commercially available.* Accelerometers provide an output proportional to acceleration which must be twice integrated with respect to time to yield displacement histories. The equivalent noise level for an accelerometer of this size is about 0.06 g based on the manufacturer signal conditioning specifications.

Assuming harmonic motion and an error free integration, the threshold amplitude level can be determined as follows. The equation defining time dependent harmonic motion is

$$y = A \sin \omega t \tag{4}$$

where y is the position or amplitude for any time t. A is the peak amplitude coefficient. ω is the circular frequency in radians.

The second derivative of y with respect to t; the acceleration ($\ddot{y}$)

$$\ddot{y} = A\,\omega^2 \sin \omega t \tag{5}$$

hence the maximum acceleration

$$\ddot{y}_{max} = \pm A\,\omega^2 \tag{6}$$

and occurs at $\sin \omega t = 1$.

Converting y from units of length per time^2 to number of g's (386 in.^{2}/sec = 1 g) and circular frequency to hertz ($\omega = 2\pi f$) reduces equation (6) to

$$A = \frac{g_n}{0.102 f^2} \tag{7}$$

when g_n is the equivalent noise level in g's.

For a frequency of oscillation of 100 Hz the threshold noise level is 0.06 mil; however, as shown in Figure 2 the threshold rises rather rapidly for lower frequencies. The accelerometer like the strain gage does not permit low amplitude, low frequencies measurements.

---

* The author is aware of three units, one a biaxial (measures in two orthogonal directions simultaneously) piezoelectric type, the other two are uniaxial piezoresistive types.

Columbia Research Laboratories Inc.
MacDade Bldv. and Bullens Lane
Woodlyn, Pa. 19094

Endevco Corporation
801 S Arroyo Parkway
Pasadena, Calif.
91109

Kulite Semiconductor Products Inc.
1039 Hoyt Avenue
Ridgefield, N.J. 07657

Conductivity Cell

The conductivity cell method has been used at Atomics International[9] for the study of mixing parameters and vibrations of bundles of fuel rods. This device consists of a conductivity cell located either in a fuel pin (or in the flow duct wall) and appropriate signal conditioning electronics to provide an electrical signal proportional to the spacing between the probe (cell) and an adjacent fuel pin. This instrument operates on the basis that probe impedance varies with distance between the cell and its mating surface in a uniform electrolytic solution.

The conductivity cell method provides a signal proportional to the relative spacing between two surfaces. Although the relative spacing between two pin surfaces may be directly related to wear, the location of one probe surface is required to establish the mode shapes. The absolute motion of the central pin in a bundle of pins using conductivity cells requires algebraically summing the relative amplitudes along a line of pins, one in each row back to the flow duct. This operation may require considerable manipulation of the output signal to establish motion in two orthogonal directions.

A prototype of the Atomics International conductivity cell was adapted to the original FTR fuel pin, (viz, 0.25 OD fuel clad and 30 mil wire wrap spacing) and was evaluated in the PNL Engineering Mechanics Laboratory. Initial testing indicated additional development was required to improve the sensitivity and response characteristics of the probe to an acceptable level for the FTR fuel pins. However because of its potential capability of measuring low amplitudes of vibration (0.1 mil, independent of frequency) the conductivity cell was chosen for PNL flow induced vibration testing of FTR fuel assemblies. The following sections describe the development of the conductivity cell instrumentation: the PNL Impedance Detector.

SUMMARY

In the Fast Test Reactor (FTR), heat generated in the fuel bundles will be removed by pumping large quantities of sodium past closely spaced, spiral wire wrapped fuel pins. The resulting turbulent flow conditions, ideal for removing heat efficiently, may generate flow induced vibrations. Analytical predictions of flow induced vibrations are extremely difficult because of the complex geometric and time varying boundary conditions present in the spiral wire wrap fuel design; hence experimental techniques are required to evaluate FTR fuel pin bundle vibrations. In the FTR development program, both water and sodium flow tests are planned. Because of the lower cost and less demanding instrumentation requirements, FTR fuel assemblies will be initially tested in water.

The slender FTR fuel pins vibrate like beams under parallel flow; frequencies and displacements can be determined by measuring the displacement histories in two orthogonal directions at several axial locations along the pin. Present commercially available strain gages and accelerometers, will not sense small deflections at frequencies corresponding to the lower pin modes. The conductivity cell however has been used to measure vibration amplitudes of much less than one mil independent of frequency of vibration.

The conductivity cell system initially developed by Atomics International was modified for the FTR fuel bundle. Several dominant parameters which affect the performance of the conductivity cell instrumentation have been evaluated: the dimensions of the cell, insulation and pin spacing respectively, the electrolyte concentration and temperature, and excitation level. In addition, since the probe impedance is dependent on the external circuit parameters, the Wheatstone bridge components must be adjusted to provide four-equal-resistance arms to obtain maximum sensitivity and linearity.

Absolute displacement histories along the length of the fuel pin is the most desirable form of vibration data. Neither strain gages nor accelerometers directly measure displacement though each provide absolute data. The conductivity cell method measures displacement directly and can sense low vibration amplitudes. However, unless the motion of one of the probe surfaces is known, this method provides only relative displacement. The major disadvantage of the conductivity cell method is that the simulated coolant must be an electrolyte solution in which the concentration and temperature can be carefully controlled.

A 19-pin instrumented bundle was tested initially as part of FTR fuel bundle development program. Fuel pin vibrations were below the noise level (0.3 mil) of the instrument and after testing for a few hours at elevated temperature and pressures, some of the conductivity probe lead cables leaked water. The instrument has since been modified to provide a threshold noise level of 0.01 mil peak-to-peak. Although inconclusive, results of a recent shaker test on the 19-pin fuel bundle have shown the conductivity cell instrumentation to be a viable method. Clear noise free signals of (1) a nearly pure sine wave (2 mil p-p) at low g levels, (2) a distorted sine wave indicating the nonlinear effect the wire wrap supports at an intermediate g level and (3) pin-to-pin and pin-to-wall impact at the upper g level have been observed.

Further testing of 217 pin, FTR fuel bundles are planned using the conductivity cell method. The current instrument will be refined to improve the annoying drift problem by replacing the operational amplifier and d-c power supply with better quality, more stable units. Additional development efforts will be directed at the design of a reliable cell and instrument lead penetration seal.

DISCUSSION

THE PNL IMPEDANCE DETECTOR

The PNL Impedance Detector Instrument contains the appropriate signal conditioning electronics to provide an electrical signal proportional to the spacing between an insulated cell and an adjacent fuel pin. A complete circuit diagram and photographs are included in Appendix I.

The PNL Impedance Detector consists of four electrical sections: (1) the middle chassis provides calibration, monitoring and the necessary switching; (2) a 100 kHz excitation oscillator provides a 100 kHz sinusoidal excitation signal for the seven bridge circuits; (3) the bridge-detector-amplifier circuit provides the major signal conditioning and the necessary resistors and capacitors for completion of a Wheatstone bridge in which (4) the probe is one leg.

The seven bridge-detector-amplifier circuits and the 100 kHz excitation oscillator are of printed circuit construction. Printed circuit design allows one to construct seven electrically identical channels and provides a compact unit. The seven bridge-detector-amplifier circuits and the 100 kHz excitation oscillator are mounted in an all metal chassis to provide shielding from electromagnetically radiated noise and hence is inherently less susceptible to noise.

Middle Chassis

The middle chassis contains a d-c power supply, switching circuits, a null meter and the calibration level set which is a voltage divider potentiometer hereafter referred to as the calibration level set. The power supply provides d-c excitation for (1) the solid state components in the 100 kHz excitation oscillator, and (2) the operational amplifier in the Bridge-Detector-Amplifier circuit, (3) a calibration signal used to adjust the operational amplifier circuit gain, and (4) a d-c reference signal for the calibration level set. The null meter is used with the calibration level set to measure the various d-c voltage levels.

100 kHz Excitation Oscillator

The 100 kHz Excitation Oscillator circuit contains an oscillator, amplifier, and rectifier. The oscillator amplifier circuit provides an adjustable level 100 kHz sinusoidal excitation signal (6 volts peak-to-peak maximum) for the seven bridge circuits. A rectifier circuit provides a d-c signal proportional to the peak-to-peak excitation signal that can be monitored and adjusted using the null meter-calibration level set circuitry.

Bridge-Detector-Amplifier

The Bridge-Detector-Amplifier circuit contains (1) the necessary resistors and capacitors for completion of a Wheatstone bridge, (2) a detector, (3) a 10 kHz low pass filter and (4) an amplifier circuit. The operation of the Bridge-Detector-Amplifier circuit can best be explained by examining the operating procedure and referring to Figure 3. Initially the operational amplifier d-c balance and gain are adjusted, and the Wheatstone bridge is balanced. In a balanced condition the bridge output of the instrument is zero. However when the probe impedance changes (due to a change in probe spacing) an unbalanced bridge results in the appearance of a 100 kHz output signal which is transformer-coupled to the detector circuit. The detector senses both the amplitude and direction of the unbalance (an increase or decrease in impedance corresponding to an increase or decrease in probe spacing) and provides a demodulated signal to the 10 kHz low pass filter. The low pass filter then removes any remaining 100 kHz excitation signal and other extraneous signal above the 10 kHz cutoff frequency. The demodulated and filtered information signal is then amplified by the operation amplifier.

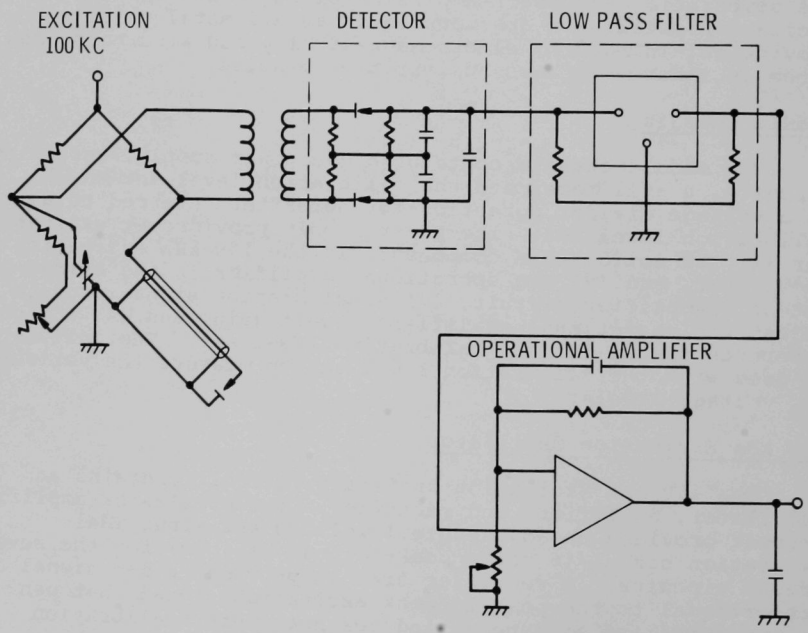

FIGURE 3. Bridge-Detector-Amplifier Circuit

PROBE DESIGN CONSIDERATIONS

The desired characteristics of a good probe design are that, (1) the probe provide sufficient sensitivity to permit accurate and reliable measurements for the amplitude range of interest; and (2) the probe and lead cable be physically small enough to mount several probes inside a fuel pin. Since the electrical characteristics of an electrolytic cell must be considered when designing a suitable probe, we will briefly discuss (1) the electrolytic conduction theory, (2) polarization, (3) electrolyte selection, (4) lead cable selection and (5) probe configurations.

Electrolytic Conduction

Current flow through an electrolytic solution takes place due to the motion of ions between the immersed electrode surfaces. Current flow through an electrolytic solution is similar to electron flow through a solid material in that the effective resistance (R) of the electrodes is directly proportional to the electrode spacing (L) and inversely proportional to the electrolyte conductivity (C) and electrode surface area (A) i.e.,

$$R \alpha \frac{L}{CA} \tag{1}$$

Furthermore, OHM's law states that the voltage (V) across the electrodes is equal to the product of the current flow (I) and the effective electrode resistance (R). That is

$$V = IR \tag{2}$$

Combining Equations (1) and (2) one can see that

$$R \alpha \frac{V}{I} \alpha \frac{L}{CA} . \tag{3}$$

Since the electrolyte conductivity (C) and the electrode area (A) are to be constant for a given test, it is possible to apply a constant voltage (current) to the electrodes, measure the resulting current (voltage) and relate the measured current (voltage) to the spacing of the electrodes.

The sensitivity (S) of the electrode or conductivity probe is the ratio of the change in output signal (V) to a change in probe spacing (L)

$$S = \frac{\Delta V}{\Delta L} \tag{4}$$

which is related to the change in probe resistance, is from Equation 1

$$S \alpha \frac{\Delta R}{\Delta L} \alpha \frac{1}{CA} . \tag{5}$$

This equation indicates that maximum sensitivity can be obtained by using a small probe area and a small electrolyte conductivity (i.e., weak electrolyte).

Polarization

Polarization[10] refers to a condition in which the ratio between the current flow and voltage of an electrolytic cell differs from a constant. That is, for two different voltage levels, all other factors being equal, the ratio between voltage and current, (the effective resistance) does not remain constant. The reliable and accurate operation of this instrument depends on the assumption that the effective probe resistance is dependent only on the probe spacing. Since polarization may cause an erroneous signal, ways to minimize polarization effects will be discussed.

Polarization phenomena are conveniently classified into two categories: concentration polarization and overvoltage. Concentration polarization implies the existence of a thin layer of solution immediately adjacent to the electrodes. Overvoltage ordinarily results from the slow rate at which the electro-chemical oxidation and reduction process occurs at one or both of the electrodes. Experimentally, concentration polarization can be reduced by (1) diluting the electrolytic concentration, (2) increasing the mechanical agitation of the solution and (3) increasing the size of the cell. Overvoltage can normally be reduced by (1) decreasing the current density at the electrode, i.e., decreasing the probe excitation voltage and (2) increasing the temperature of the electrolyte. Mechanical agitation and increased temperature is automatically accomplished for flow testing at elevated temperatures; increasing the cell size (area) and reducing the excitation level reduce the sensitivity whereas diluting the electrolyte results in an increase in sensitivity of the conductivity cell.

Electrolyte Selection

A weak concentration of $NaNO_3$ was found to be an adequate electrolyte for all the probe evaluations; hence other salts were not evaluated. Since the flow loops used for testing of the instrumented fuel bundles are of carbon steel construction, LiOH was added to raise the PH level. Raising the PH Level to 10 reduces the oxidation rate of carbon steels, limiting the formation of oxide particles which may affect the conductivity of the solution and change the electrode surface properties. Since reducing the electrolyte concentration increases the sensitivity of the probe and diminishes the effects of polarization, samples of local tap water, distilled water and a sample from the loop in which the testing was to be conducted were measured to determine their conductivity in relation to various concentrations of $NaNO_3$. A solution concentration with a conductivity slightly higher than the above samples was chosen because a solution with a conductivity much less than the

test loop sample may be subject to conductivity fluctuation due to oxidation particles forming within the loop which will create erroneous signals.

An undesirable characteristic of electrolytes is that the conductivity changes with temperature; hence the conductivity probe sensitivity depends on and must be calibrated at temperature.

Lead Cable

A miniature, low capacitance, low noise coaxial cable is required as a signal lead to the probe because: (1) the small size allows more cells to be located within a small diameter fuel pin, (2) the low capacitance keeps the capacitive reactance of the cable small compared to the probe impedance change, (3) low noise levels keep spurious signals due to cable motion at a minimum and (4) coaxial shielding minimizes stray electromagnetic pickup. Atomics International[11] has had success using a single insulated lead within the fuel pin then extending the lead to the signal conditioning equipment with a shielded cable; however, at PNL shielded cable was used throughout. In either case grounding of the shield should occur at only one location to prevent ground loops. A Microdot* "Mini-Noise" miniature coaxial cable (Microdot number 250-3808) was used; however a smaller diameter (0.0450 OD) Microdot cable could be considered.

Probe Configurations

The conductivity probes used in fuel pin vibration measurements consist of one or two insulated cells flush mounted in the surface of either the fuel pin cladding or in the flow duct wall (see Figure 4). In the one-cell design, the insulated cell faces an adjacent fuel pin which is an electrical ground. In the two-cell design, the insulated cells are aligned to face each other.

The sensitivity of the probe is affected by both the effective cell area and the portion of stray current flow to ground. Since the probe resistance change is only dependent on the portion of current flowing between the cell and the adjacent fuel pin surface, the stray current path is undesirable. The two-cell design used by Atomics International[11] may be more sensitive since the effective cell area is less. The single-cell design has provided sufficient sensitivity for the PNL instrument.

Since the stray current does not contribute to the change in resistance of the probe with spacing and may increase polarization effects at the cell surface, it is undesirable.

* Mini-Noise is the trade name for cable manufactured by Microdot Inc., and is advertised as having low noise characteristics.

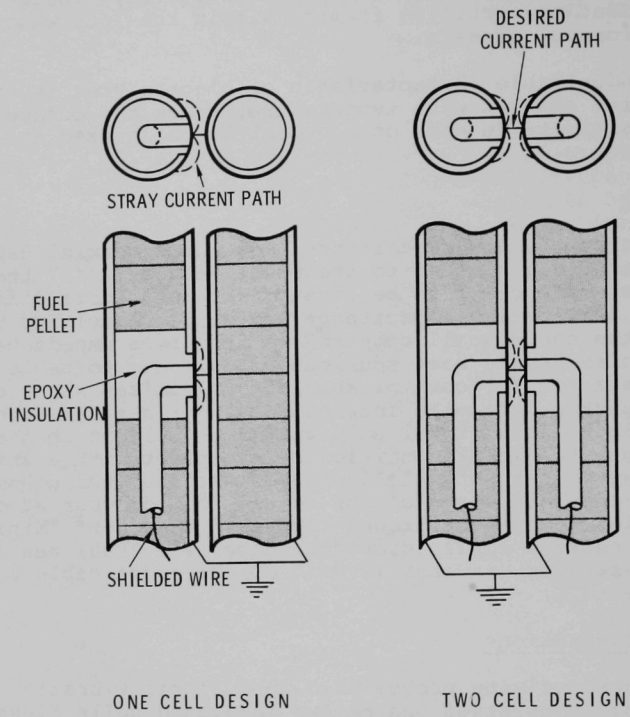

FIGURE 4. Conductivity Probe Configurations

The stray current can be reduced by increasing the insulation thickness and reducing the cell size. However the fuel pin diameter limits the insulation diameter, while polarization and construction tolerances limit the practical minimum size of the cell. Randall et al[9] have suggested an insulation thickness which is twice the mean probe spacing. Large insulation diameters may be easily provided in cells mounted in duct walls. For small pin diameters with large mean spacing, some form of thin surface insulation may be required to minimize the stray current path and increase the probe sensitivity. Small cell sizes are limited by the increase in polarization and ease of fabrication. Cell sizes ranging from 15 to 62 mils in diameter are practical.

Figure 4 shows a typical instrumented fuel pin cross section in which the fuel pellets are drilled to permit the lead cable to pass through the center of the pin; the cell insulation plug also requires removing a relatively small section of the fuel pellet. The shield on the cable is potted

into the insulation plug and hence provides shielding to the cell without having a multiplicity of ground paths. A suitable ground is provided by attaching a ground cable from the test section flow duct to chassis ground of the PNL Impedance Detector.

Constructing reliable probes requires special consideration. The major difficulty lies in getting the fuel pin end cap welded to the cladding without overheating (damaging) the lead cable insulation. The PNL probes were made using a cable with a taped teflon outer jacket. However an extruded jacket should provide a more reliable waterproof seal.

CALIBRATION AND EVALUATION

Procedure and Apparatus

For experimental calibration a test basin and a prototype cell (including the lead cable length) were constructed. Two probe configurations were calibrated: (1) pin-to-wall and (2) pin-to-pin. The cell was mounted in the flat bottom of the basin and in a short length of fuel cladding fastened to the bottom of the basin respectively. Each cell faced a short length of cladding attached to an electromagnetic shaker. The shaker was used to control the mean probe spacing as well as the dynamic amplitude. An optical displacement follower (OPTRON) provided a calibrated voltage proportional to displacement; this signal was compared with the Impedance Detector output to determine the sensitivity of the probe (see Figure 5).

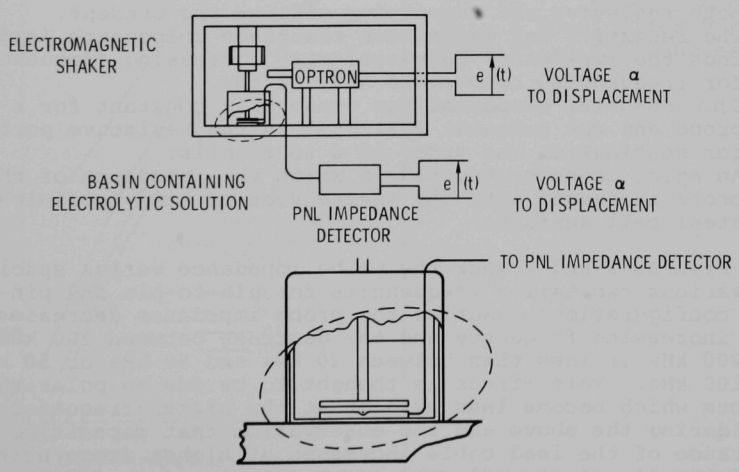

FIGURE 5. Conductivity Probe Calibration-Evaluation Apparatus

Once the calibration apparatus was constructed and set up, the Wheatstone bridge was balanced. Since the probe impedance depends on the external circuit characteristics, trial and error has provided the only reliable method of obtaining a balanced bridge. The probe resistance was determined from the potentiometer setting in the balanced bridge circuit. The resistors in the bridge circuit were adjusted to provide four equal resistance bridge legs; this optimized the bridge sensitivity and linearity. The probe sensitivity was determined with the aid of a dial micrometer by statically moving the probe a known distance and comparing with the change in output voltage of the Impedance Detector. By using the electromagnetic shaker, the probe was dynamically excited; comparing the output of the Impedance Detector with the optical displacement follower provided dynamic calibration. Accurate calibration of the conductivity probe required controlling the (1) electrolyte concentration and temperature, (2) the probe mean spacing (3) the vibration amplitude and (4) the bridge excitation level.

Experimental Probe Evaluation

Early in the conductivity cell development program several probes were constructed to experimentally determine the electrical characteristics, in particular the probe impedance to be matched in the bridge circuit. The effects of carrier frequency and probe spacing were measured. The probe impedance was calculated from oscilloscope voltage measurements across the probe and a resistor in series with an excitation oscillator. Though the loading effects of the oscilloscope and measuring circuit directly influenced the probe impedance, the following trends were observed.

(1) The impedance of an electrolytic cell is complex in that both resistive and capacitive effects are present.
(2) The resistive and capacitive reactance components (and thus the impedance) decreased with increasing frequency for frequencies between 20 and 200 kHz.
(3) The reactive component was reasonably constant for a given probe and was somewhat smaller than the resistive portion for spacings on the order of 0 to 60 mils.
(4) An aging process occurred in which the impedance of the probe increased with the square root of time (stainless steel cell surfaces).

Figures 6 and 7 show the probe impedance versus spacing for various excitation frequencies for pin-to-pin and pin-to-wall configurations. Notice the probe impedance decreases with increasing frequency and the decrease between 100 kHz and 200 kHz is less than between 20 kHz and 50 kHz or 50 kHz and 100 kHz. This effect is thought to be due to polarization effects which become less evident at the higher frequencies. Considering the above and the observation that capacitive reactance of the lead cable increases at higher frequencies, a 100 kHz signal was selected as the carrier frequency.

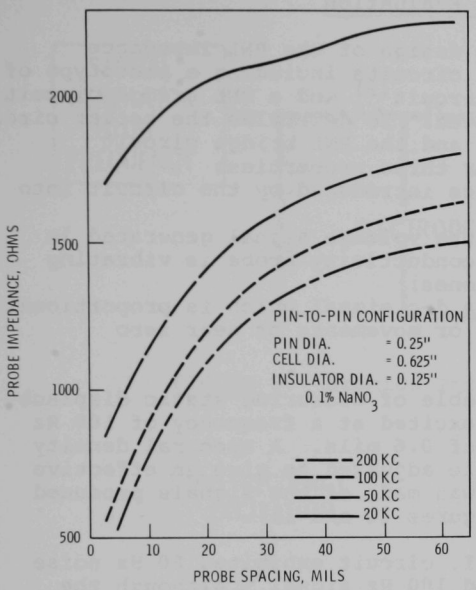

FIGURE 6. Probe Impedance Versus Spacing for Various Excitation Frequencies

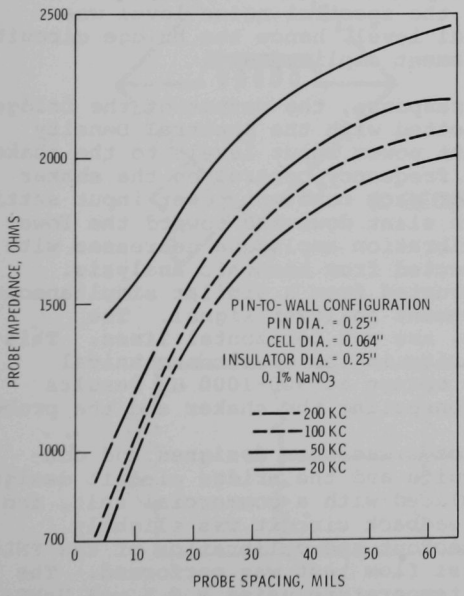

FIGURE 7. Probe Impedance Versus Spacing for Various Excitation Frequencies

Signal Conditioning Circuit Evaluation

Prior to selecting the design of the PNL Impedance Detector several breadboard circuits including a prototype of the Atomics International circuit[9] and a PNL bridge circuit were constructed and evaluated. To determine the better circuit, the A.I. circuit (Figure 8) and the PNL bridge circuit (Figure 9) were examined for three properties:

(1) 60 Hz noise and harmonics introduced by the circuit into the output signal
(2) Harmonic distortion of the voltage signal generated in the circuitry when the conductivity probe is vibrating at 100 Hz (200 Hz overtones)
(3) The ability to produce a d-c signal which is proportional to static displacements or movements of near zero frequency

Both circuits were capable of measuring static displacements. The probe was then excited at a frequency of 100 Hz with a vibration amplitude of 0.6 mils. A spectral density plot, with the vertical scale adjusted to give an effective filter band width of unity was made of the signals produced by the two circuits (see Figures 10 and 11).

The spectrum of the A.I. circuit exhibited 60 Hz noise plus harmonics of the 60 and 100 Hz signal. Although the PNL bridge circuit sensitivity is less (32 mV compared to 86 mV for the A.I. circuit) the spectral noise level was below the 100 Hz input signal level, hence the bridge circuit was capable of lower measurement amplitudes.

To evaluate frequency response, the output of the bridge circuit was measured and plotted with the Spectral Density Analyzer for various constant power input levels to the shaker as shown in Figure 12. The frequency control on the shaker was swept through a range for each constant power input setting. This created the lines which slant downward toward the lower right indicating that the vibration amplitude decreases with increasing frequency as expected from harmonic analysis. Horizontal lines were constructed from a similar simultaneous plot of the optical displacement follower signal. The actual vibration amplitudes, are not horizontal lines. This indicates a slight nonlinearity in the electromechanical shaker system. The drastic change at 900-1000 Hz results from resonance of the rod connecting the shaker and the probe.

The PNL Impedance Detector was then designed and constructed using printed circuits and the bridge circuit design. The low pass filter was replaced with a commercial unit, and the operational amplifier feedback circuit was slightly modified. After a brief checkout and calibration of the PNL Impedance Detector, the first flow test was performed. The sensitivity at 110 °F test temperature using a 0.1 wt% $NaNO_3$ solution was 60 mV/mil. The data gathering system consisted

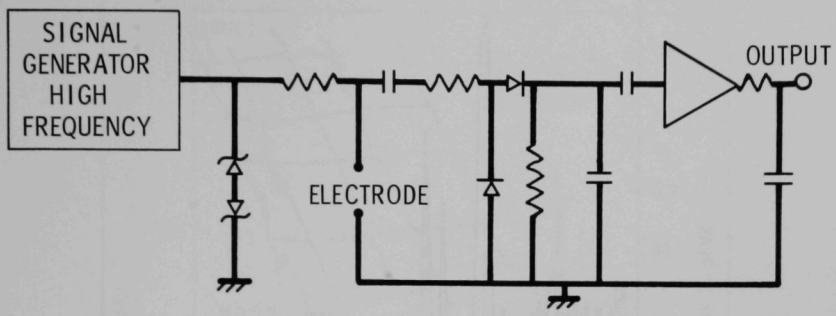

FIGURE 8. Atomics International Circuit

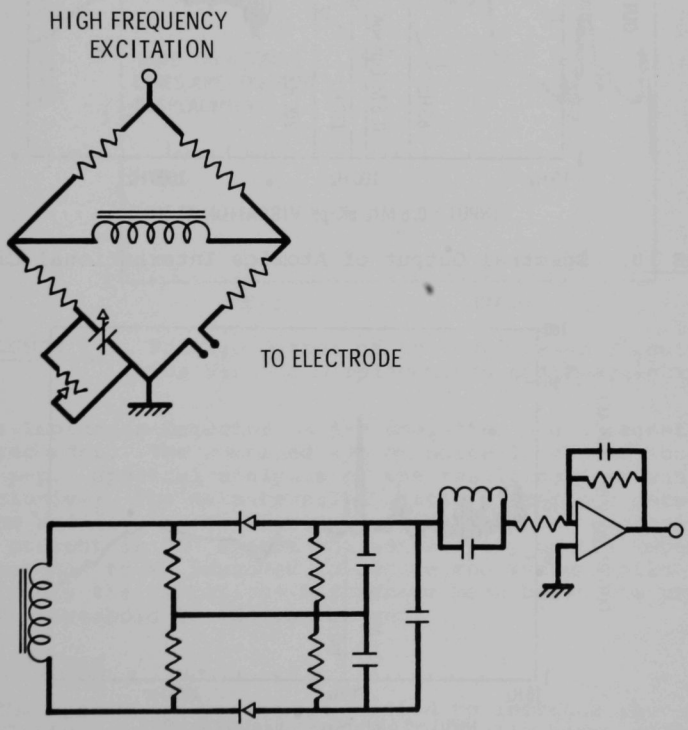

FIGURE 9. PNL Bridge Circuit

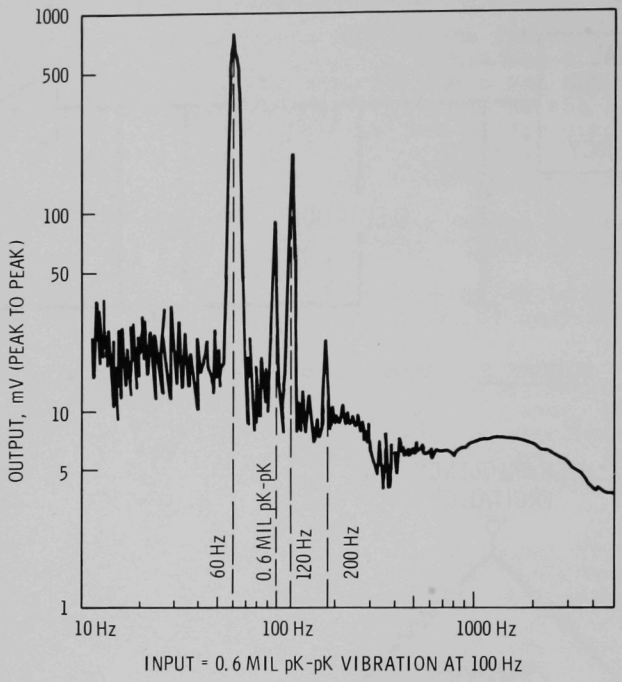

FIGURE 10. Spectral Output of Atomics International Circuit

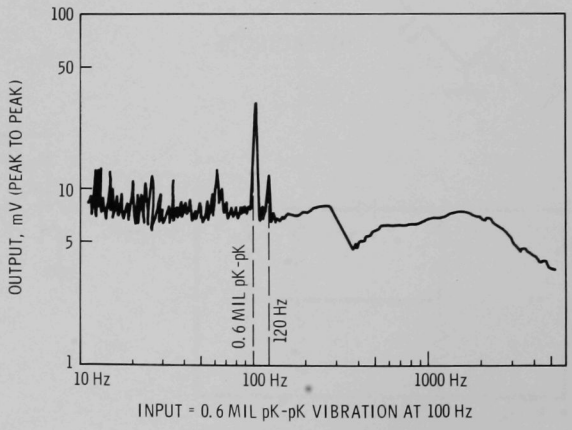

FIGURE 11. Spectral Density Plot for PNL Bridge Circuit

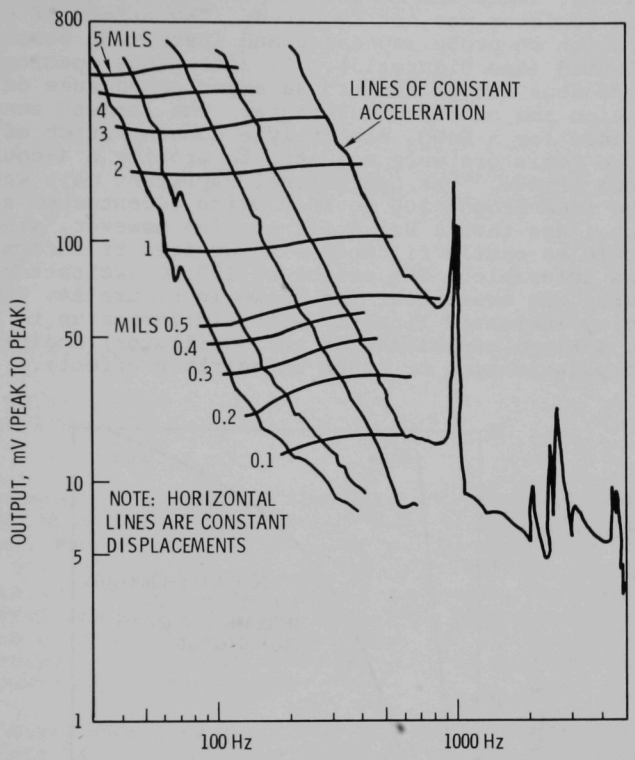

FIGURE 12. Voltage Output of the PNL Bridge Circuit for Various Displacements and Frequencies

of the Impedance Detector, a d-c amplifier and a magnetic tape recorder. The combined system noise level was about 20 mV p-p. Spectral analysis of the resulting data was inconclusive: The data revealed little difference between no-flow and flowing conditions. Because of the excessive noise present in the system the sensitivity of the Impedance Detector had to be improved to reduce the system noise level. Conceivably the vibrations might have been below the predicted 0.3 mil threshold of the instrument.

Modifications

The instrument was then modified to increase the sensitivity. A resistor which had initially been included to provide a linear output over a wide conductivity probe

displacement range was eliminated: initial flow test revealed that since the maximum amplitude may be only a few mils this resistor was not required. The effect of electrolyte concentration on probe impedance and instrument sensitivity was evaluated (see Figure 13). At zero probe spacing the probe resistance does not go to zero as expected because of polarization and contact resistance. The largest sensitivity was obtained for a $NaNO_3$ electrolyte concentration of 0.03 wt%: the bridge resistors were adjusted to provide a 4-equal-arm resistance bridge. The operational amplifier gain was increased from around 300 to 1000 which accentuated a low frequency (less than 1 Hz) drift problem however, since the drift could be easily filtered without loss of information the drift was tolerable. The effect of 100 KC excitation level on sensitivity was evaluated. As shown in Figure 14, the sensitivity increased linearly with excitation up to 12 volts p-p (the maximum capability of the oscillator) indicating no apparent polarization or other undesirable effects.

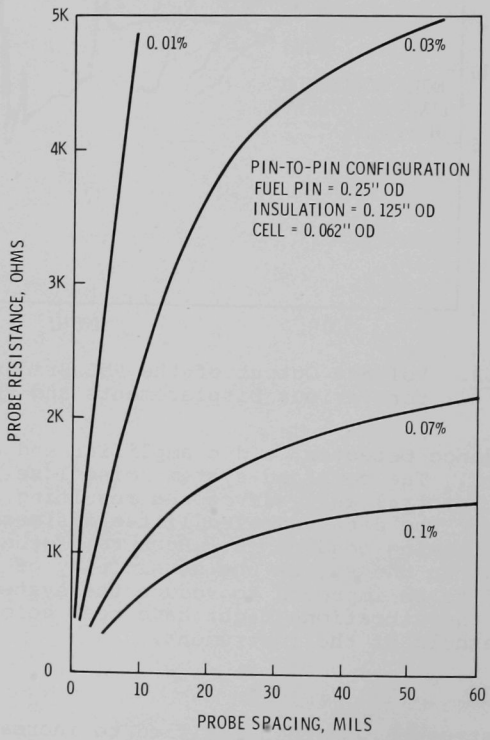

FIGURE 13. Probe Resistance Versus Probe Spacing for Various $NaNO_3$ Solution Concentrations

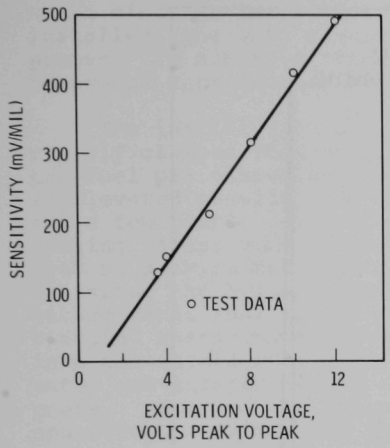

FIGURE 14. Sensitivity Versus Excitation

The spectral output of the modified instrument was then evaluated at a 100 KC excitation level of 12 volts p-p; 500 mV/mil sensitivity. The probe was excited at a constant 300 Hz, 0.2 mil p-p and the output spectrum plotted as shown in Figure 15. Except for a 120 Hz component the spectral noise level was two orders of magnitude below the signal level. A portion of the 120 Hz component was due to the shaker input as indicated on a similar spectral plot of the optical displacement follower output.

An experiment was conducted to determine the transverse sensitivity (the probe sensitivity for motion of the pin perpendicular to the cell face and to the pin axis) of the probe. For a transverse vibration of 1 mil p-p amplitude, the sensitivity was 22 times less than the normal sensitivity, hence this probe was relatively insensitive to motion in the transverse direction.

Noise measurements including spectral noise analysis with no probe vibrations were conducted in an attempt to determine the noise source. It was found that the operational amplifier noise contribution was minimal and independent of the 100 KC excitation signal level. The spectral content of the noise as shown in Figure 16 is primarily 60 Hz and 60 Hz harmonics. The measured p-p noise level was only 5 mV at the operational amplifier output. A sensitivity of 500 mV/mil provides a 0.01 mil noise level which should be quite adequate.

TEST RESULTS

Fuel pin vibration tests were conducted on a 19-pin bundle contained in a flow duct. The lower part of the duct

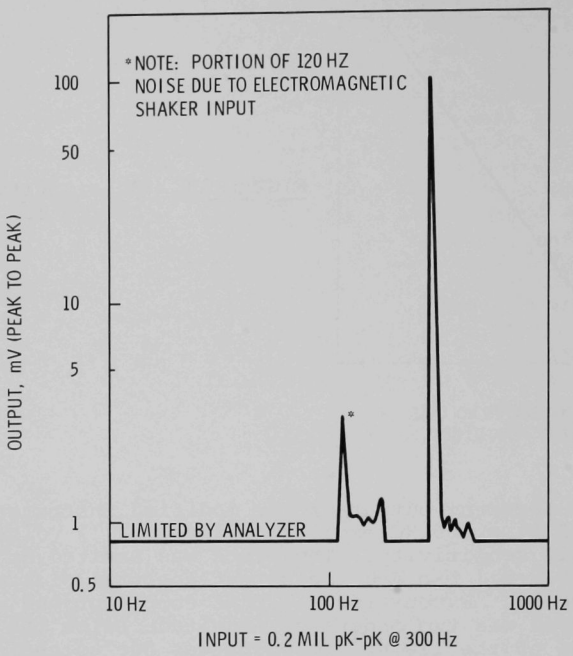

FIGURE 15. Spectral Output of PNL Impedance Detector

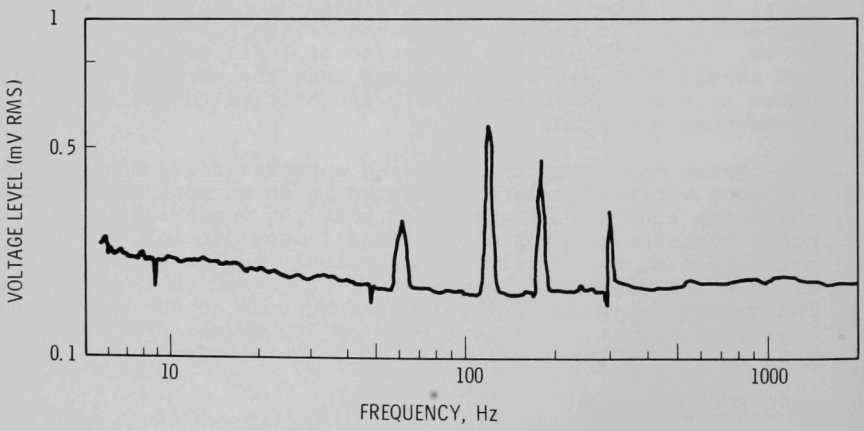

FIGURE 16. Background Noise Spectrum of PNL Impedance Detector

was hexagonal with lexan windows whereas the upper section was a circular lexan tube. Eight instrumented fuel pins were installed, one with a strain gage and seven with conductivity probes. In addition three wall probes were installed in the hexagonal duct located as shown in Figure 17.

The initial flow tests were conducted with the duct rigidly clamped to a support fixture. As discussed earlier, the fuel pin vibration data was inconclusive. After testing at elevated pressure and temperature (110 °F, 100 psig) for a few hours, several conductivity probe lead cables were leaking water; some of these probes appeared to be working with no detrimental effects while others would not permit balancing the bridge circuit and hence were inoperative. The author feels that those leaking probes which continued to operate, had permitted water to pass through the outer jacket into the shield only, whereas in those which had failed, the water had entered to the center conductor and shorted the probe. Seven of the twenty-one original probes are still in operating condition and were used in recent shaker testing.

The most recent testing was conducted with the duct mounted on bellows which permitted forced vibration of the test section. The 19-pin assembly (designated B-1) was attached to a beam which provided a nearly pure lateral translation input to the fuel bundle reducing the natural flexual modes of the nonuniform flow duct. Accelerometers were attached at various locations as shown in Figure 17 and their output recorded as the exciting force was swept through a frequency range of 2 Hz to 5 kHz. Several critical frequencies were observed i.e., where one or more accelerometers were excited at larger g levels or their output wave form was out of phase or distorted as compared to the majority of accelerometer traces indicating that the duct was not undergoing pure translation.

At a frequency of about 40 Hz, the response of all accelerometers attached to the flow duct exhibited a high complex frequency wave form obscuring the 40 Hz fundamental input. Simultaneously, an audible sound suggested a significant increase in the activity of the fuel pin bundle. At maximum g levels (3 g) the pin vibrations were easily perceptible visually--particularly when strobe light illumination was used.

The conductivity cell signals were recorded on a strip chart recorder as the shaker was swept through the frequency range discussed above. The wave forms for the conductivity cells were generally harmonic for most input frequencies. At a shaker frequency of around 40 Hz, the response signals for various pin cells became remarkably clean, i.e., free of harmonics and modulation--this is characteristic of resonance and indicated the probable lowest natural frequency of the pins. The output from a duct wall probe (2W) and a

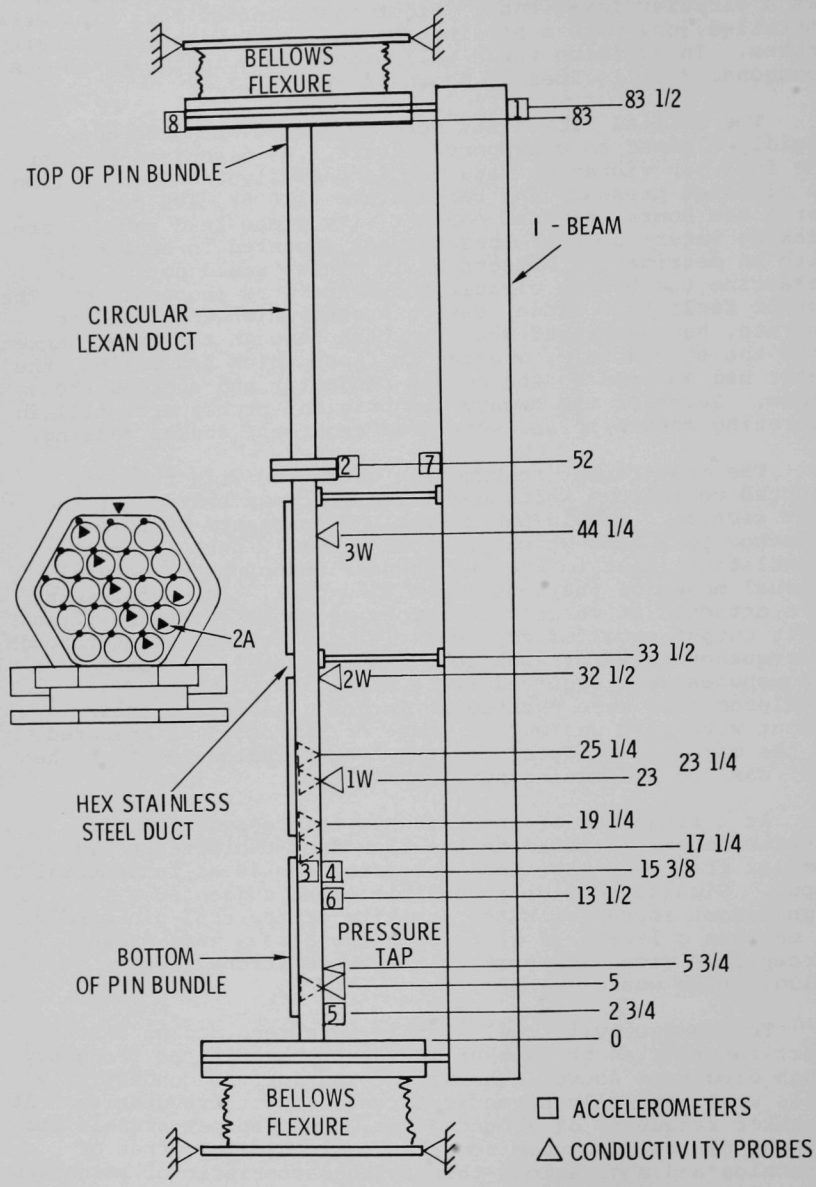

FIGURE 17. B-1 Assembly Instrument Location

pin-to-pin probe (2A) was photographed from oscilloscope traces as shown in Figure 18. Notice the response waveforms for probe 2W are nearly sinusoidal at the lower g level and becomes increasingly distorted to the point of clipping at 1.2 g. This distortion is indicative of the nonlinear constraint provided by the wire wrap support; between the pin and duct wall the wire wrap contacts at 12 inch intervals whereas at the opposite side of the pin contact will be made on each of two pins 120° apart at 6 inch intervals.

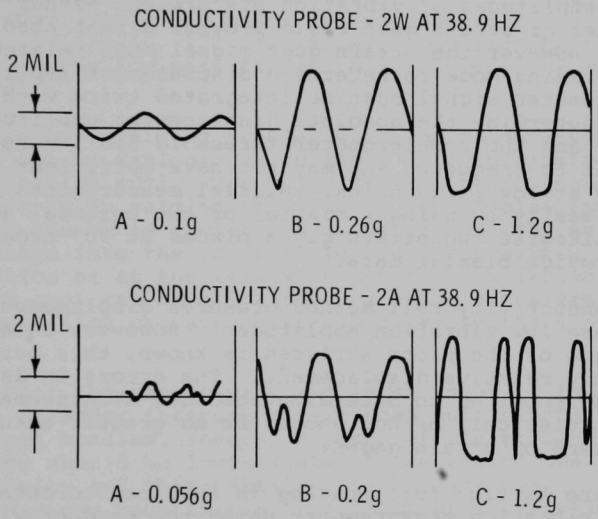

FIGURE 18. B-1 No-Flow Shaker Test Data

The trace of probe 2A is more complex because it senses the spacing between two pins rather than between the wall and a pin as in probe 2W. The maximum amplitude of the two traces at 1.2 g in which contact occurred as indicated by the clipped signal are about 10 and 12 mils respectively: the test section was designed for a duct-bundle clearance of 20 mils. The amplitude of probe 2W at 0.1 g input is 2.5 mil p-p which corresponds to a voltage amplitude of 250 mV p-p and is completely noise free. This data demonstrates the clarity of waveforms achievable with conductivity cells. One can see that much lower amplitudes should be perceptible.

CONCLUSIONS AND RECOMMENDATIONS

The PNL Impedance Detector is capable of making reasonably accurate and reliable vibration measurements to less than 0.1 mil peak to peak. Although the instrument can provide useful data, a few problems do exist--none of which are considered insurmountable. The conductivity cell method provides a signal proportional to the relative motion between two surfaces rather than an absolute strain or acceleration as in the case of a strain gage or accelerometer, respectively. None of the three major vibration sensing instruments provides a signal directly proportional to absolute motion. Where sufficient amplitudes of vibration are present either the accelerometer or strain gage could provide direct absolute amplitudes; however the strain gage signal must related to an effective bending mode to determine displacement amplitude and, the accelerometer signal must be integrated twice with respect to time to determine the absolute displacement amplitude. The strain gage and the accelerometer threshold are inversely proportional to frequency and may not have sufficient sensitivity at low frequencies. Biaxial measurements can be made quite easily by using a biaxial or two uniaxial accelerometers. Likewise two strain gages placed at 90° around the pin will provide biaxial data.

The conductivity cell method measures displacement directly and can sense low vibration amplitudes. However, unless the motion of one of the probe surfaces is known, this method provides only relative displacement. The errors in data manipulation required to determine absolute displacement with the conductivity cell method should be no greater than with accelerometers or strain gages.

A square lattice fuel spacing is required to obtain orthogonal vibration measurements using the conductivity cell method because only the two nearest surfaces in a fuel pin bundle provide an appropriate geometry. In a triangular lattice arrangement algebraic addition of two or more measurements at oblique angles is required to obtain absolute vibration displacement amplitudes.

Since each of the three major vibration sensors has inherent advantages and disadvantages, no single sensor may provide sufficient information by itself; rather two or all three sensors could be used to provide comparison and backup for reliability. However, because physical contact between pins may be more directly related to fuel pin wear (or failure), particularly in the case of the spiral wire wrap spacer design, and because of the low amplitude threshold independent of frequency, the conductivity cell method may well be the better technique for measuring fuel pin vibrations.

The PNL Impedance Detector is capable of providing a sensitivity of 500 mV/mil. A noise level of 5 mV provides an

effective displacement threshold of 0.01 mil, which should be adequate. The undesirable d-c drift characteristic can be significantly reduced by replacing the operational amplifiers and the d-c power supply with quality low drift units. Although d-c drift is tolerable since a-c coupling (filtering) will eliminate the fluctuations on the recorded data with no loss of information it is undesirable because of difficulty in maintaining amplifier balance conditions.

A low noise power supply should also reduce the power line frequency noise level. In addition since the fuel pin vibrations are expected to be below about 300 Hz, the 10 kHz low pass filter could be reduced to 500 Hz with no loss of information, however, since the major noise components, as indicated in Figure 16, are 60, 120 and 180 Hz, reducing the cutoff frequency of the low pass filter to 500 Hz may not improve the noise level.

The major remaining problem with the conductivity cell method is one of designing a reliable cell and instrument lead penetration seal. The major difficulty in installing lead cables is in welding the end cap to the cladding without destroying the cable jacket and/or the insulation material. Water leakage into the instrumented fuel pin either at the cell location or at the lead wire penetration (which is normally at the end cap) can be eliminated by using adhesives with thermal expansion characteristics similar to the cladding material.

Now that the sensitivity and noise level of the PNL Impedance Detector instrument have been sufficiently developed for FTR fuel bundles, several aspects of the probe-electrolyte interaction should be investigated to determine the effect on sensitivity and repeatability. For instance:

(1) Observations made initially at Atomics International and verified at PNL indicate a change in probe resistance occurs between a stagnant electrolyte and one which is flowing or being agitated. This apparent effect of polarization may have some effect on the sensitivity. Although the change in sensitivity is expected to be small, the effect of flow and perhaps flow velocity should be established to improve the reliability of the instrument.

(2) The cell geometry design parameters (the relation between cell and insulation size, gap, pin alignment etc.) and effects of construction tolerance variations on sensitivity should be determined. One possible way to improve the probe sensitivity is to coat one or both of the pin surfaces around (but not including) the cell with a thin (non flow disturbing) electrically insulating layer to increase the effective insulation thickness.

Future FTR fuel pins are to be instrumented with conductivity cells, accelerometers and strain gages to provide comparison and evaluation simultaneous with the gathering of

engineering data. Tests are planned to determine the limitations of the accelerometer and strain gage. Results of the no-flow shaker tests of the B-1 assembly are inconclusive because of the structurally complex nonprotypic flow duct; however future testing on prototypic flow ducts will provide information to aid in the evaluation of flow induced vibrations. The B-1 tests do indicate that the fuel pins may be excited to vibration levels several mils in amplitude at resonance conditions with very low g-level (0.05 g) inputs.

APPENDIX

This appendix contains specific information on the PNL Impedance Detector including a complete circuit diagram, component description and photos showing the printed circuit board layout and assembled instrument.

PNL IMPEDANCE DETECTOR COMPONENTS

Bridge, Detector Amplifier Circuit

R101-R104	±1% metal film resistors adjusted to provide a 4-equal-arm bridge
R105	2K to 5K trimpot - infinite resolution desirable
R106-R107	Adjusted to provide 1 volt at terminal (a)
R108-R111	100K metal film resistor
R112-R113	10K 1/2 watt carbon 10%
R114	1 Meg metal film resistor ±1%; ±50 parts per million/°C
R115-R116	Adjusted to give desired gain
R117-R118	1/2 watt carbon hand picked for operational amplifier balance 10%
C101	90 Pf glass piston trimmer
C102	Silver Mica hand picked to capacitively balance-bridge
C103-C105, C107	0.001 MFD ± 10% disc ceramic capacitor
C106	150 Pf silver mica 5%
D101-D102	IN34 glass diode
T101	3 winding, bibiliar wound, pulse transformer; 2.3 mh ratios of 1:2:1; pulse engineering type PE 2233

Relay, Calibration - Reed relay SPST with actuating coil - 12 VDC 300 - Magnecraft W101 MPCX-2

FL101	10KC low pass filter, DTC FRA4RX11YV 10K input, 10K output impedance

THE PNL IMPEDANCE DETECTOR

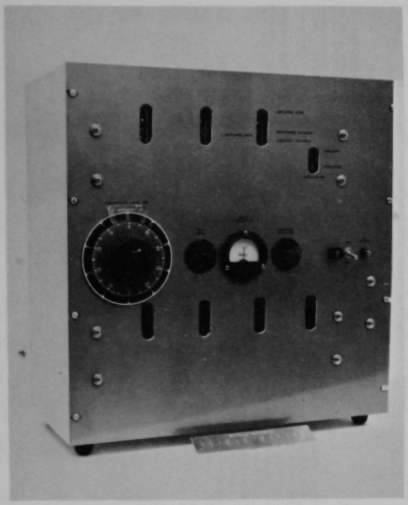

IMPEDANCE DETECTOR
FRONT VIEW

IMPEDANCE DETECTOR
REAR VIEW

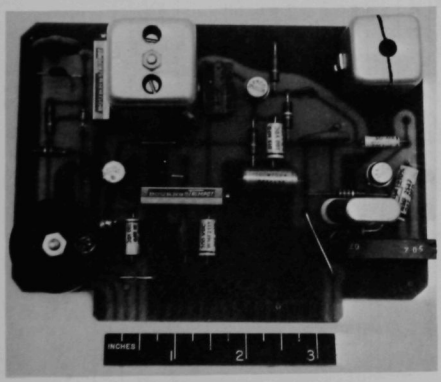

100 KC EXCITATION OSCILLATOR CIRCUIT BOARD

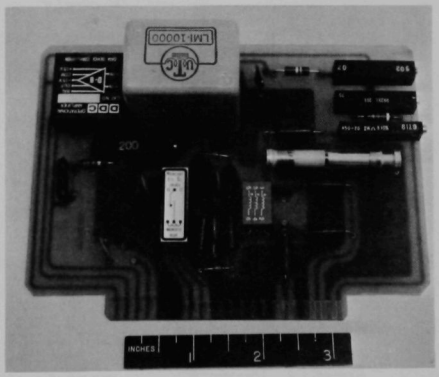

BRIDGE, DETECTOR, AMPLIFIER CIRCUIT BOARD

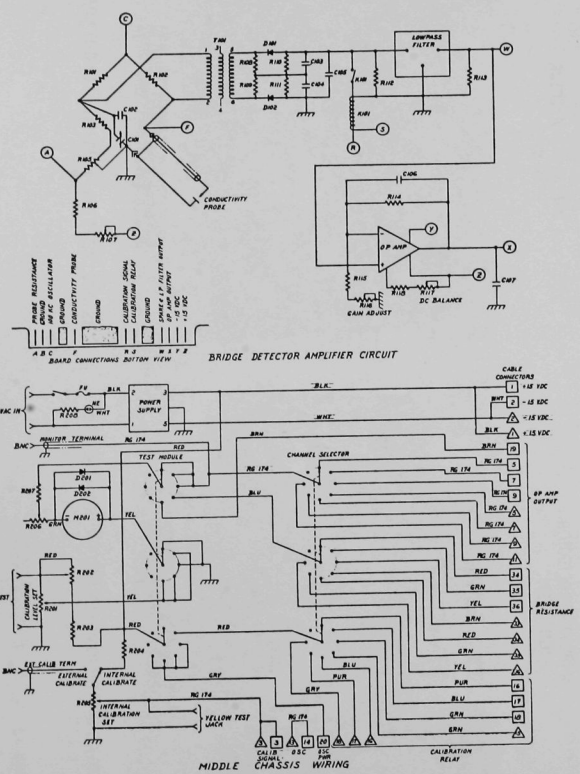

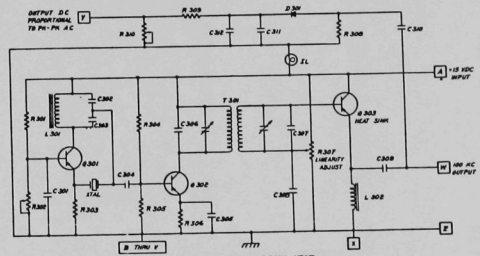

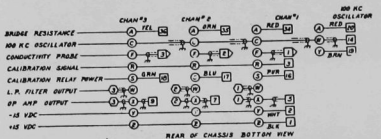

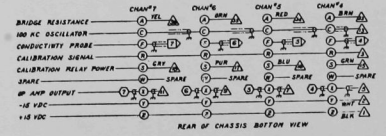

NOTES TOP & BOTTOM CHASSIS WIRING

- ○ PRINTED CIRCUIT SOCKET TERMINALS B,D,E,H,J,L,M,N,R,V ARE CHASSIS GROUNDED (AMPHENOL #143-406-01).
- △ CHASSIS CONNECTOR TERMINALS 36 PIN (AMPHENOL #57-40-360).
- ○ OUTPUT CONNECTOR ON BACK OF CHASSIS (BNC BULKHEAD).
- □ INPUT CONNECTOR ON BACK OF CHASSIS (MICRODOT).

THE NUMBERS & LETTERS INSIDE THE SYMBOLS ARE THE PIN NUMBERS & SOCKET LETTERS.

Operational Amplifier - D-8 operational amplifier, Data Device Corp. A good low drift amplifier is essential.

Middle Chassis Wiring

R201	1K ten turn pot; Helipot Model AR1K 1.25 wire wound
R202-R203	Adjusted to provide 1 volt across calibration level set (R201)
R206-R207	Adjusted to give desired sensitivity of the null meter
R208	100K part of Neon panel light
PS201	±15 VDS power supply, Ferrotran Electronics Model HMC-15, Rating +15 -15/150 ma; A stable low noise supply is essential
M201	Zero center null meter
D201-D202	IN2071 diodes for meter protection

Rotary - 11 position, 3 section, ceramic rotary switch with positive detents, switches and limit settings.

100KC Oscillator

R301	33K
R302	5K
R303	4.7K
R304	100K
R305	5.1K
R306	5.1K
R307	5K
R308	12K
R309	1K
R310	5K
L301	Slug tuned inductor. Nominal value 2.2 mh Q = 200 J. W. Miller 4400 series
L302	500 Mh Toroidal Inductor Plastic Encapsulated Triad type ET-500 A
T301	165-185KDS Air Core IF transformer with Mica Delectric Trimmer Capacitors, J. W. Miller type 112-K-2
I301	20V 10 Ma Incandescent lamp
XTAL	100KCA James Knight type G9D (500) H17T holder inserted into ELCO ceramic socket SO205COT
Z301	2N332A ETCO

Q302	2N332A ETCO
Q303	2N1308 GI with fin type heat sink
D301	IN34
C301	0.047 MFD
C302	0.005 MFD
C303	0.0015 MFD
C304	470 MMF
C305	0.015 MFD
C306	250 MMF
C307	330 MMF
C308	0.015 MFD
C309	0.01 MFD
C310	0.005 MFD
C311	220 MMF
C312	0.02 MFD

ACKNOWLEDGEMENTS

The author is deeply indebted to Dr. Wm. C. Kinsel and G. L. Fox who initiated this work; to Dr. Wm. C. Kinsel for his invaluable suggestions and encouragement throughout this investigation, but particularly for editing the final manuscript, and to H. R. Hughes for many valuable suggestions in the design and construction of the instrumentation.

REFERENCES

1. M. W. Wambsganss, Jr. "Vibration of Reactor Core Components", Reactor and Fuel-Processing Technology, vol. 10, no. 3. Summer 1967.

2. E. P. Quinn. Vibration of Fuel Rods in Parallel Flow, GEAP-4059. General Electric Co., San Jose, California, July 1962.

3. D. Burgreen, J. J. Byrnes, D. M. Benforado. "Vibration of Rods Induced by Water in Parallel Flow," ASME Trans., vol. 80. 1958.

4. M. P. Paidoussis. The Amplitude of Fluid Induced Vibration of Cylinders in Axial Flow, AECL-2225. AECL, Chalk River, Ontario, March 1965.

5. R. T. Pavlica and R. C. Marshall. "An Experimental Study of Fuel Assembly Vibrations Induced by Coolant Flow," Nucl. Eng. and Design, vol 4, pp. 54-60. (1966).

6. W. K. Winegardner. Fretting Corrosion in Plutonium Recycle Test Reactor, HW-80021. Available from Clearinghouse for Federal Scientific and Technical Information Extension, Springfield, Virginia. March 1964.

7. M. W. Wambsganss, Jr. Unpublished Data. Argonne National Laboratory, Argonne, Illinois. (Personal Communication with Author, 9-4-68.)

8. S. A. Knudson. Dynamic Response of Slender Tubes in Parallel Flow When Subjected to Time Varying Boundary Conditions. University of Nebraska, 1968. (PhD Thesis.)

9. R. L. Randall, P. J.Pekrul, G. R. Grayban. Development of Noise Analysis Techniques for Measuring Reactor Coolant Velocities, NAA-SR-11193. Engineering and Equipment Reactor Technology, Atomics International. March 25, 1966.

10. D. A. Skoog and D. M. West. Fundamentals of Analytical Chemistry. Holt, Rinehart and Winston, Inc., 1963.

11. C. R. Davidson. Unpublished Data. Atomics International, Canoga Park, California. (Personal Communication with Author, 2-3-70.)

DISCUSSION

R. L. Randall (AI): Well, I think you've done a good job of presenting the case of the conductivity cell. It's part of the paper I'm going to present following you. The solution that we've come up with for your last two problems was to use ceramic seal headers which can be soldered in place and then filed smooth with the surface. They can be made to manufacturing tolerances far greater than you can do with epoxy, and they avoid the swelling and leakage problems from our experience. Therefore, you can have precise uniformity between your cells, much easier than with the epoxy insulation.

I discovered that conductivity cell thing accidentally back in about 1965 when we were trying to do flow measurements in our system. We discovered we had flow-induced vibrations, and we turned it into a vibration sensor.

P. R. Bengel (Westinghouse-Bettis): Bentley-Nevada makes a pickup cell which is very sensitive, something like 200 millivolts per mil. It's very small and it's made in a ceramic case. Why would you be looking for a conductivity cell when there are very good pickup devices for displacement like that? What is the advantage of the conductivity cell?

Sawtelle: The Bentley-Nevada devices I am familiar with are much larger than the conductivity cells we are currently using. Also, the models we have are quite nonlinear and, in addition to that, are sensitive to temperature, although the conductivity cell is quite dependent on temperature because the conductivity electrolyte changes.

Bengel: How long ago did you look at them? They do make special cells, for money, for what you need. They will make them for temperatures of 300F. They will measure displacements on the order of tenths of mils very accurately. They are linear in the range we've been looking at them. And they are not very big, on the order of 3/8 inch in diameter and maybe 1/2 inch long.

Sawtelle: Yes, you see the fuel pin we are talking about is 0.230-inch OD, which is less than a quarter of an inch and, for instance, a typical electrode on this cell is something like 15 mils.

Bengel: These are shelf items I'm talking about, and they're too big. I imagine they could be much smaller.

Sawtelle: Yes, thank you very much. This program was started like two years ago and at that time I certainly wasn't aware of a transducer of this size. They may well be practical, particularly for mounting in the wall.

APPLICATION OF NOISE ANALYSIS TECHNIQUES TO STUDY OF FLOW INDUCED VIBRATION IN REACTOR SYSTEM COMPONENTS

R. L. RANDALL
Atomics International
A Division of North American Rockwell Corporation
Canoga Park, California

ABSTRACT

Instrumentation and analysis techniques are described for detecting and studying flow induced resonant mechanical vibrations of tubes in an intermediate heat exchanger, using accelerometers attached to the outer wall of the heat exchanger vessel.* Techniques for studying flow distribution and flow induced vibration in hydraulic models of reactor core assemblies are also discussed along with a summary of recent applications to flow measurements in 1200°F sodium.†

SUMMARY

As part of a program to investigate possible flow induced vibration in an intermediate heat exchanger, a total of seven accelerometers with natural resonant frequencies in the 40 to 45 kHz band were installed on the outer shell of the heat exchanger at four angular positions around the vessel and at four axial positions along the vessel. Signals from the accelerometers corresponding to modulation in the 40 to 45 kHz band were recorded on FM magnetic tape along with signals from the same accelerometers in the 5 to 300 Hz range, and the dc signal from a

*Work done under AEC Contract AT(04-3)-700
†Work done under AEC Contract AT(04-3)-701

permanent magnet flowmeter. Recordings were obtained while the IHX primary flow rate was varied linearly from zero to maximum IHX rated flow and back to zero.

Cross spectral density measurements were performed relating low frequency wall vibrations to modulation of ultrasonic emission in the 40 to 45 kHz range. Results indicated metal to metal impacting does occur at particular flow conditions. The method permitted experimental determination of natural frequencies of IHX system components and identification of flow conditions which induced resonant mechanical impacting.

Studies of flow induced vibration and flow distribution in hydraulic models of reactor core assemblies involve the use of conductivity sensors. Movements between elements are sensed as conductivity changes (with electrodes installed in simulated fuel elements) and measured with a spectrum analyzer. For flow studies random variations in stream conductivity are induced by injection of a thermal or conductivity tracer. The use of a thermal tracer permits continuous operation without eventual saturation that occurs with the use of conductivity tracers. A cross correlation computer with automatic transit time readout is used to measure flow rate, degree of correlation and bandwidth relating signals from each pair of sensors.

This latter work has recently led to development and successful operation of the Transit Time Flowmeter in 1200°F sodium. A miniature version of a transit time flowmeter for in-core flow measurements was also tested in 1200°F sodium.

INTRODUCTION

This paper describes experimental techniques and the equipment used to study fluid flow and flow induced vibration.

The data recording and analysis capabilities[1] described in this paper were developed from noise analysis applications in many different areas of reactor engineering, including Reactor Kinetics and Control, Structural Dynamics, Heat Transfer, Hydraulics and Detection of Incipient Malfunctions.[2,3,4,5,6]

INTERMEDIATE HEAT EXCHANGER TUBE VIBRATION TEST

Heat exchangers have been known to be subject to fatigue failure from excessive tube vibrations. One of the mechanisms which can lead to high vibration levels is vortex shedding from the tubes in the heat exchanger, particularly if flow conditions are such that vortex shedding occurs at a natural resonant frequency of the tubes.

Under flow conditions where resonant vibration of sufficient amplitude is induced, periodic metal to metal impacting may occur between tubes or between tubes and support structures. Tests conducted with accelerometers indicated that vibration resulting in metal to metal impacting generates acoustic emission that readily propagates through steel or sodium and can be detected as amplitude modulation in the ultrasonic frequency band. Each pulse of ultrasonic energy causes an accelerometer to ring at its natural frequency, if it is coupled acoustically by a steel or liquid metal path to the structure undergoing metal to metal impacting. This observation was the basis for attempts to detect resonant impacting in an intermediate heat exchanger with external sensors.

The Sodium Components Test Facility (SCTI) operates within the Liquid Metals Engineering Center (LMEC), at Atomics International. The SCTI (Figure 1) consists of a 10-in. primary sodium loop, (Figure 2) a 10-in. secondary sodium loop, and a steam loop. Heat transfer between the primary and secondary sodium loops is accomplished by a test intermediate heat exchanger (IHX).

As part of a program to assure satisfactory operation of the IHX, an investigation of possible flow-induced vibrations was considered. Neither the analytical investigations nor the in-system performance indicated a tendency towards tube vibration problems. The costs, and delays in the operating schedule which would have resulted from cutting open the IHX and installing vibration transducers inside the vessel were considered unjustified.

Therefore an attempt was made to detect resonant mechanical impacting and at least determine resonant frequencies and flow dependence, if any, using accelerometers attached to the outer shell of the IHX.[7]

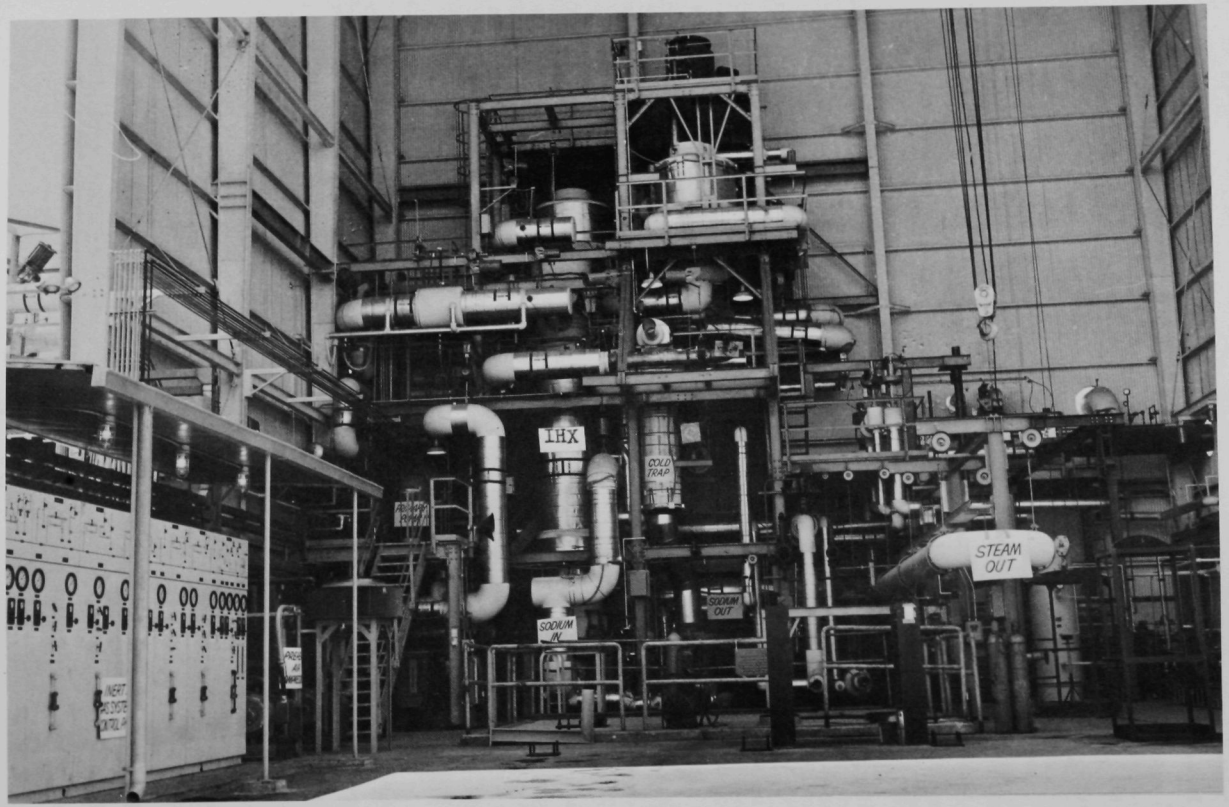

7593-5495CN

Figure 1. SCTI High Bay

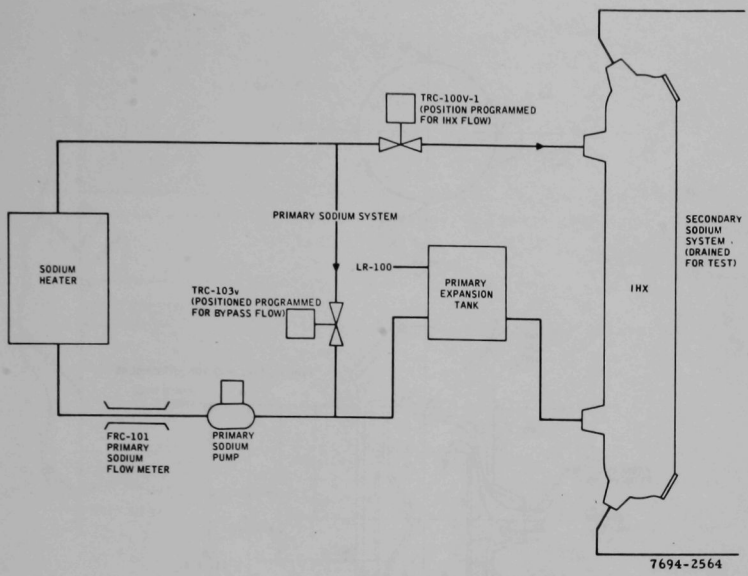

Figure 2. SCTI Primary System

Accelerometer Installation

The IHX is a vertical shell and tube design with primary flow on the shell side, constructed of Type 316 SS. The tube bundle consists of 462 tubes which have a 0.5-in. OD and 0.035-in. wall thickness. Twenty-seven disc and doughnut baffles are employed such that primary sodium flow in the region of the tube bundle is in crossflow. Shell-to-tube differential thermal expansion is allowed by the flexure of three-dimensional sine-wave tube bends located at one end of the tube bundle. The unsupported tube length in the sine-wave region (Figure 3) is about 58 in. as opposed to about 8 in. between baffles. Therefore, the sine-wave region was selected as being the most probable location of excessive tube vibrations.

A total of seven accelerometers with natural resonant frequencies in the 40 to 45 kHz band were installed on the outer shell of the heat exchanger at four angular positions around and at four axial positions along the vessel, as shown in Figure 3.

The accelerometers were mounted to the IHX shell by 1/2 in. OD by 9 in. long Type 316 SS studs. The studs were Heli-arc welded to the shell

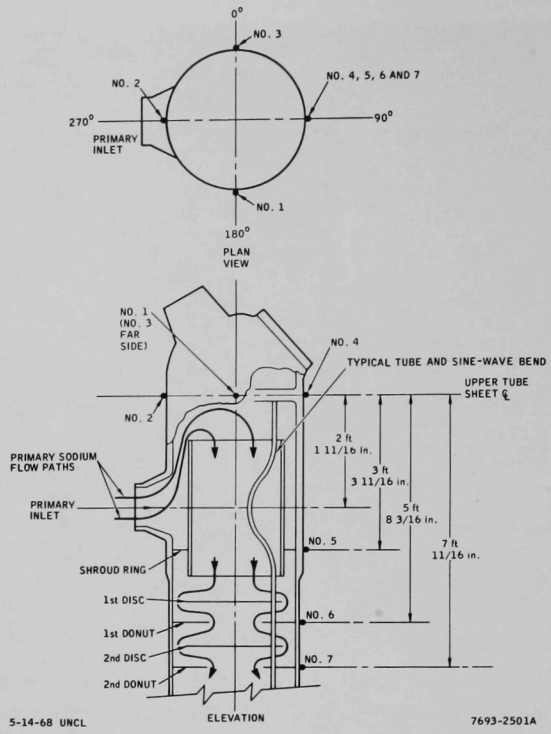

Figure 3. Accelerometer Installation Locations

and the accelerometers were bolted to the studs as shown in Figure 4. The fundamental resonant frequency of the combined accelerometer-stud was about 150 Hz.

Test Method

The basic technique involved recording simultaneously on magnetic tape the unfiltered signals from the accelerometers and a permanent magnet flowmeter, during various flow and background noise conditions. Recordings were obtained while the IHX primary flow rate was varied linearly from zero to maximum IHX rated flow and back to zero.

During recordings, selected signals were displayed on rms voltmeters, an oscilloscope and a loudspeaker. Prior or subsequent to each test calibration signals were recorded on the data tape to permit normalization of playback signals to known acceleration and voltage levels.

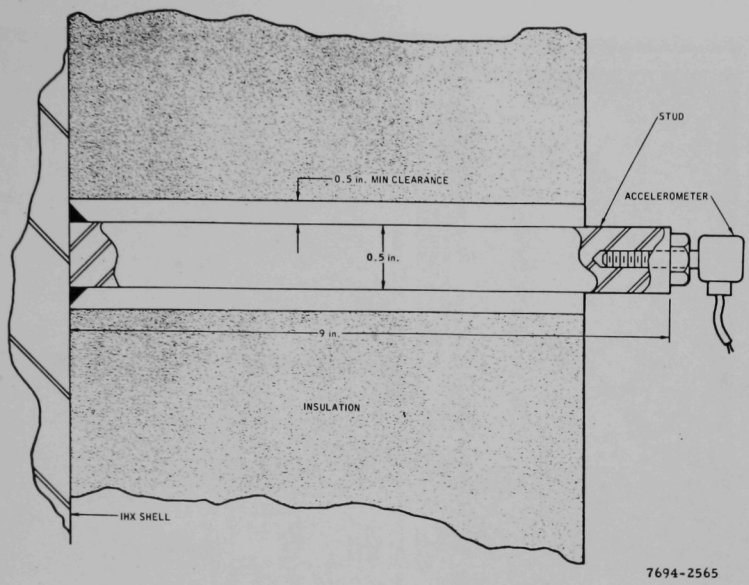

Figure 4. Accelerometer Mounting

After evaluation of the preliminary broad-band recordings, additional recordings were made using band-pass filters for isolation of specific frequency components to permit increased recording sensitivity.

Data Acquisition Instrumentation

The data acquisition instrumentation used in the tests is listed in Table 1. A recording system with tape and amplifier units similar to those used on the IHX vibration tests, is shown in Figure 5.

For the preliminary recordings, the emphasis was placed on unfiltered broad-band response. The total frequency band included in these recordings extended from 1 Hz to as high as 200 kHz. In later recordings, the emphasis was placed on high sensitivity in narrow-frequency bands. Signals from the accelerometers corresponding to modulation in the 40 to 45 kHz band were recorded on FM magnetic tape along with signals from the same accelerometers in the 5 to 300 Hz range, and the dc signals from a permanent magnet flowmeter.

Figures 6 and 7 show typical instrument configurations used for data acquisition. Figure 8 shows the frequency response of band-pass filters and demodulators used in the narrow band tests.

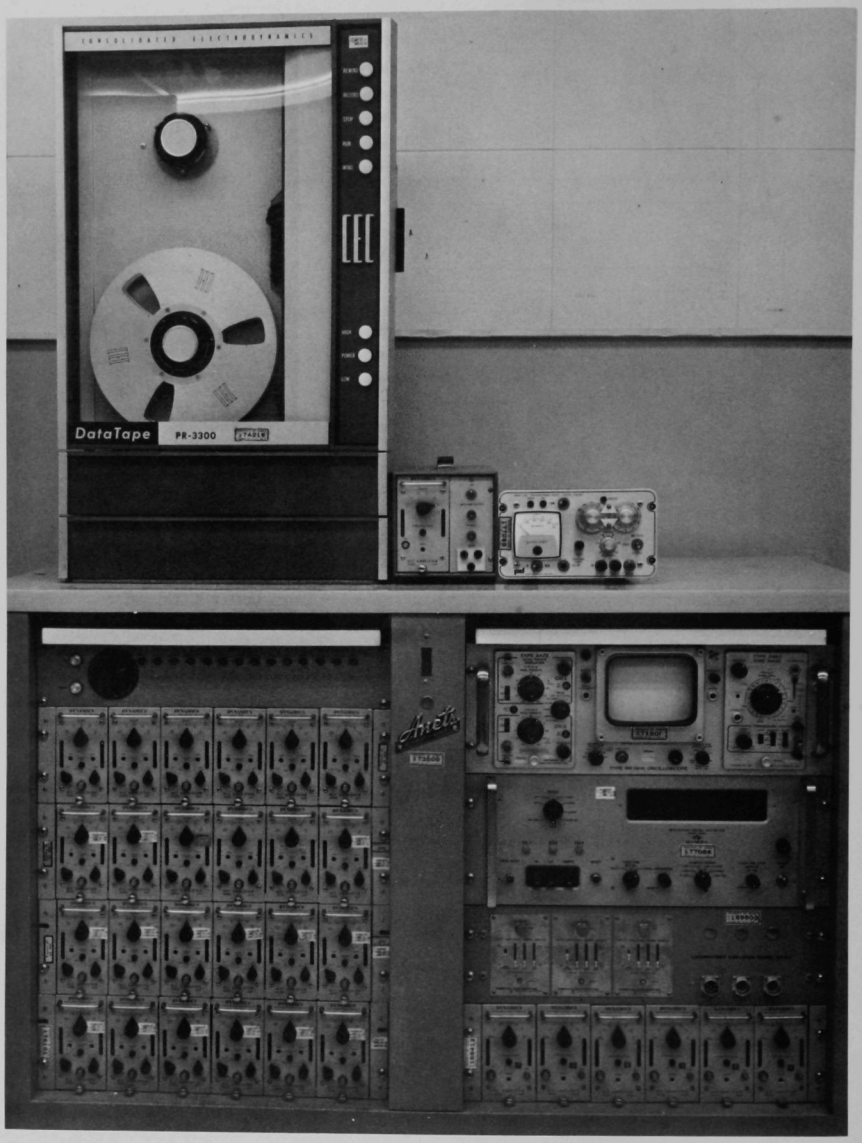

4-25-68

7757-4001

Figure 5. Data Recording System with Tape and Amplifier Units Similar to Those Used for IHX Vibration Tests

TABLE 1

DATA ACQUISITION INSTRUMENTATION

Equipment	Identification	Description
Accelerometer	Endevco Model No. 2217	Hermetically sealed unit, 8 mv/g
Microphone	Shure Model No. 51	Dynamic microphone
Tape Recorder	Consolidated Electrodynamics Model No. VR3300	14-channel bandwidth – Up to 50 kHz FM Up to 200 kHz direct
Accelerometer Preamplifier	Endevco Model No. 2616B	Bandwidth – 1 cps to 500 kHz Gain range of 1 to 10
Data Amplifier	Dynamics Model No. 6631	Bandwidth – 0 to 312 Hz Gain range of 10 to 1000
Data Amplifier	Dynamics Model No. 6109	Bandwidth – 0 to 50 kHz Gain range of 0.1 to 100
Data Amplifier	Dynamics Model No. 6106	Bandwidth – 0 to 10 kHz Gain range of 0.1 to 1000

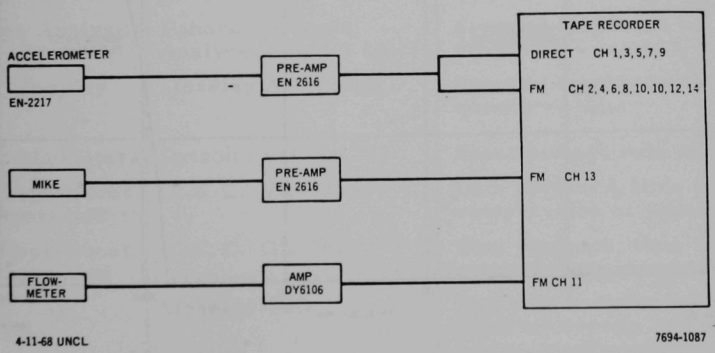

Figure 6. Block Diagram of Recording System for Wide Band Tests

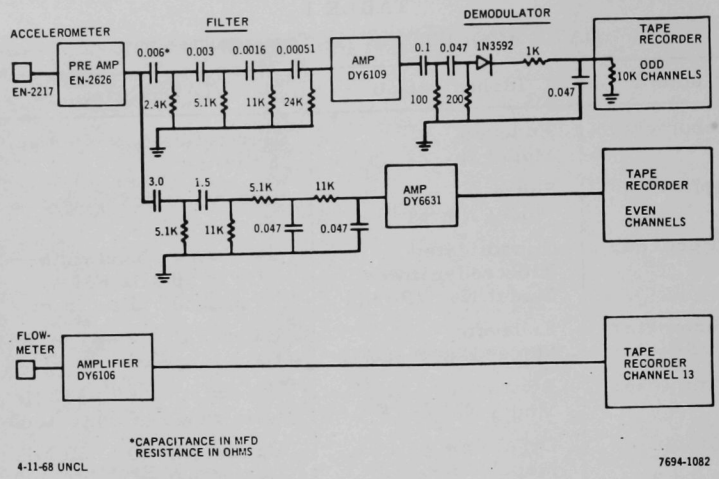

Figure 7. Schematic Diagram of Recording System for Narrow Band Tests

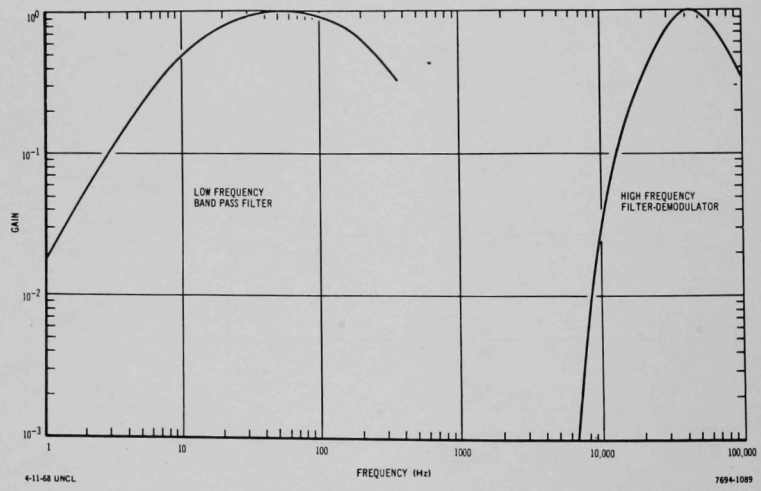

Figure 8. Normalized Frequency Response of Band Pass Filters Used for Recording Accelerometer Signals in Narrow Band Tests

Data Reduction Instrumentation

Table 2 is a list of the data reduction equipment used for this program. The laboratory where the tape recorded signals were processed is shown in Figure 9. Instrumentation block diagrams for measuring and displaying various functions are shown in Figures 10 to 14. The Analog Cross Spectral Density Analyzer System used to measure spectral amplitude, power spectral density and coherence is described in References 1 and 3. The mathematical significance and the means for measuring the coherence function, which is used to determine cause and effect relations between noise contaminated random signals as a function of frequency, are also described in References 1 and 3.

TABLE 2

DATA REDUCTION INSTRUMENTATION

Equipment	Identification	Used for Measuring or Displaying
Analog Cross Spectral Density Analyzer System	Modified Gulton, Ortholog O-F3	Spectral amplitude, power spectral density, coherence
Eight-Channel Chart Recorder	Brush, Mark 200	Amplitude, voltage spectral amplitude, coherence, rms level vs time
X-Y Recorder	Electro-Instruments Model 320	Amplitude vs frequencey amplitude vs flow power spectral density spectral amplitude
On-Line Analyzer	Panoramic Sonic Analyzer, Model LP-1	Spectral amplitude vs frequency vs time
X-Y-T Display	Moseley Autograph	Spectral amplitude vs frequency vs time
Adjustable Filters	Dytronics Model 722	Spectral amplitude vs time
Tape Reproducer Reel Operation	C.E.C. VR-3300	Data playback, time base compression or expansion
Tape Reproducer Loop Operation	C.E.C. GL-2810	Data playback, time base compression or expansion
AC-DC Log Converter	Moseley-60D	Log rms vs time, log power spectral density vs frequency, log spectral amplitude vs frequency
Data Amplifier	Dynamics Model 6109	Signal amplification 0 to 50 kHz bandwidth

9-9-66

00-40120

Figure 9. Data Reduction Instrumentation

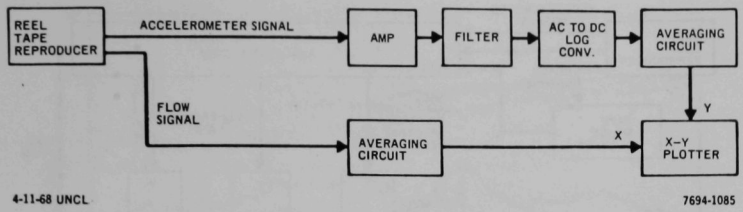

Figure 10. System for Measuring Vibration Levels in Various Frequency Bands vs Flow

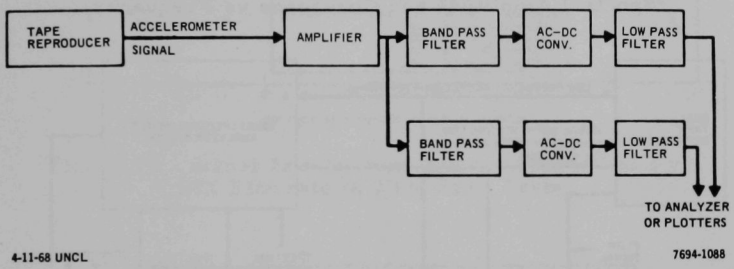

Figure 11. System for Studying Modulation on Various Frequency Bands

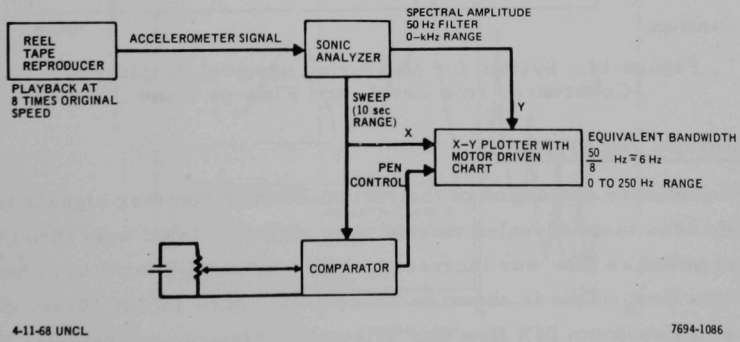

Figure 12. System for Measuring Amplitude vs Frequency vs Time

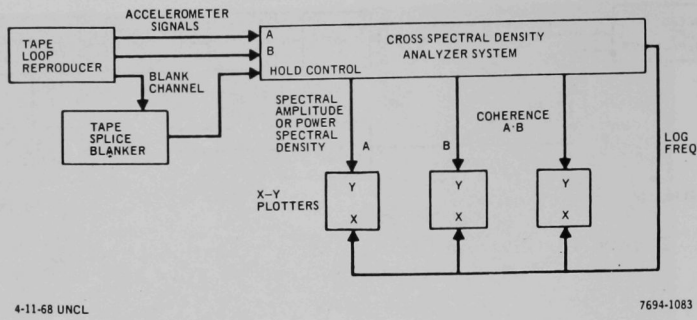

Figure 13. System for Measuring Power Spectral Density, Spectral Amplitude and Coherence vs Frequency

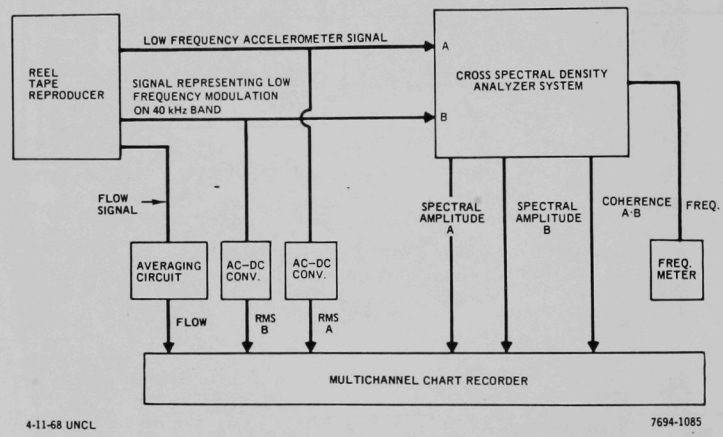

Figure 14. System for Measuring Spectral Amplitude, Coherence, rms Level, and Flow vs Time

Test Results and Evaluation

Preliminary evaluation of the recorded accelerometer signals from the wide band tests revealed that the rms vibration level went through several peaks as flow was increased, with a maximum level at or near maximum flow. This is shown in Trace 1 of Figure 15. A 10-sec data sample at maximum IHX flow was selected for frequency analysis. Figure 16 is typical of the spectral amplitude observed from the upper accelerometers, while Figure 17 shows the spectral amplitude observed at a lower position on the IHX. The major spectral components common

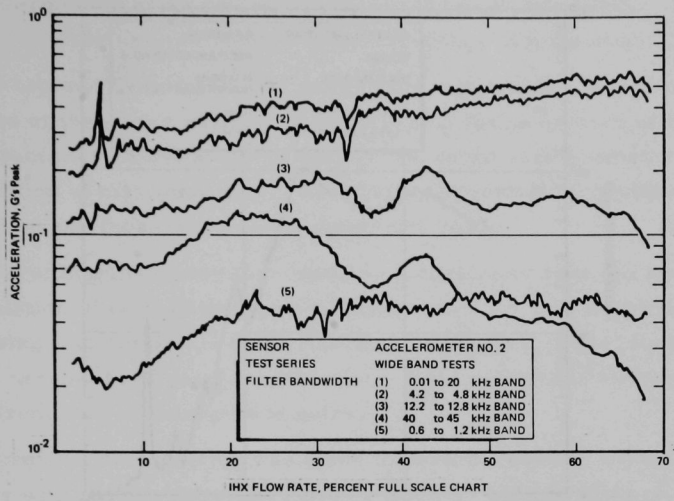

Figure 15. Signal Levels from Accelerometer No. 2 vs IHX Flowrate in Wide Band Tests

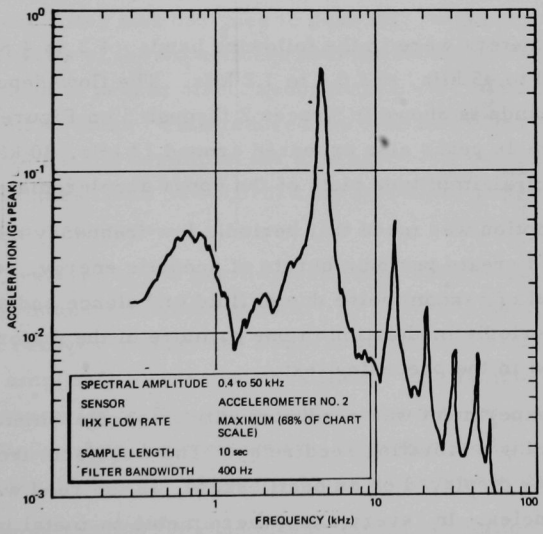

Figure 16. Spectral Amplitude of Signal from Accelerometer No. 2 at Maximum IHX Flowrate in Wide Band Tests

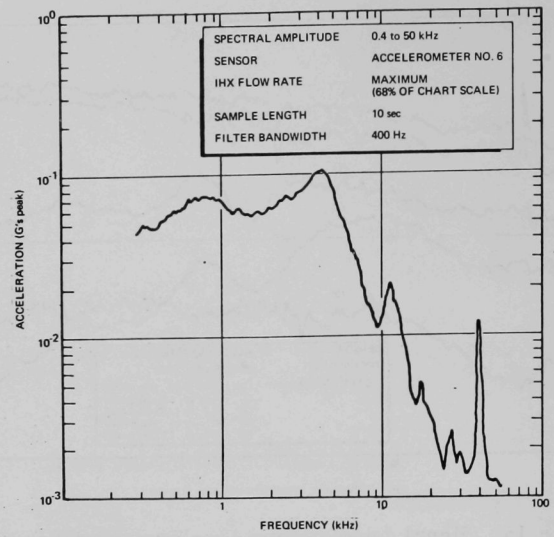

Figure 17. Spectral Amplitude of Signal from Accelerometer No. 6 at Maximum IHX Flowrate in Wide Band Tests

to all accelerometers were in the following bands: 4.2 to 4.8 kHz, 12.2 to 12.8 kHz; 40 to 45 kHz, and 0.6 to 1.2 kHz. The flow-dependence of each of these bands is shown in Traces 2 through 5 on Figure 15. As shown in Figure 16 peaks also appeared around 22 kHz, 30 kHz, and 50 kHz in the spectral amplitude plots of the upper accelerometers.

The assumption was made that periodic low frequency metal to metal impacting would create periodic bursts of acoustic energy, superimposed on a background of random noise due to fluid turbulence and appear as narrow-band periodic modulation in one or more of the major spectral peaks discussed in the preceding text.

A simple experiment was conducted with an accelerometer attached to a box containing a vibrating reed relay. The waveform from the accelerometer was displayed on an oscilloscope, as the reed was driven at various frequencies. In every case where metal-to-metal impacting occurred, two predominant frequency components were observed. One was related to the impacting frequency, the other to periodic ringing of

the accelerometer at its natural frequency (40 to 45 kHz band). The period of modulation was related to the frequency of impacting.

The attempt to find periodic modulation began with a series of measurements of the power spectral density of modulation on each of five major frequency components for each of the seven accelerometers for the condition of maximum flow. No significant periodic modulation was detected on any frequency band at maximum flow.

Several attempts were then made to qualitatively scan the spectrum of modulation of each of the spectral peaks from the continuous flow ramp data, using the Panoramic Sonic Analyzer. However, signal levels were low and narrow-band resonant vibrations could not be statistically resolved from random background noise.

Therefore, the decision was made to perform another series of recordings with narrow-band-pass filters and high-gain amplifiers. This increased recording sensitivity by one or two orders of magnitude in the selected frequency bands.

Since the expected frequency of tube vibration was in the band from 10 to 80 Hz, one filter was designed to pass this frequency band. On the basis of the results of the experiment with the vibrating reed a detector circuit was added to permit direct recording of low-frequency modulation in the 40 to 45 kHz band. This reduced the tape bandwidth requirements to less than 312 Hz and permitted the tape speed to be reduced. Thus longer data samples could be recorded for increased statistical accuracy of spectral measurements.

Spectral analyses of the narrow band recordings at specific flow conditions did not indicate periodic events. To provide a continuous frequency analysis with changes in flow, the Panoramic Sonic Analyzer was used to plot spectral amplitude vs frequency vs time. An example of these measurements is presented in Figure 18, which shows a complex interdependence of amplitude, flow, and frequency. Note that the largest components are on the order of 3×10^{-3} g, with a 6 cps filter bandwidth.

In an attempt to obtain higher measurement resolution with the existing data, one last series of measurements was made using the Cross Spectral Density Analyzer.[1,3] The Analyzer System was set up to

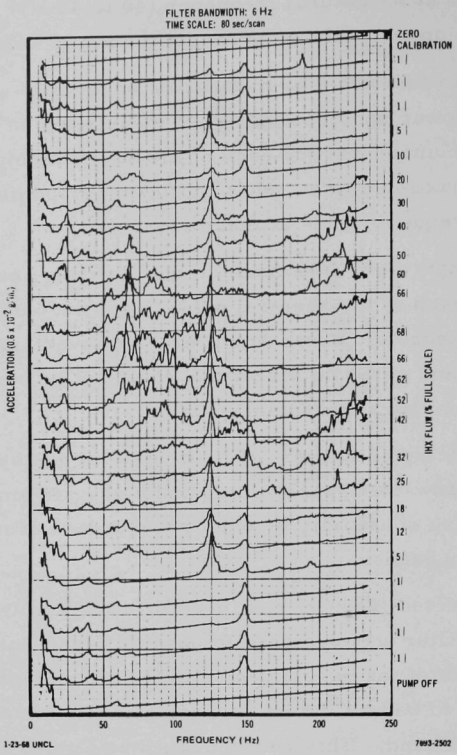

Figure 18. Analysis Showing Amplitude vs Frequency vs Time and IHX Flow-rate, Signal from Accelerometer No. 2 in Narrow Band Tests

provide simultaneous plots of spectral amplitude, coherence, and flow, vs time. The coherence measurements were used to relate the low-frequency vibrations at particular frequencies to modulation on the 40 to 45 kc band, for each accelerometer. The results of these measurements are summarized for Accelerometer 2, in Figures 19 and 20. The trace next to the bottom on each plot shows the total average signal level vs flow. Note in Figure 20 the nonsymmetry in the level of noise in the 40 to 45 kc band with flow. The peaks around 20 and 40% on the up ramp are absent on the down ramp. The observed noise in the 40 to 45 kc band could be largely void collapse sounds or bubble noise due to some type of

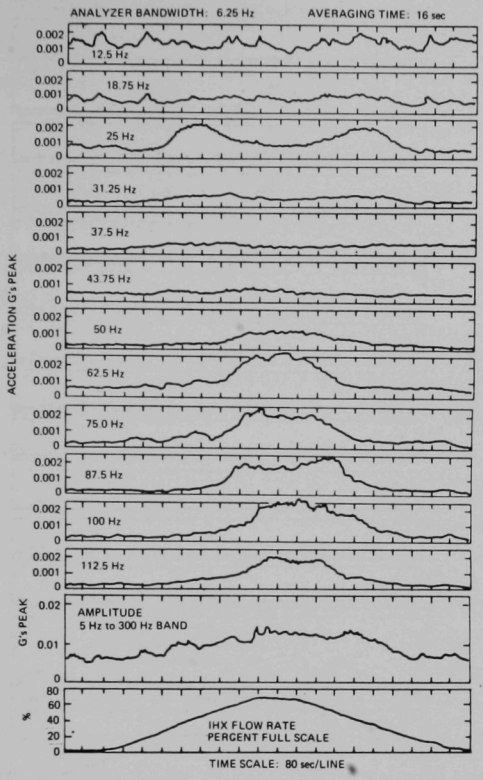

Figure 19. Spectral Amplitude, Total Signal Level in 5 to 300 Hz Band and IHX Flowrate vs Time, Signal from Accelerometer No. 2 in Narrow Band Tests

flow-dependent gas entrainment. The conditions for gas entrainment and entrapment could vary as a function of flow rate, accounting for the observed amplitude variations. If gas, entrapped in part of the system at low flow rates, was completely swept away when the system reached maximum flow, the bubble noise would be at a minimum and could gradually increase as low flow conditions were again approached.

The coherence function represents the fractional portion of a noise contaminated signal statistically correlated with, or linearly dependent upon, an observed random excitation signal at each frequency. This is

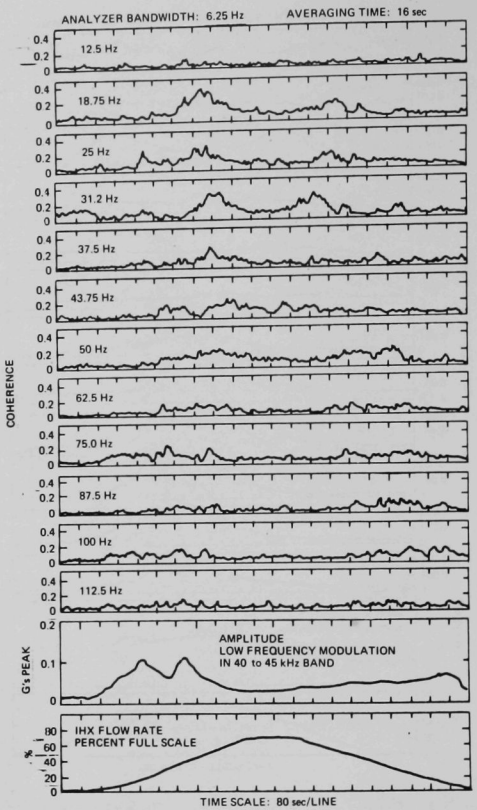

Figure 20. Coherence, Total Signal Level in 40 to 45 kHz Band and IHX Flowrate vs Time, Signal from Accelerometer No. 2 in Narrow Band Tests

useful for verifying cause and effect relations between noise-contaminated random signals, as a function of frequency. The coherence plots in Figure 20 were obtained using an equivalent analyzer filter bandwidth of 6.25 cps and with a smoothing time constant of 16 sec. The machine accuracy of the coherence display (not considering statistical factors) is approximately ±0.05 on the scale of 0 to 1. The test conditions were not stationary, signal levels varied erratically with changing flow level, resulting in further coherence uncertainties of around ±0.1 on the scale of 0 to 1. Thus, if tube vibrations and their respective impacting sounds are

to be detected from the coherence plots, the expected level of marginal significance would be approximately 0.15 to 0.20.

The coherence plots in Figure 20 showed the flow, frequency, and time dependence of coherence for Accelerometer 2. Considering all coherence levels above 0.20 to be significant, there are a number of flow and frequency regions where these measurements provide qualitative evidence of a statistical relationship between modulation of signals in the 40 to 45 kHz range and observed low-frequency IHX vibrations. According to the original assumptions of the test, this indicates resonant mechanical impacting does occur at particular flow conditions.

The spectral amplitude and coherence measurements for the various accelerometers were then used to construct contour maps showing the frequency and flow dependence of these functions. The method permitted experimental determination of natural frequencies of IHX system components and identification of flow conditions which induced resonant mechanical impacting.[8]

This example illustrates studies of flow induced vibrations in a complex operating system, must include analyzes at all possible frequencies at all flow conditions. The severe background noise created by cavitation, gas entrainment and the pump, and the complex dependence of vibration frequency on the flow rate of the system, made it particularly difficult to find appropriate combinations of analysis frequency and flow where periodic impacting was eventually detected.

FLOW AND VIBRATION TESTS IN REACTOR CORE MOCKUPS

Noise analysis techniques have been used extensively at Atomics International to study flow velocity, flow distribution, mixing and flow induced vibration in hydraulic models of reactor core or fuel bundle assemblies.[4,9,10] The following includes a brief summary of the basic approach with reference to recent improvements in the equipment and techniques.

As part of the design and development of fuel element assemblies, hydraulic models of the proposed configurations are instrumented with conductivity sensors and tests performed to experimentally determine

characteristic hydraulic parameters, flow partitions, velocity profiles, and cross flow. Such testing is essential to assure optimized transfer of heat energy from fuel to coolant, minimize fuel cladding temperature and lengthen core life.

Conductivity electrodes are installed at a number of axial positions along the wall of dummy fuel elements. The electrodes are made from ceramic seal headers, to insure size uniformity and avoid problems of water absorption and swelling which occurred with epoxy insulated electrodes. After being soldered in place, the entire header assembly is filed flush with the surface of the fuel element so the sensor does not interfere with flow. The enameled or teflon insulated lead wires are brought out through the top of the hollow fuel elements.

For flow studies, the sensors are aligned with the selected flow channels. Conductivity variations are observed at two or more in-line sensors as a thermal on conductivity tracer is added at a point upstream from the test model. A cross correlation computer with automatic transit time readout[11] is used to measure flow rate, degree of correlation and bandwidth, relating the signals from two sensors. Thermal tracers, detected as changes in electrical conductivity, permit continuous operation without eventual saturation that occurs with the use of conductivity tracers.

The same conductivity electrodes used for measuring velocity profiles and flow distribution in hydraulic models are also used to detect and measure fuel element vibrations. However, for the vibration measurements, a constant resistivity solution is used, and the electrodes are pointed at the adjacent fuel rods, instead of into the coolant channels. Movements between elements are sensed as conductivity changes and measured with a spectrum analyzer.

Tests conducted to date in reactor core models were limited to spectral analysis at fixed flow rates, usually maximum rated flow. Results from the IHX tests showed little or no evidence of resonant effects at constant flow, particularly maximum flow.

This indicates that in future studies of flow induced vibration, provision should be made to include analyses at all possible frequencies at

all flow conditions. This was achieved in the IHX vibration tests by measurements of spectral amplitude vs frequency vs time as flow was slowly and continuously varied through the desired range.

TRANSIT TIME FLOWMETER

The studies of flow distribution and flow induced vibration in reactor core models have led to the development of a Transit Time Flowmeter (TTF). The transit time method is a fundamental measurement of volumetric flow velocity and has been proposed for use in high temperature sodium systems as a standard against which other types of sodium flowmeters can be calibrated. The TTF is being considered for flow calibration in the Sodium Pump Test Facility (SPTF) and the Fast Flux Test Facility (FFTF), and for measuring the flow from individual fuel assemblies in the FFTF.

The technique provides accurate volumetric flow determination based on measurements of channel size, distance between sensors, and transit time of temperature patterns between the sensors.

Random temperature fluctuations, in the range of 1.0 to 0.01°F peak-to-peak, are detected at two axial positions in a flow channel, using sheathed thermocouples with matched time response installed on replaceable fins. An instrument system called the Transit Time Computer[11] measures and provides a continuous readout of the transport delay relating the signals with an accuracy of 0.2%. Reference 12 describes demonstration tests of a 2-in. diameter transit time flowmeter in water at flow rates to 15 ft/sec and in sodium at operating temperatures to 1200°F.

A small diameter Transit Time Flowmeter for in-core flow measurements was also tested in 1200°F sodium.[13] The TTF for in-core applications included an acoustic wave guide for external detection and study of: (1) boiling and void inception; (2) massive fuel cladding rupture of the type that can propagate to other regions of core; (3) gas entrainment; (4) cavitation; (5) pump noise; and (6) flow induced vibration of reactor system components.

REFERENCES

1. R. L. Randall, The Analog Cross Spectral Density Analyzer System, The Shock and Vibration Bulletin, Bulletin 35, Part 4, pp. 223-230 (U.S. Naval Research Laboratory, Washington, D.C.), February 1966.

2. R. L. Randall and C. W. Griffin, Application of Power Spectra to Reactor System Analysis, in Symposium on Noise Analysis in Nuclear Systems, pp. 107-130, AEC Symposium Series, No. 4 (TID-7679), Gainesville, Fla., 1964.

3. R. L. Randall and P. J. Pekrul, "Applications of Analog Time and Frequency Correlation Computers to Reactor System Analysis," in Symposium on Neutron Noise, Waves and Pulse Propagation, pp. 357-380, AEC Symposium Series, No. 9 (CONF. 660206), Gainesville, Fla., 1967.

4. R. L. Randall, P. J. Pekrul, and G. R. Grayban, "Development of Noise Analysis Techniques for Measuring Reactor Coolant Velocities," Report NAA-SR-11193, Atomics International, Div. of North American Rockwell Corp., February 1966.

5. R. L. Randall and D. Logan, "Application of Noise Analysis Techniques to Hydraulic Measurements in Liquid Metal Systems," in Proceedings of the Symposium on Liquid Metal Instrumentation and Control, pp. 71-76, ANL-7380, Idaho Falls, Idaho, 1967.

6. R. L. Randall, "The Application of Noise Analysis Techniques to Detection of Incipient Malfunctions," in Symposium on Incipient Failure Diagnosis for Assuring Safety and Availability of Nuclear Power Plants, pp. 71-86, CONF-671011, Gatlinburg, Tennessee, 1967.

7. R. L. Randall and R. E. Toews, "Alco Intermediate Heat Exchanger Tube Vibration Test," LMEC-SR-MEMO-68-16, Liquid Metal Engineering Center, Atomics International, Div. of North American Rockwell Corp., June 1968.

8. K. A. Gardner, "Alco Intermediate Heat Exchanger Vibration Studies and Tests," LMEC-SR-MEMO-68-16, Liquid Metal Engineering Center, Atomics International, Div. of North American Rockwell Corp., April 1969.

9. P. J. Pekrul and R. D. Phelps, "U-305 Vibration and Pressure Drop Test," Report AI-CE-TDR-1005, Atomics International, Div. of North American Rockwell Corp., July 1965.

10. P. J. Pekrul, "RBA Flow Velocity and Vibration Tests," Report AI-CE-TDR-1017, Atomics International, Div. of North American Rockwell Corp., January 1966

11. R. L. Randall,""Transit Time Flowmeter Employing Noise Analysis Techniques, Part 1. Water Loop Tests," AI-AEC-12802, Atomics International, Div. of North American Rockwell Corp., March 1969.

12. R. L. Randall, "Transit Time Flowmeter Employing Noise Analysis Techniques, Part 2, 2-in. Sodium Tests," AI-AEC-12941, Atomics International, Div. of North American Rockwell Corp.,(to be published 1970).

13. R. L. Randall and C. W. Wheelock, "Reactor Core Parameter Probe, Assembly and Test of a Prototype Flowmeter Assembly," AI-AEC-SR-MEMO-12907, Atomics International, Div. of North American Rockwell Corp., December 1969.

DISCUSSION

H. A. Nelms (ORNL): Do I understand from what you said that you recommend the use of external sensors as a way of looking for your vibration problems in heat exchangers?

Randall: The classical case is they have an operating system already in use, and they suddenly become worried about flow-induced vibrations and they want something done about it. So, in the area where the vibrations lead to impacting, those would be flow conditions where you'd have the most serious resonant effects. We can then use this technique to obtain experimental information about the basic, or the most serious, resonant frequencies of the internal components and their flow dependence.

Nelms: It seems to me, though, that it's got a serious limitation in that you've still got to go in the system and find out where the vibrations are, and therefore you might better have just gone ahead and done that in the first place.

Randall: Well, they wanted to find out if there were particular flow conditions they should avoid. This did point out that there were certain flow conditions, very narrow flow conditions, and if they avoided those regions, they could operate without at least the impacting effects. When they knew the resonant frequencies involved, they could use that to predict fatigue lifetime of the components.

Nelms: You mentioned you met your primary objective. Would you care to comment on what other objectives you'd hoped to make at the time that you didn't meet.

Randall: If it hadn't been for the terrific noise of gas entrainment, we had hoped to use triangulation methods to help point out the particular regions where the vibration was occurring. But because of the very bad statistical relationship here, the fact that we had to detect signals buried by a factor of 100 or 1000 down into the void entrainment noise, we were not able to use triangulation in this particular case. This may very well be typical of what you'd expect in a large sodium-cooled reactor.

A. Lohmeier (Westinghouse): When you talk about impacting, can you tell us something about the difference between the possibility of central

span impacting, which would appear to me to be more violent that the impacting at the tube support plates? Are you able to distinguish between the two? If one had a vortex-shedding phenomenon, resonance with vortex shedding, it would appear to me to be a much more violent and discernible noise. However, the rubbing of tubes in the supports might be a very low level. Could you clarify that some more?

Randall: Can you help me, Mr. Gardner? You're the one that evaluated this data.

K. A. Gardner (LMEC): (Comments not audible on tape.)

Randall: So the method does work, and if the gas entrainment could have been held down by a couple of orders of magnitude, we would probably have been able to obtain as clean a response in the amplitude at the high-frequency range as we were on the wall vibrations, only with much better resolution.

Lohmeier: I also would like to add that it's possible that this is not completely a fatigue protective device. One might not have impacting and large amplitudes.

Randall: That's right.

D. R. Miller (GE-KAPL): I would expect the first impacting noise you would hear would occur when the tube is rattling between, or within, the clearance of the support plates; in this case, the first support plate nearest the sine wave bends. If the tubes were banging against each other, I should think the noise associated with rattling in the support plates would build up continuously; but then finally you would run into a situation in which tubes would be banging against each other. I should think the noise due to rattling in the support plates would be discernible at amplitudes far less than those sufficient to cause tubes to bang against each other. Then, I would think that the first problem, just as important as the fatigue problem, is the problem of where the tubes vibrate in the support system. I find it difficult to visualize the torsional vibration that we presume is torsional and bending combined in these sine wave bends.

Gardner: (Comments not audible on tape.)

Miller: I see. Well, it's combined bending and torsion.

Randall: But you're right. What we're really afraid of is the damage of impacting.

Miller: I wondered how you arrived at a correlation between deflection and noise, that is, between stress and the signals you got on the exterior of the heat exchanger. It sounds like a very good trick to arrive at such a correlation without benefit of a direct measurement of tube motion. I'm glad I didn't have the problem of converting the signals to stresses.

Randall: It's virtually impossible from the outside.

Miller: But this technique very clearly does have value. I can cite two instances: In one instance, I diagnosed the noise problem very easily from the outside. We passed the boiler plate of the boiler; it was rattling badly. That was easy. Another interesting situation I observed was during a tour at the Naval Boiler and Turbine Laboratory. (I was there in regard to condenser tube vibration.) In making the tour, I passed near a condenser and that thing was banging like blazes. I could hear the tubes vibrating very severely, from just the distance of 10 or 20 feet or so. Of course, if I put my ear against the shell, I could hear it much more plainly. So I wonder why I heard nothing said about listening to these tones also.

Randall: The instrumentation required involves a screwdriver about this long that you put against the pipe, and you put your thumb against that and against your ear, and you listen and you can hear the impacting. You can hear the impacting and the gas entrainment sounds. Try it on some sodium loops around. You may be kind of discouraged at your gas entrainment problems, bubbles moving through the system, and so on.

D. D. Reiff (USAEC): I have two comments with regard to the previous comments. First of all, ideally it would have been preferable to have something akin to a signature analysis of a unit before it's operating, and then compare that with some of the work which would be the same as the presentation of Mr. Randall. But, since the problem sort of caught us unawares after series of failures in other heat exchangers, we started examining every single heat exchanger in the AEC operated facilities, and this one in particular looked like potentially it could be a problem. I say potentially because of the complex geometries associated with the flow and the tubes. We were concerned of a failure and went backwards. Instead, we wanted to know if we are chasing a ghost; should we ignore the problem, or are we in fact in bad trouble? If we were definitely in trouble, we would have probably opened up the unit and done something in addition to what has already been done. But as a first step to find out if there is anything that could give us trouble, we were going to try to avoid it. The results of these tests told us that while we're not absolutely sure that there is a problem which would lead to a destruction of the unit, we certainly would feel a lot safer operating away from the velocities that gave coherence in excess of 0.2. The other point of consideration is if the gas entrainment in the IHX has been a problem both from the standpoint of heat transfer and with respect to reading out the response to the accelerometers. I wonder if any consideration has been given to the opportunity to perhaps reverse the flow in that IHX, then see if you can correlate the direction of flow with gas entrainment and thereby further confirm the results you have in Fig. 20 of your paper.

Randall: That was repeatable. We did it test after test.

Reiff: I'm referring to reversal of flow in the IHX.

Randall: Right, but I mean that particular function of this nonsymmetry was repeatable. No matter how fast we went up or hit those particular flow conditions, we had those peaks.

Reiff: The fact you don't have the gas-entrainment response shown on the downtrend of flow, is that an indication that it's beginning to accumulate somewhere?

Randall: That's what we felt.

Reiff: Well, if that's the case, and I don't know how you would do this right now, I haven't thought about it, but could you reverse the flow direction, have it upflow instead of downflow?

Randall: Well, we probably would have had a little bit better luck just doing a series of these and keeping it swept out.

AN ENGINEERING APPROACH TO TUBE FLOW-INDUCED VIBRATIONS

C. R. Gerlach and F. T. Dodge

Department of Mechanical Sciences
Southwest Research Institute
San Antonio, Texas

ABSTRACT

This paper presents a critical review of existing open literature for flow-induced vibrations, and points out to what extent this information may and may not be applied to heat exchangers for the cross-flow situation. Particular attention is given to the critique of available vortex force data, the form it is presently in, and the influence of tube vibration amplitude. Next, the paper presents a fresh approach to the heat exchanger tube problem, drawing heavily on experience gained in the study of flow-induced vibrations of other types of structures. This new approach will emphasize the design aspects of the problem, largely neglected to this point, and will aim at the development of a method for the prediction of critical area stress levels and vibration amplitudes of tubes in heat exchangers. This new approach is based on the use of an effective vortex force coefficient which conveniently eliminates the need for describing vortex force in terms of an amplitude and a phase angle relative to tube motion. Available data are used to show preliminary values of the effective vortex force coefficient which is argued to be a function of only the tube stiffness and size, system damping, and fluid velocity and density.

NOMENCLATURE

b	-	damping for lumped model in Fig. 8
C_e	-	effective vortex force coefficient
$\overline{C}_e$	-	reduced effective vortex force coefficient
C_L	-	vortex lift coefficient, see Eq. (3)
d	-	tube internal diameter
D	-	tube external diameter
E	-	tube elastic modulus
f	-	frequency
f_s	-	vortex shedding frequency
f_{tn}	-	tube lateral mode nth vibration frequency
F_L	-	vortex lift force
F_o	-	vortex force for lumped model in Fig. 8
k	-	spring rate for lumped model in Fig. 8
ℓ	-	tube length
ℓ_c	-	correlation length for vortex shedding
m	-	equivalent mass for lumped model in Fig. 8
P	-	a parameter defined in Eq. (16)
Q	-	dynamic amplification factor
R_e	-	Reynolds number
S	-	Strouhal number
t	-	time
V	-	fluid velocity
V_o	-	fluid velocity for tube maximum vibration amplitude condition
x	-	displacement
x_o	-	tube vibration amplitude
ζ	-	damping ratio, see Eq. (14)
θ	-	phase angle of vortex force relative to tube motion
ν	-	fluid kinematic viscosity
ρ	-	fluid mass density

INTRODUCTION

Flow-induced vibrations of tubes in heat exchangers have been a problem for many years. A recent survey by Nelms and Segaser[1] presents brief case histories on failures in several installations, and these results dramatically emphasize the magnitude of this problem area. In very blunt terms, these failures must be attributed to inadequate heat exchanger design practices which do not always preclude the possibility of flow-induced vibrations in new heat exchanger configurations. The designer is not totally at fault, however, since available technical literature dealing with tube vibrations falls far short of giving the information really needed, and, in some cases, the available data are misleading.

The present paper deals only with the cross-flow problem and has been written with the designer in mind. The objectives of the paper are essentially twofold: first, to critically review the existing open literature of flow-induced vibrations and point out inadequacies and problem areas from an engineering or design point of view; second, to present or suggest a new approach which might be taken, with the end result leading to a reliable design procedure for heat exchangers. This new approach is based on work by one of the writers, and his colleagues[2, 3], to study and define flow-induced vibrations of metal bellows, which has been a critical problem area for liquid-fueled launch vehicles. The basic phenomena of flow excitation of bellows is identical with that of heat exchanger tubes. The work on bellows has now progressed to the point where reliable predictions of vibration amplitudes and stress levels can be made. We are convinced that the same type of approach will work equally well for heat exchanger problems.

BACKGROUND INFORMATION AND TYPICAL TEST RESULTS

To provide a firm foundation for subsequent discussions of heat exchanger tube vibrations, it is desirable at this point to look carefully at the physical picture of vortex excitation of an elastic (or elastically restrained) cylinder. Consider, therefore, a tube which is contained within a tube bank and which passes through two support plates, as shown in Fig. 1. The manner in which the tube is supported is important to the overall result; however, for the present, it will be assumed that the tube is rigidly clamped at each plate. The tube may be characterized by a length ℓ, outside diameter D, inside diameter d, and elastic modulus E. Clamped as described, the tube lateral vibration resonant frequencies will be

$$f_{tn} = C_n \sqrt{\frac{g\,EI}{w\ell^4}}\,, \quad C_n = 3.58,\ 9.82,\ 19.2\ldots \tag{1}$$

Next, it is assumed that a fluid of density ρ is flowing perpendicular to the tube axis with uniform velocity V, and at a Reynolds number $R_e = VD/\nu$. This flow situation results in periodic shedding of vortices from the cylinder, and, when no significant tube vibration occurs, the fluid velocity and vortex shedding frequency f_s may be correlated with

$$\frac{f_s D}{V} = S \tag{2}$$

where S is a dimensionless Strouhal number (see Ref. 4, for example).

The vortex shedding process may also be characterized by a correlation length ℓ_c which is defined as a length of the cylinder over which the vortex shedding process is coherent or consistent[5]. Over lengths of the cylinder greater than ℓ_c, the vortex shedding, therefore, is not totally uniform or consistent, which means that the same vortex behavior is not present over spans greater than ℓ_c.

Next, consider the vibrational response of the tube to the flow excitation as the fluid velocity is varied. Figures 2 and 3 show actual data taken from a rigidly clamped cantilever tube. These data provide a good qualitative picture, for the present discussion purposes at least, of what the response of the tube in Fig. 1 would be like. As illustrated in Fig. 2, at very low fluid velocities, no significant tube response occurs. This is because the ideal vortex shedding frequency f_s is considerably below the first tube modal frequency; thus, no coincidence (or near coincidence) of the ideal vortex frequency and the structural frequency occurs. Therefore, no resonant condition exists, and the tube response is consequently of a very low level. An analysis of the spectral content of the tube response in this low velocity range shows energy predominantly at two frequencies; one is the vortex shedding frequency f_s, and the other is the tube lowest modal frequency. The response amplitudes at these frequencies are quite random in nature.

As the fluid velocity is further increased, the tube begins to vibrate in a resonant condition which results from a coupling of the tube and vortex dynamic phenomena so that the two are "working together" to feed energy from the fluid stream. Hence, we have an instability of a fluid-structural dynamic system. As may be seen from Fig. 2, the resonant coupling of the tube and vortex shedding actually occurs over a considerable fluid velocity range, called the "lock-in range." The peak tube response in the lock-in range occurs when the frequency is equal to the fluid-structural resonant frequency. This lock-in range is of great importance since its existence means that destructive vibrations are possible over a rather broad velocity range, as opposed to a narrow range of resonance for conventional structural vibration problems.

From Fig. 3 it may be seen that the Strouhal number at the start of the lock-in range is about equal to the classically reported value of 0.20 to 0.22. Over the remainder of the lock-in range, however, the Strouhal number generally decreases considerably to a minimum value of about 0.14, with the value at the peak response point being about 0.17. The reason for this decreasing Strouhal number over the lock-in range is a result of the vortex shedding frequency adjusting progressively downward from the ideal value given in Eq. 2, to "accommodate" the stiffer tube dynamic system. Apparently, the phase angle of the vortex shedding

dynamic system is changing over this lock-in range, but, so long as the phase angle does not change too much, the vortex shedding can still feed energy from the fluid stream to the tube, and the vibration is sustained.

It is interesting to note in Fig. 3 the apparent discontinuity in system frequency, and Strouhal number, at a velocity of about 6.6 fps. The reason for this phenomenon is not presently known; however, it is likely caused by a condition of rapidly changing vortex shedding phase angle through this region. This same phenomenon has been noted in other flow-excited tube vibration data.

In summary, the physical explanation for the lock-in phenomenon follows largely from the fact that it is possible for the shedding vortices to feed energy to the vibrating tube at frequencies other than the ideal shedding frequency $f_s = SV/D$. In fact, the Strouhal number corresponding to optimum energy transfer appears to be about 0.17, or considerably below the Strouhal number for vortex shedding from stationary cylinders. The velocity range over which lock-in is possible extends roughly 40 percent either side of the peak response velocity.

A final important observation is to note what happens to the tube flow-induced response as the tube structural damping is increased, other factors remaining the same. Typical results are indicated qualitatively in Fig. 4; it is readily seen that increased damping reduces the vibrational amplitude, as might be expected, but it also can reduce the extent of the lock-in range. If damping is increased sufficiently, the lock-in type response disappears, and the excitation is of very low amplitude and very random in nature.

CRITIQUE OF CURRENTLY AVAILABLE INFORMATION

Suppose a heat exchanger designer, with some experience in fluid mechanics, is faced with the task of analyzing the flow-induced vibrations of a heat exchanger tube-bank such as that shown in Fig. 1. The designer knows that the liquid flowing across the tubes may cause destructive vibrations of the type described in the previous section. Since during normal operation the liquid velocity varies over some range from V_{min} to V_{max}, the designer suspects that tube vibration and vortex shedding might couple over some velocity range in this operating range. Consequently, the designer wants to (1) determine the range of vortex shedding frequencies that might occur; (2) determine the modes of tube vibration that can be excited in this frequency range; (3) calculate the oscillating forces exerted on the tubes, and thereby predict the stresses for each of the anticipated modes of vibration; and (4) take corrective measures as indicated.

In studying the literature, the designer finds a lengthy list of references that deal with the shedding frequency of vortices as a function of flow conditions and geometry. He finds that the ideal vortex shedding frequency f_s can be calculated from the Strouhal number $S = f_s D/V$ for each geometry, say by Chen's correlations[4]. A little further reading, however, turns up the fact that these correlations are only valid for stationary tubes (as shown also in the previous section). When the tubes vibrate, the vortex shedding process and the tube dynamics couple to give a nonlinear dynamic system as discussed earlier. The result is that the shedding frequency has a lock-in range which can extend the velocity range for excitation by as much as $\pm$ 40 percent around the peak response point. There is serious question, therefore, as to the relationship between the Strouhal number at the peak response point for vibrating tubes and the vortex shedding Strouhal number for stationary tubes. Furthermore, there are frequency components in the vortex wake other than the Strouhal frequency f_s ; for example, the shedding vortices also cause a drag force on the tubes at a frequency equal to 2 f_s , although this drag force is usually about an order of magnitude less than the lift force associated with the Strouhal frequency f_s.

Considering all of this, the designer proceeds to calculate the natural frequencies of the first few modes of vibration of the tubes, using standard strength of material equations, and allowing for the "added mass" of the liquid.

Next, he likely will use the existing Strouhal correlations to calculate the velocity at which peak excitation should occur (although this value may be in error as noted previously). To account for lock-in, he will next probably include a range of $\pm$ 40 percent around the calculated peak excitation velocity to get the critical velocity range for each tube vibration mode. Finally, the designer may anticipate the possibility of double frequency excitation to arrive at a complete picture of the predicted velocity ranges for flow excitation of the heat exchanger tubes.

The designer wishes now to determine the flow-induced forces acting on the tubes so that he can estimate the amplitude of the vibration for each critical velocity range. He finds there are many experimental determinations of a lift-force coefficient C_L (for a stationary tube); it is defined as

$$C_L = \frac{F_L}{(1/2\ \rho V^2)\ (\ell D)} \tag{3}$$

where F_L is the amplitude of the oscillatory lift force, ρ is the fluid density, V the velocity, and ℓ and D the tube length and diameter.

However, in studying the data, it is apparent that few of the C_L correlations compare very well with each other. Part of the reason for this is that C_L depends on the "correlation length," which was discussed earlier. If the tube is longer than the correlation length, not all the shed vortices cause forces in phase with each other, and a reduction in both the net oscillating lift force and C_L occurs. For stationary cylinders, it seems that the correlation length depends primarily on the Reynolds number R_e ; for the $40 < R_e < 150$, the correlation length is about 15D to 20D; for $150 < R_e < 10^5$, the correlation length is reduced drastically and is roughly constant at about 2D to 3D; for $R_e > 10^5$, the correlation length is reduced again to about 0.5D. But, the photographs of Koopmann[6] definitely show that the correlation length for a vibrating tube increases, at least at low Reynolds numbers. Further, for oscillating tubes, the literature shows that the lift force per unit length for long cylinders is less than for short cylinders when the oscillation amplitude is small; but, as the amplitude is increased, the lift-force/length for a long cylinder increases more rapidly than does the force/length for a short cylinder until, at some amplitude, the force/length for both cases is about the same. These observations, as indicated in the literature, show that the tube vibration must organize the vortex shedding process since this organization would be more apparent on long tubes, for which there are originally many regions of out-of-phase vortex shedding, than for a short tube.

In addition to the correlation length difficulties, the designer finds that the reported C_L correlations are based on many kinds of lift force measurements, for example, peak force over some period of time, or average force over some period, or root-mean-square force. Figure 5 shows a plot of most of the C_L data available for stationary cylinders; as can be seen, the scatter of the data is fairly large. But, by replotting in terms of rms data only (some of which must be estimated), better agreement is obtained, as shown in Fig. 6. The remaining discrepancies are due primarily to differences in the correlation lengths ℓ_c.

Even with these improved correlations, however, the designer is still not ready to make any stress computations. He discovers in his literature search that the C_L values for <u>stationary cylinders</u> do not necessarily apply to <u>vibrating cylinders</u>. For the stationary case, the lift force on a tube is simply

$$F_L = C_L \, (1/2 \; \rho V^2) \; (\ell D) \sin (2\pi \; f_s t) \qquad (4)$$

where C_L, as shown previously in Fig. 6, is a real number that depends on ℓ/D and R_e. Because of the feedback and coupling between the cylinder motion and the vortex shedding, the fluid-induced force on a vibrating cylinder is more complicated and must be written in the form

$$F_L = C_L (1/2 \rho V^2) (\ell D) \sin (2\pi ft + \theta) \tag{5}$$

where f is the frequency of the cylinder motion. C_L is now a function not only of ℓ/D and R_e but also of the ratios of the cylinder vibration amplitude to the tube diameter x_o/D and the vibration frequency to the Strouhal frequency f/f_s; thus,

$$C_L = C_L (R_e, \ell/D, x_o/D, f/f_s) \tag{6}$$

The phase angle θ of the fluid force relative to the cylinder motion is also a function of these parameters, so

$$\theta = \theta (R_e, \ell/D, x_o/D, f/f_s) \tag{7}$$

Figure 7 shows typical correlations of C_L and θ with f/f_s and x_o/D. It is clear from the drastic changes in C_L and θ for small changes in f/f_s and x_o/D that the dynamics of vortex shedding is quite sensitive to the tube motion.

The designer is still somewhat dubious about these plots since they were obtained under forced oscillation conditions, although he is interested in self-excited conditions. At any rate, he decides to make some stress calculations. He has already determined the modes of vibration of interest; for the purposes of discussion, consider that these modes are the two shown in Fig. 8. But now he discovers that no procedure is presently available to allow him to predict the nonuniform distribution of vortex force on a tube vibrating in an arbitrary bending mode; all of the compiled data are for a tube vibrating as a rigid body normal to its axis. However, the designer is willing to idealize his problem and assume a constant vortex force distribution over the tube; then, the problem actually is resolved into the investigation of the lumped mass model shown in Fig. 8c. The equations of motion for this model are

$$m\ddot{x} + b\dot{x} + kx = F_o \sin (2\pi ft + \theta) \tag{8}$$

with

$$x = x_o \sin (2\pi \ ft) \tag{9}$$

Substituting Eq. (9) into Eq. (8) results in two simultaneous equations to determine x_o and f:

$$(k - 4\pi^2 mf^2) x_o = F_o \cos \theta \tag{10}$$

$$2\pi \ bfx_o = F_o \sin \theta \tag{11}$$

Since both F_o (i.e., C_L) and θ depend on x_o and f, it is readily seen that tremendously large errors in x_o can result unless C_L and θ are very accurately known. Furthermore, an accurate determination of the system damping, b, is required.

Finally, reviewing his entire analysis, the designer is forced to conclude that the available force data are not accurate enough in their present form to allow a satisfactory vibration amplitude prediction. Consequently, he must resort to testing to determine if his proposed design will be adequate.

A NEW ENGINEERING APPROACH TO TUBE FLOW-INDUCED VIBRATIONS

Based on the discussion in the previous sections, it must be admitted that the presently existing vortex force information is of questionable value for predicting tube vibration amplitudes, even on single, isolated tubes. Further, existing Strouhal number data are not completely valid for predicting the velocity at which peak excitation of tubes will occur. It is the opinion of the writers that a new approach to the problem is needed which will essentially bypass the difficulties of defining and using force amplitude, and phase, data of the type shown in Fig. 7. Such an approach is suggested below and will, it should be noted, also improve our knowledge of Strouhal numbers for vibrating tubes. This proposed method resulted from previous work performed by one of the writers on the problem of flow-induced vibrations of metal bellows which, like a tube with cross flow, can be excited to large amplitudes by vortices periodically shed from the convolute tips[2, 3]. Our justification, therefore, for suggesting this new approach, is the success which has resulted from application of the same approach to bellows.

Recall the hypothetical tube vibration problem discussed in the previous section. As illustrated in Fig. 8, the cylinder flow-induced motion will likely result in a nonuniform vortex force amplitude, and phase angle, distribution over the cylinder length. Assume, for the present, that by proper integration of this nonuniform force the tube can be replaced dynamically with the single-degree-of-freedom system shown in Fig. 8. The response of this model was previously described by Eqs. (8) and (9), and this led to Eqs. (10) and (11). Now, since it is desired to avoid exactly solving these expressions using data of the type given in Fig. 7, some approximations will be made to see what can be learned about the important parameters of the coupled fluid-elastic system. Experience gained in flow-induced vibration studies of bellows and metal tubes has shown that when peak resonance amplitude occurs the frequency is very close to the actual structural frequency ω_o (actually the coupled fluid-structural frequency). This implies that assuming the phase angle θ equal to 90 degrees should be approximately valid*. Therefore, Eqs. (10) and (11) reduce to

$$b \omega x_o \approx F_o \tag{12}$$

Replacing F_o by its equivalent force coefficient form and dividing both sides by k, the model spring rate, gives

$$\frac{b \omega x_o}{k} \approx \frac{(1/2 \ \rho V^2) D\ell}{k} C_L \tag{13}$$

where C_L is understood to be a function of x_o/D, f/f_s and R_e. Now, since the damping ratio is defined by

$$\zeta = \frac{b}{2\sqrt{km}} \tag{14}$$

---

*The accuracy of this assumption is, we believe, associated with the relative stiffness of the fluid and the elastic system. If the elastic system is quite stiff (short thick-walled metal tubes), then assuming $\theta \approx 90$ degrees is valid. If, on the other hand, the elastic system is not very stiff (say a long thin-walled plastic tube), then the assumption may break down. This remains to be proven or disproven.

and, the amplification factor $Q = 1/2\ \zeta$, then Eq. (13) may be rewritten in the form

$$\frac{x_o}{D} \approx \frac{(1/2\ \rho V^2)\ D\ \ell\ Q}{Dk}\ C_L = \frac{(1/2\ \rho V^2)\ \ell\ Q\ C_L}{k} \tag{15}$$

Values of x_o/D (and therefore C_L) which satisfy Eq. (15) will be a function of only the parameter

$$P = (1/2\ \rho V^2)\ (\frac{\ell\ Q}{k}) \tag{16}$$

This implies that the peak response amplitude is determined by a force coefficient value which is a function of the parameter P, of the Reynolds number R_e, and of the tube configuration and mode of vibration. This force coefficient, which we will call an effective force coefficient C_e, now determines the system peak response amplitude through the expression

$$\frac{x_o}{D} = (1/2\ \rho V^2)\ (\frac{\ell\ Q}{k})\ C_e = PC_e \tag{17}$$

By way of review, it has been shown that the flow-induced vibration of heat exchanger tubes can be reduced to an equivalent mass-spring-damper analog and that the vortex force at the peak response point can be treated with an effective vortex force coefficient. This effective force coefficient C_e is a function of the tube Reynolds number, the tube configuration (i.e., cantilever, fixed or simply supported ends, etc.), and of a dimensionless parameter P [given by Eq. (16)]. The parameter P is a quantity which includes flow variables, tube geometric and stiffness information, and the fluid-structural system dynamic amplification factor Q. If we can make available, through rather simple experiments, a tabulation of C_e values, then heat exchanger tube vibration amplitudes could be readily predicted if Q values were also known.

To illustrate the proposed approach, some preliminary C_e data have been generated for the rigidly mounted cantilever tube of Fig. 2. This was simply done using Eq. (17), and with experimentally determined values of Q and the tube stiffness k; the results are shown in Fig. 9. Note that C_e values have been calculated throughout the

lock-in range and not just at the peak response point as discussed earlier. Also, effective force coefficient values have been reduced from flow-induced vibration data for a tube rigidly supported at both ends. The results are shown in Fig. 10.

The C_e data shown in Figs. 9 and 10 are not necessarily in a convenient form for prediction purposes because the maximum response amplitude point does not correspond to the maximum C_e point. Therefore, an alternate form for presentation of effective vortex force coefficients has been developed and is shown in Fig. 11. Here, $\overline{C_e} = C_e(V/V_o)^2$ is shown as a function of V/V_o, where V_o represents the velocity for maximum response amplitude. Since $\overline{C_e}$ is directly proportional to the tube amplitude, the same constant of proportionality at all velocities, the maximum value of $\overline{C_e}$ corresponds to the maximum response amplitude. The response amplitude at any velocity V now becomes

$$\frac{x_o}{D} = (1/2\ \rho V_o^2)\left(\frac{\ell Q}{k}\right)\overline{C_e} \tag{18}$$

In general, $\overline{C_e}$ is of the functional form

$$\overline{C_e} = \overline{C_e}\,(V/V_o,\ R_e,\ P,\ \text{geometry}). \tag{19}$$

It is interesting to note in Fig. 11 the apparent amplification of the vortex force coefficient because of increased tube vibration amplitude. The lower curve, which was for the tube supported at both ends, showed an effective force coefficient at the maximum response point of $C_e = 0.15$ with the amplitude at the tube center equal to $x_o/D = 0.128$. For the cantilever tube, the C_e value at maximum response was 0.87 for $x_o/D = 1.32$. Based on these results, we see a probable amplification of effective force coefficient because of increased displacement.

It is important to note here that these values of C_e are significantly lower than the motion-amplified values reported by, for example, Bishop and Hassan[7] and Protos, Goldschmidt, and Toebes[14]. Figure 12 shows a composite plot of the estimated* RMS C_L values reported

---

*Estimation of the absolute C_L values, with motion amplification, was necessary because the data in Refs. 7 and 14 were given in terms of a ratio of C_L/C_{Lo}, where C_{Lo} was the lift coefficient with no motion.

in Refs. 7 and 14, and RMS C_e values corrected from the Fig. 11 data. We believe this difference is primarily because the peak C_L values reported in Refs. 7 and 14 for externally excited cylinders show largely an apparent amplification. A close examination of the data in Ref. 14 shows that at the excitation frequency corresponding to the peak C_L the energy fed from the fluid to the tube was actually negative. This means that the tube motion was indeed causing a large increase in the vortex force, but only when energy was fed from the external excitation mechanism to the fluid. From the data in Ref. 14, there appears to be little or no force amplification at the frequency corresponding to maximum energy transfer from the fluid.

Based on these observations, it must be concluded that we have much to learn about motion amplification of vortex forces on flow-excited cylinders.

CONCLUSIONS

It has been shown that existing tube vortex force coefficient data, obtained largely from rigid tube forced excitation experiments, are generally inadequate for accurately predicting heat exchanger tube vibration amplitudes. The primary reason is because the measured force amplitudes and phase angles are critical and complicated functions of tube amplitude and frequency. Large errors can be expected when using these type data for predicting flow excitation of elastic tubes. Further, existing Strouhal number data do not allow proper prediction of the velocity at which peak response amplitudes can be expected. Finally, the real effect of reported motion-induced amplification of vortex forces is subject to question for flow-excited tubes.

The effective vortex force coefficient approach presented herein offers the possibility of bypassing the force data problem denoted above. By using effective force coefficient data, which can be easily and accurately obtained from rather simple experiments, tube vibration amplitudes could be reliably predicted from known tube operational data and from a knowledge of the system amplification factor Q.

REFERENCES

1. Nelms, H. A. and Segaser, C. L., "Survey of Nuclear Reactor System Primary Circuit Heat Exchangers," Report ORNL-4399, Oak Ridge National Laboratory, April 1969.

2. Gerlach, C. R., "Flow-Induced Vibrations of Metal Bellows," Journal of Engineering for Industry, Trans. ASME, 91, pp. 1196-1201, November 1969.

3. Gerlach, C. R. and Schroeder, E. C., "Study of Minimum Pressure Loss in High Velocity Duct Systems," Interim Technical Report No. 1, Contract No. NAS8-21133, Southwest Research Institute, July 1969.

4. Chen, Y. N., "Flow-Induced Vibrations and Noise in Tube-Bank Heat Exchangers Due to Von Karman Streets," ASME Preprint 67-VIBR-48, ASME Vibrations Conference, Boston, Massachusetts, March 1967.

5. Graham, C., "A Survey of Correlation Length Measurements of the Vortex Shedding Process Behind a Circular Cylinder," Report 76028-1, Contract Nonr 3963(25), Engineering Products Laboratory, MIT, October 1966.

6. Koopman, G. H., "The Vortex Wakes of Vibrating Cylinders at Low Reynolds Numbers," Journal of Fluid Mechanics, 28, Part 2, pp. 501-512, 1967.

7. Bishop, R. E. D. and Hassan, A. Y., "The Lift and Drag Forces on a Circular Cylinder in a Flowing Fluid," Proceedings of the Royal Society (London), 277A, pp. 32-50, 1964.

8. Humphreys, J. S., "On a Circular Cylinder in a Steady Wind at Transition Reynolds Numbers," Journal of Fluid Mechanics, 9, pp. 603-613, 1960.

9. Goldman, R. L., "Karman Vortex Forces on the Vanguard Rocket," Shock and Vibration Bulletin, Part II, pp. 171-179, 1958.

10. Fung, Y. C., "Fluctuating Lift and Drag Acting on a Cylinder in a Flow at Supercritical Reynolds Numbers," Journal of the Aerospace Sciences, 27, pp. 801-814, November 1960.

11. Macovsky, M. S., "Vortex-Induced Vibration Studies," David Taylor Model Basin Report 1190, July 1958.

12. Keefe, R. T., "An Investigation of the Fluctuating Forces Acting on a Stationary Circular Cylinder in a Subsonic Stream and of the Associated Sound Field," University of Toronto, UTIA Report 76, 1961.

13. Schmidt, L. V., "Measurements of Fluctuating Air Loads on a Circular Cylinder," AIAA Journal of Aircraft, 2, pp. 49-55, January 1965.

14. Protos, A., Goldschmidt, V. W., and Toebes, G. H., "Hydroelastic Forces on Bluff Cylinders," ASME Preprint 68-FE-12, ASME Fluids Engineering Conference, Philadelphia, Pa., May 1968.

DISCUSSION

D. A. Wesley (Gulf General Atomic): I have a couple of questions. The first one concerns your normalizing displacement, x_o. It seems that this has to be a function of the mode shape.

Gerlach: Yes, it definitely is. I was apparently going too quickly. I meant to say that for a given mode of vibration and a given set of end conditions, we can roughly model it in this manner. So, really you need to get this kind of data for different mode shapes and different end conditions.

Wesley: The next thing I have, if you look at the amplification factor Q, for any structural materials, it will also be a function of this normalized displacement?

Gerlach: Yes.

Wesley: So it seems like we should do exactly the same thing with that.

Gerlach: Okay. Let me show you what we've done in the case of the bellows, and this worked real well. When we're getting the Q-value data, we go ahead and get it for different amplitudes, and like you say it varies. So actually what we've come up with in that case is a plot of the parameter P/Q. In other words, take Q out of P, so that it's only $\frac{1}{2}\rho V^2$ times L over K; it's a function of the geometry and the fluid properties excluding Q. Now, it turns out then that x_o/d is a function of this thing right here, but you can actually reduce the data out so that you can put Q in this form. Okay?

P. M. Moretti (Westinghouse): You showed this locked-in band and showed a couple of data points. Did you find that there was any difference depending on whether you were running the flow up or running the flow down?

Gerlach: If you have a system which gives relatively small vibration amplitudes when it's locked in, then you have the hysteresis effect. If, however, you have a system which exhibits very large amplitudes at resonance, then we have not really been able to find any hysteresis effect. In other words, let's say this is the vibration amplitude, and let's say this is velocity. Now let's take the case of the rather highly damped system where we have something like this. Now if we were sweeping up very slowly, then we see, more or less, a jump phenomenon here. Sweeping down, we see the jump phenomenon here, and so on. But if you have a very vigorously

vibrating system, one lightly damped, then we have not been able to see much hysteresis effect. In other words, if you go up to this point and wait a while, it will get there. You don't see much hysteresis, if any.

Moretti: I've seen some data which showed quite a bit of hysteresis effect, and the difference in Q I think would explain a lot of that. I think how much background noise you have would be important too, because you have basically a bistable situation. Whether you get across your "continental divide," so to speak, to the other stable situation, which is the large-amplitude vibration, would be a function of the amount of random disturbance you have. It seemed like theoretically, from just the basic mathematics of bistable systems, you have to have a jump phenomenon and I've seen it in quite a few data, although usually it was very much stronger, more strongly visible running up than running down.

Gerlach: I would agree with this. And maybe part of the explanation for that is, as I recall, most of these curves (based on the bellows, anyway) are rather skewed over like this. In other words, they have a steep trailing edge over here and not so much over here.

Moretti: That would be explained by the fact that at the lower velocities you have a lower energy involved.

Gerlach: Right. And a lower turbulence level and less likelihood of external disturbances.

D. R. Miller (GE-KAPL): I would just like to ask whether you are familiar with a paper by, well, I think it's a translation of a paper, by Meier-Windhorst. [Editor's Note: Meier-Windhorst, A., Flutter Vibrations of Cylinders in a Uniform Flow (Flatterschwingungen Von Zylinder in Gleichmässigen Flüssigkeitsstrom), David Taylor Model Basin Translation 333; München Technische Hochschule Hydraulishe Inst. Mitt., Volume 9, 1933; pp. 1-29.] It's available in the AE series. I presume others here have seen it. He made a very extensive study of the response of a single cylinder to crossflow. He studied the effects of variations in damping, in cylinder-to-fluid mass-density ratio, and things of that sort. He found a very pronounced difference between the characteristic, or the response, due to increasing flow and decreasing flow. That's the best paper I've seen. I believe there was a recent ASME paper, a very good paper, on crossflow, too, but I don't remember the author. But the paper by Meier-Windhorst is the best paper I had seen, at least until very recently.

G. H. Toebes (Purdue U.): Your data again showed the maximum responses obtained at values of the ratio of Strouhal frequency over structural frequency less than 1. Quite a number of explanations have been advanced for this. I may wish to add another one. Two years ago I made an extensive study of the flow field around an oscillated cylinder, a forced oscillation cylinder of 6-inch diameter. A flow field was measured with as many as eight simultaneous hot wires, and many of these wires were mounted with the cylinders so they did vibrate with it. Only a fraction of the data were published, and even from those data I think you can see that at resonance the wake narrows and, due to the narrowing, its frequency goes up. As a consequence, you will have a lesser ratio.

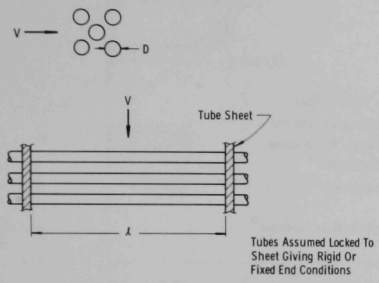

Fig. 1. Illustration of Typical Tube Installation

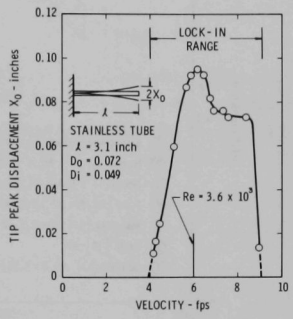

Fig. 2. Flow-induced Response of Cantilever Tube in Water

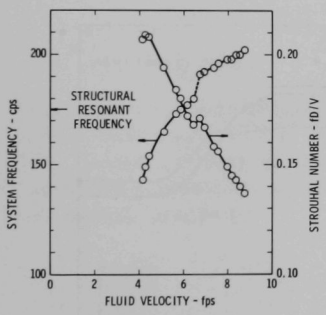

Fig. 3. System Frequency and Strouhal Number Data for the Cantilever Tube of Fig. 2

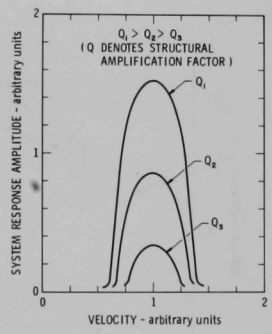

Fig. 4. Qualitative Effect of Increased Structural Damping on Tube Flow-induced Vibrations

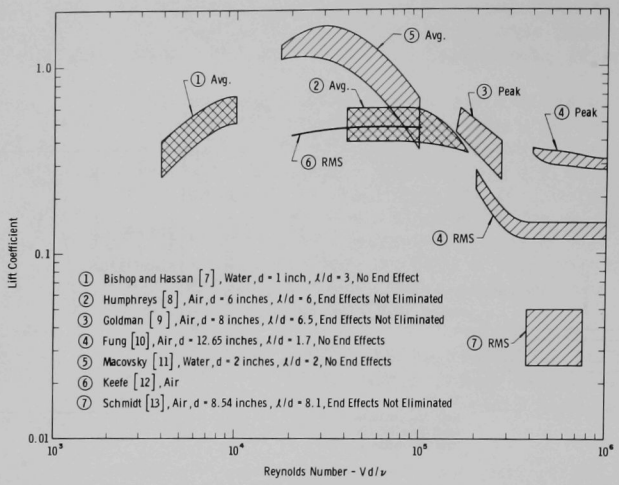

Fig. 5. Compilation of Available Vortex Force Coefficients for Stationary Cylinders

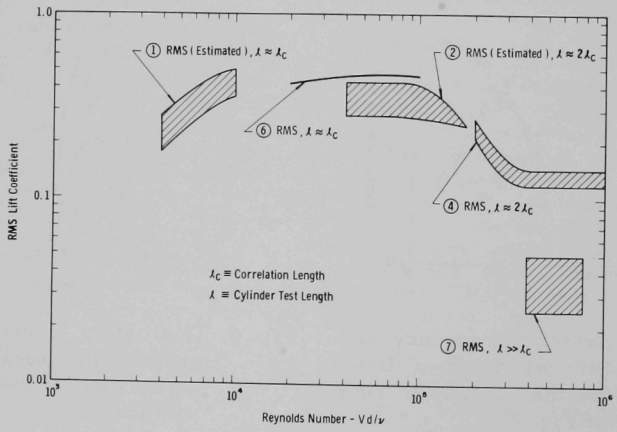

Fig. 6. Compilation of RMS Lift Coefficients. (See Fig. 5 for Legend.)

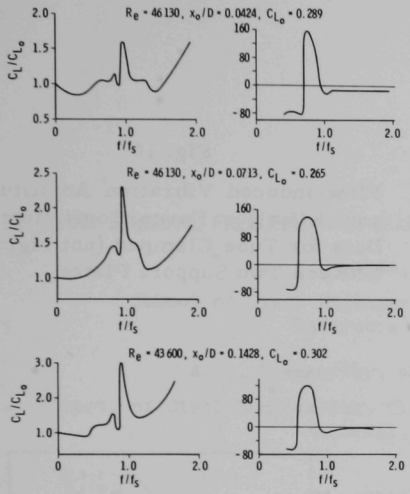

Fig. 7

Example of Available Experimental Force Coefficient Amplitude and Phase Angle Data for Oscillating Circular Cylinders - Taken from Ref. (1)

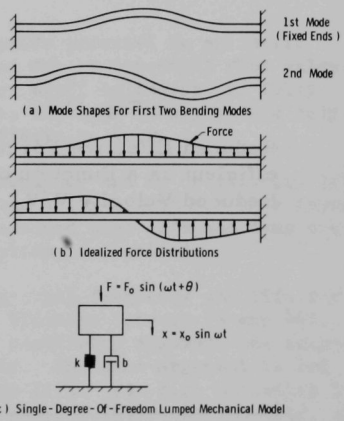

Fig. 8

Illustration of Mode Shapes and Force Distribution for First Two Modes of Heat Exchange Tubes, Also Idealized Mechanical Model

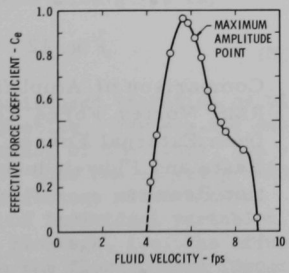

Fig. 9

Effective Force Coefficient Data for Rigidly Mounted Cantilever Tube. (See Fig. 2.)

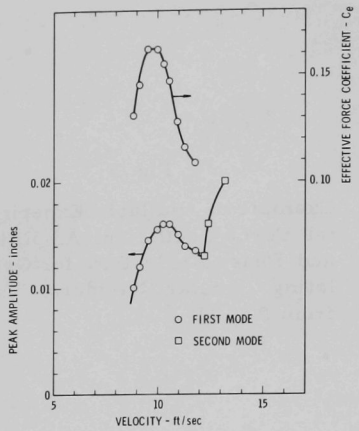

Fig. 10

Flow-induced Vibration Amplitude and Effective Force Coefficient Data for Tube Clamped (not rigidly) between Two Support Plates

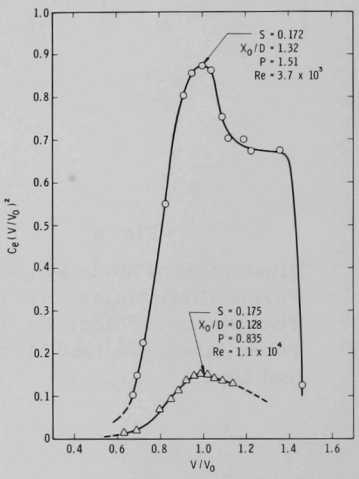

Fig. 11

Reduced Effective Force Coefficient as a Function of the Reduced Velocity V/V_0

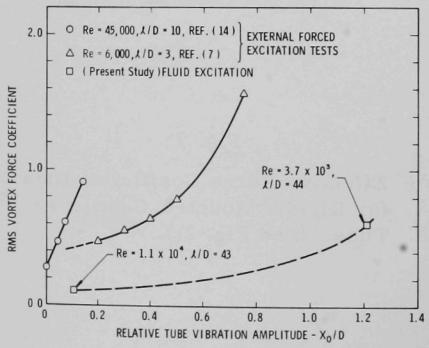

Fig. 12

Comparison of Amplification of RMS Vortex Force Coefficients from External Forced Excitation Tests and Flow-induced Excitation Results

LIFT AND STROUHAL FREQUENCY FOR BLUFF SHAPES IN CONSTRICTED PASSAGES

G. H. Toebes, Professor

School of Civil Engineering, Purdue University,
Lafayette, Indiana

A. S. Ramamurthy, Assistant Professor

Dept. of Civil Engineering, Sir George Williams University
Montreal, Canada

ABSTRACT

Flow constraint effects due to boundaries parallel to prismatic bodies, called "blockage", can be accounted for by potential flow calculations if the prisms are streamlined. For bluff cylinders, no fully theoretical solution is possible. To date, blockage theory exists only for blockages below 6% and only for the effects on drag.

The effect of blockage on Strouhal frequency and on oscillatory lift, which are of primary concern in fluidelastic design, have not been investigated systematically. It is generally assumed that lift and drag are proportional. The validity of this assumption is examined.

This note presents initial data on Strouhal frequency and lift for circular and triangular cylinders and for blockage between 7% and 44%. It is found that, in that range, a simple continuity argument can account for blockage effects on the Strouhal number. The same argument is not satisfactory for correcting the oscillatory lift. For high blockages the oscillatory lift for steady cylinders decreases relative to the drag. The tendency towards self-excitation, however, may well increase when vortex-induced vibration gives way to a single-degree-of-freedom flutter.

INTRODUCTION

Flow-induced vibration of bluff shapes in cross-flow is a multi-faceted problem. Few are the experimental arrangements that permit adequate ranging of the fluid, the structural and the statistical parameters involved. None has as yet provided workers in this area with truly comprehensive reference measurements. In fact, there are still occasions where the role of individual variables requires a first delineation. One of these is blockage, i.e. the effect of the proximity of other solid boundaries on the flow-induced forces exerted on a given test geometry.

Too long blockage has been ignored when it comes to fluidelastic studies. Without considering it, the work by different investigators is not properly comparable. What is more, its understanding offers the possibility to alleviate the unusual number of experimental constraints and to do better in research planning.

Blocking is a well-known worry in wind tunnel work where it received attention from many gifted workers. They devised complicated correction formulae. These corrections, however, are mainly for streamlined shapes where potential flow models are applicable. Test section wall constraints are then handled by computing velocities induced by infinite series of images of the shape's singularity presentation.

For bluff cylinders flow separation precludes an entirely theoretical solution. Yet two potential flow models have dominated the treatment of bluff body flows. These are the von Karman vortex street model and the even older free streamline models.

EXISTING MODELS

The characteristics of the title problem may be set forth by a simple review of models for bluff body flows with and without consideration of flow constraint effects.

a. Classical Hodographs - The classical hodograph models originated with Helmholtz (1868) and Kirchhoff (1869). Referring to Figure 1 they conceived of an outer potential flow separated from a relatively quiescent wake by vortex sheets of strength $\Gamma(s)$, where $s = 0 \equiv$ separation point. Across a vortex sheet the pressure was continuous but the tangential velocity discontinuous.

Neglecting all instability or dissipation questions, the strength of the sheets was assumed constant. Consequently, the velocity difference across the sheet was constant

$$d\Gamma/ds = U_s - U_w = \text{constant} \tag{1}$$

Infinitely far downstream, the free streamlines become parallel. Hence for $s \to \infty$ one has $U_s \to U_1$ (where U_1 is the undisturbed approach velocity) and the wake pressure $p_w \to p_1$ = the ambient pressure in the approach flow).

Since the wake is assumed quiescent, $U_w = 0$ and $p_w = p_1$ throughout, which implies

$$p(s) = p_b = p_w = p_1 \tag{2}$$

Herein $p(s)$ = pressure along the sheet and the base pressure $p_b = p(0)$ = pressure at the separation point(s) and hence the pressure at all points of the body contour beyond the separation points. Clearly the pressure p_b is the most important parameter in regard to the magnitude of the cylinder's drag force, F_D.

In the outer flow the Bernoulli sum is constant

$$E_1 = \frac{1}{2}\rho U_1^2 + p_1 = \frac{1}{2}\rho U_b^2 + p_b \tag{3}$$

From Eq.'s 2 & 3 it thus follows that

$$U_b = U_1 \tag{4}$$

Now the magnitude of the tangential velocity U_b along the free streamline is an important determinant of the wake shape. It also is related directly to p_b and hence the drag F_D. Thus wake shape and drag can be related when discussing blockage effects.

b. Modified Hodographs - The assumption of constant pressure throughout the wake region led to having constant velocity along the free streamline. This in turn made possible the hodograph mapping which transforms free streamlines into circular arcs which facilitated their analysis.

Unfortunately the above method underestimates F_D by no less than 100%. The reason is that the free shear layers are unstable and deform dragging fluid downstream. Interacting with each other, periodic deflection towards and even crossing of the wake centerline occurs. Thus a substantial mean pressure difference is required to replenish the fluid carried downstream from near the body base. This difference is

$$\Delta p_b = p_w - p_b \tag{5}$$

where the pressure p_w is found say 4-8 L downstream of the cylinder. Here L is the largest cylinder dimension perpendicular to both the flow and the cylinder axis.

Several investigators have proposed "notched hodograph" models wherein

$$U_b = kU_1 \tag{6}$$

so that

$$p_b = p_1 - \frac{1}{2}\rho(k^2 - 1)U_1^2 \tag{7}$$

or

$$(p_b - p_1)/\frac{1}{2}\rho U_1^2 = -(k^2 - 1) \tag{8}$$

In these models, U_b remains constant until the wake reaches its maximum width W. Beyond this U_b decreases gradually to U_1.

In reality U_b starts decreasing along the (mean) vortex sheet from the outset. Also the replenishment flow cannot be analyzed. The factor k must be deduced from measurement of either the drag, F_D, or the base pressure, p_b. The only exception is a model by Weinig (1957).

Roshko (1954) constructed, as part of a trial and error solution for a "universal Strouhal number", the relation between maximum wake width and

base pressure coefficient

$$W = W(L,k) \tag{9}$$

for several cylinder shapes. No relation between Eq. 9 and constraint effect was considered.

c. Modified Hodograph for Constrained Flow - Recently Shaw (1969) worked out the case of the hodograph modified according to Eq. 6 for the case of a normal flat plate in a channel. Shaw's discussion, however, centered on very high blockages (defined as L/B where B = channel width) from say 50% to 90%. In this range a well-defined dependence of k on L/B was found resulting from the well-known fact that the contraction coefficient for flow under a gate becomes independent of the free surface boundary condition if that free surface is far removed (in terms of the gate opening dimension).

Shaw's analysis was based on the available potential flow solution of a gate set normal to the flow and protruding from one of the walls of a channel. In potential flow calculations, this is identical to one-half of the case of a flat plate centered in the channel (see Figure 2). Unfortunately, in seeking experimental confirmation of his analysis, Shaw did test gates in the water tunnel section forgetting that physically the configuration is not identical to one-half of the "plate centered in the channel" case. For the gate one will find an eddy in the upstream corner due to the boundary layer growth along the wall from which the gate protrudes. Such an eddy is, of course, absent near the stagnation point of a normal plate. Thus for the plate, U_b makes a larger angle with the mean flow than for the gate. This effect is important exactly in the blockage range of interest here, namely $L/B < 0.5$.

Shaw, noticing descrepancies for low L/B values, was able to perform but one test with a flat plate. On the basis of this and the theoretically known value of $k = 1.46$ (in Eq. 6) for a flat plate when $L/B \to 0$, he drew a curve (his Figures 10 and 11) showing $k = k(L/B)$. Shaw's one measurement with a plate permits one to obtain the relation

$$k = 1.45(1 - L/B)^{-1} \tag{10}$$

It is finally possible to deduce from Shaw's work (Figure 13-Shaw) that, giving regard to Eq. 10, the drag coefficient in the range $0.15 < L/B < 0.45$ can be represented by

$$C_D \simeq - 0.3 + 2.3(1 - L/B)^{-2} \tag{11}$$

d. Momentum Model - The potential flow models discussed above involved facets of the problem of bluff body drag influenced by flow field constraints. Within the framework of "mean-flow" models, the momentum approach is more comprehensive.

The momentum approach towards the indirect measurement of profile drag, evolved early in the context of wind tunnel measurements, seeks to relate the energy reduction in the flow behind streamlined bodies to the drag force (Betz, 1925). More specifically, it relates the drag force,

F_D, with experimentally determined mean longitudinal velocity and mean pressure profiles taken across the wake.

This procedure is not immediately applicable to the bluff body drag problem since in the wake of stalled profiles, the energy expended in the generation of vorticity does not appear as a drop in linear momentum. For this reason Maskell (1963), following Glauert (1933), applied the momentum relation to the flow outside of the mean wake structure. For any required notions concerning the wake he relied tacitly on elements of the free streamline models mentioned above.

Maskell's work may be reviewed briefly with aid of Figure 3, which shows a control volume bounded by: a. two sections 1 and 2 perpendicular to the mean flow; b. the constraining test section walls parallel to the mean flow; undetermined position of Section 2, a maximum mean wake width, W. The shape of the free shear layers is equally undetermined. It should be noted that Maskell's work implied a control volume defined only by the sections 1 and 2 and by the test section walls.

Neglecting test section wall shear stresses, the momentum thickness of its boundary layer, and the contributions of fluctuating components to the momentum integrals over section 2, one may write

$$p_1 B - F_D - p_2(B-W) - p_w W = \rho(B-W)U_2^{\,2} - \rho B U_1^{\,2} \tag{12}$$

This relation is based on the typical free streamline assumption that over the portion W of section 2 the velocity is zero. Also over the remainder of section 2 the velocity is taken to be uniform. The Eq. 12 differs from Maskell's Eq. 8 which incorporated the term $(-p_b W)$ rather than the term $(-p_w W)$ in accord with Eq. 5. This change was first suggested by Cowdry (1968).

Rearranging terms and using the continuity equation

$$U_2(B-W) = BU_1 \tag{13}$$

one may obtain

$$F_D = (p_1 - p_2)W + \left\{p_1 - p_2 - \frac{1}{2}\rho U_2^{\,2}\right\}(B-W) + \frac{1}{2}\rho U_1^{\,2}\left\{\frac{B^2 - 2BW}{B - W}\right\} \tag{14}$$

Using the Bernoulli relation for the outer flow

$$p_1 - p_2 - \frac{1}{2}\rho U_2^{\,2} = -\frac{1}{2}\rho U_1^{\,2} \tag{15}$$

and further rearrangement of terms gives

$$F_D = (p_1 - p_w)W - \frac{1}{2}\rho U_1^{\,2}\,\frac{W^2}{B - W} \tag{16}$$

Constraint effects are generally referenced to the completely unconstrained case, i.e. $W/B \to 0$. It is convenient to prime all parameters for this zero blockage condition. Introducing a wake width parameter

$$m = W/L \tag{17}$$

one thus obtains from Eq. 16

$$C_D' = \lim_{B\to\infty}\left[m\,\frac{p_1 - p_w}{\frac{1}{2}\rho U_1^{\,2}} - m\,\frac{W}{B-W}\right] = m'\left[\frac{p_1 - p_w'}{\frac{1}{2}\rho U_1^{\,2}}\right] \tag{18}$$

In keeping with free streamline model notions Maskell introduced the questionable assumptions

$$p_w' = p_b' \quad ; \quad p_w = p_b \tag{19}$$

This does permit the simplification of Eq. 18 to

$$C_D' = m'[(k')^2 - 1] \tag{20}$$

Maskell then rewrote Eq. 16 as

$$C_D = m\left[\frac{p_1 - p_b}{\frac{1}{2}\rho U_1^{\,2}} - (m\,\frac{L}{B}) - (m\,\frac{L}{B})^2 - (m\,\frac{L}{B})^3 - (m\,\frac{L}{B})^4\right] - \ldots \tag{21}$$

and confining attention to small blockages such that

$$(mL/B)^2 \ll (mL/B) \tag{22}$$

he replaced Eq. 21 by

$$C_D = m[(k^2 - 1) - mL/B] \tag{23}$$

where $k > k'$ of Eq. 20. Using the emperical relation (for small blockages)

$$C_D'/(k')^2 = C_D/k^2 = \text{constant} \tag{24}$$

and a weakly motivated supposition that

$$m/m' = 1 - \frac{(C_D - C_D')L/B}{(k^2-1)(k'^2-1)} \tag{25}$$

Maskell arrived at the relation (per unit of cylinder length)

$$F_D = \left[1 + \frac{L/B}{(k')^2 - 1}\,C_D\right] C_D \cdot \frac{1}{2}\rho U_1^{\,2} \tag{26}$$

which is again obtained by neglecting terms of order $\{(L/B)^2\}$. Knowing the value of k' for the unconstrained case, say from a base pressure measurement, the Eq. 26 would permit calculation of the C_D value appropriate to having the body placed in an unconstrained stream of velocity $U_1' = U_1$.

The Eq. 25 and the match with emperical data taken over a limited range of small blockages are difficult to criticize in the absence of data

for larger blockages. Thus Maskell's work earned the designation of "theory".

e. Dynamic Model - The effect of constraint on drag was considered above. However, it is the dynamic lift that is of ultimate concern. For small blockage it is commonly assumed that lift and drag remain proportional. The only picture of sufficient simplicity to be of use here is still based on von Karman's vortex street model.

For two staggered vortex rows symmetrically placed in a channel of width B, one has (Goldstein, 1965)

$$F_D = \rho a U^2 \left[c_1 \frac{u}{U} - c_2 \frac{u^2}{U^2} + 16 \left(\frac{u}{U}\right)^2 \frac{W^2}{LB} \right] \tag{27}$$

in which a = vortex spacing in one row and u = vortex pattern velocity relative to the main flow U. Comparison with Eq. 11 shows that Eq. 27 is untenable; Eq. 27 is typically a correction relationship with validity only for small L/B-values.

Assuming that a fraction β of the vorticity generated near the separation points is preserved in the vortices one has for the maximum instantaneous lift:

$$(F_L)_{max} = \rho U_1 \Gamma_v = (\rho U_1)\beta\left(\frac{1}{2} k^2 U_1^{\,2} f^{-1}\right) = \frac{1}{2}\rho\left(\frac{L}{1 - L/B}\right)\beta k U_1^{\,2} S_s^{-1} \tag{28}$$

where Γ_v is the strength of each shed vortex.

The ratio of drag and lift coefficients obtained from Eq.'s 10, 11 and 28a becomes (if the small first term on the r.h.s. of Eq. 11 is neglected)

$$\frac{C_D}{C_L} = 1.6\ S_s/\beta \tag{29}$$

This shows that drag and lift would be proportional if β remains constant in accord with established notions. Data presented below will be seen to be at variance with Eq. 29.

PRESENT WORK

a. Experimental Facility - The experimental work reported herein was performed in the test section of a low velocity water tunnel. The test section had a height H = 8" and a width B = 18". A variety of cylinders all 8" long, but of different cross-sectional size L were mounted vertically and at right angles to the flow.

The cylinders were mounted onto a force gage as indicated in Figure 4. This portal gage had an LVDT as the transducing element. Generally it measured the dynamic lift. By turning it over 90° it was possible to measure the drag force.

For the equilateral triangular cylinders the orientation or "attitude" could be varied between $\alpha = 0°$ (i.e. a symmetrical position with an apex downstream) and $\alpha = 60°$ (i.e. a symmetrical position with an apex upstream).

b. Procedures and Tests - The flow rate and possible static head ranges of the equipment were limited. Therefore, the tests were performed at only two fixed flow rates equivalent to clear tunnel velocities of $U_1' =$ 1.30 and 2.00 ft/sec.

The parameter of interest was the blockage, L/B. Since the cylinder size L varied, the Reynolds number varied from cylinder to cylinder. This is held to be but a minor concern. More consequential may have been the fact that it was not feasible to keep the cylinder aspect ratio, L/H, constant.

Although the equipment was designed to subject the cylinders to forced oscillations, these were not imposed. The greater tendency towards self-induced oscillation with displacement, noted earlier, is therefore a qualitative observation.

An overview of test conditions is given in Table 1. Therein C_D and C_L stand for mean drag and lift values whereas C_D' and CLO stand for rms values of drag and lift, respectively.

Shape and Orientation	U_1 ft/sec	α degrees	L/B -	H/L -	C_D -	C_D' -	C_L -	CLO -
U_1	1.30	-	0.067 through 0.445	6.4 through 1.0	-	none	-	7x
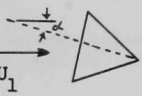 U_1	1.30	$\Delta\alpha = 5°$	0.097	4.6	13x	13x	13x	13x
U_1	1.30 2.00	60°	0.097 through 0.445	4.6 through 1.0	none	none	-	5x
U_1	1.30 1.20	0°	0.097 through 0.445	4.6 through 1.0	none	none	-	5x

Table 1 - Test Conditions

PRESENTATION AND DISCUSSION OF RESULTS

a. Cylinder Orientation - For non-circular cylinders the angle of orientation α is an additional variable whose role is not generally documented for all pertinent force and frequency variables. Therefore, tests were made for the triangular cylinder at the lowest blockage ratio of 0.97 and at increments of $\Delta\alpha = 5°$ from $\alpha = 0°$ through $\alpha = 60°$. The resulting data have been collected in Figures 5 and 6.

Figure 5 shows that there can be a considerable mean lift force coefficient C_L (up to $C_L = 1.56$) whenever the cylinder has a non-symmetrical attitude. The mean drag coefficient too shows considerable variation between a maximum of $C_D = 2.7$ to a minimum of $C_D = 1.0$. Two of the values agree well with those found by Lindsey (1937). The Strouhal number, STRNO, based on the dimension L shows a variation that is roughly the inverse of the drag coefficient variation. This is anticipated and associates with the variation in relative wake width, W/L. Note that all data were normalized using the same cylinder dimension L, i.e. the projected area was not adjusted for the orientation effect.

Note that C_D, C_L, and STRNO all reach a relative extreme at $\alpha \approx 40°$ illustrating their interrelationship.

Figure 6 shows the rms-values of the fluctuating component of drag, C_D', normalized with the value of C_D' at $\alpha = 0°$. This normalization was selected because C_D' is quite small; its absolute value is thus of rather limited accuracy. It is noteworthy that the maximum C_D' does not associate with extremes in C_D. The same is true for the rms-value of the lift CLO. There is reasonable similarity in the variation of C_D' and CLO with α as would be expected.

The data of Figure 5 and 6 appear to be the first that show complete information on the role of attitude for the equilateral triangular prism. In the present context the data's significance is in comparing blockage behavior for the two cases of $\alpha = 60°$ and $\alpha = 0°$.

b. Data Reduction for Blockage

The Strouhal number and the oscillatory lift, based on the clear tunnel velocity, U_1', were affected appreciably by the blockage L/B. The question how to "correct" STRNO and F_D for blockage effect, i.e. the usual point of view in wind tunnel test scaling, may also be taken as an inquiry how to normalize measured data such that they become independent of blockage.

The accepted theory for normalizing the drag force is given by the Eqs. 22 through 25. An attempt to employ these relations gave entirely inconsistent results. This made suspect the neglect of higher order terms in Eq. 20 in accord with Eq. 21. However, retaining these terms for a blockage L/B = 0.445 leads to even greater inconsistencies. It must be concluded that Eq. 18 is inadmissible for larger blockages.

Thus a new, preferably simple approach to normalization of data is required. As a first step a new reference velocity

$$U_s = \frac{B}{B-L}$$

will be defined. This is the mean velocity of flow in the narrowest passages between cylinder and test section walls. Using this "slit" velocity amounts to normalizing the oscillatory lift and the Strouhal number as follows

$$CL1 = F_D/\frac{1}{2}\rho L U_s^2 \tag{30}$$

and

$$STRNO1 = fL/U_s \tag{31}$$

There is also justification for a normalization based on the velocity U_2 where the wake attains its maximum width W, i.e. one may introduce

$$STRNCC = fL/U_2 \tag{32}$$

with equal justification. The velocity U_2 was found from Eq. 9 and $U_2 = kU_1/C_c$ where $C_c = (1 - mL/B)(1 - L/B)^{-1}$.

c. Circular Cylinder

The upper curves in Figure 7 portray the lift and lift frequency data for a circular cylinder as a function of blockages between 7% and 44%. When normalized by the mean test section speed $U_1 = U_1'$, the blockage effects are evident and pronounced.

The use of Eq. 31 is seen to be quite satisfactory in giving a nearly constant Strouhal number, STRNO1, over the entire range of blockages. The use of Eq. 32 will give over-correction, however.

The use of Eq. 30 gives less satisfactory results. The lift force is underestimated at low and high blockages, whereas it is overestimated at intermediate L/B values. For a circular cylinder the value of $m' \approx 1.2$ whereas wake blocking would give a monotonous decrease to $m = 1.0$. This further refinement of the reference velocity will, therefore, not lead to a normalization CL1, that would eliminate the relative maximum in CL1.

The reason is that, in contradiction to Eq. 29, the ratio of drag to lift does not remain constant. Rather, it will approach infinity as C_D keeps increasing with L/B, whereas C_L must approach zero for $L/B \to 1.0$. The reason for the latter is that the image of a shed vortex will decrease the net lift experienced by the body. This attenuation increases with proximity of test section wall and shed vortex, i.e. with increasing blockage. The initial increase in lift coefficient at the lowest L/B values could well be due to the changes in aspect ratio.

It is concluded that the two established relationships for these situations, namely Eq.'s 26 and 29, are disproven.

d. Triangular Cylinders

The data for the triangular cylinder at $\alpha = 60°$ (Figure 8) show similarity with those of the circular cylinder. The decrease in lift with

blockage, however, is now much more pronounced. This could be due to the higher effective blocking for the same L/B value of this geometry. The higher effective blockage is confirmed by the somewhat higher drag coefficient as compared to a circular cylinder (1.5 vs 1.2). However, it is not confirmed by the Strouhal frequency value which is slightly higher rather than lower relative to that for the circular cylinder.

In Figure 9 the same data for a 65% higher flow rate are shown. It is seen that Reynolds number effects are not significant. The same conclusion is reached by comparing the Figures 10 and 11.

Note the very low values for the lift coefficients. This is not due to the fact that the vortex strength, Γ_v, would be so much smaller relative to the circular cylinder case. Rather, the cylinder in this orientation lacks an afterbody (i.e. the geometry beyond the separation points) on which the transient wake pressure distributions may act. Such an afterbody is pronounced for the $\alpha = 0°$ orientation of the triangular cylinder for which Figures 10 and 11 provide data. Indeed, the (oscillatory) lift coefficient for the lowest blockage is almost an order of magnitude higher than the $\alpha = 60°$ case.

As expected the Strouhal number at the lowest blockage, i.e. STRNO = 0.15 is well below the corresponding value of STRNO = 0.23 for the $\alpha = 0°$ orientation. However, for the highest blockage (L/B = 0.44) the vortex shedding frequencies for both orientations approach the same value. This is again due to the fact that the $\alpha = 0°$ attitude gives, for the same L/B-value a larger effective blockage (defined as W/B) than the $\alpha = 60°$ case, i.e. the contraction coefficient of the flow beyond the separation points is larger for $\alpha = 0°$ than for $\alpha = 60°$.

As a consequence, it was attempted to normalize the data by means of the mean velocity of the contracted flow, U_2, as defined by Eq. 32. This yielded the lower curves in the four sets of three curves found in the Figures 10 and 11.

It is seen that this is a correct procedure as far as the Strouhal number data is concerned. However, the force data appear to be yet more overcorrected at the highest blockages.

Finally it is noted that the drag plotted as function of blockage would show a continuous increase of C_D according to Eq. 23 whereas the experimental C_L show a decrease beyond a blockage of about 1/3 disproving Eq. 29.

SUMMARY AND CONCLUSIONS

This note presents data on the Strouhal frequency and hydrodynamic forces for circular and triangular cylinders in cross flow as they are effected by flow blockage. Blockage in test sections is defined as L/B, where L = largest cross sectional cylinder dimension and B = test section width. This note may be summarized as follows:

1. The effect of flow constraint is to produce increased drag coefficient if force data are normalized with approach velocity values. This

increase has not been studied experimentally for blockages beyond 4 ~ 7%.

2. The effect of flow constraint on the Strouhal frequency and the oscillatory lift has not been systematically studied at all.

3. This note presents data on the mean Strouhal frequency, STRNO, and the oscillatory lift coefficient CLO for a range of blockages between 7% and 44%.

4. The existing methods of blockage analysis imply constancy of the drag to lift ratio under varying blockage. Data presented herein disprove this notion.

5. It is concluded that free streamline models, or more generally that mean flow models, which are at the base of attempts to correct hydrodynamic force coefficients for blockage effects require substantial revision if not abandonment. This question calls for detailed measurements in the outer flow and throughout the early wake region.

6. The Strouhal frequencies can be normalized satisfactorily on the basis of continuity arguments.

7. The oscillatory lift data cannot be normalized satisfactorily in the same manner.

8. This note presents a complete frequency and force characteristic for a triangular cylinder (L/B = 0.097) as function of attitude.

LIST OF SYMBOLS

f = Mean Frequency of Unsteady Lift

h = Length of Test Cylinder Mounted Vertically.

$k = U_b/U_1$

m = Wake Width Parameter = W/L

p_1 = Ambient Pressure in the Approach Flow

p_2 = Pressure in Outer Flow at Section 2

p_b = Base Pressure

$p(s)$ = Pressure Along the Vortex Sheet

p_w = Pressure in the Wake

u = Vortex Pattern Velocity

A = Area Considered in the Definition of Force Coefficients (A=L.h)

B = Width of Test Section

C_D = Constrained Steady Drag Coefficient =

$$C_D = \frac{\left\{\frac{1}{T}\int_c^T (\text{Drag Force})\ \Delta t\right\}}{\frac{1}{2}\rho A U_1^{\,2}}$$

CDO = Constrained Unsteady Drag Coefficient =

$$\text{CDO} = \frac{\left\{\frac{1}{T}\int_o^T (\text{Unsteady Drag Force})^2 \Delta t\right\}^{1/2}}{\frac{1}{2}\rho A U_1^{\,2}}$$

CDO_o = CDO at $\alpha = 0$

C_L = Constrained Steady Lift Coefficient =

$$C_L = \frac{\left\{\frac{1}{T}\int_o^T (\text{Lift Force})\ \Delta t\right\}}{\frac{1}{2}\rho A U_1^{\,2}}$$

CLO = Constrained Unsteady Lift Coefficient =

$$CLO = \frac{\left\{\frac{1}{T}\int_{o}^{T}(\text{Unsteady Lift Force})^2 \Delta t\right\}^{1/2}}{\frac{1}{2}\rho A U_1^{\,2}}$$

CL1 = Modified Unsteady Lift Coefficient =

$$CL1 = \frac{\left\{\frac{1}{T}\int_{o}^{T}(\text{Unsteady Lift Force})^2 \Delta t\right\}^{1/2}}{\frac{1}{2}\rho A U_2^{\,2}}$$

CLCC = Modified Unsteady Lift Coefficient =

$$CLCC = \frac{\left\{\frac{1}{T}\int_{o}^{T}(\text{Unsteady Lift Force})^2 \Delta t\right\}^{1/2}}{\frac{1}{2}\rho A U_2^{\,2}}$$

H = Height of Test Section

L = Characteristic Linear Dimension of the Test Bodies

STRNO = Strouhal Number = STRNO = (fL/U_1)

STRN1 = Modified Strouhal Number = STRN1 = (fL/U_s)

STRNCC = Modified Strouhal Number = STRNCC = (fL/U_2)

U_1 = Clear Tunnel Velocity = Free Stream Velocity U_1'

U_2 = Mean Velocity in The Cross-Section of the Test Region Having Maximum Wake Blockage

U_b = Outer Flow Velocity Along Free Shear Layer Near Separation

U_s = Mean Velocity in the Cross-Section of the Test Region Having Maximum Solid Blockage

W = Wake Width (Maximum)

α = Angle of Orientation of Triangular Cylinder

Γ_v = Strength of Shed Vortex

ρ = Density of Fluid

ACKNOWLEDGEMENT

The reported study is part of a program on Fluidelastic research supported by the National Science Foundation via Grant GK-414, by the School of Civil Engineering, Purdue University and the Purdue Research Foundation.

The authors are grateful for the support by these various sponsors.

REFERENCES

1. Betz, A.: "Ein Verfahren Zur Directen Ermittlung der Profilwiderstandes," Flugtechn. Motorluftschaft, Vol. 16, pp. 42 (1925).

2. Cowdry, C. F.: "Application of Maskell's Theory of Wind Tunnel Blockage to Very Large Solid Models," - Proc. Symposium on Wind Effects on Buildings and Structures, London, pp. 29.1 - 29.9 (1968).

3. Glauert, H.: "Wind Tunnel Interference on Wings, Bodies, and Airscrews," ARC Res. & Mem. 1566 (1933).

4. Goldstein, S.: "Modern Developments in Fluid Mechanics II," pp. 566, 567, Dover Edition (1965).

5. Kirchhoff, G.: "On the Theory of Free Fluid Jets," (In German), Journ. fur die Reine und Angew. Math. 70, pp. 289-98 (1869).

6. Lindsey, W. F.: "Drag of Cylinders of Simple Shapes," NACA Rept. 619, pp. 1-8, (1937).

7. Maskell, E. C.: "A Theory of the Blockage Effects on Bluff Bodies and Stalled Wings in a Closed Wind Tunnel," - R.A.E. Aero Rept. No. 2685 (1963).

8. Roshko, A.: "On the Drag and Shedding Frequency of Two-Dimensional Bluff Bodies," - NACA T.N. 3169 (1954).

9. Shaw, T. L.: "Steady Flow Past Flat Plate in Channel," - ASCE Proc., Hydraulics Division, pp. 2013 - 2028 (1969).

10. von Helmholtz, H.: "On the Discontinuous Motion of Fluids," (translated from the German and published in) Phil. Mag. Series 4, 36, pp. 337-45 (1868).

11. Weinig, F.: "Computations of Drag in Separated Flow by Use of Rolling up Free Streamlines," Proc. 9th Int. Congress Appl. Mech. Bruxelles, pg. 215-20, Vol. I (1957).

DISCUSSION

S. C. Rose (GE-KAPL): Could you comment on your experimental technique to get such nice movies of these vortices?

Toebes: Yes. What it is is a compound that is used in lipstick which consists of very small platelets which tumble in the flow. They are reflective, like little mirrors. They are mixed up with the fluid and lighted with a strong light from above which is reflected.

R. Katz (Gulf General Atomic): I was pleased to see the one shot there that you had a splitter plate to avoid the problems of vortex shedding and the frequencies and some of the problems that were talked about earlier this morning. Do you have results or any rules for the location, length, and placement of these splitters in these confined passageways to avoid the periodic vortex shedding?

Toebes: Oh, it is approximately 1½ times the width of the wake--the width between the shear layers. Why should this be the case? It is an inertial flip-flop, and I have measurements of pressure as well as velocity fluctuations in this region. It would probably take too long to try to set up a model for this, but it is not illogical that this happens.

Katz: I wonder if I understood the movie correctly. It seemed that you were getting boundary-layer separation at the walls at the time the wake was aiming or moving toward that particular wall. Is that correct?

Toebes: Yes. I could explain it more in detail if there were more time, but what happens is that there is self-induction. Due to self-induction, they start to roll up. And this vortex here, its strength will increase up to the point that it induces velocities in this region that are so strong that this flow is swept in, and this flow is moving. And so you get that this stream of flow is, so to say, being stopped, and it either has to go this way or that way and it flips in. At the same time, you see, this flow has a stagnation point in this region and that is what you were seeing. In other words, you have the boundary layer here that encounters temporarily an increasing pressure gradient and then you have a zone of boundary-layer separation. That is what you were seeing.

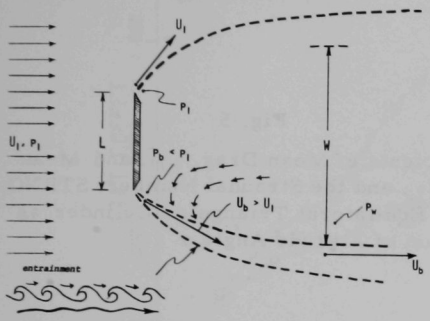

Fig. 1. Classical and Modified Hodograph Model Features

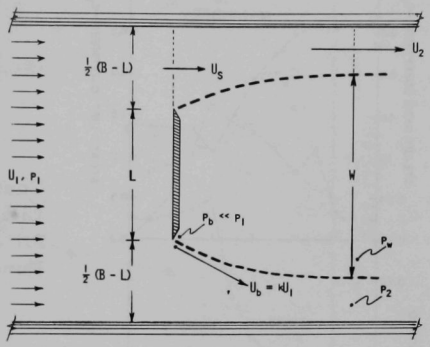

Fig. 2. Hodograph Model for a Flow with Side Wall Constraints

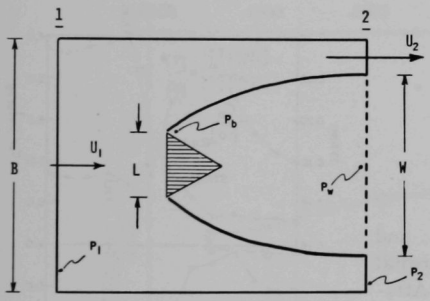

Fig. 3. Momentum Mean Flow Model for Bluff Cylinder Located Symmetrically in a Channel

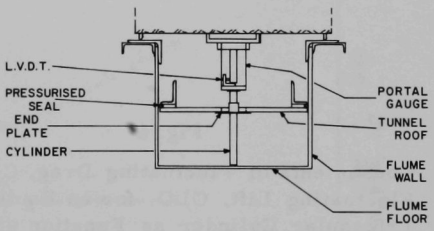

Fig. 4. Experimental Equipment

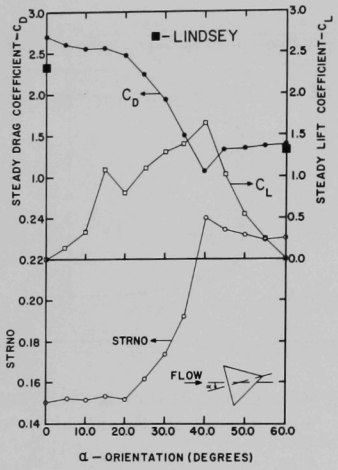

Fig. 5

Coefficients of Mean Drag, C_D, and Mean Lift, C_L, and the Strouhal Number, STRNO, for an Equilateral Triangular Cylinder as Function of Attitude Angle α

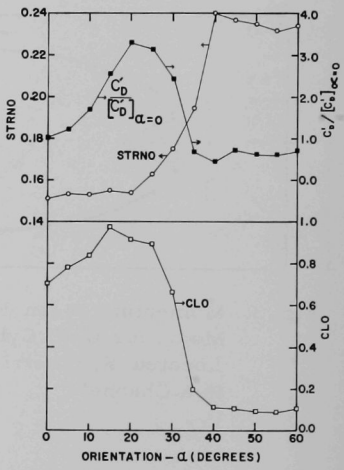

Fig. 6

Coefficients of Fluctuating Drag, C_D', and Fluctuating Lift, CLO, for an Equilateral Triangular Cylinder as Function of Attitude Angle α

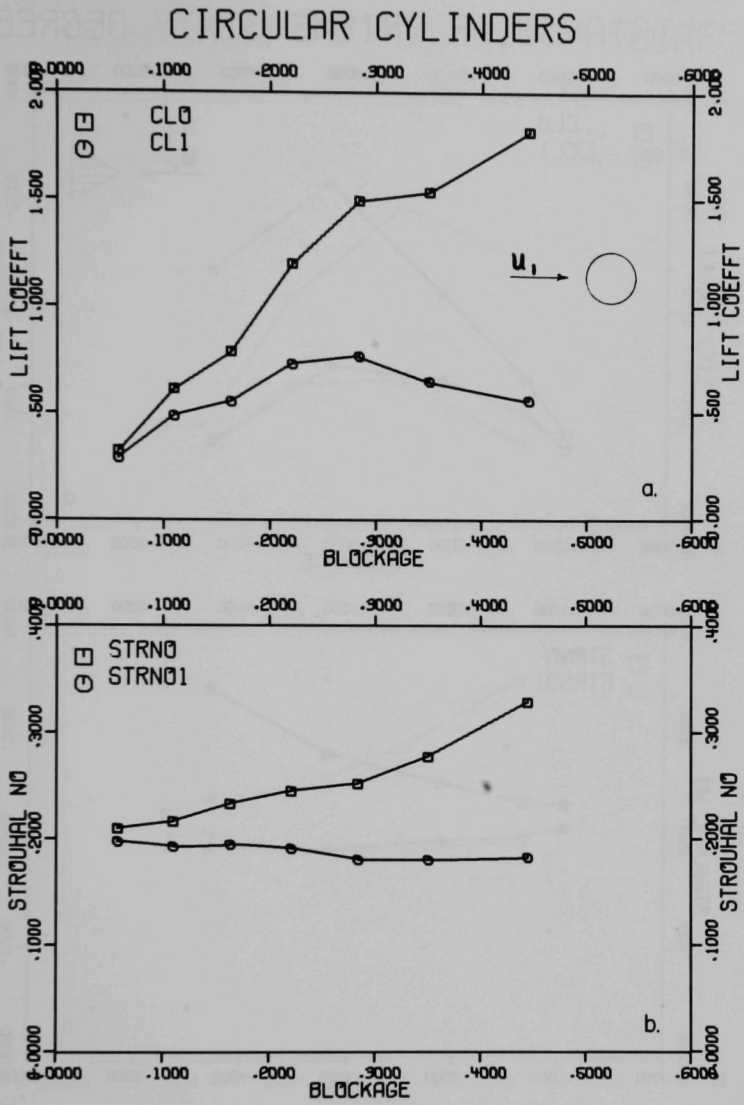

Fig. 7. a. Coefficient of Fluctuating Lift, CLO, and Coefficient of Fluctuating Lift, CL1, Normalized with the Slit Velocity, U_s, for a Circular Cylinder as Function of Cylinder Diameter to Channel Width Ratio, L/B, or Blockage. b. Strouhal Number, STRNO, and Strouhal Number, STRNO1, as Function of Cylinder Size to Channel Width Ratio, L/B, for U_1 = 1.3 ft/sec.

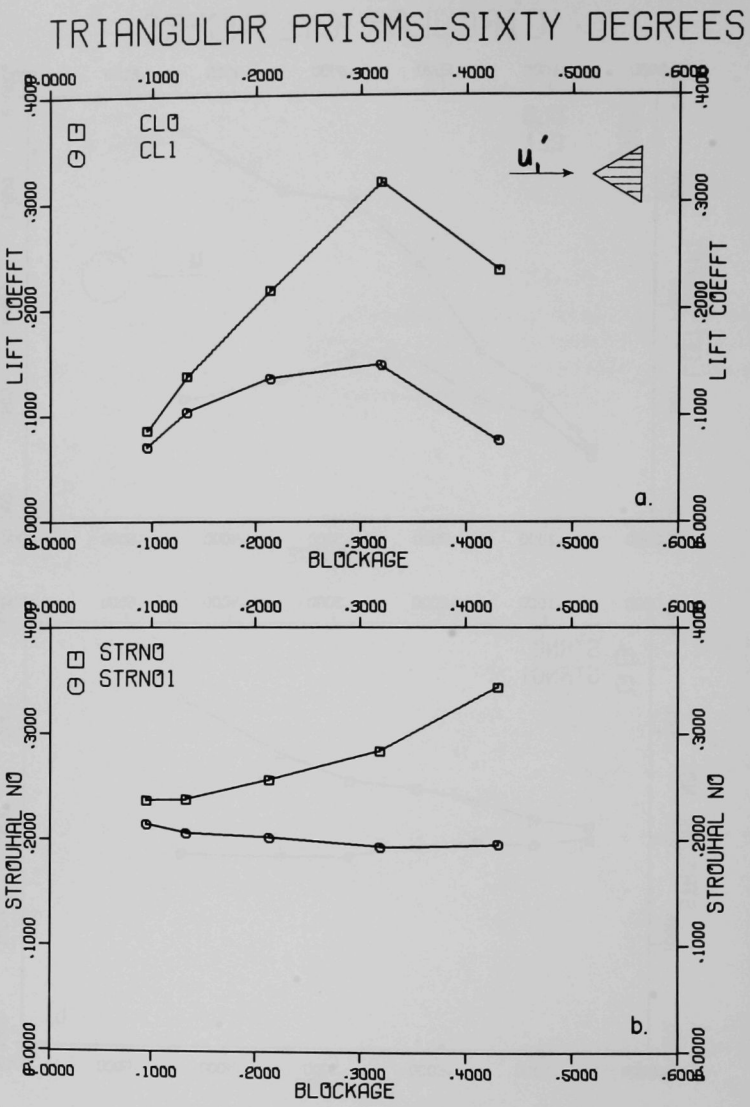

Fig. 8. a. Coefficient of Fluctuating Lift, CLO, and Coefficient of Fluctuating Lift, CL1, Normalized with the Slit Velocity, U_s, for a Triangular Cylinder at $\alpha = 60°$ as Function of Cylinder Size to Channel Width Ratio, L/B, for $U_1 = 1.3$ ft/sec. b. Strouhal Number, STRNO, and Strouhal Number, STRNO1, as Function of Cylinder Size to Channel Width Ratio, L/B, for $U_1 = 1.3$ ft/sec.

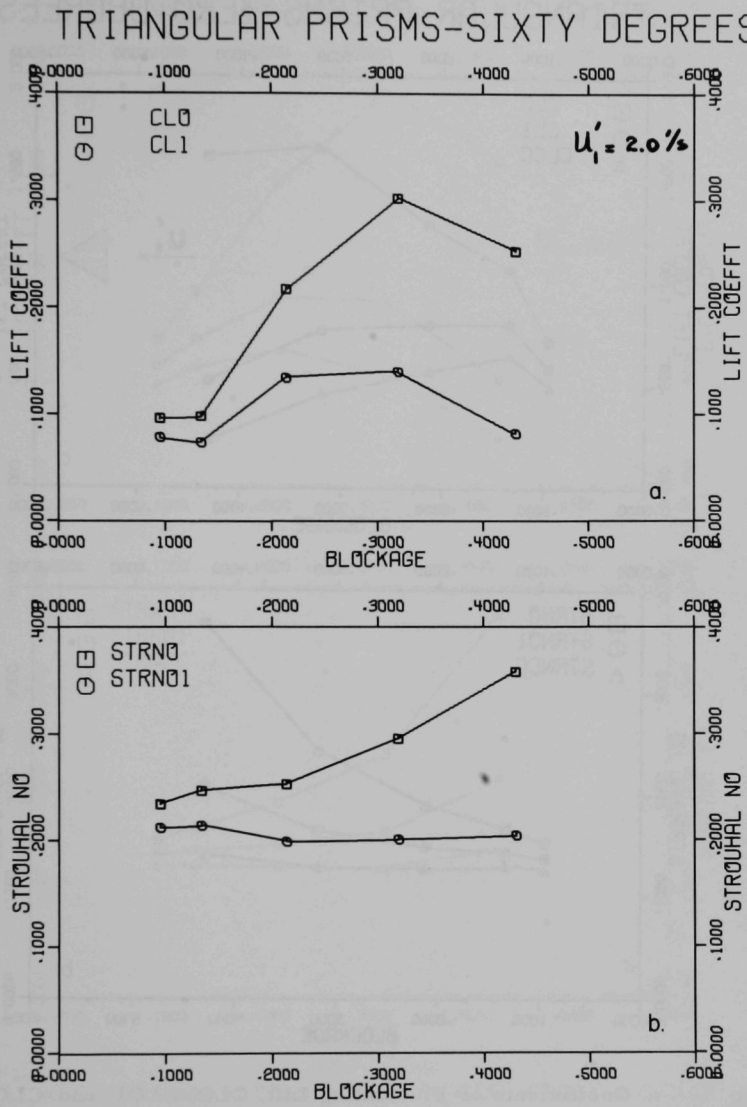

Fig. 9. a. Coefficient of Fluctuating Lift, CLO, and Coefficient of Fluctuating Lift, CL1, Normalized with the Slit Velocity, U_s, for a Triangular Cylinder at $\alpha = 60°$ as Function of Cylinder Size to Channel Width Ratio, L/B, for U_1 = 2.0 ft/sec. b. Strouhal Number, STRNO, and Strouhal Number, STRNO1, as Function of Cylinder Size to Channel Width Ratio, L/B, for U_1 = 2.0 ft/sec.

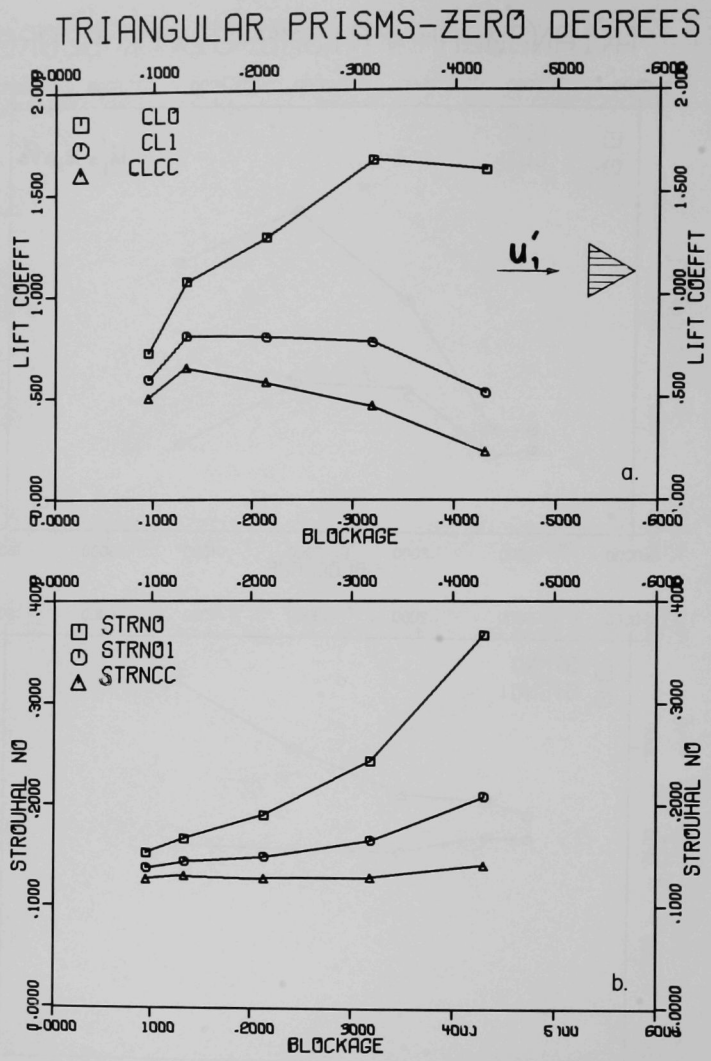

Fig. 10. a. Coefficients of Fluctuating Lift, CLO, CLO1, and CLCC, Normalized with U_1, U_s, and U_2, Respectively. Data are for triangular cylinder at $\alpha = 0°$, $U_1 = 1.3$ ft/sec and are shown as function of cylinder size to channel width ratio, L/B. b. Strouhal Numbers, STRNO, STRNO1, and STRNCC, Normalized with U_1, U_s, and U_2, Respectively. Data are for triangular cylinder at $\alpha = 0°$, $U_1 = 1.3$ ft/sec and are shown as function of cylinder size to channel width ratio, L/B.

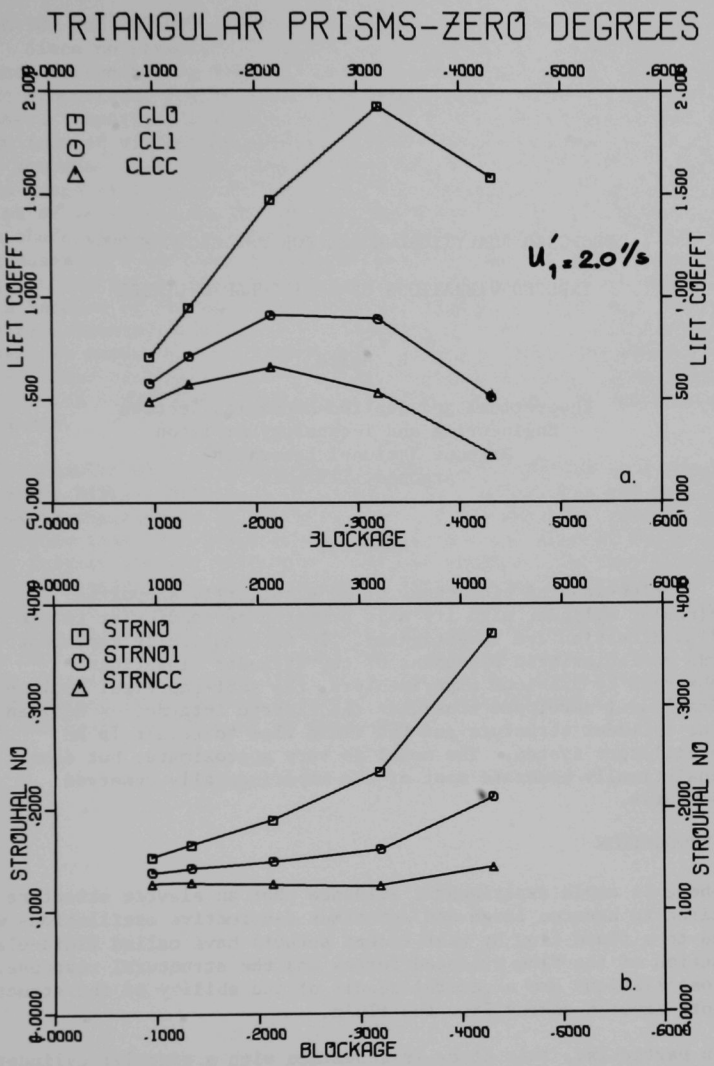

Fig. 11. a. Coefficients of Fluctuating Lift, CLO, CLO1, and CLCC, Normalized with U_1, U_s, and U_2, Respectively. Data are for triangular cylinder at $\alpha = 0°$, $U_1 = 2.0$ ft/sec and are shown as function of cylinder size to channel width ratio, L/B. b. Strouhal Numbers, STRNO, STRNO1, and STRNCC, Normalized with U_1, U_s, and U_2, Respectively. Data are for triangular cylinder at $\alpha = 0°$, $U_1 = 2.0$ ft/sec and are shown as function of cylinder size to channel width ratio, L/B.

PROPOSED ANALYTICAL MODEL FOR THE CROSS-FLOW-INDUCED VIBRATIONS OF A CIRCULAR CYLINDER

H. Halle

Theoretical and Applied Mechanics Section
Engineering and Technology Division
Argonne National Laboratory
Argonne, Illinois

ABSTRACT

Flow-induced vibrations of an elastically supported circular cylinder with its axis oriented perpendicular to the flow direction are investigated. To mathematically represent the characteristic phenomena of the cylinder vibrations observed by previous experimenters, the semi-empirical analytical model developed considers the elastic interaction between the cylinder structure and the fluid flow to result in an oscillatory system. The model is very approximate, but does analytically generate most of the experimentally observed features.

I. INTRODUCTION

There is ample experimental evidence that an elastic structure may be excited to undergo large and sometimes destructive oscillations when exposed to a fluid flow by what recent authors have called fluid-elastic interaction of the flow produced forces and the structural response. These oscillations are a general result of the ability of the structure to absorb kinetic energy from the fluid.

In particular, this study is concerned with a circular cylinder subjected to cross flow, i.e. flow directed transversely to the cylinder axis. When the cylinder is held fixed, fluid vortices are shed with a frequency determined by

$$f_f = \frac{SU}{D} , \tag{1}$$

where S, the Strouhal number, is an approximate constant equal to 0.2 within a range of flow conditions characterized by Reynolds' numbers

between 300 and 200,000. Many practical applications fall within this range. Since no structure is perfectly rigid, it will have a natural frequency determined by damping and by its suspensions and/or its own elastic properties, for instance the beam properties of a tube in a heat exchanger. Experiments show that a cylinder is particularly vulnerable to flow induced vibrations when the vortex shedding frequency is at and/or somewhat above the natural frequency of the cylinder. Within a certain range of flow conditions cylinder vibrations and vortex shedding occur at or very near to the natural frequency of the cylinder. The vortex shedding remains locked to the cylinder frequency until the flow is increased to a certain, not always well defined point at which the strong interaction is broken. The analysis of such a system is very complex because of the many nonlinear relationships involved. While most of the experimental work has been conducted by forced oscillation of the cylinder, an experiment by Ferguson and Parkinson (Ref. 1) allowed the vortex-excited oscillation of a spring mounted cylinder. This cylinder vibrated with translation displacement only, there was no deformation of cylinder.

The results of this experiment in turn were analyzed in a recent paper by Di Silvio (Ref. 2). The results of the Ferguson and Parkinson experiments represented by Di Silvio are further analyzed herein, for this purpose this work proposes an analytical model that is hoped to provide further insight into this difficult problem. In this process, the author combines the observations of Ferguson and Parkinson and Di Silvio with those of Toebes and Ramamurthy (Ref. 3) and, in a sense, applies the "fluid- or wake-oscillator" concept proposed by Bishop and Hassan (Ref. 4). This "fluid-oscillator" approach was also used by Hartlen, Baines, and Currie (Ref. 5) to establish a mathematical model quite different from the one proposed herein and unknown to this author during the basic development of this work.

II. NOMENCLATURE

Symbol	Definition
a	Peak vibration amplitude of cylinder as a result of power spectral density effect (random turbulence excitation)
b	Damping coefficient characterizing cylinder-fluid interaction
c	Damping coefficient of cylinder
D	Diameter of cylinder
f	Frequency
k	Spring constant of cylinder
k_g	Spring constant of fluid
H	Refer to Eq. 37
L	Lift force
m	Mass of cylinder including added mass of fluid vibrating with it
m_g	Mass of fluid (considered by proposed model)
n	Constant
Q	Quality factor = 1/2 reciprocal of damping factor
R	Resultant force
S	Strouhal number
t	Time
U	Flow velocity
W	Displacement spectral density function
x	Amplitude of cylinder vibration
y	Amplitude of fluid vibration
y_o	Peak amplitude of fluid vibration
α	Phase angle with which fluid lags cylinder displacement
ε	Peak amplitude of cylinder vibration
ζ	Damping factor or fraction of critical damping
ϕ	Phase angle of component
Φ	Power spectral density function
ω	Circular frequency

Subscripts	
c	Pertaining to cylinder when immersed in stagnant flow
e	Effective property
f	Pertaining to fluid, vibration amplitude effects neglected
g	Pertaining to fluid, vibration amplitude effects considered
m	Pertaining to condition at that frequency where a maximum vibration amplitude, considered as a function of frequency, is encountered
r	Reference condition
s	Pertaining to cylinder and/or its frequency of vibration, when exposed to flow conditions

III. DESCRIPTION OF BASIC MODEL

Even though the involved phenomena are very complex, the resulting flow induced vibration of the cylinder have been observed to be of a common sinusoidal nature. In some cases a modulation of the basic natural frequency of the cylinder has been observed. The simplified semi-empirical model developed herein proposes to treat the cylinder-fluid system as the interaction of two vibrating masses coupled by a mutual frictional force. The spring mounted cylinder is constrained to pure translation in the plane normal to the flow direction. There is no deformation of the cylinder surfaces exposed to the flow, e.g. no bending. Sketches of the setup and of the model system are presented in Figs. 1 and 2.

The cylinder is considered to be energized by random disturbances characterized by the power spectral density function Φ_s of the fluid flow. Since the damping of the cylinder is very small, the mechanical properties of the cylinder provide a very narrow band filter that, for all practical purposes, extracts energy only at a resonant frequency of vibration ω_s, which is almost the same as the natural frequency ω_c of the cylinder when immersed in stagnant fluid.

By using what may be called an artifice, the fluid is also considered to be a vibrating mass. To determine its natural frequency the cylinder is held fixed. As a result of flow turbulence the fluid is subject to random excitation characterized by the power spectral density function Φ_f (related to Φ_s) and will shed vortices at the vortex shedding frequency given by Eq. 1. This study proposes that this inherent vortex shedding frequency is to be taken as the natural frequency of the fluid. At this point, it is not necessary to know the derived spring constant and mass of the fluid, except that they are both assumed very small. However, as far as fluid damping is concerned, it will be assumed that a damping factor is known or can be determined.

Now, let the cylinder be unlocked. With the pre-condition that the flow is within the wide Reynolds' number region within which vortex shedding occurs, the effect of this shedding will generally not influence the cylinder unless the shedding frequency is at or somewhat above the natural frequency of the cylinder where vibrations with large amplitudes at or near the latter frequency may be induced. This study presumes that a lift force L created by the cylinder motion drives the fluid which is coupled to the cylinder via the mutual damping force. The effect on the cylinder is to change the effective damping that permitted the buildup of the cylinder vibration to a large amplitude in the first place; perhaps after some small perturbation initiated the process. This study takes the position that the phase angle α between the cylinder and fluid displacements is essentially the phase angle of the fluid determined by its damping ratio and its natural frequency, i.e. the inherent vortex shedding frequency that it would have had if the cylinder were held stationary.

This phase angle α has <u>two</u> critical effects on the vibration: with a <u>cos α</u> component it determines not only the relative components of <u>direction</u> of motion but with a <u>sin α</u> component it also provides a

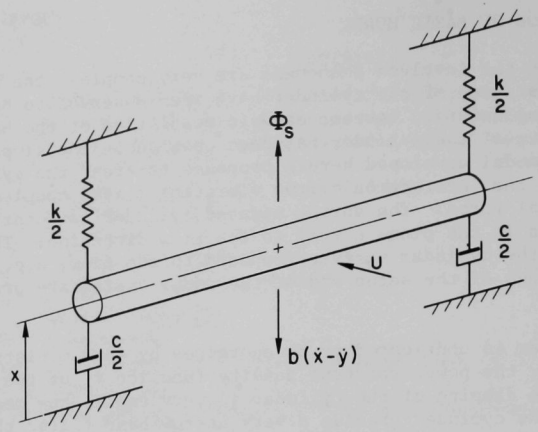

CYLINDER CONSTRAINED TO PURE TRANSLATION IN PLANE NORMAL TO U

TOTAL SPRING CONSTANT = k

TOTAL STRUCTURAL DAMPING = c

Fig. 1. Cross-flow-induced Vibration Setup

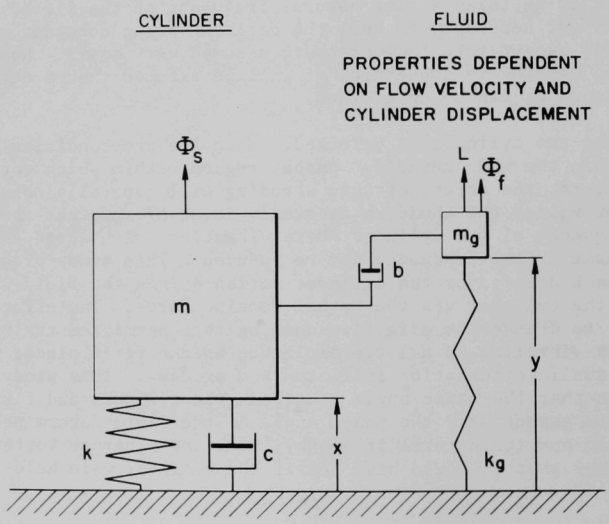

Fig. 2. Proposed Cross-flow-induced Vibration Model

resonance or magnification factor that relates the amplitudes of cylinder and fluid motions as a very sensitive function of frequency. These two effects can have supplementary as well as opposing tendencies, and the overall behavior of the model may, at least in part, explain the almost abrupt vibration amplitude and phase angle changes observed by experiments.

IV. DEVELOPMENT OF EQUATIONS

1. Initial Statements and Assumptions.

This analysis will be based on the model and the pertinent vector diagrams shown in Figs. 2 and 3 respectively. It is presumed that the basic properties of the cylinder and the fluid flow are known or can be determined, including the damping factor of the fluid

$$\zeta_g = \frac{b\omega_g}{2k_g} = \frac{1}{2Q_g} \quad , \tag{2}$$

which is taken to be constant over the relatively narrow flow velocity range of locked-in vortex shedding, even though recent tests (Ref. 6) indicate that this variation may not always be insignificant.

The analysis will involve four different frequencies:

ω_c the natural frequency of the cylinder when immersed in stagnant fluid,

ω_s the frequency of the flow induced vibration of the cylinder when interacting with the fluid,

ω_f the inherent vortex shedding frequency of the fluid flow as determined by Eq. 1,

ω_g the effective inherent vortex shedding frequency of the fluid flow which accounts for the modified width of the cylinder or wake resulting from the amplitude of the flow induced vibration.

The mass and the spring constant of the fluid will be assumed to be negligible with respect to those of the cylinder. Consequently, since the natural frequencies of both are of comparable magnitude, the displacement and the velocity of the cylinder are assumed to be negligible with respect to those of the fluid. The implications are that the force component $b\dot{x}$ is negligible compared to $b\dot{y}$ as well as to $c\dot{x}$, noting that

$\frac{b}{c} = \frac{k_g \omega_c Q_c}{k\omega_g Q_g}$. Another way of stating this is the following: the frictional force coupling the cylinder and the fluid depends on the vector difference of the respective velocities, however, since the cylinder velocity is assumed to be negligible in comparison, the fluid velocity alone determines this force.

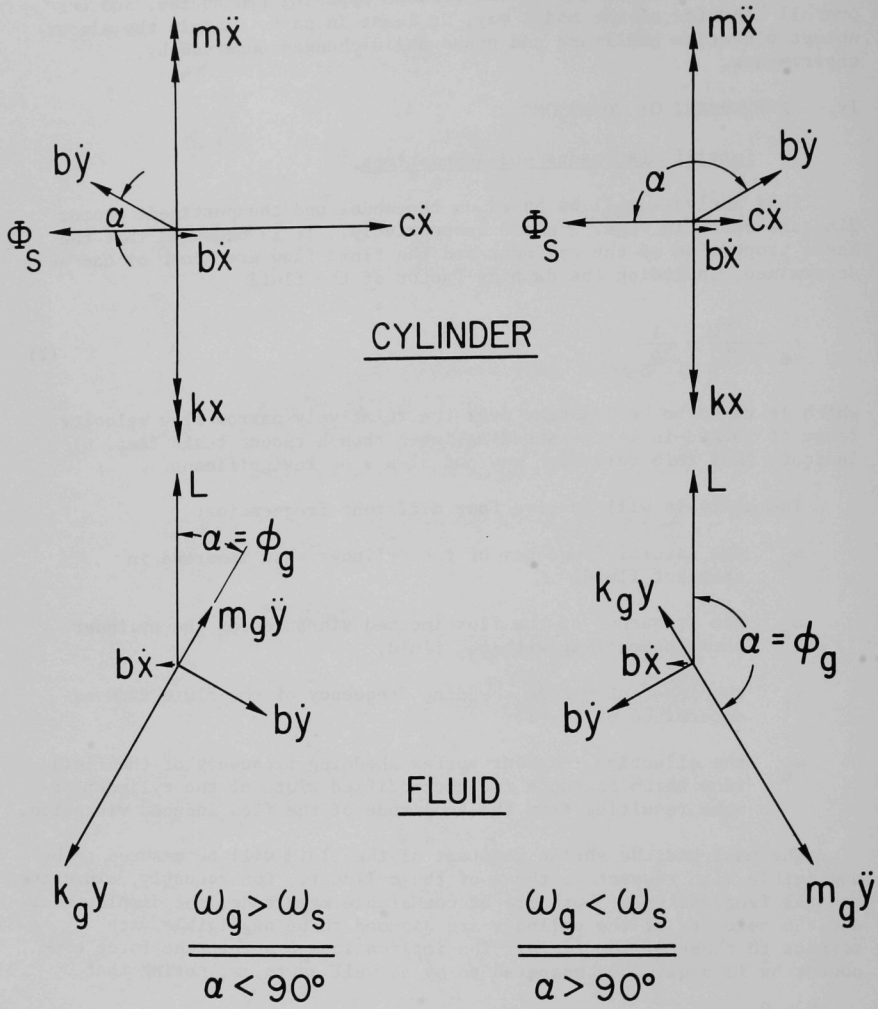

Fig. 3. Vector Diagram ($b\dot{x}$ assumed to be negligible)

This study will also assume that as long as the vortex shedding of the fluid is "locked-in" with the cylinder vibration frequency, the contribution of the power spectral density function Φ_f to the motion of the fluid can either be completely neglected or that the effect can be considered to be included in the damping characteristics of the fluid. A later section will examine the relative contribution of the force L and the power spectral density function Φ_s (acting on the cylinder) with respect to the locked vibration phenomena. It may be helpful to keep in mind that the Φ_f and Φ_s functions are expected to be closely related.

2. Motion of Fluid

The fluid is considered to be a simple one degree of freedom system driven by a force L $\sin\omega_s t$ acting in phase with the cylinder displacement

$$x = \varepsilon \sin\omega_s t \tag{3}$$

and a frictional component resulting from the cylinder velocity

$$b\dot{x} = b\varepsilon\omega_s \cos\omega_s t \quad . \tag{4}$$

The resulting forcing function

$$R = (L^2 + b^2\varepsilon^2\omega_s^2)^{1/2} \sin(\omega_s t + \phi_g - \alpha) \tag{5}$$

results in a derived fluid displacement $y = y_o \sin(\omega_s t - \alpha)$. As previously stated, the component $b\dot{x}$ will be assumed negligible, thus $\alpha = \phi_g$ and $R = L \sin\omega_s t$.

Applying common vibration analysis, it can be shown that the fluid displacement is given by

$$y = \frac{L}{k_g} \frac{\omega_g}{\omega_s} Q_g \sin\alpha \sin(\omega_s t - \alpha) \quad , \tag{6}$$

where it is noted that α is equal to ϕ_g and

$$\tan\phi_g = \frac{1}{Q_g\left(\frac{\omega_g}{\omega_s} - \frac{\omega_s}{\omega_g}\right)} \quad , \tag{7}$$

$$\sin\phi_g = \frac{1}{Q_g\left[\left(\frac{\omega_g}{\omega_s} - \frac{\omega_s}{\omega_g}\right)^2 + \frac{1}{Q_g^2}\right]^{1/2}} \quad , \tag{8}$$

$$\cos\phi_g = \frac{\left(\frac{\omega_g}{\omega_s} - \frac{\omega_s}{\omega_g}\right)}{\left[\left(\frac{\omega_g}{\omega_s} - \frac{\omega_s}{\omega_g}\right)^2 + \frac{1}{Q_g^2}\right]^{1/2}} \quad . \tag{9}$$

The frictional coupling force is given by

$$b\dot{y} = b\,\frac{L}{k_g}\,\omega_g Q_g \sin\alpha \cos(\omega_s t - \alpha) \quad , \tag{10}$$

which becomes

$$b\dot{y} = L \sin\alpha \cos(\omega_s t - \alpha) \tag{11}$$

when Eq. 2 is applied. A glance on the vector diagram Fig. 3 would have shown this directly.

3. Motion of Cylinder.

The motion of the cylinder is determined by the differential equation

$$m\ddot{x} + c\dot{x} + b\dot{x} - b\dot{y} + kx = \Phi_s \quad . \tag{12}$$

Since $b\dot{x}$ is assumed to be negligible and the cylinder is considered to be vibrating at the resonance frequency ω_s, with the displacement $x = \varepsilon\sin\omega_s t$, Eq. 12 can be written

$$(k - m\omega_s^2)\varepsilon \sin\omega_s t + c\varepsilon\omega_s \cos\omega_s t - L \sin\alpha \cos(\omega_s t - \alpha) = \Phi_s \quad . \tag{13}$$

Expanding the $\cos(\omega_s t - \alpha)$ term leads to

$$(k\varepsilon - m\omega_s^2\varepsilon - L \sin^2\alpha)\sin\omega_s t + (c\varepsilon\omega_s - L \sin\alpha \cos\alpha)\cos\omega_s t = \Phi_s \quad . \tag{14}$$

This equation represents an extension of Eq. 29 given by Toebes and Ramamurthy in Ref. 3. One may define effective damping and an effective spring constant, respectively, by

$$c_e = c - \frac{L \sin\alpha \cos\alpha}{\varepsilon\omega_s} \quad , \tag{15}$$

$$k_e = k - \frac{L \sin^2\alpha}{\varepsilon} \quad . \tag{16}$$

This study considers the vibration to occur at the resonance condition of the system with a phase angle $\phi_s = 90°$. Thus the frequency of vibration of the cylinder is determined by setting the $\sin\omega_s t$ components of Eq. 14 equal to zero, consequently

$$\omega_s = \omega_c \left(1 - \frac{L \sin^2\alpha}{\varepsilon k}\right)^{1/2} \quad . \tag{17}$$

Vibration at the resonant frequency ω_s reduces Eq. 14 to

$$(c\varepsilon\omega_s - L \sin\alpha \cos\alpha)\cos\omega_s t = \phi_s \quad , \tag{18}$$

which controls the amplitude of the cylinder vibration. The determination follows below.

The system described by Eq. 18 will have an effective quality factor given by

$$Q_e = \frac{k_e}{c_e \omega_s} \quad . \tag{19}$$

If we assume the system is energized by white noise random excitation with a power spectral density that is characterized by the displacement spectral density function W[units:(length)^2/cps], the amplitude of the lightly damped system vibrating at frequency ω_s will be given by

$$[x(\text{rms})]^2 = \frac{\varepsilon^2}{2} = \frac{\pi}{2} Q_e f_s W \tag{20}$$

or

$$\varepsilon^2 = \frac{Q_e \omega_s W}{2} = \frac{W k_e}{2 c_e} \quad . \tag{21}$$

Substituting from Eq. 15,

$$\varepsilon^2 = \frac{W k_e}{2\left[c - \frac{L \sin\alpha \cos\alpha}{\varepsilon\omega_s}\right]} \quad . \tag{22}$$

Rearranging terms and noting that $c = k/(\omega_c Q_c)$, leads to

$$\varepsilon^2 - L \sin\alpha \cos\alpha \frac{Q_c \omega_c}{k\omega_s} \varepsilon - \frac{W k_e \omega_c Q_c}{2k} = 0 \quad . \tag{23}$$

This quadratic equation determines the amplitude of vibration, but before we use it we must realize that both energy sources L and W vary with the flow velocity. To facilitate the application of this equation for the analysis of experimental data, it will be assumed that the lift L varies with the square of the flow velocity (this appears justifiable) and that W varies with the fourth power of the flow velocity. Recent testing (Ref. 6) performed at this laboratory indicated that the rms deflection of parallel flow induced vibrations varied with the about the

1.85th power of flow velocity, thus implying a variation of the power spectral density with the 3.7th power. This reduction was probably caused by an increase of fluid damping. The equations to be developed could be modified accordingly if necessary.

It is now possible to establish some constant reference values L_r and W_r at the flow velocity that corresponds to a reference frequency ω_r. Consequently Eq. 23 takes the form

$$\varepsilon^2 - L_r \left(\frac{\omega_f}{\omega_r}\right)^2 \sin\alpha \cos\alpha \frac{Q_c \omega_c}{k\omega_s} \varepsilon - W_r \left(\frac{\omega_f}{\omega_r}\right)^4 \frac{k_e \omega_c Q_c}{2k} = 0 \quad . \tag{24}$$

The above assumption to treat L_r and W_r as constants is probably a great oversimplification of a complex problem, however it is hoped that Eq. 24 as stated above will provide insights in addition to those previously available.

Two basic methods of conducting experimentation will be considered:

Method A: variation of the flow velocity

and

Method B: variation of the natural frequency of the cylinder without any change of its external dimensions.

In general, this paper will focus on Method A, because it seems that this approach was and will be used for most experimentation. It is fully realized that Method B can also have very practical applications, for instance the presence or lack of liquid within a heat exchanger tube influences its natural frequency. For a Method B approach one may choose $\omega_f = \omega_r$ and reduce Eq. 24 to Eq. 23. This will be assumed for any future occasional discussion of Method B.

When conducting experimentation according to Method A, it seems appropriate to choose $\omega_r = \omega_s \approx \omega_c$ and to define an amplitude of vibration "a" when $\omega_g = \omega_s$ and $\alpha = 90°$ such that

$$a^2 = \frac{W_s k_e \omega_c Q_c}{2k} = \frac{W_s Q_c \omega_s^2}{2\omega_c} = \frac{W_s Q_c \omega_c}{2} \left(1 - \frac{L_s}{ak}\right) , \tag{25}$$

or since (ω_s/ω_c) is approximately unity (Eq. 17)

$$a^2 \approx \frac{W_s Q_c \omega_s}{2} \quad . \tag{26}$$

Strictly speaking the peak amplitude "a" represents 1.414 times the rms value of the amplitude resulting from random excitation. Eq. 24 may now be written

$$\left(\frac{\varepsilon}{D}\right)^2 - L_s \left(\frac{\omega_f}{\omega_s}\right)^2 \sin\alpha \cos\alpha \frac{Q_c \omega_c}{k\omega_s} \frac{\varepsilon}{D^2} - \left(\frac{\omega_f}{\omega_s}\right)^4 \left(\frac{a}{D}\right)^2 = 0 \quad . \tag{27}$$

Solving the quadratic, Eq. 27 provides

$$\frac{\varepsilon}{D} = \left(\frac{\omega_f}{\omega_s}\right)^2 \left\{ \frac{L_s Q_c \omega_c}{2kD\omega_s} \sin\alpha \cos\alpha + \left[\left(\frac{L_s Q_c \omega_c}{2kD\omega_s} \sin\alpha \cos\alpha \right)^2 + \left(\frac{a}{D}\right)^2 \right]^{1/2} \right\} , \tag{28}$$

which controls the amplitude of the flow induced vibration.

Inherent in the mathematical model is the assumption that the Strouhal number remains constant. Since we have corrected above for velocity effects and will correct for amplitude effects in the following section, this assumption appears justified.

4. Effective Vortex Shedding Frequency.

Before Eq. 28 can be employed to determine the vibration amplitude, an additional problem must be faced. Unless this amplitude is very small, its presence will change the effective width of the wake and thus change the effective frequency of vortex shedding. Di Silvio in Ref. 2 presents a detailed discussion of this problem and proposes that the effective frequency be defined by his Eq. 20 as

$$\frac{\omega_g}{\omega_f} = \frac{D}{D + 2\varepsilon \sin \phi(\text{Di Silvio})} , \tag{29}$$

where ϕ(Di Silvio) is defined as the phase angle between zero displacement time and the vortex origin time, apparently corresponding to the maximum fluid displacement time of this study. It is proposed to adopt Di Silvio's principle with regard to phase angle relationship, noting but, like him, not accounting for his observations that there may be an additional phase difference coming into effect. Since α is essentially equivalent to ϕ(Di Silvio) - 90° the following relationship was initially employed:

$$\frac{\omega_f}{\omega_g} = 1 + 2\frac{\varepsilon}{D} \cos\alpha \quad . \tag{30}$$

In the process of trying to analyze the experimental data of Ferguson and Parkinson presented by Di Silvio and subsequently checking references 4 and 7 it appeared that the $2\varepsilon/D$ term is overcorrecting the effect of the amplitude on the vortex width, particularly at larger amplitudes.

Let us examine first the slope of the ω_f/ω_g ratio as a function of the ε/D relationship at small amplitudes. Differentiating Eq. 30 provides a slope of $2\cos\alpha$. Referring to Fig. 16 of Reference 4, a slope of frequency ratio (in terms of Strouhal number) versus amplitude of

about unity is indicated at a zero amplitude ratio. Estimating that the phase angle α was in the vicinity of 45°, and that the wake width (without oscillation) is larger than the diameter D (Ref. 2 mentions 1.13 D, others have indicated 1.21 D), the term $2\cos\alpha/1.13$ is not too far from unity, thus the relationship of Eqs. 29 and 30 may be roughly acceptable for small amplitudes. However, the discussion of References 4 and 7 and further examination of Fig. 16 in Reference 4 indicates that some modification is indicated for larger amplitudes. Assuming the $2\cos\alpha$ term to be unity in the region $0 < \varepsilon/D < 0.3$, the curve of Fig. 16 of Reference 4 can be roughly fitted by the relationship

$$\frac{\omega_f}{\omega_g} = 1 + (2\cos\alpha)\left[\frac{\varepsilon}{D} - \left(\frac{\varepsilon}{D}\right)^2\right] \tag{31}$$

or by

$$\frac{\omega_f}{\omega_g} = 1 + \frac{1}{3}\left(\frac{\varepsilon}{D}\right)^{1/2}(2\cos\alpha) \quad . \tag{32}$$

Even though the relationship of Eq. 32 is admittedly improper for very small ε/D ratios, it was used by the author in the form

$$\frac{\omega_f}{\omega_g} = 1 + n\left(\frac{\varepsilon}{D}\right)^{1/2}\cos\alpha \tag{33}$$

with a constant n somewhat smaller than 2/3 because this form greatly facilitated the computational effort.

V. CHARACTERISTICS OF PREDICTED MOTION

1. Inherent Vortex Shedding Frequency Equal to Vibration Frequency.

The characteristics of the motion predicted by the basic equations 17, 28, and 33 may now be examined. Consider first the situation when $\omega_f = \omega_g = \omega_s$. Since $\alpha = 90°$, the frictional force coupling the cylinder and the fluid has no component effecting the cylinder damping. The amplitude of vibration is given by $\varepsilon = a$ and the resonant frequency of vibration is

$$\omega_s = \omega_c\left[1 - \frac{L_s}{ak}\right]^{1/2} \quad . \tag{34}$$

Even though "a" may be a small quantity, the lift force for air flow is relatively small too. Experimental evidence of gaseous flow (air) indicates that the reduction of ω_s from ω_c is very small. It seems that at this time a more critical investigation of Eqs. 17 and 34 and their derivation is not justified, and that, for all or most practical purposes one can assume $\omega_s = \omega_c$.

2. Inherent Vortex Shedding Frequency Larger Than Vibration Frequency. Amplitude Effects Neglected.

When the flow velocity is increased moderately above the level where ω_g was equal to ω_s, extensive experimental evidence indicates that the vortices will continue to be shed at or near the natural frequency of the cylinder, provided that the cylinder is not held fixed. The model proposed in this study indicates that a fluid will be excited at a frequency below its natural frequency, and that the phase angle $\alpha < 90°$.

For clarity, let us assume for the initial discussion that the amplitudes of vibration remain negligibly small compared to the cylinder diameter, thus $\omega_g = \omega_f$. Let us start with $\omega_g = \omega_s$ and examine what is predicted by the model as the flow velocity is increased in accordance with Method A. At $\omega_g = \omega_s$, only the power spectral density, represented by the a/D term in Eq. 28 is effective. As the flow velocity is increased, the $\cos\alpha$ term increases from zero and brings the $L_sQ_c/2kD$ term into effect ($\omega_s = \omega_c$ for all practical purposes). For any substantial increase of amplitude to occur, this term must be larger than a/D, in other words: the amplitude created by the lift forces, if and when allowed to act, must be larger than the amplitude extracted from the power spectral density of the random vibration when acting alone. In many practical situations, this is evidently the case.

Let ω_g be increased only very slightly beyond ω_s, perhaps to ω_c. The powerful $\cos\alpha$ function can influence the amplitude so greatly that a casual observer, relating "resonance" with ω_c rather than ω_s, may get the impression that the amplitude increases before the resonance frequency is reached.

As the ω_g/ω_s ratio increases with increasing flow the amplitude reaches a maximum. Assuming that the contribution of the random vibration is negligible at this point, (and remembering that $\omega_g = \omega_f$ for this consideration), the maximum amplitude ε_m occurs when

$$\tan\alpha_m = \frac{1}{Q_g\left[\left(\frac{\omega_g}{\omega_s}\right)_m - \left(\frac{\omega_s}{\omega_g}\right)_m\right]} = \left[\frac{3 - \left(\frac{\omega_g}{\omega_s}\right)_m^2}{3\left(\frac{\omega_g}{\omega_s}\right)_m^2 - 1}\right]^{1/2} . \tag{35}$$

Given Q_g, this equation is readily solved by trial and error for $(\omega_g/\omega_s)_m$. This angle α_m, determined subsequently, is seen to be less than 45°.

As the flow is further increased, the $\sin\alpha$ term decreases the influence of the lift term and the power spectral density comes into prominence again. Theoretically, the amplitude decreases towards the level it had when $\omega_g = \omega_s$, multiplied only by the square of the flow velocity ratio since we are considering Method A.

The preceeding prediction is theoretical. Ample experimental evidence indicates that at a certain ω_g/ω_s ratio the vortex shedding frequency suddenly unlocks from ω_s and the vortices begin to shed at the inherent frequency ω_f. It thus appears that as the lift influence is reduced, a certain level is reached beyond which the power spectral density effect begins to dominate. One surmises that as soon as the frictional force tie can be overpowered, the fluid liberates itself from the grip of the cylinder and extracts energy via the power spectral density function Φ_f at what this study proposes to call its inherent natural frequency, and the vortex shedding proceeds at the frequency ω_f predicted by Eq. 1. One can speculate that Eq. 28 may provide a clue or perhaps even a criterion on when the unlocking process can be expected. There is a possible additional complication, in that the unlocking point may be influenced by the direction from which it was approached, i.e. a hysterisis effect as mentioned in Ref. 4.

3. Inherent Vortex Shedding Frequency Larger Than Vibration Frequency. Amplitude Effects Considered.

The contribution of the amplitude to the inherent vortex shedding frequency, ignored in the previous section, will now be considered. For clarity Eq. 28 is restated as

$$\frac{\varepsilon}{D} = \left(\frac{\omega_g}{\omega_s}\right)^2 \left(\frac{\omega_f}{\omega_g}\right)^2 H \quad , \tag{36}$$

where

$$H = \frac{L_s Q_c \omega_c}{2kD\omega_s} \sin\alpha \cos\alpha + \left[\left(\frac{L_s Q_c \omega_c}{2kD\omega_s} \sin\alpha \cos\alpha\right)^2 + \left(\frac{a}{D}\right)^2\right]^{1/2} \quad . \tag{37}$$

Substituting Eq. 36 into Eq. 33 and solving for ω_f/ω_g results in

$$\frac{\omega_f}{\omega_g} = \frac{1}{1 - n\left(\frac{\omega_g}{\omega_s}\right) H^{1/2} \cos\alpha} \quad . \tag{38}$$

Combining Eqs. 36 and 38 provides

$$\frac{\varepsilon}{D} = \frac{\left(\frac{\omega_g}{\omega_s}\right)^2 H}{\left[1 - n\left(\frac{\omega_g}{\omega_s}\right) H^{1/2} \cos\alpha\right]^2} \quad . \tag{39}$$

At this point, it must be realized that the computational process may be utilized in two ways, synthesis and analysis. In other words, respectively, given input data can be employed to predict a vibration

performance or existing experimental data can be used to estimate and analyze what the input quantities may have been. The author has to admit that he has not used the proposed model to predict performance but has used it to analyze experimental data as previously stated.

To predict vibration performance, the values of (L_sQ_c/kD), n, Q_g, and a must be given. The general amplitude versus frequency curve is obtained by choosing sets of α and (ω_g/ω_s) values (related by Eq. 7, ω_g/ω_s can be expressed as a function of α and Q_g) as the independent variable and solving Eqs. 38 and 39. The procedure is straightforward provided one assumes that $\omega_s = \omega_c$ which is expected to be satisfactory for most if not all practical applications.

The magnitude of the maximum amplitude is of interest, however the associated frequency cannot be directly determined unless "a" is taken to be zero. Since at maximum amplitude there will generally prevail conditions resulting in substantial amplitude magnification, the contribution of the power spectral density can either be neglected or, to be conservative, can be adjusted for by a slight upward adjustment of the $(L_sQ_c/2kD)$ ratio to be able to omit the $(a/D)^2$ in Eqs. 28 or 37. Taking $\omega_s = \omega_c$ simplifies Eq. 37 to

$$H = \frac{L_sQ_c}{kD} \sin\alpha \cos\alpha \quad . \tag{40}$$

With the above assumptions it can be shown that the maximum amplitude ε_m occurs when the following equation is satisfied:

$$1 - \frac{2}{Q_g\left[\left(\frac{\omega_g}{\omega_s}\right)_m + \left(\frac{\omega_s}{\omega_g}\right)_m\right]\tan\alpha_m} = 2\sin^2\alpha_m \left\{1 + n\left(\frac{L_sQ_c}{kD}\right)^{1/2}\left(\frac{\omega_g}{\omega_s}\right)_m \sin^{\frac{1}{2}}\alpha_m \cos^{\frac{3}{2}}\alpha_m\right\} \tag{41}$$

This equation must be solved by trial and error simultaneously for α_m and $(\omega_s/\omega_s)_m$, which of course are not independent but related by Eq. 7. However, this process is not difficult at all if one solves for α_m, because (ω_g/ω_s) and $(\sin\alpha \cos\alpha)^{1/2}$ can be expected to be very weak function of this angle which will be somewhat less than 45°. Note that Eq. 41 is equivalent to Eq. 35 when n = 0.

Let us now turn to the analysis of the existing experimental data presented by Di Silvio. This task was initiated by determining the frequency ratio $(\omega_f/\omega_s)_m$ at the occurrence of the maximum amplitude from these data. Prior to solving, Eq. 41 was equipped with

$$n = \frac{\left(\frac{\omega_f}{\omega_s}\right)_m \left(\frac{\omega_s}{\omega_g}\right)_m - 1}{\left(\frac{\varepsilon_m}{D}\right)^{1/2} \cos\alpha_m} \tag{42}$$

and

$$\left(\frac{L_s Q_c}{kD}\right)^{1/2} = \frac{\left(\frac{\varepsilon_m}{D}\right)^{1/2}}{\left(\frac{\omega_f}{\omega_s}\right)_m \sin^{1/2}\alpha_m \cos^{1/2}\alpha_m} \tag{43}$$

to provide

$$1 - \frac{2}{Q_g\left[\left(\frac{\omega_g}{\omega_s}\right)_m + \left(\frac{\omega_s}{\omega_g}\right)_m\right]\tan\alpha_m} = 2\sin^2\alpha_m\left[2 - \left(\frac{\omega_g}{\omega_s}\right)_m\left(\frac{\omega_s}{\omega_f}\right)_m\right] . \tag{44}$$

Note that Eq. 44 is independent of the amplitude ε_m. What is required, however, is an estimate of Q_g. The influence of this factor is discussed in the section concerned with the analysis of the experimental data. With the experimental $(\omega_f/\omega_s)_m$ value it is then possible to solve Eq. 44 for α_m and $(\omega_g/\omega_s)_m$, these values are entered in Eqs. 42 and 43 to determine n and (L_sQ_c/kD), these in turn are used to compute the amplitude versus frequency curve as previously described. It is to be remembered that Eqs. 40 through 44 assume that a = 0.

To analyze existing data for $a/D \neq 0$ this author solved Eqs. 42, 43, and 44 as described above for a/D = 0 and assumed the α_m and n values to remain unchanged for $a/D \neq 0$. Calling the (L_sQ_c/kD) parameter obtained from Eq. 43 $(L_sQ_c/kD)_{a=0}$, an adjusted value of this parameter was computed from

$$\left(\frac{L_s Q_c}{kD}\right)_{a/D} = \left(\frac{L_s Q_c}{kD}\right)_{a=0} - \frac{(a/D)^2}{\left(\frac{L_s Q_c}{kD}\right)_{a=0}(\sin\alpha_m\cos\alpha_m)^2} . \tag{45}$$

All the above discussion refer to a Method A approach. Utilization of a Method B approach simplifies the mathematics, because $\alpha_m = 45°$ under all conditions.

4. Inherent Vortex Shedding Frequency Smaller Than Vibration Frequency.

When the flow velocity is lowered (considering Method A) so that the inherent vortex shedding frequency ω_g falls below the natural frequency ω_s of the system, the effect of the negative $\cos\alpha$ term ($\alpha > 90°$) quickly reduces the amplitude below the level "a" determined by the power spectral density contribution. Because of the increased effective damping the amplitude of vibration is small, ω_f/ω_g does not deviate much from unity. With only minor influence exerted by the ω_f/ω_g term, the angle α will move very quickly toward 180° as a function of ω_g/ω_s alone. Again the decreasing $\sin\alpha$ function brings the power spectral density

contribution into dominance, but at a ω_f/ω_s ratio that is much closer to unity than is the case when ω_f/ω_s is larger than 1. This could explain the experimentally observed phenomena of locked in vibration during only a narrow frequency span below ω_s, beyond which the vortex shedding prevails at the inherent frequency ω_f. Since the frequency ratio ω_f/ω_s is still quite close to unity even after unlocking has taken place, the observance of beat phenomena (Ref. 1) is perhaps not unexpected.

VI. ANALYSIS OF EXPERIMENTAL RESULTS AND CONCLUSION

As already mentioned in the introduction, the mathematical model proposed herein will now be applied to the experiment conducted by Ferguson and Parkinson (Ref. 1) and reported and analyzed by Di Silvio (Ref. 2).

The experimenters exposed an elastically supported cylinder in a low speed wind tunnel and determined the amplitude of the transverse cylinder vibrations, frequency of both vortex shedding and the cylinder vibration, and the phase angle between lift and displacement. For the calculations of this investigation, reference conditions were established at a flow velocity of U_s = 11.5 ft/sec = 3.5 m/sec, which is related by a Strouhal number of 0.196 to the 9.0 Hz vibration frequency that the cylinder experienced under almost all test conditions. With this reference value, the data plotted on Fig. 3 of Di Silvio's Ref. 2 indicate that a maximum deflection ε_m = 0.29 D occurred at U_f/U_s = 1.22 at U_f = 4.27 m/sec. This U_f/U_s value was taken to be equal to $(\omega_f/\omega_s)_m$.

The model did require the assumption of a value for the fluid damping as represented by the factor Q_g. It was found that a value of Q_g = 20 would provide a reasonable match with the experimental data. Using this value and $(\omega_f/\omega_s)_m$ = 1.22, and taking "a" to be zero, a phase angle α_m = 39.6° was determined from Eq. 44. Subsequently, the experimental ε_m/D = 0.29 value was used to obtain n = 0.442 and (L_sQ_c/kD) = 0.397 from Eqs. 42 and 43; these parameters provided a match at the point of maximum amplitude. Estimating a slight power spectral density contribution a/D = 0.02 resulted in (L_sQ_c/kD) = 0.393 (Eq. 45). The amplitude and ω_f/ω_s frequency computations were performed and plotted on Fig. 4. The consideration of a/D = 0.02 lifted the skirts of the curve accordingly but did not have much effect on the peak. Also shown on Fig. 4 are the data points presented by Di Silvio on Fig. 3 of his paper. It is seen that fair agreement is obtained.

The experimental data indicate the vortex shedding was at least partially locked to the cylinder vibration frequency between the approximate limits of U_f = 3 and 4.8 m/sec which correspond to ω_f/ω_s = 0.86 and 1.37, respectively. The corresponding phase angles α would have been approximately 168° and 8° respectively, whose $\sin^2\alpha$ $\cos^2\alpha$ functions (see Eq. 28) cannot be said to be in agreement but still indicate a trend with respect to the locking criterion discussed in earlier sections. As far as phase angles are concerned, the calculated α values crudely match the graphical data of Refs. 1 and 2, which show an approximate 45° relationship (135° in terms of these references' definition) at the frequency ratio associated with the maximum amplitude.

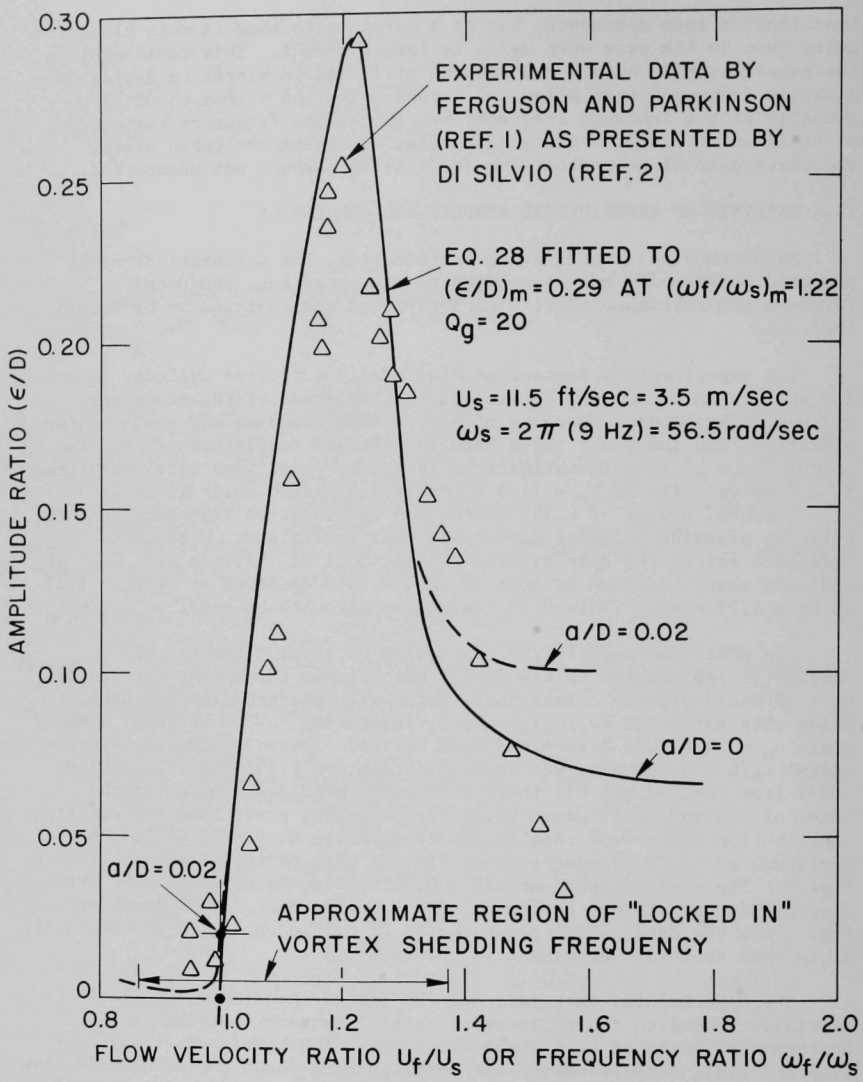

Fig. 4. Vibration Amplitude versus Flow Velocity

This author will readily admit that the selection of Q_g was made with some discretion. Choice of a larger or smaller value would have narrowed or broadened the peak, respectively. As a matter of fact, a higher Q_g value will actually move the right side of the curve sufficiently to the left to create an "overhang" of the peak and suggest abrupt changes or instabilities, depending from which direction the peak is approached. This indeed has been observed and reported as a "hysterisis" or "jump" phenomena by Parkinson, Feng, and Ferguson in Ref. 8, these data just recently came to the attention of this author and will be studied as soon as possible. In the future it may be possible to establish a valid Q_g value, if not by direct determination then perhaps by relation of experimental results. With respect to "overhang," it may be shown that when "a" = 0 this will occur if

$$Q_g n \left(\frac{L_s Q_c}{kD}\right)^{1/2} > 9.61 \quad , \tag{46}$$

however freedom of "overhang" is not guaranteed by a reversed inequality even though the exact criterion is probably not too distant.

At this point, it is interesting to examine the experimental stiffness and damping components presented by Jones in Figs. 10a and 10b of Ref. 9 (reproduced as Fig. 10 and correlated on Fig. 37 by Ref. 5) and to note the qualitative agreement with the respective $L \sin^2\alpha$ and $L \sin \alpha \cos \alpha$ relationships proposed by this study.

In conclusion, in spite of the uncertainty that exists about the choice of the proper Q_g value, and about the effective vortex shedding frequency correction, and beyond that about the many other assumptions made to establish this oversimplified model, the basic character of the proposed model has been clearly demonstrated. Endeavoring to represent experimentally observed cross-flow induced vibration performance of a circular cylinder, this analytical model offers the following features:

1. Frequency band of "locked-in" cylinder and vortex-shedding oscillations straddling the natural frequency of vibration of the cylinder.

2. Proper trend of phase angle relationships.

3. Adjustment for the effects of cylinder amplitude on vibration.

4. Estimate of the maximum value of the vibration amplitude versus flow velocity curve at a flow velocity corresponding to an inherent vortex shedding frequency larger than the actual frequency of the cylinder and the locked-in vortex shedding.

5. Vibration frequency slightly smaller than the natural frequency of the cylinder when immersed in stagnant fluid.

6. Effect of fluid (or system) damping that may explain the "hysterisis" or "jump" phenomena.

7. Reasonably clear identification of the influence of the basic parameters on the performance of the system.

Acknowledgment

This work was performed under the sponsorship of the Special Technology Branch, Division of Reactor Development and Technology, U. S. Atomic Energy Commission.

References

1. Ferguson, N., and Parkinson, G. V., "Surface and Wake Flow Phenomena of the Vortex-Excited Oscillation of a Circular Cylinder," Journal of Engineering for Industry, Trans. ASME, Series B, Vol. 89, Nov. 1967, pp. 831-838.

2. Di Silvio, G., "Self-Controlled Vibration of Cylinder in Fluid Stream," Journal Engineering Mechanics Div., ASCE, Vol. 95, No. EM2, April 1969, pp. 347-361.

3. Toebes, G. H., and Ramamurthy, A. S., "Fluidelastic Forces on Circular Cylinders," Journal Engineering Mechanics Div., ASCE, Vol. 93, No. EM6, December 1967, pp. 1-20.

4. Bishop, R. E. D., and Hassan, A. Y., "The Lift and Drag Forces on a Circular Cylinder Oscillating in a Flowing Fluid," Proceedings of the Royal Society, London, Series A, Vol. 277, 1964, pp. 51-75.

5. Hartlen, R. T., Baines, W. D., and Currie, I. G., "Vortex-Excited Oscillations of a Circular Cylinder," University of Toronto, UT Mech E, TP 6809, November 1968.

6. Wambsganss, M. W., Argonne National Laboratory, internal communication.

7. Marris, A. W., "A Review on Vortex Streets, Periodic Wakes, and Induced Vibration Phenomena," Journal of Basic Engineering, Trans. ASME, Series D, Vol. 86, June 1964, pp. 185-196.

8. Parkinson, G. V., Feng, C. C., and Ferguson, N., "Mechanisms of Vortex-Excited Oscillation of Bluff Cylinders," Symposium on Wind Effects on Buildings and Structures, Loughborough University of Technology, April 1968.

9. Jones, G. W., Jr., "Unsteady Lift Forces Generated by Vortex Shedding About a Large, Stationary, and Oscillating Cylinder at High Reynolds Numbers," ASME Paper 68-FE-36, May 1968.

DISCUSSION

D. R. Miller (GE-KAPL): I'd just like to say it's very impressive.

Halle: Well, thank you. We hope to do some experimentation these days and maybe we can show some of these things, but I've been forewarned by Dr. Toebes here, who has eleven years of experience in this fields, that this can be quite a job and maybe we can learn from him to avoid some of the pitfalls.

R. R. Rippel (GE-KAPL): I noticed on your plots of amplitude versus frequency that your amplitude increases from unity right up to a maximum at 1.2. It seemed that the previous paper by Dr. Gerlach indicated that the amplitude started to increase at a lower frequency, and I was wondering if Dr. Gerlach could comment on that aspect.

Halle: One comment I might make is this: We have the curve here, and I actually have used ω_s which is a system frequency, the actual vibration of the cylinder. But this is not necessarily the natural frequency of vibration of the cylinder. The natural frequency of vibration of the cylinder can be a little bit larger. As a matter of fact, the paper gives the formula for this system frequency which is

$$\omega_c\left(1 - \frac{L \sin^2 \alpha}{\epsilon k}\right)^{\frac{1}{2}} .$$

Remember that this correction results from the consideration of the mass component. Now what I said essentially is that this is a very small correction. It may not be for water. I'm not so sure for air, either, but judging from the experimental results, I more or less neglected this. On the other hand, since these are very steep functions, the casual observer may look for his natural frequency here at ω_c, and if here at ω_s is our reference point, it is possible that at ω_c you have already some amplitude, and this may be what you are seeing.

INTRODUCTION TO SESSION 3

M. Bender
Oak Ridge National Laboratory
Oak Ridge, Tennessee

From yesterday's discussion, one must recognize that in any nuclear reactor system there are many types of vibration problems. Yesterday, we heard a lot about near-field vibration. Today we will hear something about far-field vibration. What we must recognize is that because the variety of problems is so great, the investigational techniques are equally varied. Most of us who are familiar with these systems are satisfied that there are a number of techniques that have to be used. The ones we heard about yesterday were divided into two categories, the first one being the kind of vibrational problems pertaining to nuclear control elements and fuel assemblies, and the other pertaining to heat exchangers. These have been two of the more chronic problem areas in nuclear systems. While listening to Nick Grossman yesterday, I tried to remember how many reactor systems have been built without any vibrational problems. I did not recall any, so it is fairly evident that we have not come very far toward licking the problem since the days of the MTR, when people worried about fuel plate vibration. Moreover, the effort so far has concentrated on problems pertaining to fuels; it has been only in the last two or three years that people in the nuclear business began to recognize that other structures were equally problematical.

Before getting into the subject matter of this meeting today, I thought I might review for you why things are different in different parts of reactors. Mr. Corr has been kind enough to draw a reactor vessel on the board showing that it has a core structure with fuel elements and control plates inside, and heat exchangers usually outside. You will hear something this morning about steam separators which exist in the upper area above the core and you may also hear something about thermal shields and shrouds which surround the cores. Generally speaking, most of us look at these as different kinds of flow regimes. The fuel elements usually operate with fluid velocities of about 30 to 50 feet per second (a fairly common range), and Reynolds numbers of the order of 100,000. Consequently, we become interested in a whole range of frequencies--50 cycles per second in the lower region and maybe 2,000 in the upper region. But certainly one is interested in vibration effects over this entire frequency range. That is one reason why in the investigations concerning fuel assemblies people frequently want to know what the energy inputs are doing and how the fine structure of the fuel is responding. Because of this, the highly refined experimental techniques that were described yesterday have a tremendously important place in the experimental programs. But people tend to confuse

the value of these techniques with what might be done with components that are outside the core structure.

Another area that we heard about yesterday is heat exchangers. Those designing heat exchangers ten years ago thought five feet per second was a fairly good flow rate to work with. Numbers of about that value (6, 7, or 8 feet per second) for water systems were quite common, but now we are seeing designs that approach 15 feet per second. Rates may be going even higher in sodium-cooled systems.

Higher flow rates cause increased Reynolds numbers and more energy has to be absorbed in the structural systems. Problems arise when one reaches the point where the energy input into the heat exchanger causes an important vibrational response in the tube bundle structure. The structure will respond in the frequency range of about 10 to 100 cps. I will not speculate on whether this is the absolute upper limit or the lower limit, but it is the general range.

Typically, the direction of fluid flow in reactor cores is parallel to the axis of the core and the vibrational mechanism is introduced by local disturbances in the flow path or perhaps instability in the flow passage that may cause cyclic drag and pressure forces. In most heat exchangers where vibration is a matter of conern, the flow moves perpendicular to the axis of a tube bundle with the result that vortex shedding at low flow rates is the most common cause of vibrations. Both parallel and transverse flow conditions exist in these flow systems but in the discussions thus far, one or the other is dominant. The final area for consideration covers all of the other potential causes of vibration in combination with the above mentioned. That is the subject of today's discussions.

The subject matter that we will hear about today, some people say, is associated with the design kinds of vibrational problems. I choose to describe it is the vibrational response of miscellaneous structures; structures that have no well-defined geometry that is predictable in advance and useful for experimental purposes; structures that, because of their size, are generally relatively flimsy and probably thin because of nuclear factors, and are generally associated with rather low fluid flows, something less than 5 feet per second. Nevertheless, they can vibrate and they may transmit their vibrational energy to other components that may have a different vibrational response. The types of structure we are going to hear about today are not generally treated in the same way that one would consider a fuel element; we cannot afford the time, the money, or the experimental work required to treat the problem rigorously. Nevertheless, we have had as many problems with such structures as with any other kind of reactor system component. People have tended to handle these problems on a qualitative basis by rather simple methods. I suppose if one anticipated many such structural problems, he might want to tackle the design problems on the basis of a very generalized analysis of the structure and the fluid system. There may be some hope of using this approach.

We will hear something about all of these matters this morning.

BIG ROCK POINT VIBRATION ANALYSIS

J. E. Corr

Manager, Materials and Mechanics Development Engineering
Atomic Power Equipment Department
General Electric Company
San Jose, California

ABSTRACT

Industry experience has not been free of nuclear reactor vibration problems. This specific case of a General Electric-designed plant concerns the diagnosis and remedial action based on mathematical analysis. Subsequent longterm operation has confirmed the validity of the solution.

The thermal shield configuration of the Big Rock Point nuclear reactor is unique among General Electric designs. It is a cylindrical shell 92" long by 102-7/8" O. D. It is supported at its bottom so that there is a 1-1/2" water filled annulus between it and the reactor pressure vessel wall. Originally, a 3/8" X 2-3/16" Belleville washer element served as a bottom seal to prevent water from by-passing the core. See Figure 1.

In September 1964, several thermal shield retainer bolts were found to be broken. In consequence, the support structure was stiffened by a factor of over 100. The modification required precision machine work under thirty feet of water and is described elsewhere (1). The problem was generally considered due to a flow induced vibration mechanism and so the reactor was instrumented for its restart in April, 1965. Two runs to maximum attainable core pressure drop of 12 psi revealed no vibration (i.e. less than 50 μ in.). During the next run, the shield displayed low level "nervousness" at 4 Hz and at maximum flow suddenly began to oscillate at about 25 mils amplitude. One pump was tripped and the amplitude dropped by 20%; following trip of the other pump the amplitude decayed with a log decrement of about 0.4 (Figure 2). The shield was brought into vibration twice more before this test series was ended.

The vibration was characterized by:

1. Shield rigid body transverse translation such that its center described an elongated ellipse.

2. Intolerably large amplitude.

3. Symptoms of self-excitation:

   a. The initial low level nervousness indicated decreasing damping with increasing flow.

   b. Sudden onset of high level response.

   c. Highly nonlinear: a major flow reduction had only a minor effect on response. Vibration frequency changed from 4.1 Hz to 3.7 Hz as the amplitude increased.

4. Incidence of vibration was flow (or pressure drop) dependent.

5. Vibration decayed with a very high damping.

6. There was no core pressure drop variation at or near shield frequency.

7. Reactor flow vs. pressure drop characteristic changed during the tests so as to suggest increased leakage.

Since the shield support fatigue usage at 25 mils amplitude was 1% per minute, it was clear that a serious problem had been uncovered. In response, a four pronged attack was launched to: (1) determine the cause of vibration, (2) analyze one hypothesized case, (3) modify the design, and (4) improve the follow-on test program.

Many possible sources of vibration stimuli were hypothesized, but most could be ruled out by data from the initial tests and will not be treated further here. The analyses of what was later shown to be the true cause of the vibration is given in the Appendix. What follows deals with the follow-on test program.

It was early surmised that the annulus seal might leak at higher core flows and provide a self-excitation mechanism by the coupling between its variable leakage and changing shield displacement. This seal is shown in detail in Figure 1. It was decided to check this theory by immobilizing the seal ring with twelve assemblies of three one-inch thick plates tied together by cable and lowered into the annulus to rest upon the seal ring. The three plates "stacked" haphazardly in the annulus leaning against the shield and vessel walls. With these assemblies in place, the shield was "dead" over the entire flow range. This agreed with theory, but left the question open as to whether the weights simply immobilized the shield - rather than the seal ring.

Another device for checking the seal leakage hypothesis was an inflatable rubber "inner tube" which was constrained to fit in the annulus near the top of the shield. It was theorized that the rubber tube, when inflated, would prevent flow through the lower seal and thus destroy its excitation mechanism. Similarily, when deflated, the rubber seal would leak and permit the lower seal to produce high level self excitation of the shield. However, only low level "nervousness" was noted with the seal deflated. This disappointing result was later explained by analysis (see Appendix).

The most significant analytical result is presented on Figure 3 which depicts hydrodynamic damping due to seal leakage as a function of core pressure drop. It is seen that the original design was unstable even for small leakage flows, while the modified design had a wider range of stability and produced high damping for small seal leakage. The change was in the proper direction, but didn't go quite far enough to preclude further trouble. With this result in hand, the direction of a repair program became clear:

1. Immobilize the bottom seal (it was done with wedges).

2. Install a top seal (shown to be stable by analysis - see Appendix).

3. Insert the hold-down weights to immobilize the shield and interrupt annulus flow.

It is considered that anyone of the above modifications would have sufficed to eliminate the problem. Inspections made since the reactor returned to service in September 1965, have supported the adequacy of the above "fix".

ACKNOWLEDGMENT

The writer wishes to gratefully acknowledge the many helpful discussions with S. W. Tagart during the troublesome period described in this paper, as well as the excellent support of E. C. Eckart in analogue computations, and of R. Plunkett in data interpretation.

REFERENCES

1. Hausler, L. M., Haueter, R. L., and Christianson, R. C., "In Vessel Modification of Irradiated Reactor Internals at Big Rock Point", presented at ANS Conference on Reactor Operating Experience, Grand Teton National Park, Wyo., July 28-30, 1965.

2. Eckert, E. C., Big Rock Point Analog Studies of Thermal Shield Vibration: NUSA-146, May 1965 and July 1965.

APPENDIX

ANALYSIS

The following analysis provides criteria for the stability of small displacements from static equilibrium. For this condition, it is considered valid to linearize the system.

Nomenclature is established below:

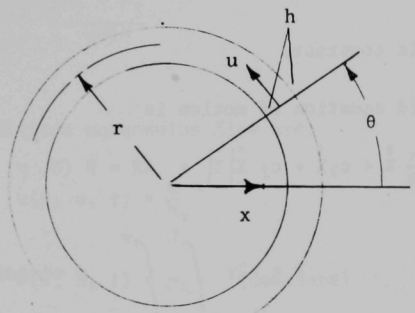

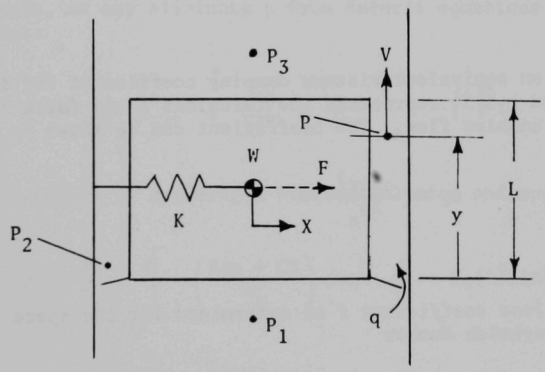

Neglecting velocity variations across the 1-1/2" annulus, the linearized Euler equations for annulus water are:

$$-\frac{1}{\rho r}\frac{\partial p}{\partial \theta} = \frac{\partial u}{\partial t} \tag{1}$$

$$-\frac{1}{\rho}\frac{\partial p}{\partial y} = \frac{\partial v}{\partial t} \tag{2}$$

The continuity equation for small motions ($X << h_o$) is:

$$\frac{1}{r} \frac{\partial u}{\partial \theta} + \frac{\partial v}{\partial y} = \frac{\dot{X}}{h_o} \cos\theta \tag{3}$$

where the annulus width h was defined by

$$h = h_o - X \cos\theta \tag{4}$$

for which h_o is constant.

The shield equation of motion is

$$\frac{w}{g} \ddot{X} + c_1 \dot{X} + c_2 \dot{X}|\dot{X}| + KX = F(\theta, y, t) \tag{5}$$

where

$$F = -2r \int_0^L \int_o^\pi p \cos\theta d\theta dy \tag{6}$$

and c_1 is an equivalent viscous damping coefficient for structural damping and $c_2 \dot{X}|\dot{X}|$ represents the turbulent shear force for circumferential annulus flow. The coefficient can be shown to be estimated by:

$$c_2 = \frac{\rho f L r^3}{3h_o} \tag{7}$$

where the loss coefficient f is determined for the space and time averaged Reynolds Number

$$\bar{\bar{N}}_R = \frac{4r\omega}{\pi^2 \nu} X_o \tag{8}$$

for which X_o is the amplitude of the shield harmonic translation and ω its circular frequency (rad/sec).

The volumetric seal leakage may be represented by the linearized form:

$$q = A - [B\,\Delta p(t) + CX]\cos\theta \tag{9}$$

where,

$$\Delta p = \frac{p_2 - p_3}{\cos\theta} \tag{10}$$

The boundary conditions on annulus flow are:

$$v(\theta,\ o,\ t) = \frac{q}{h_o} \tag{11}$$

$$P(\theta,\ L,\ t) = p_3 \qquad \text{(constant)} \tag{12}$$

The above equations suffice to solve the system and define p or X. For example, we may eliminate p from Euler's equations (1), (2) and show that:

$$\frac{1}{r^2}\ \frac{\partial^2 v}{\partial\theta^2} + \frac{\partial^2 v}{\partial y^2} = 0 \tag{13}$$

This may be solved by assuming a product solution and applying (11) to yield:

$$v = \frac{A}{h_o} + \left[-\left(\frac{B\Delta p + CX}{h_o}\right)\cosh\frac{y}{r} + f_4(t)\sinh\frac{y}{r}\right]\cos\theta$$

which may be used to determine

$$u = f_5(y,t) + \left[\left(\frac{B\Delta p + CX}{h_o}\right)\sinh\frac{y}{r} - f_4(t)\cosh\frac{y}{r} + \frac{rx}{h_o}\right]\sin\theta$$

We may now eliminate u, v from Euler's equations, and integrate to provide

$$p = G_4 + \rho r\left[\left(\frac{B\Delta\dot{p} + C\dot{X}}{h_o}\right)\sinh\frac{y}{r} - f_4\cosh\frac{y}{r} + \frac{r\ddot{X}}{h_o}\right]\cos\theta$$

After applying the second boundary condition (12) we find

$$p = p_3 + \frac{\rho r}{h_o}\left\{(B\Delta p + CX)\sinh\frac{y}{r} - \left[r\ddot{X} + (B\Delta\dot{p} + C\dot{X})\,\mathrm{Sinh}\,\frac{L}{r}\right]\frac{\cosh\frac{y}{r}}{\cosh\frac{L}{r}} + r\ddot{X}\right\}\cos\theta \tag{14}$$

By (10) and since $p_2 = p(\theta, o, t)$, we may replace (14) by

$$\Delta\dot{p} + \xi_1\Delta p = \xi_2\ddot{X} + \xi_3\dot{X} \quad , \tag{15}$$

where

$$\xi_1 = \frac{h_o}{\rho r b \tanh\frac{L}{r}}\ ; \quad \xi_2 = \frac{\cosh\frac{L}{r} - 1}{\sinh\frac{L}{r}}\ ; \quad \xi_3 = -\frac{C}{B}$$

Tests showed that X was a simple harmonic function, even for large amplitudes, so we may assume that

$$X = X_o \sin\omega t \tag{16}$$

$$\Delta p = \Delta p_1 \sin\omega t + \Delta p_2 \cos\omega t \tag{17}$$

The above relations may be used to establish $\Delta p(X)$. After eliminating Δp from (14), we finally have the dynamic pressure distribution:

$$p = p_3 + \frac{\rho r}{h_o}\left[r\left\{1 - \frac{\cosh\frac{y}{r}}{\cosh\frac{L}{r}} + \rho B\tanh\frac{L}{r}\left[\frac{\rho r^2\omega^2(1-\mathrm{sech}\,\frac{L}{r})B - h_o C}{h_o^2 + (\rho\omega B\tanh\frac{L}{r})^2}\right] \times \left(\mathrm{Sinh}\,\frac{y}{r} - \tanh\frac{L}{r}\cosh\frac{y}{r}\right)\right\}\ddot{X}\right.$$

$$\left. + h_o\left\{\frac{h_o C - \rho r\omega^2(1-\mathrm{Sech}\,\frac{L}{r})B}{h_o^2 + (\rho r\omega B\tanh\frac{L}{r})^2}\right\}\left(\mathrm{Sinh}\,\frac{y}{r} - \tanh\frac{L}{r}\cosh\frac{y}{r}\right)\dot{X}\right]\cos\theta \tag{18}$$

and (6) may be used to define

$$F = -\frac{\pi\rho r^4}{h_o}\left\{\frac{L}{r} - \tanh\frac{L}{r} - \rho B\left[\frac{\rho r^2\omega^2(1\text{-Sech}\,\frac{L}{r})B - h_oC}{h_o^2 + (\rho r\omega B\tanh\frac{L}{r})^2}\right](1\text{-Sech}\,\frac{L}{r})\tanh\frac{L}{r}\right\}\ddot{X}$$

$$-\pi\rho r^3\left[\frac{\rho r^2\omega^2\ (1\text{-Sech}\,\frac{L}{r})B - h_oC}{h_o^2 + (\rho r\omega B\tanh\frac{L}{r})^2}\right](1\text{-Sech}\,\frac{L}{r})\ \dot{X} \tag{19}$$

The shield equation of motion may be written in the form:

$$\ddot{X} + s_1\dot{X} + s_2\dot{X}\left|\dot{X}\right| + s_3 X = 0 \tag{20}$$

where

$$s_1 = \frac{c_1 + c_3}{m} = \frac{1}{m}\left\{c_1 + \pi\rho r^3\left[\frac{\rho r^2\omega^2(1\text{-Sech}\,\frac{L}{r})B - h_oC}{h_o^2 + (\rho r\omega B\tanh\frac{L}{r})^2}\right](1\text{-Sech}\,\frac{L}{r})\right\} \tag{21}$$

$$s_2 = \frac{c_2}{m} \tag{22}$$

$$s_3 = \frac{K}{m} \tag{23}$$

and: $$m = \frac{W}{g} + m' + m'' \tag{24}$$

with

$$m' = \frac{\pi\rho r^4}{ho}\left(\frac{L}{r} - \tanh\frac{L}{r}\right) \tag{25}$$

$$m'' = \frac{\pi\rho r^4 B}{ho}\left[\frac{h_oC - \rho r^2\omega^2 B(1\text{-Sech}\,\frac{L}{r})}{h_o^2 + (\rho r\omega B\tanh\frac{L}{r})^2}\right]\tanh\frac{L}{r}\,(1\text{-Sech}\,\frac{L}{r}) \tag{26}$$

In the above, m' is the virtual mass due to the annulus flow effects and m'''' is the perturbation of the virtual mass due to the effect of seal leakage. It is small relative to m' for cases of interest.

The coefficient s is the sum of structural damping (c_1/m) and damping due to seal leakage (c_3/m).

If we neglect the relatively small effects of structural damping and fluid turbulence shear damping, we may conclude that the thermal shield is stable for small displacements about equilibrium for which

$$c_3 > 0 ,$$

or

$$C < \frac{r^2\omega^2}{ho}(1 - \text{Sech}\,\frac{L}{r})\,B \tag{27}$$

We note that the stability margin increases with shield natural frequency ω, thus, the initial "fix" at Big Rock Point was in the proper direction.

Values for the seal leakage coefficients A, B, C are plotted on Figures 4 to 6. The factor Δp_o is the core pressure drop at which the seal becomes unseated and steady leakage begins. Note that the hydrodynamic effect of seal leakage was to provide a significantly high damping at core pressure drops too low to induce instability, and then a sudden onset of instability - as observed during the plant tests. The two limiting cases of corner and wall flow may be understood by examining Figure 1 for which initially the flow is corner limited and then with further rotation of the seal ring the flow becomes wall limited. This change corresponds to the onset of instability.

A similar analysis was made for the case of a top seal only, as sketched below:

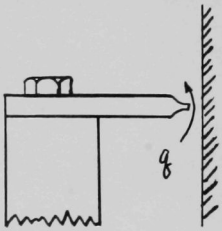

The corresponding hydrodynamic damping value is:

$$c_4 = \frac{\pi\sqrt{2\rho}\,C_d\,r^3}{h_o}\left[\frac{\rho r^2\omega^2}{2}(1-\text{Sech}\,\frac{L}{r})\,\frac{h_o}{\sqrt{\Delta\rho c}} + \sqrt{\Delta\rho c}\right] \tag{28}$$

It is apparent that the value of c_4 cannot be less than zero. Indeed, it represents a powerful hydrodynamic damper.

The case with both top and bottom seals was solved by Eckert using an analogue computer with the results shown by Figure 8. Note that the collapsed rubber tube acted like a top seal and provided sufficient positive damping to override the destabilizing effect of the open bottom seal as observed during the rubber seal test program.

DISCUSSION

M. Bender (ORNL): In attacking a problem like this, where you didn't anticipate it in advance, what kind of analysis would you recommend at the beginning for designating something of that sort?

Corr: Subsequently, we have performed similar analyses in places where we were suspicious, for example, on the KRB reactor at a place where there was leakage. I would say to be alert to the possibility of high-velocity leakage. Wherever you can get a large pressure drop across the leakage path, wherein the effect of changing that pressure drop is reflected into a force, a significant force on the structure, be alert to whether you should try to do an analysis like this. For example, in the KRB reactor, it proved to be unstable, but the damping was so low, that is, the negative damping was so low, that the structural damping was adequate to swamp it out; that wasn't true in the Big Rock case. Any place where you turn a lot of momentum, be careful.

G. H. Toebes (Purdue U.): I would like to reinforce what you said. Wherever you have a seal that is flexible, and which on opening can permit flow, you may have a potential problem. The problem is known since about 10 years in hydroelectric plants where large tunnels have been sealed off with flexible seals. You will find, in the proceedings of the ASME, several papers on the particular subject.

Corr: Butterfly valves, for example, have been notoriously bad.

Bender: What you've seen is a practical solution to a problem that had to be fixed after the fact, and with the variety of problems that one has to anticipate in reactor systems, it would be very desirable if we could ideally have a good generalized solution that would fit any problem.

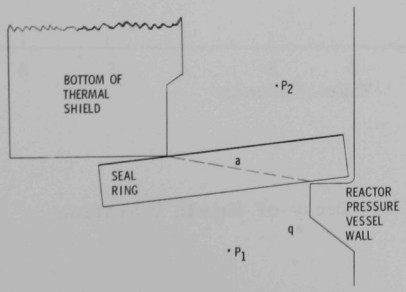

Fig. 1

Annulus Seal

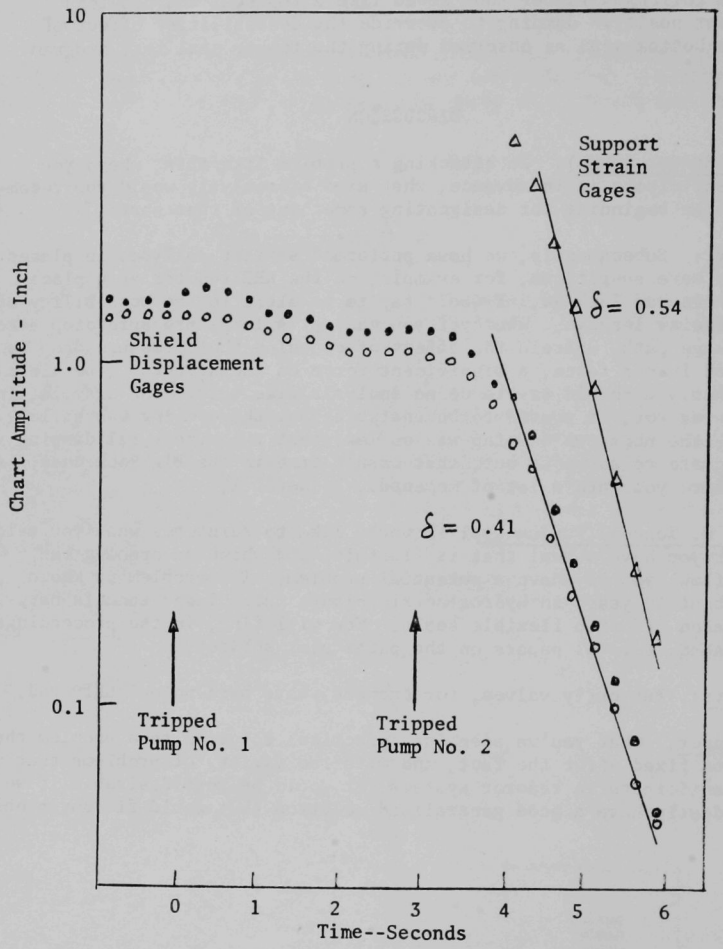

Figure 2. Decay of Shield Vibration

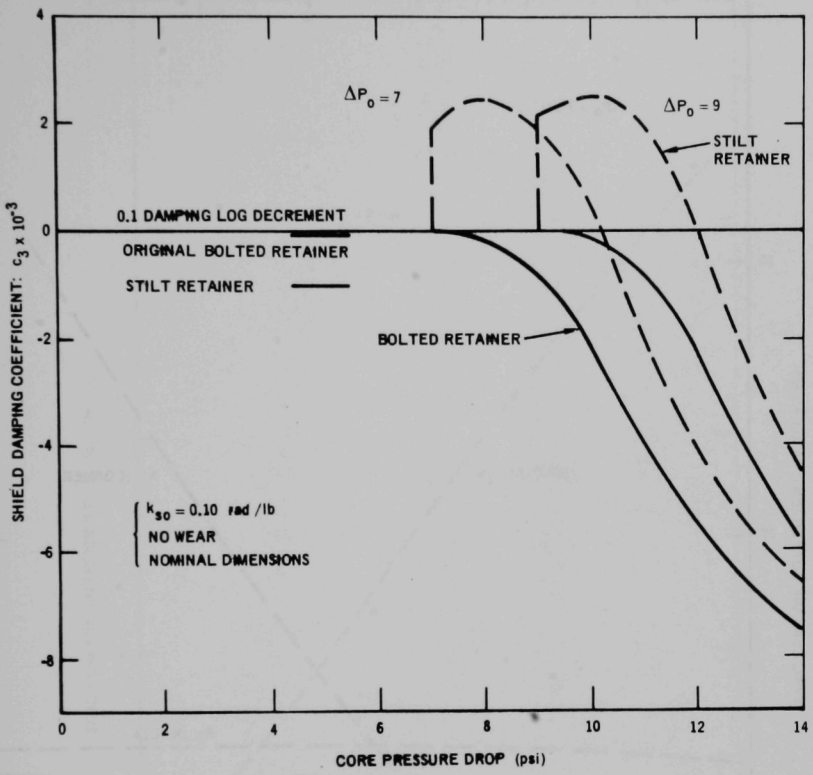

Figure 3. Shield Damping Coefficient Resulting from Annulus Seal Leakage Cold Operation

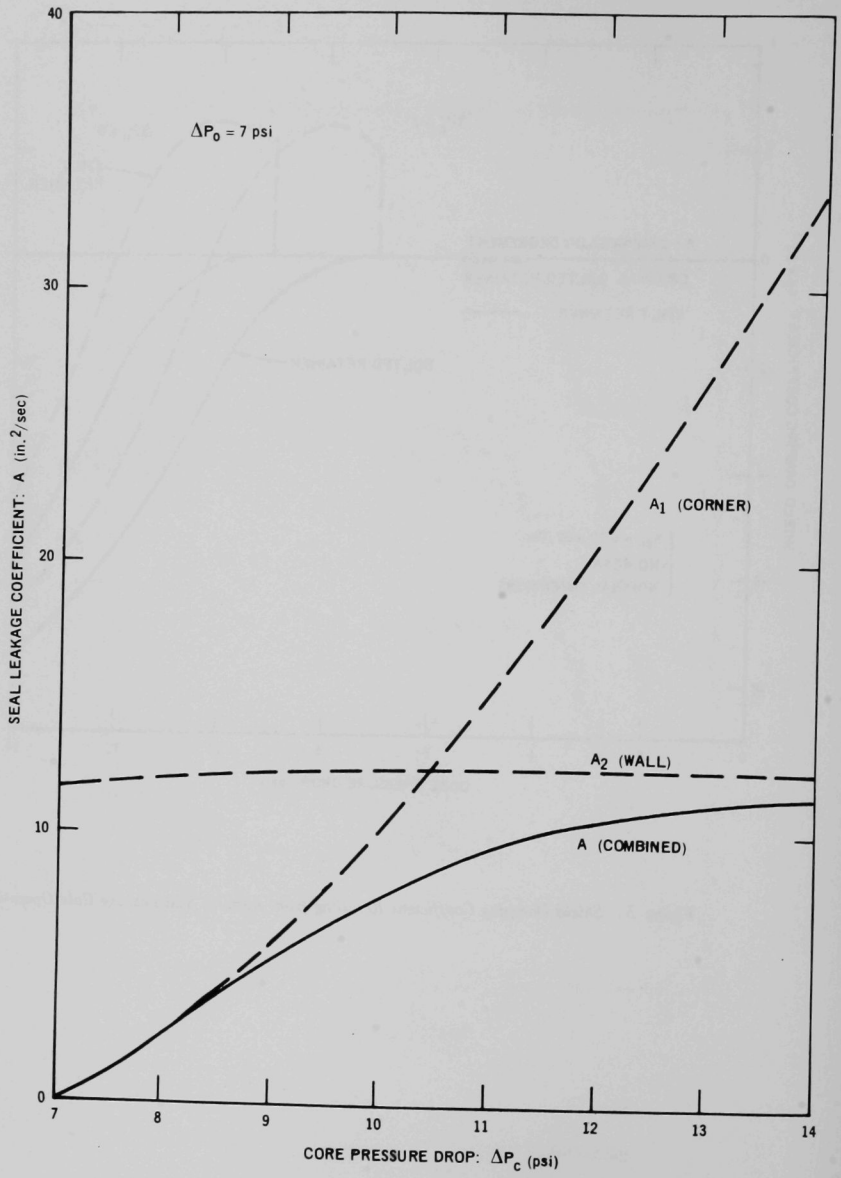

Figure 4. Annulus Seal Leakage Coefficient : A

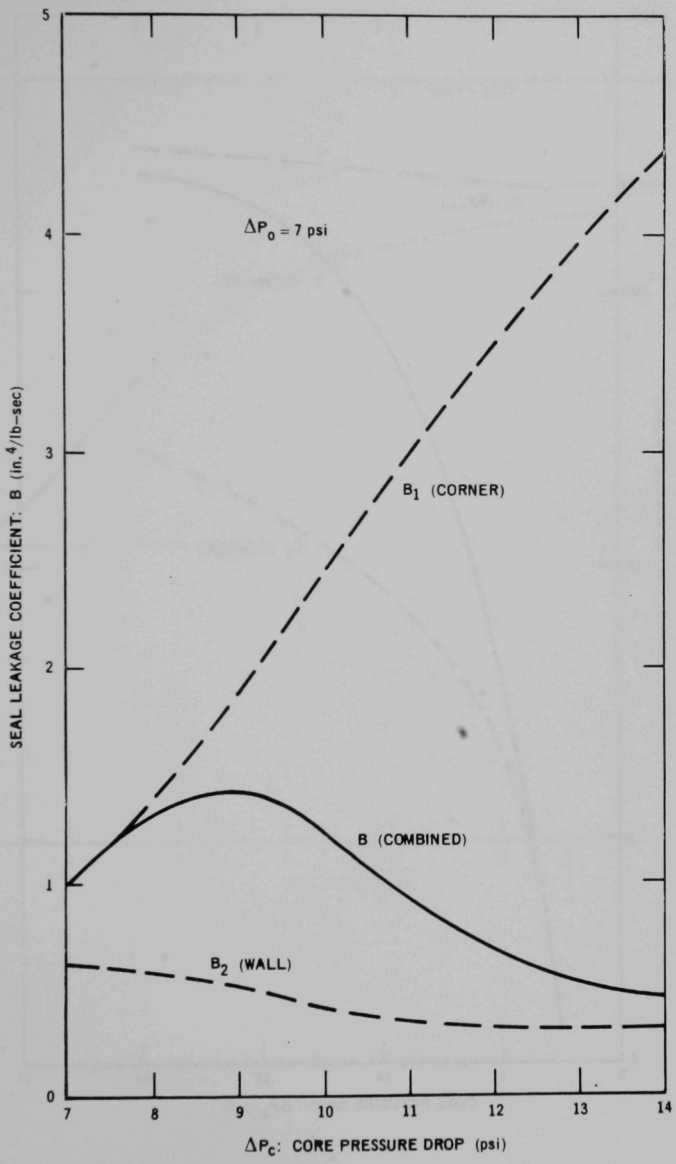

Figure 5. Annulus Seal Leakage Coefficient : B

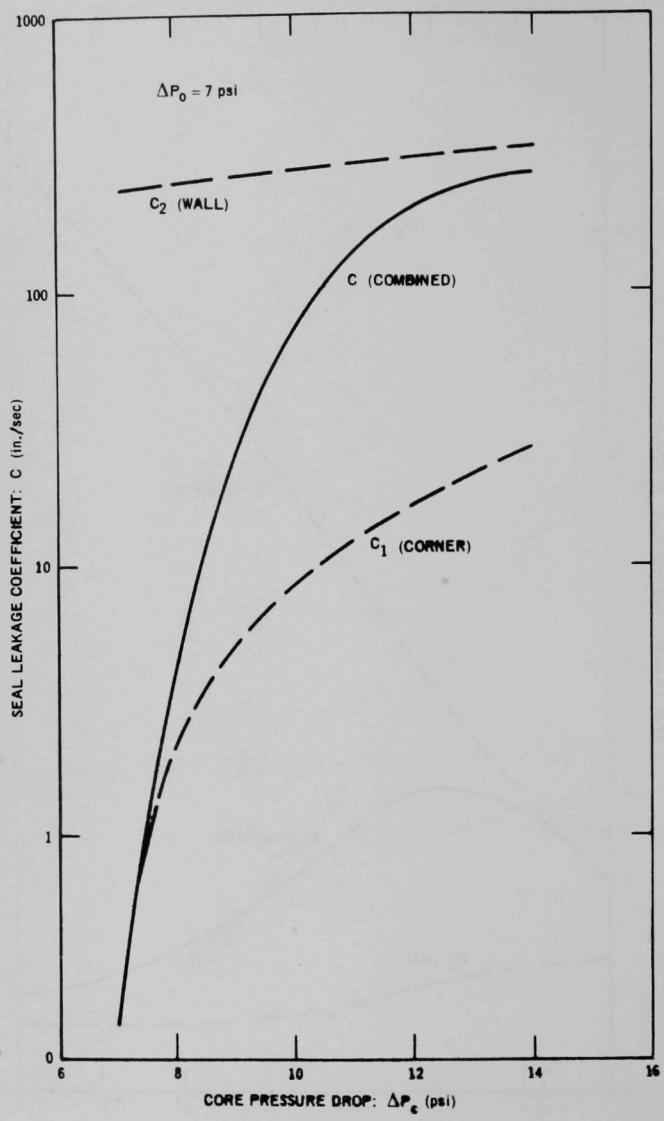

Figure 6. Annulus Seal Leakage Coefficient : C

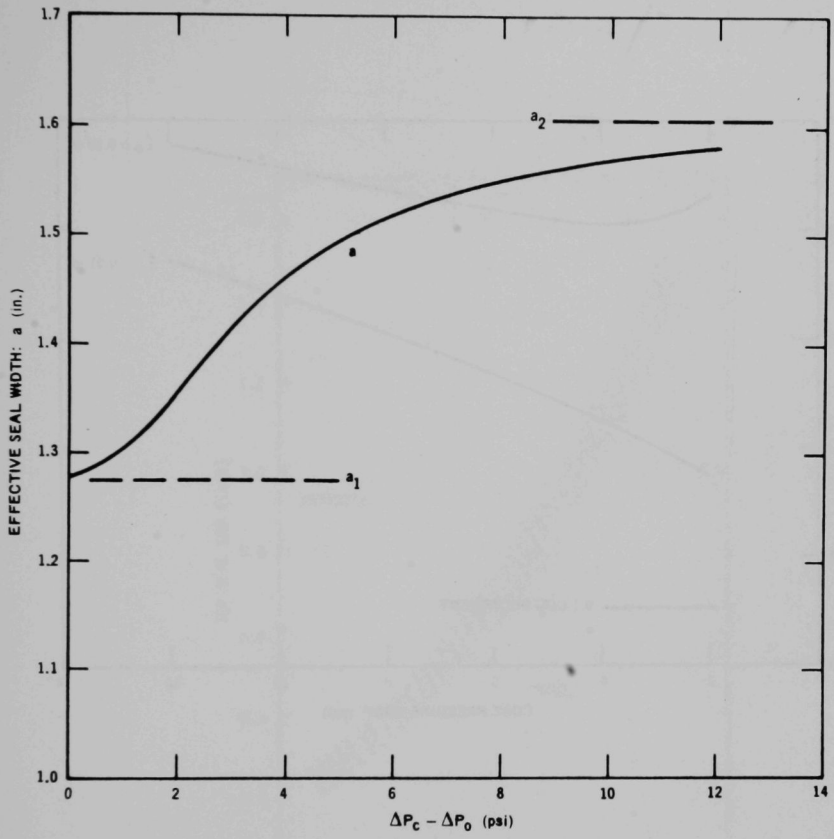

Figure 7. Effective Pressure Exposed Width of Annulus Seal

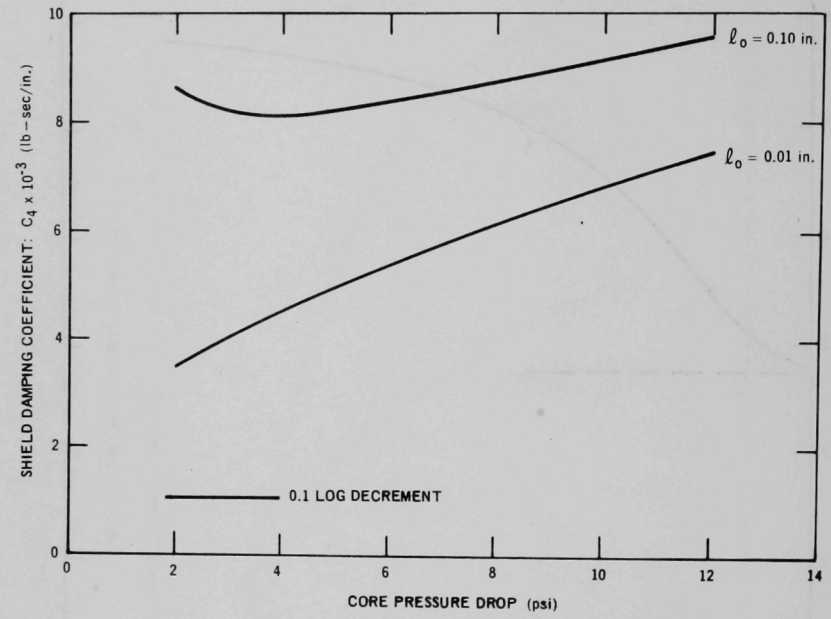

Figure 8. Hydrodynamic Damping Coefficient for Top Seal

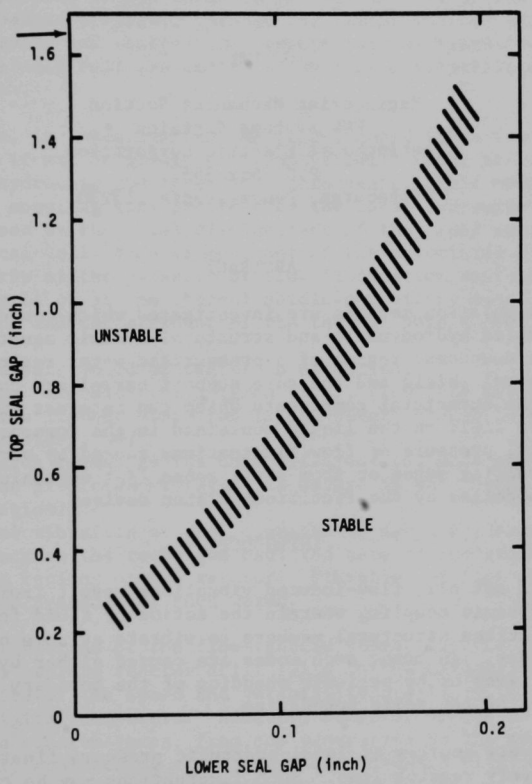

Figure 9. Effect of Top and Bottom Seal Gap on Shield Stability (Analog Computer Results by Eckert)

INVESTIGATION OF METHODS FOR COUPLED STRUCTURAL - HYDRODYNAMIC ANALYSIS OF REACTOR INTERNALS

S. Fabic

Engineering Mechanics Section
PWR Systems Division
Westinghouse Electric Corporation
P.O. Box 355
Pittsburgh, Pennsylvania 15230

ABSTRACT

Calculation methods are investigated which could solve the coupled hydrodynamic and structural-dynamic equations for the downcomer region of a pressurized water reactor. The thermal shield and the core support barrel are considered to be the structural components which can interact with the pressure field in the liquid contained in the downcomer region. The local pressure or flow fluctuations caused by vortex shedding from trailing edges or from stall zones (jet switching) are to be modelled by the fictitious piston devices.

INTRODUCTION

Many, if not all, flow-induced vibrations result from hydrodynamic structural-dynamic coupling wherein the action of fluid forces (local pressures) excites structural members to vibrate at some of their natural vibration modes. In turn, such modes are caused either by the presence of standing waves or by periodic shedding of the boundary layers attuned to the motion of the solid boundaries.

The primary sources of local hydraulic pressure fluctuations are present in every reactor loop. Such fluctuations may be caused by pump pulsations, by vortex shedding at pipe bundles or at trailing edges, by periodic separation of the boundary layer, or by periodic formation and shedding of vortices at "stall" regions.

The pressure fluctuations arising from these primary sources can become greatly amplified if their frequencies happen to coincide with some of the natural frequencies of acoustic vibration of the neighboring body of fluid. Furthermore, some of the walls bounding this fluid may themselves have natural frequencies (in liquid), which coincide with the

frequencies of the local primary sources. Such resonances can lead to severe vibrational problems.

The remedy can be obtained either by elimination of the primary sources, by structural/hydrodynamic de-tuning, or both. The primary sources of fluctuations are difficult to avoid, and the de-tuning process is the only practical alternative.

The approach adopted in this investigation was based on the premise that both the localities and the ranges of frequencies of some of the primary sources of pressure fluctuations are known functions of the fluid velocity. The purpose of the analysis is then to predict how these pressure disturbances propagate through the fluid; whether they "feed" some standing waves; and whether they excite natural vibration modes of the reactor internals that are deemed to be most susceptible to flow-induced vibration.

For example, in investigating the flow-induced vibration of the thermal shield, it may be possible to analytically model the whole downcomer region's hydraulic and structural components. This model would account for the coupling link provided by the local hydraulic forces (pressures) caused by the local displacement of the fluid caused, in turn, by the local deflection or movement of the structural component. The primary source of the pressure or flow fluctuation could be positioned at the inlet nozzle or at the thermal shield's trailing edge, its frequency varied, and the response of the thermal shield computed.

Such an analysis would be useful to establish:

a) The "trouble-free" region (i.e., flow rate below which the flow induced vibration is not severe enough to pose a problem); and
b) which remedy is the most efficient and most economical if the predicted vibration is severe in the normal operating region.

Flow induced vibration of fuel elements is not considered in this paper, mainly because the technique explored here tracks gross pressure waves in various regions of the reactor. Vibration of fuel elements is not caused by the presence of such waves.

Precise calculation of the flow-induced vibrations for as complicated a structure as a nuclear reactor still falls in the category of wishful thinking, in spite of the speed and versatility available in the current generation of digital computers. However, computer speeds and capacities have advanced in quantum jumps, from one generation to the next. We are therefore rapidly approaching the stage where hardware will not limit our ability to attack such complex problems; the limitations will be imposed by the fact that the development of the methods of analysis has not sufficiently advanced. The emphasis of this paper is directed at investigating the presently available means for attacking the problem as economically as possible.

Section 2 describes two methods of solution of the coupled structural/hydrodynamic equations. The first method applies to simple geometries involving one or more flexibly mounted parallel plates. The second method,

which is now under investigation, involves the merging of existing Westinghouse structural dynamics and hydrodynamic computer codes. This method would be applicable to complex geometries, such as found in the PWR downcomer region.

Section 3 describes the modelling techniques investigated for multi-dimensional hydraulic passages.

Section 4 outlines the description of the primary excitation sources.

2. METHODS OF ANALYSIS

Consider the flow channels proportioned such that their dimensions in directions perpendicular to the flow axis or in the direction of motion of some flexible wall, are small compared with the length along the flow axis. The flow cross section area is assumed to be uniform along the channel, although it may vary with time, and from channel to channel. Hence, we are assuming that channel walls are flexible, although in a restricted sense; and that wall motion is caused either by the action of some external force or by the liquid pressure acting over the wetted surfaces.

The method of characteristics allows us to transform the set of partial differential equations into the following four equations which, together with specified boundary conditions, describe the relationship between the local (and instantaneous) pressure, p, velocity, u, and the flow area A:

$$\alpha_1 \frac{dp}{dt} + \frac{du}{dt} + F + \beta_1 \frac{1}{A} \frac{dA}{dt} = 0 \qquad (1)$$

$$\text{with } \frac{dx}{dt} = c + u \qquad (2)$$

$$\text{and } -\alpha_2 \frac{dp}{dt} + \frac{du}{dt} + F - \beta_2 \frac{1}{A} \frac{dA}{dt} = 0 \qquad (3)$$

$$\text{with } \frac{dx}{dt} = u - c \qquad (4)$$

The first two equations describe conditions along one characteristic, the last two along the other. The term F is a one-dimensional approximation for the frictional force, proportional to $|U|\ U$. Formulation of such equations for the case of rigid walls, i.e., when $dA/dt = 0$ (together with the description of the numerical solution method) can be found in References 1 and 2. The values of the coefficients α, β, and F are updated after each time increment of computation. This allows consideration of phase changes (flashing) of the fluid as implemented (for example) in the Westinghouse BLODWN-2 computer code(3).

To obtain information on the value of the dA/dt term one must add to the above set the differential equation of motion for each of the flexible walls. For walls which can move only in one direction these are of the form

$$M_i \frac{d^2 y_i}{dt^2} + K_i y_i = f_i(t) + \sum_{K=1}^{j} \gamma_K \bar{p}_K \tag{5}$$

where the subscript i defines the particular flexible wall; y_i is its deflection from initial value, M_i and K_i, the wall's mass and stiffness, respectively; $f_i(\underline{t})$ is an externally applied force (which may or may not be present); and $\bar{p}_K$ is the mean pressure acting over the length of the channel K. There may be a number of such channels wetting that particular flexible wall.

For example, a flexible partition of mass M and stiffness K, located in a fluid passage bounded by rigid boundaries shown in Figure 1, forms two flow channels, both having a common flexible wall. The latter is assumed to move only in a direction perpendicular to the channel axis and there may be an external force applied to the partition.

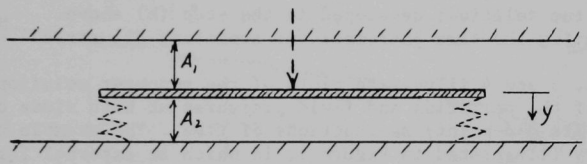

Figure 1 Flexibly Mounted Partition in One-Dimensional Flow Channel

One final equation is needed to describe the relationship between the deflections y of all flexible walls bounding a channel and that channel's flow area A_i:

$$\frac{dA_i}{dt} = \sum_J \lambda_j \frac{dy_j}{dt}$$

For the example of Figure 1, assuming that the flexible partition spans the whole width of the channel,

$$\frac{dA_1}{dt} = \frac{dy_1}{dt} \tag{6}$$

$$\frac{dA_2}{dt} = -\frac{dy_1}{dt} \tag{7}$$

The initial condition may, for example, be a specified liquid pressure and velocity just upstream of the partition's leading edge which, by the solution of the steady flow equations, defines the local pressures and velocities in each channel. The boundary conditions for p and u at the leading and trailing edges of the partition may either be some specified functions of time, or may be specified through conservation of mass flow in case the adjacent regions are also considered in the dynamic evaluation.

One method of solution which proved applicable to multiple parallel channels consists of:

a) Expressing all the above listed equations in the finite difference form.
b) Solving equations (1) through (4) for $p(x,t)$ in terms of $A(t)$, hence in terms of $y(t)$ by means of equations (6) and (7). Obtaining, for each channel K (K = 1, 2. . ., j), the mean channel pressure $p_K(t)$ by summation over all discrete values of x. One thus obtains $p_K(t)$ in terms of $y_K(t)$ and $y_{K-1}(t)$.
c) Substituting the appropriate members of this set of $p_K(t)$ into the last term of equation (5), thereby obtaining an algebraic expression for $y_i(t)$ in terms of other wall deflections $y_K(t)$.
d) When this is done for every flexible wall, one obtains a set of algebraic equations for all wall deflections. These are then solved simultaneously, thus obtaining the magnitudes of $y_i(t)$.
e) The knowledge of $y_i(t)$ hence, $A_i(t)$, enables us to find the values of $p(x,t)$ and $u(x,t)$ for all channels by back-substituting into the relations developed in the step (b) above.
f) Advancing the time increment and repeating all steps.

Figures 2, 3 and 4 illustrate plots of the computer solution for the displacement of the partition and fluid pressures at both sides of the partition (at its mid-point) as functions of time. The example consisted of the geometry illustrated in Figure 1, in which an external force of 1000 lbs oscillating at 600 c/sec acted on a partition weighing 1 lb and having a stiffness of 150 lbs/inch. The partition was 3 inches long and channel thickness (on both sides) and width were 1/4 inches and 5 inches, respectively. The initial pressure of the liquid was 500 psi as were the boundary pressures at the partition's leading and trailing edges. The displacement curve shows the 600 c/sec component and the natural vibration frequency to be smaller than the natural frequency of this plate in air.

Another method of solution now being investigated shows more promise for the cases in which the structural elements are considerably more complex, requiring interfacing with a separate structural-dynamic code. For example, Westinghouse's STASYS-II structural dynamics code solves, by numerical integration, the equation of motion for a structural system:

$$[M]\{\ddot{y}\} + [C]\{\dot{y}\} + [K]\{y\} = \{F(t)\} \qquad (8)$$

where [M] is the structure mass matrix
[C] the structure damping matrix
[K] the structure stiffness matrix
{y} the vector of nodal displacements
{F(t)} the node forcing function

The structure is approximated as an assembly of discrete structural elements connected at a finite number of nodal points. If the force-displacement relationship for each of these discrete structural elements is known (the element "stiffness matrix"), then the force-displacement relationship for the entire structure can be assembled, using standard matrix methods.[4]

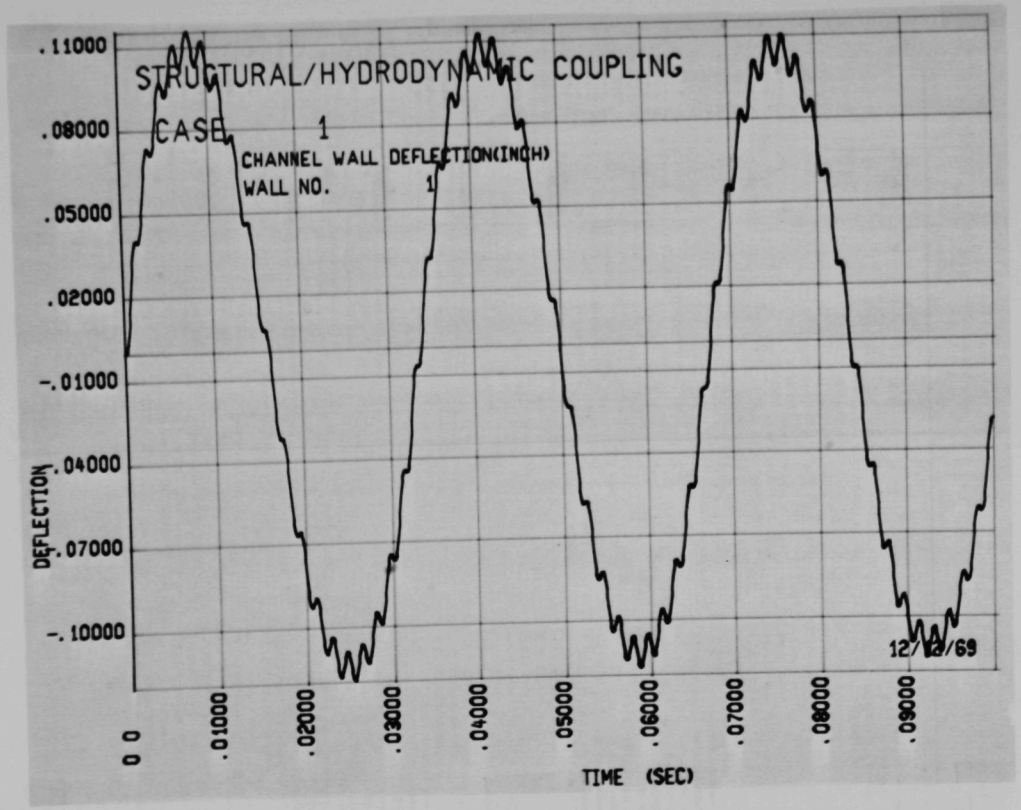

Figure 2 Time History of Deflection of the Center Partition

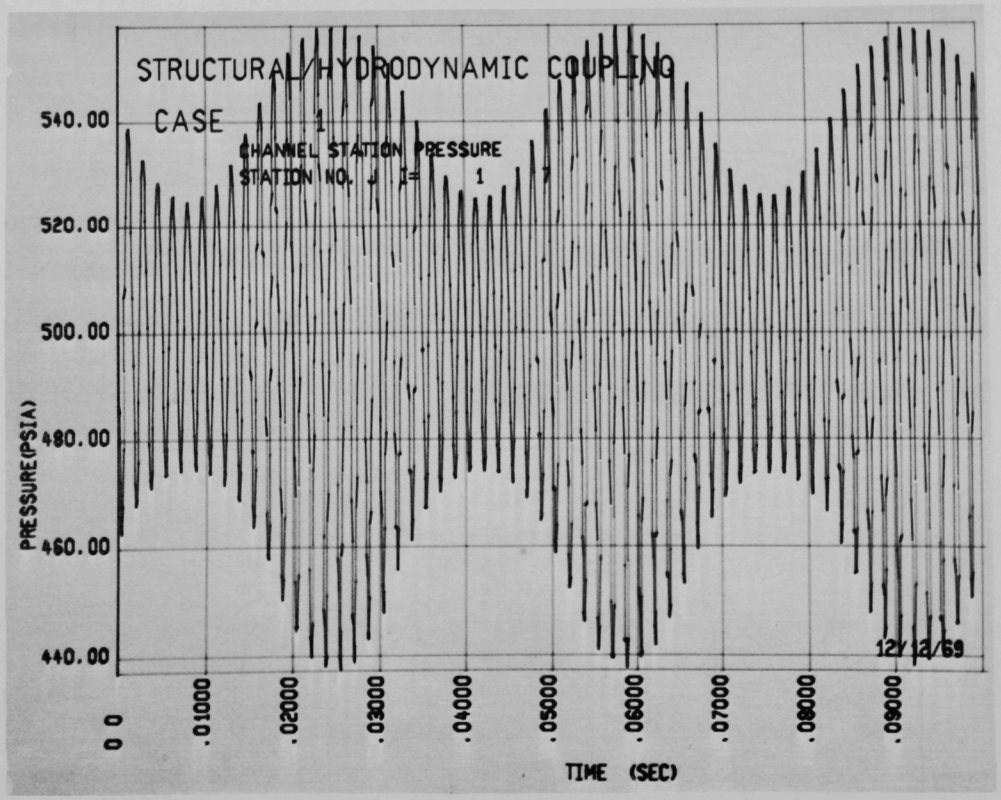

Figure 3 Time History of Liquid Pressure Above the Partition (Midplane)

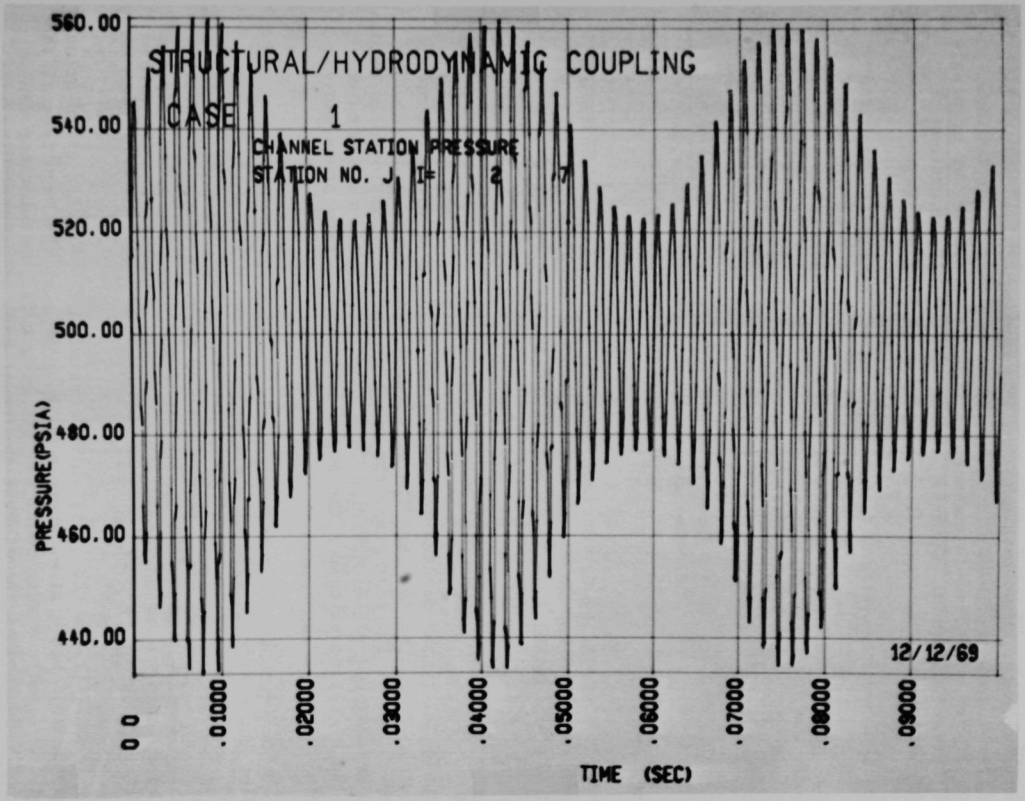

Figure 4 Time History of Liquid Pressure Below the Partition (Midplane)

The available library of finite elements numbers more than 20 for static and dynamic analyses. These include frames, plane stress and axisymmetric triangles, three-dimensional solids, springs, masses, dampers, plates, axisymmetric shells, general shells, and friction interface elements.

Having approximated the structure by an assembly of discrete structural elements, the fluid passages are also subdivided into sub-assemblies of hydraulic elements. The latter may consist of a single channel, of two and three-dimensional networks of channels, or of single two and three-dimensional regions. These various representations of hydraulic elements are described in Section 3 of this paper.

The next step consists of generating two transfer matrices: One identifying the local nodal deflections of structural elements with the local changes in the flow area of hydraulic elements; the other expressing the forces acting on the nodes of the structural elements as products of the local pressure and the corresponding portion of the wetted surface area.

Assuming for the moment that both the structural and hydraulic calculations are to be performed at each time increment of computation (which is not always necessary), such calculations will form the predictor/corrector loop.

The first operation in the loop consists of the computation of all $dA_i(t)/dt$, based on the knowledge of two previous magnitudes; i.e., $dA_i(t - \Delta t)/dt$ and $dA_i(t - 2\Delta t)/dt$ and on the previous estimate of $dA_i(t)/dt$.

In the next operation, hydrodynamic equations, such as equations (1) through (4), are solved for all local p(t) and u(t). In the third step, the transfer matrix is applied to compute the structural element's nodal forces and, in the fourth step, the structural code computes all nodal displacements. In the last step, the transfer matrix is employed to obtain the new estimate of all $dA_i(t)/dt$. This loop is repeated once more to obtain the corrected values of the nodal deflections, flow areas, local pressures, etc.

The time increments for hydraulic calculations, Δt_{HYD}, are limited by the hydraulic element's spatial increments and the velocity of sound in liquid. It is therefore quite likely that these Δt_{HYD} will be much smaller than the Δt_{STR} needed for the solution of the structural equations. Hence, in practical applications the above mentioned loop calculations need not be performed for every Δt_{HYD} but, rather, only once for every Δt_{STR}.

The second step in the loop, which consists of hydraulic calculations, will then be repeated n times where $n = \Delta t_{STR}/\Delta t_{HYD}$. The magnitude of the selected Δt_{STR} must be such that: a) the structural calculations can follow the frequency of the highest important mode of natural vibration (determined at the time of formulation of the total stiffness and mass matrices); b) can follow the highest frequency of an imposed external load if it exists; and c) the magnitudes of all $dA_i(t)/dt$ computed between the

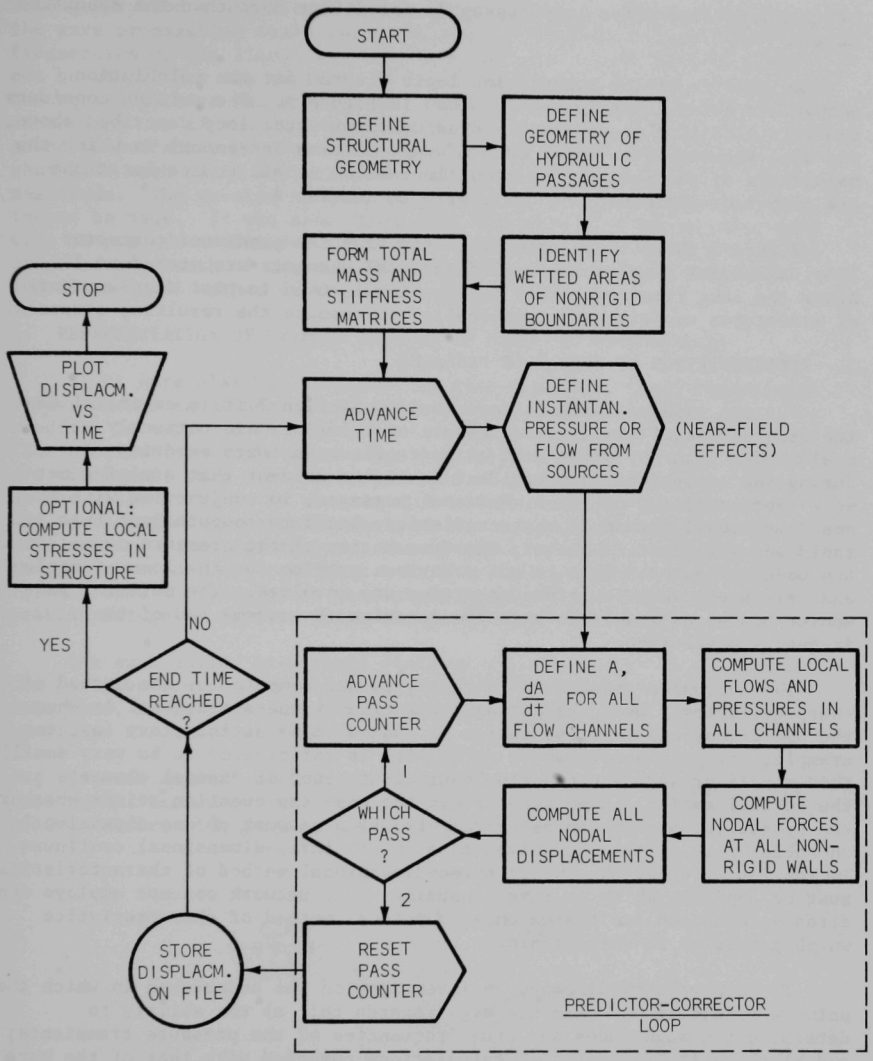

Fig. 5. Computation Logic Diagram for Flow-induced Vibrations

two predictor/corrector loop passes do not differ more than the specified amount.

An outline of the computation logic diagram for the calculation method now being investigated is shown in Figure 5. The outline considers the initialization steps and the predictor/corrector loop described above, and also shows a step (after each advance of time increment) in which the magnitudes of the pressure or flow fluctuation at all source locations are computed. This will be dealt with in Section 4.

Figure 5 shows that, after the exit from the predictor/corrector loop, all nodal displacements of structural elements are stored on file. After the last time step, this information is used to plot displacements of structures vs. time and, optionally, to compute the resulting stresses.

3. REPRESENTATION OF HYDRAULIC PASSAGES

For the type of analysis described in Section 2 it is essential that the frequencies of the liquid pressure oscillations are correctly evaluated. From our prior work on hydraulic transients experienced during the loss-of-coolant accident it became evident that a piping network representation of two-dimensional passages, in conjunction with the one-dimensional method of characteristics, leads to computations that are rapid and efficient. However, the frequencies of the pressure oscillations are underestimated. This is not a serious problem for the loss-of-coolant analysis since very few pressure cycles are involved. The material presented addresses itself to both the question of economy and of the frequency prediction.

The hydraulic transients in the fluid are computed by the method of characteristics. When the passages are clearly one-dimensional or when the one-dimensional representation is judged to be satisfactory (as, for example, for passages in which $dA(t)/A(t)$ is anticipated to be very small), then single or series connected "equivalent pipe" or channel elements are the logical choice. When such is not the case the question arises whether the hydraulic passage can be represented by a network of one-dimensional channels or if it must be solved as a two or three-dimensional continuum. In the latter case, the two or three-dimensional method of characteristics must be applied, which is time consuming. The network concept employs the already developed and tested one-dimensional method of characteristics which proved to be quite rapid.

To resolve this dilemna, an investigation was undertaken in which the network modelling was examined with regards to: a) the ability to determine the magnitudes and true frequencies of the pressure transients; and b) the efficiency of such calculations compared with that of the more precise two or three-dimensional method of characteristics.

To date our investigation was centered on representation of two-dimensional regions. The results show that branching of waves into the network, with attendant reflections and partial transmissions at the branch points, causes the waves to propagate with an apparent velocity that is smaller than the velocity of sound in the fluid. The same effect was noted by Streeter and Wiley[5] in their work with the square,

triangular, and diamond type lattices of the piping network. A delay in the wave propagation would result in the prediction of lower than true frequencies of the liquid pressure oscillations. Such results would not be useful for the analysis of flow induced vibrations. In our work the square lattice was adopted and the lattice size varied in order to establish: a) if and what adjustments could be made to the velocity of sound to correctly predict the frequencies of the oscillations and b) what size mesh gives satisfactory prediction of the wave shape and magnitude. The results to date show that a suitable adjustment can indeed be made. It was also found that the mesh size which gives good wave shapes and magnitudes leads to computation times which are of the order of one tenth of the computation time needed for the more exact two-dimensional method of characteristics.

4. REPRESENTATION OF PRIMARY SOURCES OF PRESSURE OSCILLATIONS

If it were possible to solve the time-dependent three-dimensional Navier-Stokes equations in the regions where vortex formation and shedding is expected to occur, some of the primary sources of pressure or flow oscillations would appear automatically. As far as pump pulsations are concerned, they are easily modelled as an imposed boundary condition at the inlet nozzle. As the computer speeds keep increasing and our understanding of numerical techniques for solution of nonlinear partial differential equations deepens, the feasibility of such computations becomes more and more realistic. At this stage, however, we shall refrain from the attempt to accurately model all the primary sources, seeking refuge in devices which may produce similar effects.

One such device is a short piece of pipe, attached at one end to the location where vortex induced pressure fluctuations occur. At its other end, it is provided with a piston which can oscillate with any specified frequency and amplitude.

In each channel next to the thermal shield trailing edge one could model such fictitious devices and couple their piston movements to produce alternating pressure oscillations, as shown in Figure 6 .

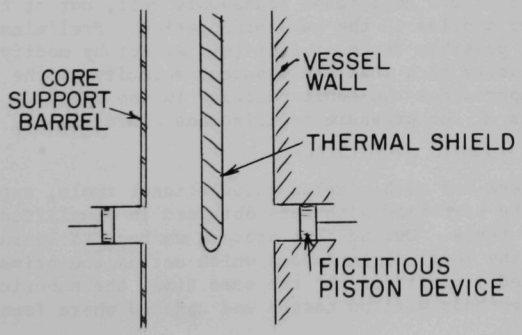

Figure 6 Modelling of Sources of Pressure Oscillations Caused by Vortex Shedding at Trailing Edge

The amplitude of the piston movement can be made such as to cause a few psi pressure differential across the thermal shield's trailing edge. The frequency of the piston movement may be either an externally specified function of the local velocity, or it may be coupled with the motion of the thermal shield to produce, through a feedback, the observed "capture" of the vortex shedding frequencies.

A similar piston device could be located just below the location where the inlet nozzle joins the downcomer region. Tests presently being conducted at Westinghouse Research Laboratories can provide information as to what pressure or flow oscillation may be expected to occur at that location. If the test results show that jet switching or periodic stall vortex formation at the inlet nozzle is affected by the thermal shield vortex shedding, some means of cross-coupling of the piston devices must be introduced.

The laboratory tests could also identify other important primary sources.

5. CONCLUSIONS

This paper outlines one among a number of calculation methods presently being investigated at Westinghouse. The method here discussed applies to hydraulic passages or channels in which the wall deflection, during vibration, is a significant fraction of the channel thickness. Hence, this particular method shows promise in describing the flow induced vibration of the reactor internals located in, or bounding, the PWR downcomer region.

Since the downcomer region is mainly two-dimensional (owing to the thinness of its annular gap), emphasis was placed on obtaining the most appropriate method for solving hydraulic transients in two-dimensional geometries. The term "most appropriate" here implies the method having sufficient accuracy and with the best economy in running time.

The piping network modelling of two-dimensional regions was found to reproduce pressure amplitudes reasonably well, but at the expense of introducing a delay in the wave propagation. Preliminary work has shown that it is possible to counteract this effect by modifying the wave propagation velocity such that the apparent velocity of the wave (through the network) approaches the sonic velocity in the liquid. In this way the frequencies of the pressure oscillations could also be reasonably well predicted.

To check out such complex calculational tools, extensive comparisons remain to be performed with data obtained in simplified yet realistic laboratory tests. During that process we hope to learn how best to represent the local disturbances which act as the primary sources of the flow induced vibrations. At the same time, the numerical solutions and modelling methods will be tested and updated where found necessary.

6. REFERENCES

1. V. L. Streeter and E. B. Wiley, "Hydraulic Transients," McGraw-Hill.

2. A. Ralston and H. S. Wilf, "Mathematical Methods for Digital Computers", John Wiley and Sons.

3. S. Fabic, "Loss-of-Coolant Analysis: Comparison Between BLODWN-2 Code Results and Test Data," WCAP-7401, Topical Report, November, 1969.

4. V. C. Zienkiewiez and Y. K. Chueng, "The Finite Element Method in Structural and Continuum Mechanics," McGraw-Hill, 1967.

5. V. L. Streeter and E. B. Wiley, "Two and Three-Dimensional Fluid Transients," Trans. ASME, Vol. 90 pp. 501-509, December, 1968.

DISCUSSION

M. Bender (ORNL): What Dr. Fabic has said this morning reminds us that a lot of what we're proposing to do in the way of analysis will only be confirmed by a lot of experimentation on real hardware, but it's encouraging to know that people are still trying to develop analytical solutions to these things that at least will give the designer a start on doing it the right way.

GENERATION OF POSITIVE AND NEGATIVE DAMPING WITH A FLOW RESTRICTOR IN AXIAL FLOW

D.R. Miller

Technical Operation
KNOLLS ATOMIC POWER LABORATORY
General Electric Company
Schenectady, New York

ABSTRACT

A fluid flowing past a vibrating body may absorb energy from the body, or it may supply energy to the body thereby generating positive or negative damping of the vibration of the body. A simple model is used to show how a fluid can generate either positive or negative damping.

A modification proposed by the author has been incorporated in the Advanced Test Reactor (ATR) at the National Reactor Testing Station to reduce to acceptable levels the flow-induced vibration of a number of pressure tubes which will contain irradiation experiments. Each pressure tube is essentially centered within a tubular insulation jacket by means of spacer collars. A hollow circular safety rod surrounds the insulation jacket over part of the length of the pressure tube and insulation jacket assembly. These tubes are long and slender and have low natural frequencies of transverse vibration, which makes them more prone to vibrate than if their natural frequencies were higher. High-velocity longitudinal flow of reactor coolant in the annuli between the safety rods and the insulation jackets induced objectionable vibration of the pressure tube and insulation jacket assemblies in their original configuration. This vibration problem was alleviated, but not adequately corrected, by the addition of flow-restricting sleeves in the upstream portion of the annuli which reduced the volume flow rate. Based on KAPL studies of the self-excited vibration of a rigid elastically supported blade in a flow channel(1), it was evident to the author that the flow restrictors would have been more effective in suppressing flow-induced vibration if they had been placed at the downstream ends of the annuli rather than near the upstream ends. Tests in the ATR confirmed this expectation.

Fig. 1 shows why a flow restrictor at the downstream end of a flow channel tends to suppress flow-induced vibration of a rigid body

suspended in the channel, while a flow restrictor at the upstream end tends to enhance or even cause vibration. The following assumptions were made as a basis for preparation of the figure:

1. The body is a rigid blade with a flow-restricting enlargement at one end, as is shown in cross section in Fig. 1.

2. The blade is constrained to have freedom only for translation across the flow channel.

3. Flow is two-dimensional in the plane of the figure.

4. The fluid is single-phase and incompressible.

5. The loss factor for flow between the flow restrictor and either channel wall is not affected by a translatory displacement of the blade across the channel.

6. The pressure drop across the flow restrictor is very large in comparison with the pressure difference from the righthand end of a channel to the flow restrictor.

7. The pumping action of the moving blade produces negligible axial accelerations of the fluid compared with those that are produced by changes in clearance between the channel walls and the flow restrictor.

8. Fluid friction along the blade is negligible.

Now consider what would happen if the blade had a small upward velocity v while the direction of fluid flow is from left to right. The flow velocity between the flow restrictor and the channel walls remains essentially the same above and below the flow restrictor but, because of the changing clearance between the flow restrictor and the channel walls, the total inflow rate past the upper side of the flow restrictor is decreasing with time. The opposite situation exists with respect to the flow that passes the lower side of the flow restrictor. These changes in inflow rate to the upper and lower channels at the right of the flow restrictor cause a decreasing flow velocity (deceleration) in the upper channel at the right of the flow restrictor and an increasing velocity (acceleration) in the lower channel. For deceleration of the fluid in the upper channel to occur, there must be in this channel an axial pressure gradient with pressure rising with increasing distance from the flow restrictor. Similarly, there must be an axial pressure gradient of opposite algebraic sign in the lower channel. The resulting distribution of static pressures acting on the blade is shown directly below the diagram of the physical model in Fig. 1. Since the pressure in the lower channel is everywhere higher than it is in the upper channel, the net hydraulic force on the blade is upward. Because this is also the direction of the velocity of translation of the blade, the hydraulic forces are supplying energy to the motion of the blade. Under this condition, the flow restrictor and blade interact with the fluid to produce negative damping.

Similar reasoning shows that if the blade had an upward velocity but the flow was from right to left, the pressure gradients would have reversed their algebraic signs, and the pressure distribution in the two channels would be as sketched in the bottom part of the figure. Under this condition the net hydraulic force acting on the blade in the vertical direction acts in the direction opposite to the velocity of translation of the blade. This effect corresponds to positive damping.

A source of negative damping in a linear elastic system tends to increase the response of the system to fluctuating exciting forces. If the source of negative damping is strong enough to overcome the stabilizing effects of the positive damping in the system, a self-excited vibration will develop. Any source of positive damping will reduce the response of the system to fluctuating exciting forces and will oppose a tendency for a self-excited vibration to occur.

A simple model was constructed to demonstrate the principles that are described above. It consisted of a 1/2-in. inside diameter (ID) by 11-1/2 in.-long glass tube with a standard wooden lead pencil ($\sim$5/16 in. diam) suspended with an axial coil spring (rubber bands could have been used) at each end so as to give the pencil a lateral natural frequency on the order of five cps. A coil 1.6 in. long consisting of 14 turns of about 0.06 in.-diam wire was placed on one end of the pencil to form a flow restrictor. One could easily excite a severe vibration of the pencil by blowing through the tube with the flow restrictor at the upstream end of the pencil, but little vibration could be excited by blowing in the opposite direction.

In the model visualized in the above discussion it was assumed, for simplicity, that the flow was entirely axial, i.e., that there was no flow across the longitudinal edges of the blade. In the cases of the ATR pressure tube and the lead-pencil model, the pressure difference which is developed across the diameter of the tube or pencil is diminished by circumferential flow within the annulus. This seems to affect the magnitude of the damping effect, but not its algebraic sign.

Reference

1. Miller, D.R. and R.G. Kennison. "Theoretical Analysis of Flow-Induced Vibration of a Blade Suspended in a Flow Channel." ASME Paper 66-WA/NE-1. (Also published as KAPL-M-6959).

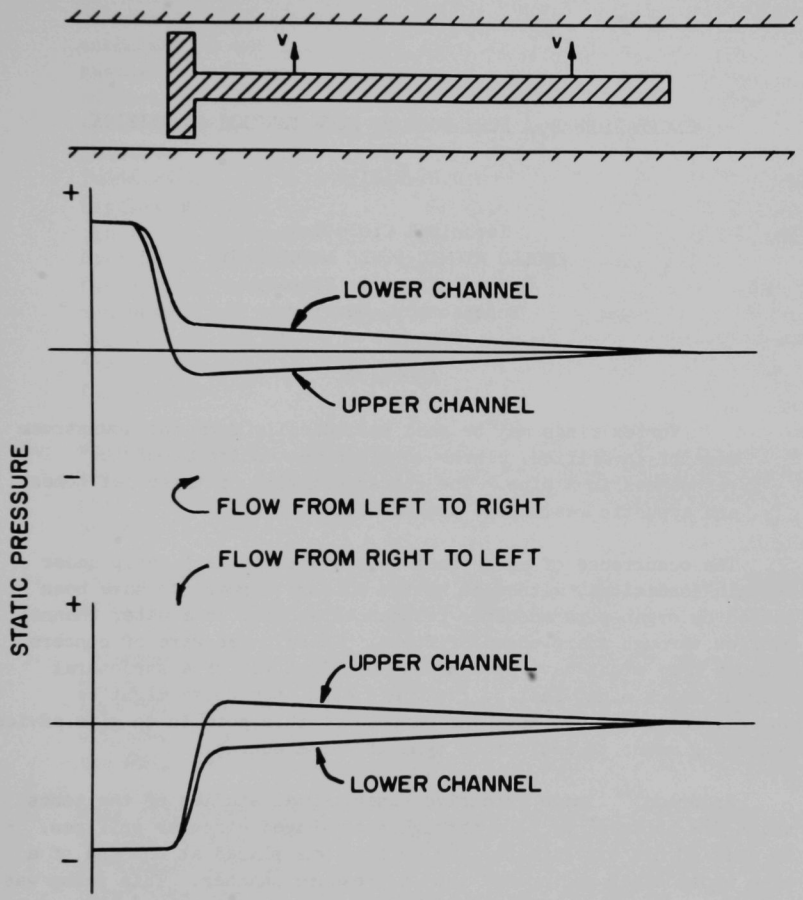

Fig. 1. Generation of Positive and Negative Damping

EXCITATION OF A PURE TONE BY FLOW THROUGH AN ORIFICE

D.R. Miller

Technical Operation
KNOLLS ATOMIC POWER LABORATORY
General Electric Company
Schenectady, New York

ABSTRACT

Vortex rings may be shed periodically from the downstream side of an orifice. These vortices may excite acoustic resonances in a pipe. The characteristics of these jet tones and acoustic resonances are described.

The occurrence of pure tones in a hydraulic test setup under certain conditions, witnessed by the author, appears to have been caused by organ-pipe acoustic resonances excited in a water channel by flow through sharp-edged orifices. These tones were of concern because they might have been caused by vibration of a structural element which might fail by fatigue. Also, the noise might be objectionable in service. The purpose of this note is to give advice regarding means to avoid this type of noise source.

Anderson[1-7] made extensive experimental studies of the tones which are produced by flow through sharp-edged circular orifices. In some of his experiments, the orifice was placed at one end of a pipe whose other end opened into a pressure chamber. This setup was used to study the influence of the pipe on the jet tones produced by flow through the orifice to the atmosphere. Anderson also discussed other observations of jet-tone and pipe-tone phenomena. The following information is from Anderson.

1. Jet tones are associated with the shedding of vortex rings from the downstream side of the orifice. Excellent shadowgraphs of the vortex rings have been obtained.[6-7]

2. The jet tones from an orifice may have components which are integral multiples (harmonics) and integral submultiples (subharmonics) of a fundamental tone frequency. The fundamental usually is the strongest tone, and the strength of the harmonics diminishes with increasing multiples of the fundamental. The subharmonics are less steady than the fundamental and its harmonics. For plate-thickness-to-orifice diameter ratios between 0.5 and 1.25, and Reynolds numbers (based on orifice-plate thickness) between 1200 and 2000 the dimensionless parameter $(ft/\sqrt{\Delta p/\rho})$ has a value of about 0.8 for the fundamental. In this parameter: f is the frequency of the tone (cycles per unit time); t is the thickness of the orifice plate; Δp is the pressure drop across the orifice; and, ρ is the mass density of the fluid. The value of the parameter for the fundamental tone rises to about unity, as the Reynolds number is increased, and remains there for Reynolds numbers up to 5000 to 10,000. As the Reynolds number increases to high values, first the subharmonics die out, then the harmonics, and finally the fundamental.[4]

3. When a liquid is discharged through a sharp-edged circular orifice into a large body of the same liquid, sound is produced over a range of plate-thickness-to-orifice diameter ratios between 0.1 and 2.[4]

4. The loudest jet tones are produced by orifices whose thicknesses are approximately equal to their diameters.[5]

5. "Studies have been made of the effect of sharpness of orifice edges on the character of jet-tones. It is especially important that the entrance edge of the orifice be sharp for maximum efficiency in the production of tones. This is not as true for the exit. Wide variation in geometry of this may be tolerated."[4]

6. When pipe tones are generated by flow through a sharp-edged orifice, a succession of acoustic resonances can occur in a particular configuration as the flow rate is increased. The first tone usually occurs abruptly at a fundamental frequency when the pressure drop across the orifice reaches a particular level. As the pressure drop across the orifice is increased further, the frequency may rise as much as 10% while the pressure drop is increased by $\sim$100%. The second multiple of the fundamental then occurs, sometimes before the fundamental tone has stopped. This process repeats, as the pressure drop is increased, with higher multiples of the fundamental occurring, and being replaced by still higher multiples.

Sometimes one or more of the tones in the sequence does not occur. Each new frequency occurs when increasing flow brings about a resonance of the orifice-pipe system to a jet-tone frequency which would be produced by the orifice in the absence of the pipe.(1)

Based on the above, it is evident that pipe-tone acoustic resonances can be excited by flow through an orifice in a fluid channel which, in combination with the orifice plate and other influencing factors, has an acoustical natural frequency in the range of the frequencies generated by flow through the orifice in the absence of an acoustic resonance. It appears reasonable that in most hydraulic systems these acoustic resonances will not occur, since only one instance of this occurrence has come to the author's attention. However, it is desirable to guard against this problem, if the protective measures do not unduly compromise the design or test objectives.

Evidently, rounding of the edges of the entrance side of the orifice or use of an orifice plate whose thickness is over twice the orifice diameter will prevent excitation of acoustic resonance by the jet issuing from the orifice. Factors which tend to damp acoustic oscillations will be beneficial in reducing the response of a fluid column or chamber to the orifice vortex-ring excitation.

References

1. Anderson, A.B.C. "Dependence of Pfeifenton (Pipe Tone) Frequency on Pipe Length, Orifice Diameter, and Gas Discharge Pressure," JASA. 24, No. 6. Pp. 675-681. 1952.

2. Anderson, A.B.C. "Dependence of the Primary Pfeifenton (Pipe Tone) Frequency on Pipe-Orifice Geometry," JASA. 25, No. 3 Pp. 541 - 545. 1953.

3. Anderson, A.B.C. "A Circular-Orifice Number Describing Dependency of Primary Pfeifenton (Pipe Tone) Frequency on Differential Pressure, Gas Density, and Orifice Geometry," JASA. 25, No. 4. Pp. 626-631. 1953.

4. Anderson, A.B.C. "A Jet-Tone Orifice Number for Orifices of Small Thickness-Diameter Ratio," JASA 26, No. 1. Pp. 21-25. 1954.

5. Anderson, A.B.C. "Metastable Jet-Tone States of Jets from Sharp-Edged, Circular, Pipe-Like Orifices," JASA 27, No. 1 Pp. 13-21. 1955.

References (Continued)

6. Anderson, A.B.C. "Structure and Velocity of the Periodic Vortex-Ring Flow Pattern of a Primary Pfeifenton (Pipe Tone) Jet," JASA. 27 No. 6. Pp. 1048-1053. 1955.

7. Anderson, A.B.C. "Vortex-Ring Structure-Transition in a Jet Emitting Discrete Acoustic Frequencies," JASA 28,No. 5. Pp. 914-921. 1956.

FLOW-INDUCED INSTABILITY OF A THIN-WALLED CYLINDRICAL SHELL

D.R. Miller

Technical Operation
KNOLLS ATOMIC POWER LABORATORY
General Electric Company
Schenectady, New York

ABSTRACT

The author's previously published theoretical analysis of the flow-induced collapse of flat plates is extended to the case where an incompressible fluid flows axially within a thin annulus bounded by one or two elastic thin-walled tubes. Expressions for the critical flow velocity for these two cases are derived. Some implications of flow velocities approaching the critical value are discussed.

Introduction

Theoretical expressions for the velocity of fluid flow at which static instability occurs in assemblies of flat and curved plates such as are used in some nuclear reactor fuel assemblies(1) were previously derived. The type of instability on which the derivations were based is analogous to the elastic buckling of a column which occurs when the critical axial load is applied. In the column, a small lateral deflection of the column in the presence of the axial load develops bending moments in the column which are sufficient to maintain the deflection.

The analogous situation for plate collapse can be explained for the simple case of a single elastic plate which bisects a long rigid flow channel. Assume a small deflection of the plate over an axial distance that is small compared with the plate length. The volume flow rate of an incompressible fluid remains essentially the same in the two channels; in accordance with Bernoulli's theorem, however, the linear velocity rises and the static pressure acting on the plate falls on the side where the channel is contracted by deflection of the plate. The reverse effect occurs on the other side of the plate. The resulting pressure difference, tending to bend the plate, is proportional to the square of the linear velocity of flow in the undeformed channel. With this velocity at a critical value, the pressure difference acting

on the deflected plate is sufficient to overcome the elastic stiffness of the plate to maintain the deflection.

This analysis of plate collapse was prompted by observation of tests on an array of plates in which static elastic deflections could be developed and then eliminated by increasing and then decreasing the flow rate. In tests at Oak Ridge,[2] flow-induced plate deflections entered the plastic range and permanent deformations remained when the flow was reduced to zero. A number of papers and reports[3-22] have presented experimental data on this problem and extended the theoretical analysis. Despite some factors which were not accounted for in the analysis, the expressions for critical velocity give a reasonably good indication of the velocities at which significant plate deflections will occur.

The current note calls attention to the possibility of the same type of instability in the case of axial flow of a fluid in an annulus bounded by one or two thin-walled cylindrical shells. Expressions are derived below for the critical value of the average axial flow velocity in the annulus for this type of configuration. The following assumptions are made during derivation of the expressions for critical velocity:

1. Shells are homogeneous, elastic and isotropic and, in the absence of flow, are circular and concentric.

2. Shell thickness is very small in comparison with the radius.

3. Fluid is incompressible and frictionless.

4. Flow-induced deflections are small when compared with the annular clearance.

5. Flow-induced deformations do not produce a significant circumferential flow or nonuniformity of volume flow rate per radian around the deformed annulus.

6. Annular clearance is small when compared with the radius of the boundaries of the annulus.

7. Hoop stress in the shells is negligible.

8. Pressure difference across the wall of the shell(s) in the absence of distortion of the shell(s), is negligible in comparison with the net external pressure which would collapse the shell(s) in the absence of flow.

Two cases are considered: in the first case, a pair of thin-walled concentric cylindrical shells of equal thickness has an incompressible fluid flowing longitudinally in the annulus between them; the second case differs from the first case in that one of the bodies bounding the annulus is so resistant to distortion of its cross section relative to the thin-walled shell that the former can be assumed to be rigid, i.e., a solid cylinder within a thin-walled tube or a thin-

walled tube within a thick-walled tube.

Nomenclature

a = average value (subscript)

c = critical value (subscript)

g = gravitational acceleration

h = radial depth of annulus

ℓ = axial length of ring

p = local static pressure in annulus

p_o = amplitude of circumferential variation of p

t = thickness of thin-walled shell

w_o = maximum radial deflection of shell relative to average deflection

E = Young's modulus of elasticity

I = moment of inertia of cross section of ring

R = mean radius of annulus or shell

V = local linear velocity of fluid in annulus

V_c = critical value of V_a

W = total weight flow rate in annulus

ρ = weight density of fluid

θ = angular coordinate

ν = Poisson's ratio

Analysis of Concentric Thin-Walled Cylindrical Shells of Equal Thickness

The lowest critical velocity corresponds to the mode of deformation in which the shells locally assume an elliptical cross section with the major axes of the two ellipses perpendicular to each other. This type of deformation can be produced by a pressure variation in the annulus of the form

$$p = p_o \cos 2\theta + p_a \tag{1}$$

Alford[23] has given an expression for small radial deflections of a narrow circular cylindrical ring under the action of this pressure distribution. For elliptical deformation, Alford's expression reduces to

$$p_o = \frac{9 w_o EI}{R^4 \ell} \tag{2}$$

To provide an expression applicable to a cylindrical shell, $t^3/12$ is substituted for I/ℓ, and $(1-\nu^2)$ is added in the denominator. This results in the relation

$$p_o = \frac{3w_o t^3 E}{4R^4(1-\nu^2)} . \tag{3}$$

Neglecting fluid friction and gravitational heads, application of Bernoulli's theorem gives

$$p + \frac{\rho V^2}{2g} = p_a + \frac{\rho V_a^2}{2g} . \tag{4}$$

With the assumed deformation, the circumferential variation of annular gap is

$$h = h_a\left(1 + \frac{2w_o}{h_a}\cos 2\theta\right). \tag{5}$$

It is assumed, for conservatism, that the volume flow rate per radian around the annulus remains uniform despite deformation of the shells. On this basis

$$V = V_a h_a/h \tag{6}$$

For the critical condition, where the deformation generates a static pressure distribution sufficient to maintain the deformation, $V_a = V_c$ and the following relations can be written on the basis of Equations 4, 5, and 6:

$$p - p_a = \frac{\rho}{2g}(V_c^2 - V^2)$$

$$= \frac{\rho}{2g}V_c^2 - \frac{\rho}{2g}\left[\frac{V_c h_a}{h_a\left(1 + \frac{2w_o}{h_a}\cos 2\theta\right)}\right]^2 \tag{7}$$

Assume that $2w_o/h_a \ll 1$; then Equation 7 reduces to

$$p - p_a = \frac{2\rho w_o V_c^2}{gh_a}\cos 2\theta \tag{8}$$

This is the variation of pressure defined by Equation 1. Hence,

$$p_o = \frac{2 \rho w_o V_c^2}{g h_a} . \tag{9}$$

Combining Equations 3 and 9 to eliminate p_o and w_o,

$$V_c = \sqrt{\frac{3 g E h_a t^3}{8 \rho R^4 (1-\nu^2)}} . \tag{10}$$

is obtained.

Conversion of Equation 10 to an expression for the critical value of total weight flow rate gives

$$W_c = \sqrt{\frac{3 \pi^2 \rho g E h_a^3 t^3}{2R^2 (1 - \nu^2)}} . \tag{11}$$

Analysis of the Thin-Walled Cylindrical Shell with Rigid Boundary on Other Side of the Annulus

This case is equivalent to that of a pair of concentric thin-walled shells of equal thickness which have an annular gap twice that between the single thin-walled cylindrical shell and the rigid boundary. Expressions for the critical velocity and flow rate for this case can therefore be obtained by inserting the factor 2 in the numerator under the radical sign in Equations 10 and 11. The resulting expressions are

$$V_c = \sqrt{\frac{3 g E h_a t^3}{4 \rho R^4 (1 - \nu^2)}} . \tag{12}$$

$$W_c = \sqrt{\frac{3 \pi^2 \rho g E h_a^3 T}{R^2 (1 - \nu^2)}} . \tag{13}$$

Discussion

The existence of a uniform static pressure difference across the wall of one or both of the thin-walled shells will cause a significant change in the critical axial flow velocity, if this pressure difference is significant in comparison with the net external pressure required to cause elastic buckling of the shell in the absence of axial flow. A pressure difference which causes a tensile hoop stress in a circular shell increases the critical velocity; one which causes a compressive hoop stress decreases the critical velocity. The latter case is analogous to that of compressive loading across the width of flat plates, which decreases their critical flow velocity.(1)

Some interesting possibilities of interaction exist between the tendency for flow-induced collapse in a thin-walled shell which forms a boundary of an annulus, and a tendency for vibration to occur. If the annular clearance varies with axial position or if there is an entrance hydraulic loss, axial flow may excite an elliptical mode of vibration of the shell when the flow velocity approaches the collapse velocity. Such vibrations might result from solid-fluid interactions which generate negative damping. The generation of negative damping by such interactions was discussed by Miller and Kennison in regard to flow-induced vibrations of a rigid blade suspended in a flow channel(24). If an angular velocity of the fluid in the annulus or in one or both of the solids forming the boundaries of the annulus exists, generation of circumferential traveling waves such as have occurred in turbines(23) may be possible. The natural angular velocity of the elliptical-mode wave apparently would be reduced by the proximity of the axial flow velocity to the critical value.

If the axial length of the narrow annulus is not large in comparison with the diameter, the critical velocity tends to increase. Smith(22) has shown how the critical-flow velocity for a plate increases with reduced ratio of length to width. He found a large increase in critical velocity when the plate dimension in the direction of flow was much smaller than the plate span.

References

1. Miller, D.R. "Critical Velocities for Collapse of Reactor Parallel-Plate Fuel Assemblies," Trans. ASME, 82, A. Pp. 83-95. 1960.

2. Stromquist, W.K. and O. Sisman. "High Flux Reactor Fuel Assemblies-Vibration and Water Flow." ORNL 50. June 15, 1948.

3. Zabriskie, W.L. "An Experimental Evaluation of the Critical Flow Velocity Formulas for Parallel Plate Assemblies." G.E. Co., General Engineering Laboratory Report No. 58GL297. October 31, 1958.

4. Zabriskie, W.L. "An Experimental Evaluation of the Effect of Length-to-Width Ratio on the Critical Flow Velocity of Single Plate Assemblies," G.E., General Engineering Laboratory Report No. 59GL209, September 1, 1959.

5. Zabriskie, W.L. "Report of Tests to Determine the Effect of Plate Length-to-Width Ratio on the Pressure Differentials Developed Across Single Aluminum Plates Dividing a Flow Channel," G.E., General Engineering Laboratory Report No. 60GL73. April 14, 1960.

6. Johansson, E.B. "Hydraulic Instability of Reactor Parallel-Plate Fuel Assemblies." Preprint Paper No. 57, Nuclear Engineering and Science Conference. New York City. 1960.

7. Morehouse, D.J., and J.A. Christenson. "Vibration and Collapse Testing of SM-2 Fuel Elements." APAE Memo 265. July 5, 1960.

8. Shallenberger, J.M. "A Radiographic Method of Determining Collapse Velocity in Flat Plate Fuel Assemblies." WAPD-BT-23. Pp. 83-92. August 1961.

9. Rosenberg, G.S., and C.K. Youngdahl."A Simplified Dynamic Model for the Vibration Frequencies and Critical Coolant Flow Velocities for Reactor Parallel Plate Fuel Assemblies." Nuclear Science and Engineering. 13. Pp. 91-102. 1962.

10. Schlosser, J. "On the Stability of Flat Plates Under the Influence of Coolant Flow," Journal of Nuclear Energy. A and B 16. Pp. 351-4. 1962.

11. Scavuzzo, R.J. "An Experimental Study of Hydraulically Induced Motion in Flat Plate Assemblies." WAPD-BT-25. Pp. 37-45. May 1962.

12. Beck, S.D., and J.V. Miller. "Mathematical Analysis of Rippling of Type I Fuel Plates, Part I." ALCO Products Co. APAE Memo-318. July 5, 1962.

13. Griffin, D.S. "Inelastic Deflection of Fuel Plates Due to Coolant Flow and Compressive Edge Loads," Journal of Nuclear Energy. A and B 17. Pp. 551-7. 1963.

14. Kane, J.J. "The Effect of Inlet Spacing Deviations on the Flow-Induced Deflections of Flat Plates." Nuclear Science and Engineering. 15. Pp. 305-8. 1963.

15. Groninger, R.D., and J.J. Kane. "Flow-Induced Deflections of Parallel Flat Plates." Nuclear Science and Engineering. 16. Pp. 218-26. 1963.

16. Remick, F.J. "Hydraulically-Induced Deflection of Flat Parallel Fuel Plates." Thesis, Pennsylvania State University, 1963 (from AEC Nuclear Science Abstract No. 1223, 1964).

17. Reports on test and in-pile experience on MTR, ETR, and ATR fuel-plate assemblies in the IDO series during 1958-1964; 16464, 16465, 16862, 24463, 24466.

References (Continued)

18. Scavuzzo, R.J. "Hydraulic Instability of Flat Parallel-Plate Assemblies," Nuclear Science and Engineering. 21. Pp. 463-72. 1965.

19. Friedrich, C.M. "Structural Analysis of a Reactor Subassembly Under Thermal, Hydraulic and Fuel Expansion Loads." Trans. ANS. 8, No. 1. Pp. 96-97. 1965.

20. Smissaert, G.E.H. "Hydroelastic Instabilities in Fuel Plate Elements." Thesis, Pennsylvania State University, 1966.

21. Wambsganss, M.W., Jr. "Second Order Effects as Related to Critical Coolant Flow Velocities and Reactor Parallel Plate Fuel Assemblies." ANL-7261. November 1966.

22. Smith, R.L. "Dynamic Pressure Limits for Flat Plates as Related to Nuclear Fuel Elements." NASA-TN-D-4417. February 1968.

23. Alford, J.S. "Protection of Labyrinth Seals from Flexural Vibration." Trans. ASME. 86,(A). Pp. 141-48. 1964.

24. Miller, D.R., and R.G. Kennison. "Theoretical Analysis of Flow-Induced Vibration of a Blade Suspended in a Flow Channel." ASME Paper No. 67WA/NE-1. 1967.

DISCUSSION

M. Bender (ORNL): Could you comment on the relationship between the analyses of the ATR pressure tube problem and that of the Big Rock Point thermal shield?

Miller: Yes, it is really quite fitting that I do so. John Corr did his analysis independently of the work of Kennison and me and, of course, he came to the same conclusions; that is, his work revealed the same principle that I've just described. I might mention that another, if you'll excuse the commercial, GE man at GE Gas Turbines in Cincinnati also has become aware of this same phenomenon and has discussed this problem as it relates to seals of gas turbines. It's also noteworthy that this determination of positive and negative damping that I discussed is also consistent with the movies that Professor Toebes showed yesterday, where when the apex of the triangular cylinder was upstream he had a stable situation, and when the apex was downstream he had an unstable situation. I presume that the explanation of that is the same. You don't agree, Dr. Toebes?

G. H. Toebes (Purdue U.): (Comments not audible on tape.)

Bender: One observation you could make from this talk is the importance of trying to model the geometry, using experimental evidence that is really representative of the condition you are trying to understand. One of the problems that most of us have run up against in trying to work with

heat-exchanger vibration is that virtually all the data applies to single tubes, and we're more interested in bundles of tubes. Further, a great deal of the data is developed for axial flow conditions, and most of us in looking at heat exchangers are far more interested in transverse-flow conditions. So I guess what all of this leads up to is that we can benefit surely from the experience that each of us is generating, and the idea of having this kind of meeting is to get most of us together every once in a while to see what experiences we are having. Further, Dan's comment about looking in the literature at what's happening to organ pipes might apply to a lot of other things, too. There's an awful lot of literature in other kinds of engineering than nuclear engineering that is adaptable to this particular problem and that we aren't taking advantage of, and we've made lots of mistakes on account of it.

STABILITY ANALYSIS OF A RIGID BLADE IN PARALLEL FLUID FLOW

E. A. Zanoni and P. A. Lowe

Bettis Atomic Power Laboratory
West Mifflin, Pennsylvania

ABSTRACT

A stability analysis for the prediction of flow-induced oscillations of a rigid flat blade in a rectangular duct is presented. The analysis permits two degrees of freedom as well as cross flow around the blade edges. The fluid conservation equations are linearized by assuming small perturbations about the steady-state-centered blade conditions. The linearized equations are introduced into the dynamic equations which describe the motion of the blade. The stability of those equations subject to the constraint of the boundary condition is investigated by solving for the system's eigenvalues and eigenvectors. Thus, pure sinusoidal motion, damped sinusoidal motion and divergent motion are allowed. The model is compared with experimental data.

INTRODUCTION

Fluid flowing past a structural member may provide an energy source which can induce and sustain motions of the structural element. This paper will discuss a stability analysis technique for a blade in confined parallel fluid flow. The physical model is shown in Fig. 1. The suspended blade as well as the walls of the containing channel are rigid. The rotational and translational springs at the downstream end allow two degrees of freedom for the rigid blade. The blade is subjected to a steady flow of an incompressible fluid.

A small perturbation approach is used to linearize the transient fluid conservation equations about the steady-state operating point. The fluid velocity is assumed to be composed of a steady-state component and a perturbation component.

If a small displacement perturbation were introduced, such that the blade would be displaced slightly from its midchannel (steady-state) position, then the resulting differential fluid pressures would tend to

produce either a divergent or stable motion of the blade. Stability is defined here to be blade motions about the steady-state position and channel perturbation velocities that decay in time.

The primary difference between the stability problem being discussed here and the classical flutter analysis of aeroelasticity is that the lateral boundaries of the fluid are in much closer proximity so that the flutter assumptions of an infinite fluid media are not reasonable.

In developing the mathematical model, a one-dimensional flow field is assumed and the desired expressions for the differential pressure (i.e., the pressure difference acting normal to the blade) acting along the blade is derived by considering a control volume of fluid bounded by the rigid wall and the blade. Cross flow around the sides of the blade is also considered. This is shown in section X-X of Fig. 1.

Some experimental results of tests conducted with a model very similar to that shown in Fig. 1 will be compared with the results of the analytical model derived herein. The experimental model used had only a rotational degree of freedom.

Although there have been at least two other published investigations of this problem in the past using the same general conceptual approach (see, for example, Refs. 1 and 2), the criterion used for stability was not as rigorous as presented herein. Also the current analysis has some additional refinements so that it may be considered quite apart from this previous work.

ANALYTICAL PROCEDURE

A. General

The equations of motion for the rigid blade of Fig. 1 are simply:

$$J\ddot{\theta} + C_T\dot{\theta} + \left(\frac{mgL}{2} + K_T\right)\theta + \left(\frac{mL}{2}\right)\ddot{y} = B_o \int_o^L z\Delta p \, dz \tag{1}$$

$$\left(\frac{mL}{2}\right)\ddot{\theta} + m\ddot{y} + C_Y\dot{y} + K_Y \cdot y = B_o \int_o^L \Delta p \, dz \tag{2}$$

Thus the problem at hand is the evaluation of the right-hand side of equations (1) and (2).

Due to the involved, lengthy algebraic expressions that occur in the analysis, it is most helpful if the analysis is presented and explained in a stepwise fashion. This will be accomplished in the next sections.

B. Identification of Key Parameters

The following parameters are defined here for the sake of continuity. Reference to Fig. 2 will aid in the visualization of these parameters. Note that for convenience, both x and z directions are defined.

V	Upstream Steady-state Velocity
$v_2(t)$	Perturbation of the Upstream Velocity
$v_1(z,t)$	Perturbation of the Velocity Past the Blade
$r \cdot V$	Steady-state Velocity Past the Blade
$r = A/A_o$	Defines the Flow Split for the Steady-state Condition
K_T	Rotational Spring Constant
K_Y	Translational Spring Constant
$\Delta P(z,t)$	Differential Pressure Acting on the Blade
$u(x,t)$	Cross-flow Velocity Moving in the Direction of Positive ΔP
K_I	Loss Coefficient at Upstream End of Blade (Inlet)
K_o	Loss Coefficient at Downstream End of Blade (Outlet)
f	Darcy Friction Factor
J	Mass Moment of Inertia of the Blade about Its Pivot Point
m	Mass of the Blade
C_Y	Translational Damping Coefficient
C_T	Rotational Damping Coefficient
L	Length of the Blade

C. Derivation of ΔP along the Blade

The following three steps will result in a general expression for the gradient of the lateral differential pressure:

Step 1 - A continuity and momentum balance are applied to the channels on the right and left sides of the blade. Cross-flow communication between the control volumes is allowed. This results in a Bernoulli-type partial differential equation which, for either channel, relates the axial pressure gradient to the channel velocity and geometry.

Step 2 - The fluid velocity is assumed to be composed of a steady-state term that corresponds to the velocity when the blade is centered in the channel and a perturbation term. When this form for the velocities is substituted into the equations of Step 1, the equations can be linearized.

Step 3 - The left-side equation from Step 2 is subtracted from the right-side equation from Step 2. This develops an equation for the axial gradient of the differential pressure in terms of the channel velocity, dimensions, and the perturbation parameter.

The resulting equation from Step 3 is:

$$\frac{\partial(\Delta P/\rho)}{\partial z} = 2\frac{\partial v_1}{\partial t} - 2Vr\frac{\partial v_1}{\partial z} + \frac{fV\cdot r\cdot v_1(B - B_S + A_o)}{A_o \cdot B} - \frac{f(V\cdot r)^2(B - B_S)(y + z\theta)}{2 \cdot B \cdot A_o^2} \tag{3}$$

and upon integration:

$$(\Delta P/\rho) = 2\int \frac{\partial v_1}{\partial t}\,dz - 2Vr\int \frac{\partial v_1}{\partial z}\,dz + \frac{fV\cdot r(B - B_S + A_o)}{A_o \cdot B}\int v_1\,dz$$

$$- \frac{f(V\cdot r)^2(B - B_S)}{2 \cdot B \cdot A_o^2}\left(yz + \frac{\theta z^2}{2}\right) + ¢. \tag{4}$$

Note that since v_1 cannot be determined explicitly, equation (4) cannot be evaluated. However, by applying continuity between the upstream end of either the right or left channel and a point in the blade region, an expression for v_1 can be derived as follows:

$$v_1 = \frac{V\left[y(1 - r) + \theta(L - rz)\right] + v_2A - (L - z)\left[\dot{y} + \dot{\theta}(L + z)/2\right] - \frac{2\cdot B_S}{B}\int u\,dx}{A_o} \tag{5}$$

The integral in equation (5) represents the effect of cross flow between the channels and u is the cross-flow velocity. From an inspection of equation (4), it can be seen that the cross-flow effect tends to reduce the differential pressure and therefore has a stabilizing effect. However, since one-dimensional flow theory is being used, an expression for the cross flow cannot be derived analytically. Thus, empirical relationships must be sought.

One simple relationship that has been used for a purely rotational blade motion is:

$$u = V\cdot r(L - x)(C_1 \cdot \theta). \tag{6}$$

One of the obvious advantages of equation (6) is that by substituting this expression into equation (5) the integration may be performed directly. Also, it will be shown later how the coefficient in equation (6) can be determined experimentally.

The experimental work presented in Ref. 3 suggests a relationship for the cross-flow velocity as a function of the differential pressure. A recent correlation of the data of Ref. 3 indicated that a suitable expression for the cross-flow velocity based on the test data was

$$u = \frac{C(\Delta P/\rho)}{V \cdot r}. \tag{7}$$

However, in Ref. 3 the cross flow between channels was accomplished by drilling holes in the fixed plate which separated the two channels. This is considerably different than the continuous slot along both blade edges shown in Fig. 1. For the purpose of this presentation, the relationship of equation (6) will be used together with an assumed relationship

for the pure translation case to give the following combined expression:

$$u = V \cdot r(L - x)(C_1\theta + C_2 \cdot y/A). \tag{8}$$

D. Boundary Conditions at Leading and Trailing Ends of Blades

The boundary conditions used at the trailing edge (z = 0) can have a considerable effect on the type of solutions obtained in the final stability analysis. Figure 3 illustrates the flow assumptions used in the present investigation.

Writing an energy balance (Bernoulli's Equation with losses) for each channel at the leading and trailing ends of the blade and subsequent subtraction of the left and right channel results will give the following expressions for the boundary conditions at the two ends of the blades:

$$\left(\frac{\Delta P}{\rho}\right)_o = \frac{2Vr(K_o - 1 + 1/r^2)}{A_o}\left\{V[y(1-r) + \theta L] + v_2 A - L(\dot{y} + \dot{\theta}L/2) - \frac{2 \cdot B_S}{B}\int u\, dx\right\} \tag{9}$$

$$\left(\frac{\Delta P}{\rho}\right)_L = 2Vr(1 + K_I)\left[\frac{V(r - 1)(y + \theta L)}{A_o} - v_2 r\right] \tag{10}$$

where K_o and K_I represent loss coefficients at the trailing and leading ends of the blade, respectively. It should be noted that these coefficients contain both recoverable and unrecoverable pressure drops. For example, in the case of pure rotation where the trailing end of the blade is fixed in the center of the channel, by using momentum balance equations, expression for K_o' reflecting the recoverable pressure drop due to a sudden channel enlargement is found to be:

$$K_o' = (1 - 1/r)^2. \tag{11}$$

The expression for the differential pressure, equation (4), can now be evaluated. Substitution of equation (8) into (5) will permit evaluation of the perturbation velocity v_1. Substitution of v_1 into equation (4) and subsequent integration using the boundary condition (9) yield the final expression for the differential pressure.

E. Final Form of the Governing Equations

Once the right-hand side of equations (1) and (2) have been evaluated, the two expressions for the dynamic motion of the blade can be conveniently rewritten in matrix form as follows:

$$[M]\begin{Bmatrix}\ddot{\theta}\\ \ddot{y}\end{Bmatrix} + [C]\begin{Bmatrix}\dot{\theta}\\ \dot{y}\end{Bmatrix} + [K]\begin{Bmatrix}\theta\\ y\end{Bmatrix} + [D]\begin{Bmatrix}v_2\\ \dot{v}_2\end{Bmatrix} = \begin{Bmatrix}0\\ 0\end{Bmatrix}. \tag{12}$$

In order to reduce the above set of equations to a set of first-order differential equations, the following substitutions are made:

$$\xi = \dot{\theta}; \quad \eta = \dot{y}. \tag{13}$$

Also let:

$$\{\Psi\} = \begin{Bmatrix} \theta \\ y \\ \xi \\ \eta \\ v_2 \end{Bmatrix}. \tag{14}$$

Equations (12) can be rewritten as:

$$\left[\begin{array}{c|c|c} I & 0 & 0 \\ \hline 0 & M & \begin{matrix} D_{12} \\ D_{22} \end{matrix} \end{array}\right] \left\{\dot{\Psi}\right\} = \left[\begin{array}{c|c|c} 0 & I & 0 \\ \hline -K & -C & \begin{matrix} -D_{11} \\ -D_{21} \end{matrix} \end{array}\right] \left\{\Psi\right\} \tag{15}$$

where D_{ij} represent the elements of matrix $[D]$.

Equation (15) represents a set of four equations in five unknowns. However, by equating the expression for the differential pressure, ΔP, evaluated at $z = L$ (equation (10)), a fifth independent equation may be added to (15) for the following final form:

$$\left[\begin{array}{c|c|c} I & 0 & 0 \\ \hline 0 & M & \begin{matrix} D_{12} \\ D_{22} \end{matrix} \\ \hline \multicolumn{3}{c}{B_1} \end{array}\right] \left\{\dot{\Psi}\right\} = \left[\begin{array}{c|c|c} 0 & I & 0 \\ \hline -K & -C & \begin{matrix} -D_{11} \\ -D_{21} \end{matrix} \\ \hline \multicolumn{3}{c}{B_2} \end{array}\right] \left\{\Psi\right\} \tag{16}$$

or

$$\left[E_1\right]\left\{\dot{\Psi}\right\} = \left[E_2\right]\left\{\Psi\right\} . \tag{17}$$

Equation (16) can be restated in the standard form of an eigenvalue problem as follows:

$$\left\{\Psi\right\} = \left[N\right]\left\{\Psi\right\} \tag{18}$$

where

$$\left[N\right] = \left[E_1\right]^{-1}\left[E_2\right] . \tag{19}$$

The stability of the original system of equations ((1) and (2)) can now be determined by inspection of the eigenvalues of the square matrix $[N]$. Standard eigenvalue routines may be used for this purpose. For the work contained herein, two different routines were used and both gave identical results. However, one routine also computed the eigenvectors. Documentation for these routines can be found in references (4) and (5).

A computer program that obtains the matrix [N] starting with the basic system parameters and a specific upstream velocity V has been written in FORTRAN IV and programmed on the CDC-6600. The eigenvalues and eigenvectors are computed and stability of the system is indicated by the sign of the real part of the eigenvalues.

The eigenvalue with the largest positive real part is the dominant eigenvalue of the system. Negative real parts of the eigenvalue represent stable behavior and positive or zero real parts represent unstable behavior. The periodic component of the blade motion is described by the imaginary values of the eigenvalues. Excursive instabilities are described by eigenvalues which have positive real components and no imaginary component. Thus, this is a definition of asymptotic stability in the sense of Lyapunov.

ANALYTICAL RESULTS

A. Pure Rotational Motion--No Cross Flow

If cross flow is omitted and only pure rotational motion is considered, the governing equations can be conveniently rewritten in dimensionless form. By introducing the mass density of the solid body, γ, one of the dimensionless ratios is γ/ρ, ρ being the mass density of the fluid. Some results of this analysis are illustrated in Fig. 4 for the case of a steel blade in water.

Referring to Fig. 4, it can be seen that according to the assumptions of the analysis presented herein, as the blade clearance A_o is made increasingly small ($H/A = 2$ corresponds to zero clearance), the system becomes more unstable. A similar set of curves would be obtained if γ/ρ were calculated for a blade in air. Some discrepancies will occur since the friction factor is assumed constant over the entire range of velocities and channel geometries. However, the curves are suitable for observing trends in the model.

B. Two-Degree-of-Freedom Analysis--No Cross Flow

The effect of considering one or two degrees of freedom can be demonstrated by another example. These results should not be interpreted as universal--they are only descriptive of the example considered. However, the results do point out the effect that an additional degree of freedom can have on the critical velocity. In the example, based upon pure rotation, an excursive instability was found at a fluid velocity of 581 in./sec. The system was stable based upon a pure translational analysis. The two-degree-of-freedom coupled motion analysis indicated that a decreasing value for the translational spring constant destabilized the system. As the magnitude of the translational spring constant increased the system response approached that of a pure rotation analysis. These results are summarized in Table I.

TABLE I.
Comparison of One- and Two-Degree-of-Freedom Analysis

Model	Fluid Velocity at Instability, in./sec	Instability Type
Pure Rotation		
K_T = 2000 in.-lb/rad.	581	Excursion
Pure Translation	Stable for V < 10000	
Coupled Motion		
K_T = 2000 in.-lb/rad.		
K_Y = 0.1 lb/in.	544	Excursion
K_Y = 10 lb/in.	577	Excursion
K_Y = 100,000 lb/in.	580	Excursion

C. Effect of Downstream Loss Coefficient
Pure Rotational Motion--No Cross Flow

The influence that the loss coefficient at the downstream end of the blade has on the calculated critical velocity was investigated for a particular configuration. The configuration used in this study corresponds to the experimental model discussed in the next section. Results from this study are shown in Fig. 5. For ease of presentation the entire term containing K_o in equation (9) was designated as $(K_o'' - 1)$ so that K_o'' represents both recoverable and unrecoverable pressure drops at the downstream end.

Figure 5 illustrates that an increase in the magnitude of the loss coefficient K_o'' from a value of zero to a value of approximately 0.11 has a very drastic stabilizing effect. Also, the mode of instability corresponds to a sinusoidal motion within this region. If K_o'' is further increased the effect is a gradual destabilizing of the system although the effect appears to reach an asymptotic limit. However, the mode of instability in this region corresponds to a divergent motion. A nondimensional analysis was performed, and it verified the trends illustrated in Fig. 5.

EXPERIMENTAL RESULTS

Recently some fundamental tests involving an aluminum blade inserted in a wind channel have been conducted at the University of Cincinnati, Department of Mechanical Engineering, under the direction of Professor Thorpe. These tests utilize essentially the same simplified model that is shown in Fig. 1 with the exception that only a rotational spring is attached to the downstream end of the blade. The channel is five inches by two inches and the blade is 4.75 inches wide by 0.25 inch thick and is 24.0 inches long.

Professor Thorpe has attempted to evaluate the cross-flow coefficient C_1 presented in equation (6) by tilting the blade a small amount and fixing this position in the channel, and then measuring the differential pressure at the leading edge of the blade for a given steady-state velocity. This information is then used in conjunction with an analytical expression for C_1 that can be derived by equating the expression for the differential pressure evaluated at z = L and the boundary condition, equation (10). The The data is obtained from static conditions so all time derivatives are set equal to zero. For pure rotation this constant is found to be

$$C_1 = \frac{\dfrac{2r^2LK_o}{A_o} + \dfrac{fr^2L^2}{4B\cdot A_o^2}(B - B_S + 2A_o) - \left(\dfrac{\Delta P}{\rho V^2\theta}\right)_L^* \left[\dfrac{K_I + K_o}{K_I + 1} + \dfrac{fL(B - B_S + A_o)}{2BA_o(1 + K_I)}\right]}{\dfrac{2B_S r^2L^2}{B\cdot A_o}\left[K_o + \dfrac{fL(B - B_S + A_o)}{3A_oB}\right]} \tag{20}$$

The term $\left(\dfrac{\Delta P}{\rho V^2\theta}\right)_L^*$ is determined experimentally and remains constant. This expression for C_1 has been included in the computer program previously mentioned. Obviously, other assumed relationships for the cross-flow velocity u will have varying effects on the solution of the stability problem.

Figure 6 presents preliminary results from Professor Thorpe's work. It should be noted that the instability observed was divergent in that the blade suddenly moved against the channel wall at the critical velocity. Prior to the inception of divergence the blade motion was not observed to be periodic in nature. Analytical results assuming only recoverable pressure drops at the ends, and no damping, are also shown on the figure. The analytical results predicted a divergent instability of the blade at the critical velocity. The preliminary nature of the data does not warrant a more exhaustive analysis. The figure clearly shows the effects of cross flow upon stabilizing the system. The cross-flow coefficient determined in accordance with Professor Thorpe's leading edge pressure differential data gives the correct data trends but it underestimates the velocity required to induce the instability. It is also possible to consider the cross-flow coefficient as a correlation parameter. In that case the data could be used to establish the magnitude of the effective cross-flow coefficient consistent with the assumptions of equation (6). The usefulness of such a technique would be established in the event that such an empirically determined coefficient could be used to predict other independent data.

CONCLUSIONS

A computer-oriented eigenvalue approach to defining flow-induced vibration stability has been shown to be feasible. Two degrees of freedom and cross-flow effects are important and must be included in the model. Experimental results from simplified geometries are needed in order to evaluate the assumptions used in developing the analytical model. Once the reliability and accuracy of the model are established it will be possible

to more extensively define the effects of various parameters upon the systems stability.

ACKNOWLEDGMENT

The authors wish to acknowledge Dr. N. C. Small for his contributions toward an understanding of the stability problem that were made while he was employed by the Bettis Atomic Power Laboratory from 1967 to 1968.

REFERENCES

1. D. R. Miller and R. G. Kennison, "Theoretical Analysis of Flow-Induced Vibration of a Blade Suspended in a Flow Channel," ASME Paper 66-WA/NE-1, Winter Annual Meeting, 1966.

2. F. T. Dodge and A. F. Muller, "Flow-Induced Vibrations of a Flat Blade Suspended in a Narrow Channel," NASA-CR-1186, September 1968; also available as N68-35086.

3. T. G. Chapman and P. N. Stevens, "Pressure Equalization by Fluid Exchange between Parallel Flow Channels," ORNL-TM-456, April 1958.

4. L. Ehrlich, "Eigenvalues and Eigenvectors of Complex Non-Hermitian Matrices Using the Direct and Inverse Power Methods and Matrix Deflation," The University of Texas Computation Center, UTF4-01, August 1961.

5. B. Parlett, "The Development and Use of Methods of LR Type," SIAM Review 6, 275-295 (1964).

DISCUSSION

S. Fabic (Westinghouse): Do you consider the effect of trailing edge unimportant? It's not modeled.

Lowe: That's right, it's not modeled. As a matter of fact, at MIT Dr. Eggelston, Dr. Toebes and other researchers did a study of the effect of trailing edges on the stability of various plates and found it to be quite important.

Fabic: We looked at the shape of the trailing edge around the reentrance and so on, and it has a very pronounced effect on the amplitude of vibration.

Lowe: Normally you think if you shape the trailing edge and get a good hydrodynamic shape you'll enhance stability, but if you miss shaping it properly and it's rounded, it tends to apparently destabilize as compared to, say, a sharp trailing edge or reentrant trailing edge.

Fabic: It depends on the degree of hydrodynamic shaping. If it's a very slow angle, like a small angle of 7°, of divergence, then you have a lot of stable operation, but if you have a round edge that may look aerodynamically nice, it may be the worst condition. So I was wondering

whether these crossflow effects that you are considering in the model are really masked by the effect of the trailing edge?

Lowe: There is one thing; the test data that Professor Thorpe is developing is at flows low enough that he isn't getting a lot of vortices shed off the end, and when he's not shedding vortices, I suspect the trailing edge has less influence except as it influences the loss coefficient at that point. The big influence of the trailing edge results when it starts shedding vortices and putting on some sort of forcing function on the trailing edge of the plate.

D. H. Pai (Foster Wheeler): I have not had a chance to look at your paper. In your governing equations, do you include the effect of a virtual or apparent mass in the calculations?

Lowe: When you integrate that term for the transverse pressure, there are some terms proportional to the second derivative of the space coordinate. You could call those apparent, or virtual, mass. We didn't arbitrarily put in apparent mass, but it comes in through the control volume formulation. So there are some terms that are related by the geometry to the second derivative. In fact, it brings in some damping-type terms and some spring-constant terms.

P. M. Moretti (Westinghouse): Just to get back to this trailing-edge problem again. One way to look at it is whether you have a well-defined separation point or not, and while there are a great number of phenomena involved in this flow-induced vibration, the movable separation point, in one way or another, is very frequently one of the things that leads to a strong forcing function. This is really one way to look at the cylinder in the crossflow problem, or the oscillating diffuser problem, or any kind of nozzle, and perhaps it's actually visually a little bit easier to tie this together. I think that's the point that Dr. Fabic was making with respect to this. Really, if you don't have well-defined separation points, you are very likely to get into trouble and find that your dominant phenomenon is right there.

G. H. Toebes (Purdue U.): I would like to disagree with this and put down some results. (Additional comments inaudible on tape.)

Lowe: One of the problems is that if you begin to shape this trailing edge and you feel you're getting a good shape and are going to improve things, if it's poorly designed it can turn out to be the worst shape, as compared to just leaving the trailing edge alone and leaving it stay square. One other problem you will encounter is the interaction due to the plate motion and the vortex shedding that is different than if you hold the plate rigid and make measurements. You have to be careful when you set up your experiments.

S. C. Rose (GE-KAPL): In your analysis and in what you have done, you have assumed what amounts to a streamlined shape at the exits, such that you don't have any vortex shedding off of this plate. I mean you just neglected that altogether. In some of the work we've done at GE, we find that the excitation mechanism for the flow induced vibration of plates can be vortex shedding giving rise to a very strong excitation force. In your analysis, what you've done is assumed some sort of streamlined body where

vortex shedding is not an excitation mechanism. If you take your analysis and were to apply it to a plate where you do have strong vortices coming off the exit, like say you had a full round or a triangle at the end, I think you could be somewhat misled in applying your results to such a case.

Lowe: That's right. We've neglected vortex shedding. The test data, of course, that Dr. Thorpe is developing is at low enough velocities that he's not getting vortex shedding. If vortex shedding occurs, there's another forcing function that we need to introduce into the model.

M. Bender (ORNL): Can I ask why you put that restraint on your investigation? I mean the low peak velocities.

Lowe: Well, first of all we are trying to determine whether the model can predict experimental results and if it was no good, then we wouldn't pursue the model and so we developed a model and then we are trying to get some test data representative of that model to determine and assess the value of the model. Then for application we will have to consider other things.

Rose: Professor Toebes might want to comment on why the reentrant notch is such an effective device for reducing the vortex excited type vibrations. Would you have any comment on that, Professor Toebes?

Toebes: (Comments not audible on tape.)

Bender: I did want to make one other observation. Yesterday, Dr. Nevitt in his opening discussion made some comment about the importance of considering materials in structural damage, and this type of discussion, and the one thing I've noticed in the discussion today is a total lack of discussion of what constitutes structural damage and how to evaluate it. Maybe the next time we have a conference like this we can hear a little bit about this.

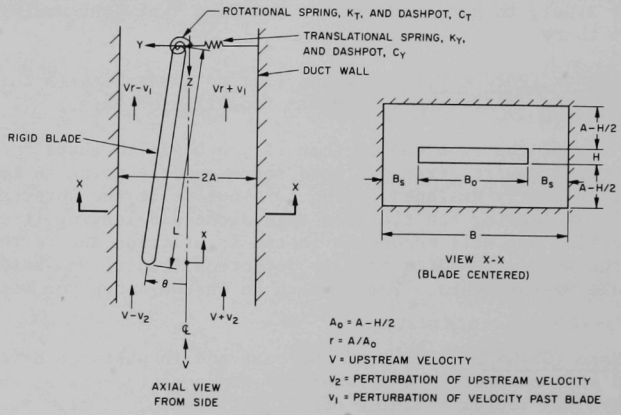

Fig. 1. Schematic of Flow Channel

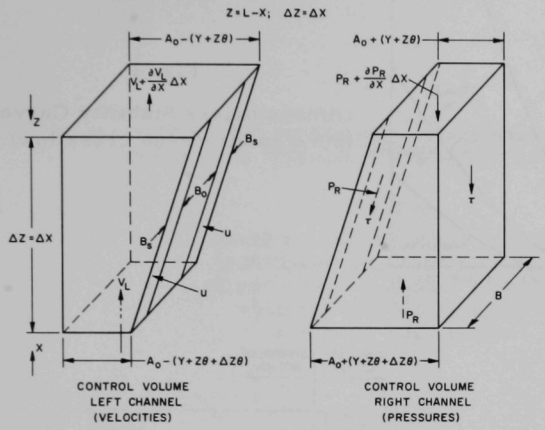

Fig. 2

Control Volumes

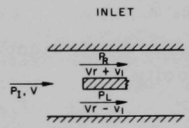

$$\frac{P_I}{\rho} + \frac{V^2}{2} = \frac{P_R}{\rho} + \frac{(K_I + 1)}{2}(Vr + v_l)^2$$

$$\frac{P_I}{\rho} + \frac{V^2}{2} = \frac{P_L}{\rho} + \frac{(K_I + 1)}{2}(Vr - v_l)^2$$

Fig. 3

Boundary Conditions

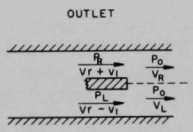

$$\frac{P_o}{\rho} + \frac{V_R^2}{2} = \frac{P_R}{\rho} + \frac{(1 - K_o)}{2}(Vr + v_l)^2$$

$$\frac{P_o}{\rho} + \frac{V_L^2}{2} = \frac{P_L}{\rho} + \frac{(1 - K_o)}{2}(Vr - v_l)^2$$

$$\rho A_o (Vr + v_l) = \rho A V_R$$

$$\rho A_o (Vr - v_l) = \rho A V_L$$

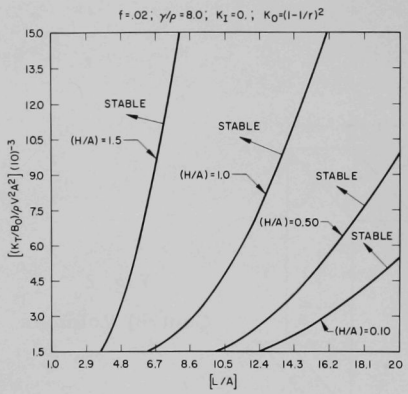

Fig. 4

Dimensionless Stability Curves (pure rotation--no crossflow)

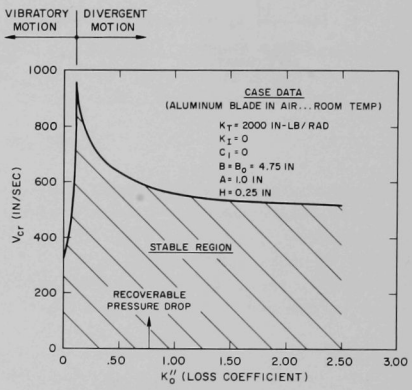

Fig. 5

Effect of Exit Loss Coefficient on Critical Velocity

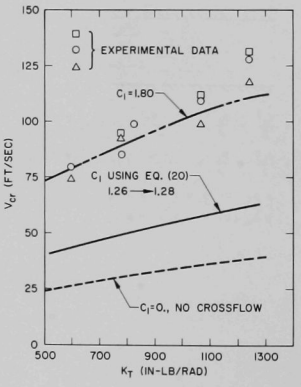

Fig. 6

Comparison of Experimental Results with Analysis

ANALYSIS OF THE FUNDAMENTAL VIBRATION FREQUENCY OF A RADIAL VANE INTERNAL STEAM SEPARATOR STRUCTURE

E. Kiss

Manager, Applied Mechanics Unit
Development Engineering Section
Atomic Power Equipment Department
General Electric Company
San Jose, California

ABSTRACT

The analysis of the fundamental vibration frequency of a Radial Vane Internal Steam Separator has been performed considering the effect of the entrapped fluid between the idealized structure and pressure vessel wall. The hydrodynamic or "virtual" mass associated with a vibrating finite length cylinder is presented in terms of a correction factor to be used with the calculated two-dimensional "mass" effect. Finally, the lateral frequency of a radial vane separator assembly has been measured and compared with the predicted value.

INTRODUCTION

For several years the General Electric Company has been evaluating the performance of Radial Vane Steam Separators for application to commercial BWR reactors. As contrasted to the axial steam separators, of which there may be several hundred required for 1100 MWe plants, only one radial vane steam separator would be needed. In the present BWR design, internal steam separators are mounted directly to the core support structure. As a consequence of this, the steam separation mechanism is considered a potential source of vibration stimuli. Indeed, measurement (1) of the vibration response of the core support structure at KRB,* during power operation, did show a direct correlation of vibration amplitude and steam flow. The measured vibration appeared random in amplitude with predominant frequency that of the minimum lateral rocking mode associated with the core support cylindrical structure on elastic supports. Although the measured vibration magnitudes were of no structural concern, the potential use of a radial vane separator represented a significant departure from past experience since the dynamic characteristics of the separator-core support structure were unknown.

* KRB Gundremmingen - AEG, General Electric

In view of these factors, a mechanical model was idealized to predict the lateral rocking frequency of the core structure including the dynamic effect of the entrapped water in the annulus formed by the radial vane steam separator and the pressure vessel wall. The hydrodynamic effect was considered important since many investigations (2,3) have shown that the mass effect of fluid entrapped in small clearances can be quite dramatic in reducing the natural frequency from that in vacuo.

Figure 1 shows a typical radial vane steam separator, while Fig. 2 shows the two-degree-of-freedom mechanical model used to predict the lateral natural frequency.

It is convenient to consider the analysis in terms of ratio of vane bending the stiffness to shell support stiffness since it easily permits evaluation of several different radial vane structure designs.

Writing the displacement and rotation of mass M_T as follows,

$$\left\{\begin{aligned} y &= \frac{V\ell_2^3}{EI_2}\,\xi(\alpha,\beta) + \frac{T\ell_2^2}{EI_2}\,\eta(\alpha,\beta) \\ \varphi &= \frac{V\ell_2^2}{EI_2}\,\eta(\alpha,\beta) + \frac{T\ell_2}{EI_2}\,\nabla(\alpha,\beta) \end{aligned}\right\} \tag{1}$$

where

$$\xi(\alpha,\beta) = \frac{1}{3} + \alpha + \alpha^2 + \alpha^3/3\beta$$

$$\eta(\alpha,\beta) = \frac{1}{2} + \alpha + \alpha^2/2\beta$$

$$\nabla(\alpha,\beta) = 1 + \alpha/\beta$$

using D'Alembert's principle, the inertia force and moment V and T can be taken as static loads:

$$\left\{\begin{aligned} V &= -M_T\ddot{y} \\ T &= -J_0\ddot{\varphi} \end{aligned}\right\} \tag{2}$$

assuming harmonic motion

$$\left\{\begin{aligned} \begin{bmatrix} y \\ \varphi \end{bmatrix} &= \begin{bmatrix} Y \\ \Phi \end{bmatrix} e^{ipt} \\ \begin{bmatrix} \ddot{y} \\ \ddot{\varphi} \end{bmatrix} &= -p^2 \begin{bmatrix} Y \\ \Phi \end{bmatrix} \end{aligned}\right\} \tag{3}$$

and substituting (3) in (1) and (2), the frequency equation (4) is determined by setting the determinant equal to zero:

$$p^4 C_1 + p^2 C_2 + 1 = 0 \tag{4}$$

where

$$C_1 = \frac{M_T J_0 \ell_2^2}{E^2 I_2^2}(\xi\nabla - \eta^2)$$

$$C_2 = \frac{\ell_2}{EI_2}(M_T \ell_2^2 \xi + J_0 \nabla).$$

The minimum natural frequency $f_1 = p_1/2\pi$ evaluated from equation (4) is shown as a function of stiffness ratio β in Fig. 3.

In order to evaluate the hydrodynamic mass (virtual mass) associated with the entrapped fluid between the internal cylinder and vessel wall, the three-dimensional fluid flow problem has been considered. Figure 4 shows the idealized model used.

Consider the cylinder (r = a) subjected to an impulsive translation x(t). Assuming potential flow exists (2), the impulsive pressure on the cylinder can be evaluated as follows:

$$\nabla^2 \phi = 0$$

$$\frac{\partial^2 \phi}{\partial r^2} + \frac{1}{r}\frac{\partial \phi}{\partial r} + \frac{1}{r^2}\frac{\partial^2 \phi}{\partial \theta^2} + \frac{\partial^2 \phi}{\partial z^2} = 0; \tag{5}$$

assuming a separable solution,

$$\phi = R(r)\Theta(\theta)Z(z)f(t) \tag{6}$$

$$\left\{\begin{aligned} \Theta &= A \sin K\theta + B \cos K\theta \\ Z &= C \sin nz + D \cos nz \\ R &= E\, I_k(\xi) + F\, K_k(\xi) \end{aligned}\right\} \quad \xi = nr \tag{7}$$

where I_k, K_k are the modified Bessel functions of the 1st and 2nd kind.

The boundary conditions are:

a. $z = 0 \qquad w = \frac{\partial \phi}{\partial z} = 0$

b. $z = H \qquad p = -\rho\frac{\partial \phi}{\partial t} = 0$

c. $r = a \qquad u = \dot{x}(t) \cos \theta = \left(\frac{\partial \phi}{\partial r}\right)_a$

d. $r = b \qquad u = \left(\frac{\partial \phi}{\partial r}\right)_b = 0.$

To satisfy boundary conditions a and b,

$$C = 0 \qquad \text{and} \qquad n = \frac{m\pi}{2H}$$

so

$$\phi = \sum_{m=1,3,5}^{\infty} D_n \, R(r) \, \Theta(\theta) \cos\left(\frac{m\pi}{2H}\right) z \, f(t). \tag{8}$$

To satisfy boundary conditions c,

$$A = 0, \qquad K = 1, \qquad f(t) = \dot{x}(t)$$

$$\sum_{m=1,3,5}^{\infty} D_m \, R'(a) \cos\left(\frac{m\pi}{2H}\right) z = 1. \tag{9}$$

From boundary conditions d,

$$\sum_{m=1,3,5}^{\infty} D_m \, R'(b) \cos\left(\frac{m\pi}{2H}\right) z = 0 \tag{10}$$

$$\frac{\partial}{\partial r} = \frac{\partial}{\partial \xi} \frac{\partial \xi}{\partial r} = n \frac{\partial}{\partial \xi}.$$

Write equations (9) and (10):

$$\sum_{m=1,3,5}^{\infty} \frac{m\pi}{2H} \left[E_m I_1'(\xi_a) + F_m K_1'(\xi_a) \right] \cos\left(\frac{m\pi z}{2H}\right) = 1 \tag{11}$$

$$\sum_{m=1,3,5}^{\infty} \frac{m\pi}{2H} \left[E_m I_1'(\xi_b) + F_m K_1'(\xi_b) \right] \cos\left(\frac{m\pi z}{2H}\right) = 0. \tag{12}$$

Expanding equation (1) as an even Fourier series in the interval 0 - H with period 2H:

$$1 = \frac{4}{\pi} \sum_{m=1,3,5}^{\infty} \frac{1}{m}(-1)^{(m-1)/2} \cos \frac{m\pi z}{2H} \tag{13}$$

$$1 = \frac{4}{\pi}\left[\cos\frac{\pi z}{2H} - \frac{1}{3}\cos\frac{3\pi z}{2H} + \frac{1}{5}\cos\frac{5\pi z}{2H} - \ldots\right].$$

Equating coefficients in equation (11),

$$\begin{aligned} &E_1 I_1'(\tfrac{\pi a}{2H}) + F_1 K_1'(\tfrac{\pi a}{2H}) = \frac{8H}{\pi^2} \\ &E_3 I_1'(\tfrac{3\pi a}{2H} + F_3 K_1'(\tfrac{3\pi a}{2H}) = -\frac{8H}{9\pi^2} \\ &\quad\vdots \qquad\qquad\qquad \vdots \qquad\qquad\qquad \vdots \\ &\text{etc.} \end{aligned} \tag{14}$$

Equations (14) are q equations with 2q unknowns. However, equation (12) is true for all z, so

$$\frac{E_m}{F_m} = -\frac{K_1'(\frac{m\pi b}{2H})}{I_1'(\frac{m\pi b}{2H})}. \tag{15}$$

Using equation (15), equations (14) can be written:

$$F_m = \frac{\frac{8H}{m^2\pi^2}(-1)^{(m-1)/2}}{K_1'(\frac{m\pi a}{2H}) + \left(\frac{E_m}{F_m}\right) I_1'(\frac{m\pi a}{2H})}, \tag{16}$$

and

$$\phi = \sum_{m=1,3,5}^{\infty} \left[E_m I_1(\tfrac{m\pi r}{2H}) + F_m K_1(\tfrac{m\pi r}{2H})\right] \cos(\tfrac{m\pi z}{2H}) \cos\theta\, \dot{x}(t). \tag{17}$$

The hydrodynamic pressure p is

$$p = -\rho\frac{\partial\phi}{\partial t} = -\rho\dot{x}(t) \sum_{m=1,3,5}^{\infty} \left[E_m I_1(\tfrac{m\pi r}{2H}) + F_m K_1(\tfrac{m\pi r}{2H})\right] \cos(\tfrac{m\pi z}{2H}) \cos\theta. \tag{18}$$

The resultant force in the x direction on the internal cylinder is

$$F_x = -2 \int_{-\pi/2}^{\pi/2} \int_0^H p \Big|_{r=a} a \cos\theta \, d\theta \, dz. \tag{19}$$

The hydrodynamic, or virtual, mass is then:

$$M_h = 2\rho a H \sum \frac{1}{m}(-1)^{(m-1)/2} \left[E_m I_1\left(\frac{m\pi a}{2H}\right) + F_m K_1\left(\frac{m\pi a}{2H}\right) \right], \tag{20}$$

where the E_m, F_m are determined from equations (15) and (16).

Equation (20) has been solved and is shown in Fig. 5 plotted as a correction factor to be used with the two-dimensional mass effect (3).

$$K_L = M_h(3D)/M_h(2D)$$

$$M_h(3D) = M_H = K_L \left\{ \pi\rho a^2 \left[\frac{1 + (a/b)^2}{1 - (a/b)^2} \right] \right\}. \tag{21}$$

Vibration tests of a radial vane separator were performed in air and in water. Results are shown below:

	c.p.s.
Air	4.5
Water	3.5

$$\frac{f_o}{f_w} = \frac{4.5}{3.5} = 1.28.$$

For the test structure, the solid mass plus internal water mass is

$$M_o = 6.16 \ \frac{\text{lb-sec}^2}{\text{in.}}.$$

From equation (20) the virtual mass is evaluated to be $M_h = 4.33 \frac{\text{lb-sec}^2}{\text{in.}}$,

so

$$M_T = M_o + M_h = 10.49.$$

Then

$$\frac{f_o}{f_w} = \sqrt{\frac{M_T}{M_o}} = \sqrt{\frac{10.49}{6.16}} = 1.31,$$

which compares quite favorably to the test results.

CONCLUSIONS

1. The hydrodynamic mass effect associated with a finite length circular cylinder surrounded by a fluid annulus has been predicted and is presented in the form of a correction factor to be used with the infinite length (two-dimensional) case.

2. The minimum lateral natural frequency of a radial vane separator-core support structure can be accurately predicted using a two-degree-of-freedom model and considering the hydrodynamic mass effect as in Eq. (1).

REFERENCES

1. Internal General Electric Memorandum - KRB, Vibration Measurements at Power, Feb. 15, 1967.

2. K. Wendel, "Hydrodynamic Masses and Moments of Inertia," DTMB Translation 260.

3. R. J. Fritz and E. Kiss, "The Vibration Response of a Cantilevered Cylinder Surrounded by a Fluid Annulus," KAPL Memo-6539, Feb. 1966.

DISCUSSION

M. Bender (ORNL): Dr. Kiss has done an excellent job of reminding us that you have to account for everything in the systems and that we are really talking about systems analysis and not individual components. I wanted to make one other observation that came to my mind as I listened to these talks over the last couple of days. There's been a tremendous furor over the last year about seismic analysis, which in principle is not unlike this but is far less complicated, except for understanding the forcing function. My belief is that the meager amount of work that has been done, considering the complexity of this problem, would warrant perhaps some change in emphasis at least among those in the structural business who are concerned with making reactors work.

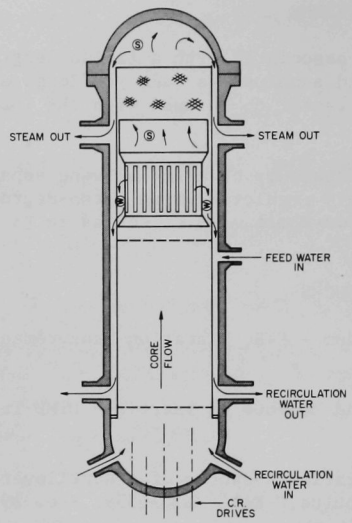

Fig. 1

Typical BWR with Radial Vane Steam Separator

Fig. 2

Two-degree-of-freedom Mechanical Model

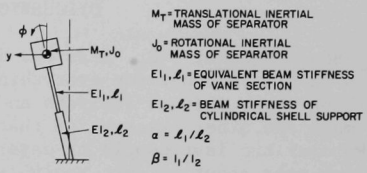

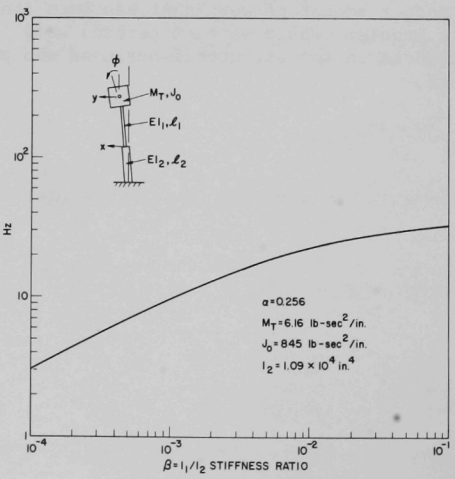

Fig. 3

Fundamental Frequency (Hz) vs β

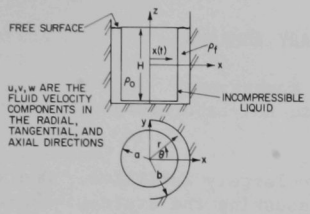

Fig. 4

Idealized Model

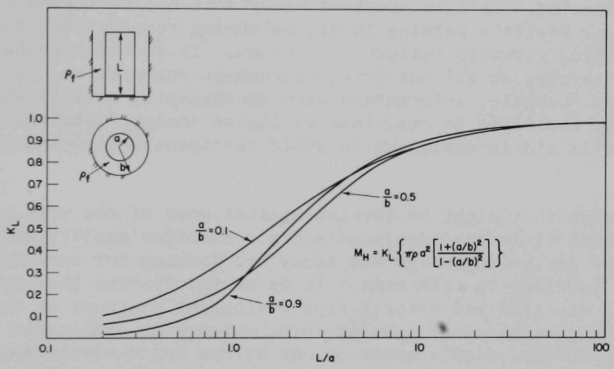

Fig. 5. End Effect Correction Factor for Virtual Mass Calculation for a Finite Length Circular Cylinder

SUMMARY REMARKS

M. W. Wambsganss
Argonne National Laboratory

The conference objectives were largely fulfilled. One of the objectives was to provide a basis for assessing the state-of-the-art. In this regard, it would have to be agreed that, while progress has been made, there is a lot of work to be done and a good deal of it will require careful experimentation. Certain areas of study were not discussed and, in particular, Dr. Nevitt's warning in his welcoming remarks should be heeded and consideration given to failure mechanisms. It should also be emphasized, that, throughout all our work, the design engineer should be kept in mind; whenever possible, information with accompanying qualifications, should be made available to him, that will give insight into the design problem and will aid in designing to avoid detrimental flow-induced vibration.

A criticism that might be leveled against most of the work which was reported is that it is too idealized and too far from reality to be of any use to reactor design engineers who today are looking for answers to practical design problems in this area. It is certainly true that we are a long ways off (in time and effort) from giving the designer an equation, or design guide in graphical or tabular form, which will enable him to predict, say, the flow-induced displacement of, or stress in, a wire-wrapped fuel element within a fuel assembly cluster. However, while results may be slow coming, progress is being made, as attested to by the conference papers, and the design engineers can benefit from our current insights if we assume the responsibility to make available what information we have in a form that is most usable.

For example, it has long been known that the Strouhal number associated with vortex shedding from a fixed cylinder in an "infinite" crossflow field is approximately a constant of 0.2 over a given range of Reynolds number. In a heat exchanger, the tubes are not rigid, the flow is not ideally crossflow, there is an effect of adjacent elements, and one can argue that well-defined vortices do not exist. Nevertheless, as Nelms and Segaser discuss in their survey,[1] tube failures did not occur in those heat exchangers in which the tube natural frequency was sufficiently greater (by a factor of 2 or 3) than the vortex shedding frequency based on a Strouhal number of 0.2. Now, while the exact mechanism of heat exchanger tube vibration is not known

[1]H. A. Nelms and C. L. Segaser, *Survey of Nuclear Reactor System Primary Circuit Heat Exchangers*, ORNL-4399 (April 1969).

and while he cannot predict the magnitude of the displacement and stresses in the tube, in checking the tube natural frequency against the vortex shedding frequency the designer has a computation he can perform with reasonable assurance of avoiding detrimental vibrations. Obviously nothing can be said about the degree of conservatism associated with the calculation; design optimization will come from more detail studies. But, this is the kind of design guide that one should look for at each step along the path toward an overall solution and command of the problem area.

While motivation for the study of flow-induced vibration and the desire to predict displacements and stresses stems from the potential for failure caused by fretting corrosion, wear and fatigue, conspicuously there was no mention of failure or failure mechanisms. It can be argued that any failure analysis that can be performed will require information from the models being developed to predict component response; therefore, why worry about failure until we have these models and methods developed and validated. Nevertheless, it might prove advantageous to consider and study potential failure mechanisms and identify the data required for their analyses. For example, with a random process, the form of the distribution function is important in determining crossing rate statistics, peak amplitudes, and in studying first-excursion failures. Nothing was said about distribution functions; however, a preliminary study has shown the Gaussian probability law to satisfactorily represent the amplitude distribution from typical displacement-time measurements of parallel-flow-induced vibration.[2] The information, transducers, and measurement technique that have so far been developed can contribute to the design of experiments for studying failure.

The majority of the work reported involved single elements with idealized geometries and flows, and not without good reason; however, designers are looking for results applicable to element bundles. In this regard, future research might be guided and the designer benefited by giving consideration to the performance of what might be termed preliminary, or scoping, tests with element bundles. These experiments might be carried out most expeditiously by those who have had experience with single element tests, the thought being that experience with making the kinds of measurements required would have been acquired previously. The purpose of these bundle experiments would be to provide insight into the effect adjacent elements might have and, with knowledge of the behavior of a single element as a reference, to provide insight into the feasibility of extrapolating single element response to obtain a first estimate of the response of an element within a bundle.

The flow-induced vibration of piping systems also was not mentioned. However, this may be a reflection of the specialization of the select group in attendance, rather than a lack of interest in the subject. Nevertheless, the vibration of piping is an important problem area to which many of the methods of analysis and testing that are being developed could be directly applicable. Mr. M. Bender mentioned there is also a need for work in the area of seismic analysis. Here, too, many of the techniques of analysis will have application.

---

[2] Argonne National Laboratory, *Reactor Development Program Progress Report for June 1969*, USAEC Report ANL-7581, pp. 103-105 (1969).

Response to two-phase flow was not discussed at the meeting; however, it is considered in the paper by T. S. Yih and P. Griffith of MIT. Some studies of vibration in two-phase flow also have been carried out at the Chalk River Nuclear Laboratories (AECL). As might be expected, vibration amplitudes are highly dependent on quality, or void fraction.

In the area of parallel-flow-induced vibration of cylindrical elements, it is generally accepted that nearfield flow noise is the dominant excitation source. (Support excitation, which may account for the orders-of-magnitude discrepancies between experiment and certain empirical correlations, would be of a different class of excitation.) However, mathematical modeling and analytical methods have reached the point where careful experimentation is now required, not only to obtain those time responses which can be used to validate the mathematical models, but also to obtain information relating to the structure and intensity of the forcing function, which is assumed to be the nearfield flow noise. Those who are, or have been, involved with experimental programs will acknowledge the difficulties that can be encountered when the quantities being measured are of small magnitude or when the components themselves are small or not readily accessible. The measurement of displacement and pressure in the study of parallel-flow-induced vibrations has required the development and construction of new transducers and measurement techniques; it is expected that these will also have use in studies of crossflow-induced vibration. Measurements and characterization of the pressure field on the surface of the element remain the cruxes of the problem and there is still a great deal of work to be done to understand the low frequency behavior of this field.

As in the area of parallel-flow-induced vibration, the work reported on in crossflow-induced vibration involved a single element in idealized crossflow. Again, this is because the real problems of interest, for example, the vibration of heat exchanger tubes, are too complicated; requiring that we develop first an understanding of the simple models and then proceed to the more complex. Here, too, careful, and what might be termed "sophisticated," experimental work is required to guide the mathematical modeling and to provide a means of evaluating the models.

Mr. D. R. Miller in his paper on the excitation of a pure tone by flow through an orifice illustrated how we can profit from work performed in related fields, in this case acoustics, to guide us in our analysis and explanation of observed phenomena. Mr. M. Bender also called our attention to being aware of the literature in other engineering fields. This deserves re-emphasis and perhaps the aerospace field could be singled out as a potential source of useful information. Most often the fluid medium will not be the same and the parameter ranges, for example, flow velocity, will be different. Nevertheless, the basic phenomenon is often the same and the methods of attack and techniques of analysis may be applicable.

In addition to the basic studies of parallel-flow- and crossflow-induced vibration, the solution of practical problems resulting in a design fix was discussed. These problems will be encountered continually and will require "immediate" solutions. It is hoped that the insights gained through basic studies and from a conference of this nature will contribute to their solution.

ATTENDEES

Achenbach, Jan D.
Northwestern University
Bender, M.
Oak Ridge National Laboratory
Bengel, Paul R.
Bettis Atomic Power Laboratory
Boers, Burdette L.
Argonne National Laboratory
Bruckx, Joseph F.
Argonne National Laboratory
Carey, John J.
Argonne National Laboratory
Carter, Ralph P.
Argonne National Laboratory
Chang, L. K.
Argonne National Laboratory
Chen, Shoei-Sheng
Argonne National Laboratory
Corr, John E.
General Electric Co., APED
Davis, Stanley A.
Argonne National Laboratory
Dhudshia, V. H.
Foster Wheeler Corp.
Fabic, Stanislav
Westinghouse Electric Corp., Power Systems
Fenech, Henri J.
University of California, Santa Barbara
Gardner, Karl A.
Liquid Metal Engineering Center
Gelman, A.
Atomics International
Gerlach, C. Richard
Southwest Research Institute
Gesinski, Leonard
Westinghouse Electric Corp., Nuclear Energy Systems
Gross, Peter J.
Div. of Reactor Development and Technology, USAEC
Grossman, Nicholas
Div. of Reactor Development and Technology, USAEC
Halle, Henry
Argonne National Laboratory
Jendrzejczyk, Joseph A.
Argonne National Laboratory
Kanazawa, Richard M.
General Electric Co., APED
Katz, Robert
Gulf General Atomic
Kinsel, William C.
Battelle Northwest Laboratory
Kiss, Edward
General Electric Co., APED
Knudson, Stanley A.
Esso Research and Engineering Co.
Krajcinovic, Dusan
Argonne National Laboratory
Lawrence, William P.
Argonne National Laboratory
Lennox, David H.
Argonne National Laboratory
Lohmeier, Alfred
Westinghouse Electric Corp., Tampa
Lottes, Paul A.
Argonne National Laboratory
Lowe, Phillip A.
Bettis Atomic Power Laboratory
Miller, Daniel R.
Knolls Atomic Power Laboratory
Minami, Henry M.
Liquid Metal Engineering Center
Monson, Harry O.
Argonne National Laboratory
Moretti, Peter M.
Westinghouse Electric Corp., Walts Mill Site
Muraoka, Jack
Battelle Northwest Laboratory
Nalezny, Charles L.
Bettis Atomic Power Laboratory
Nelms, Harry A.
Oak Ridge National Laboratory
Nevitt, Michael V.
Argonne National Laboratory
Nolan, Donald O.
United Nuclear Corp.
Pai, David H.
Foster Wheeler Corp.
Probert, Paul B.
The Babcock & Wilcox Co.
Purcell, John J.
Chicago Operations Office, USAEC
Randall, R. L.
Atomics International
Reiff, David D.
Div. of Reactor Development and Technology, USAEC
Rippel, R. Ross
Knolls Atomic Power Laboratory
Rose, Sewell C.
Knolls Atomic Power Laboratory
Rosenberg, Gerald S.
Argonne National Laboratory

Sawtelle, George R.
Battelle Northwest Laboratory
Simonis, John C.
The Babcock & Wilcox Co.
Singleton, Norman R.
Westinghouse Electric Corp., Nuclear Energy Systems
Smith, Gerald M.
University of Nebraska
Toebes, Gerrit H.
Purdue University
Valentin, Richard A.
Argonne National Laboratory
Wambsganss, Martin W.
Argonne National Laboratory
Wang, Ping Y.
Argonne National Laboratory
Wesley, Donald A.
Gulf General Atomic
Youngdahl, Carl K.
Argonne National Laboratory
Zaleski, Peter L.
Argonne National Laboratory
Zanoni, Edward A.
Bettis Atomic Power Laboratory

Left to Right, Front Row: A. Lohmeier, Westinghouse Electric Corporation--Tampa; D. D. Reiff, U.S. Atomic Energy Commission; M. W. Wambsganss, Argonne National Laboratory; G. R. Sawtelle, Battelle Northwest Laboratory; J. J. Purcell, U.S. Atomic Energy Commission; N. Grossman, U.S. Atomic Energy Commission; W. C. Kinsel, Battelle Northwest Laboratory; G. H. Toebes, Purdue University; D. H. Pai, Foster Wheeler Corporation; V. H. Dhudshia, Foster Wheeler Corporation; R. L. Randall, Atomics International; J. C. Simonis, The Babcock & Wilcox Company; J. Muraoka, Battelle Northwest Laboratory; P. M. Moretti, Westinghouse Electric Corporation. Middle Row: B. L. Boers, Argonne National Laboratory; J. J. Carey, Argonne National Laboratory; E. A. Zanoni, Bettis Atomic Power Laboratory; C. L. Nalezny, Bettis Atomic Power Laboratory; P. A. Lowe, Bettis Atomic Power Laboratory; J. E. Corr, General Electric Company--APED; E. Kiss, General Electric Company--APED; L. K. Chang, Argonne National Laboratory; P. Y. Wang, Argonne National Laboratory; J. F. Bruckx, Argonne National Laboratory; R. R. Rippel, Knolls Atomic Power Laboratory; G. M. Smith, University of Nebraska; S. C. Rose, Knolls Atomic Power Laboratory; R. M. Kanazawa, General Electric Company--APED. Standing: H. J. Fenech, University of California--Santa Barbara; S. S. Chen, Argonne National Laboratory; S. A. Knudson, Esso Research & Engineering Company; W. P. Lawrence, Argonne National Laboratory; G. S. Rosenberg, Argonne National Laboratory; P. L. Zaleski, Argonne National Laboratory; J. A. Jendrzejczyk, Argonne National Laboratory; M. Bender, Oak Ridge National Laboratory; R. P. Carter, Argonne National Laboratory; H. A. Nelms, Oak Ridge National Laboratory; D. Krajcinovic, Argonne National Laboratory; J. D. Achenbach, Northwestern University; P. R. Bengel, Bettis Atomic Power Laboratory; H. Halle, Argonne National Laboratory; D. R. Miller, Knolls Atomic Power Laboratory; C. R. Gerlach, Southwest Research Institute; C. K. Youngdahl, Argonne National Laboratory; S. Fabic, Westinghouse Electric Corporation; K. A. Gardner, Liquid Metal Engineering Center; R. Katz, Gulf General Atomic; P. B. Probert, The Babcock & Wilcox Company; D. A. Wesley, Gulf General Atomic; P. J. Gross, U.S. Atomic Energy Commission; A. Gelman, Atomics International; H. M. Minami, Liquid Metal Engineering Center.

3 4444 00014998 9

B